METAL COMPLEXES OF SCORPIONATE-LIKE POLYIMIDO SULPHUR PHOSPHANYL LIGANDS

Dissertation zur Erlangung des
mathematisch-naturwissenschaftlichen Doktorgrades
der Georg-August-Universität Göttingen

vorgelegt von
Margret Meinholz
aus Coesfeld

Göttingen 2011

Eingereicht am:	28.03.2011
Referent:	Prof. Dr. D. Stalke
Co-Referenten:	Prof. Dr. F. Meyer Prof. Dr. L. Ackermann
Datum der mündlichen Prüfung:	11.05.2011
Prüfer Anorganische Chemie:	Prof. Dr. D. Stalke
Prüfer Makromolekulare Chemie:	Prof. Dr. M. Buback
Prüferin Kristallographie:	Prof. Dr. H. Sowa
Erweiterte Prüfungskommision:	Prof. Dr. F. Meyer Prof. Dr. L. Ackermann Prof. Dr. O. Wenger

"Oft bringt ein Tag,

worauf man sonst ein Jahr lang wartet.“

Menander

CONTENTS

ABBREVIATIONS

Å	*Ångstrom*
AMMM	alkali metal mediated metalation
approx.	approximately
av.	average
calc.	calculated
cp	cyclopentadienyl
CVD	chemical vapour deposition
decomp.	decomposition
dme	dimethoxyethane
dmp	2,6-dimesitylphenyl
DOSY	diffusion ordered spectroscopy
e. *g*.	for example (*lat.: exemplia gratia*)
Et	ethyl
et al.	and others (*lat.: et alii*)
GoF	goodness of fit
h	hour(s)
HMBC	heteronuclear multiple bond correlation
HOESY	heteronuclear Overhauser effect spectroscopy
HSAB	hard and soft acids and bases
HSQC	Heteronuclear single quantum coherence
i. e.	that is (*lat.: id est*)
IμS	Incoatec Microfocus Source
*i*Pr	*iso*-propyl
LDA	lithium diisopropyl amide
M	molar
Me	methyl
*n*Bu	*n*-butyl
NMR	nuclear magnetic resonance
NOESY	nuclear Overhauser effect spectroscopy
Ph	phenyl
pmdeta	pentamethyldiethylenetriamine
pic	picolyl
ppm	parts per million

pz	pyrazolyl
rt	room temperature
*t*Bu	*tert*-butyl
thf	tetrahydrofurane
thp	tetrahydropyrane
tmcda	tetramethylcyclohexane-1,2-diamine
tmeda	tetramethylethylenediamine
tmmda	tetramethylmethylenediamine
tmp	tetramethylpiperidine
trmeda	trimethylethylenediamine
vs.	*versus*

LIST OF COMPOUNDS

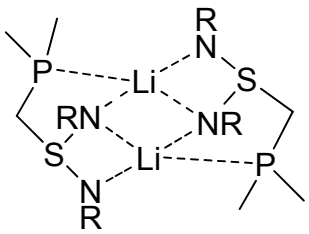

1: R = *t*Bu; **4**: R = $SiMe_3$

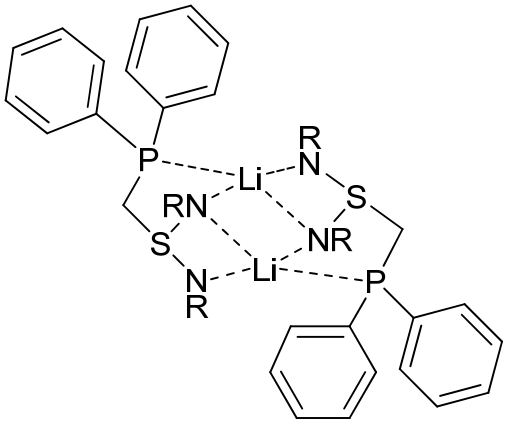

2: R = *t*Bu; **5**: R = $SiMe_3$

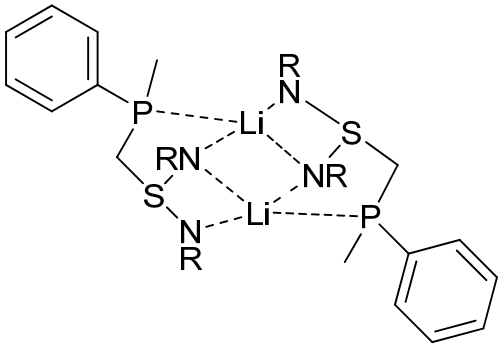

3: R = *t*Bu; **6**: R = $SiMe_3$

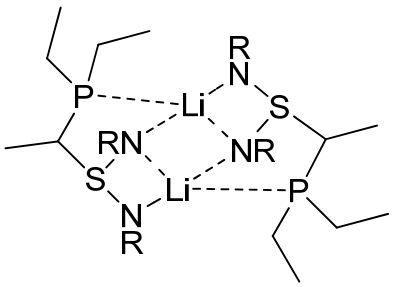

7: R = $SiMe_3$

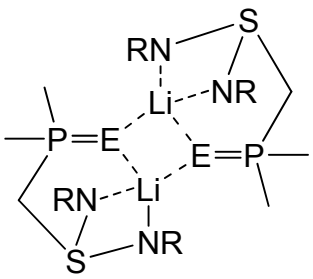

8: E = S, R = $SiMe_3$; **9**: E = Se, R =$SiMe_3$

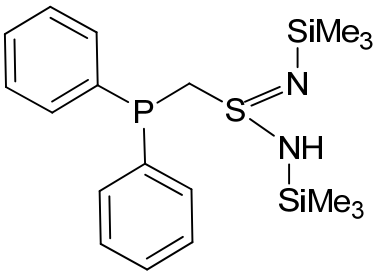

10

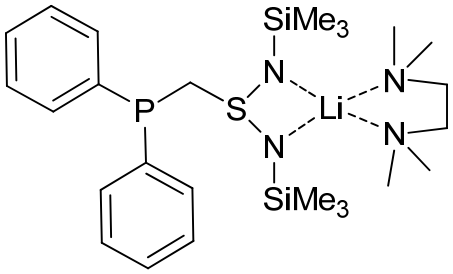

11

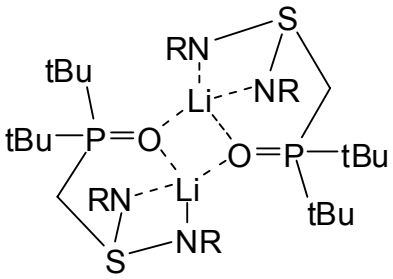

12: R = $SiMe_3$

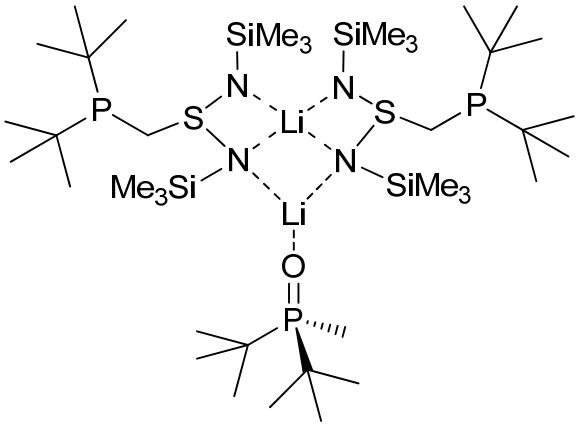

13

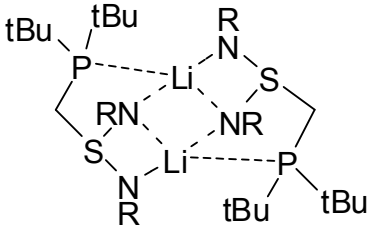

14: R = $SiMe_3$

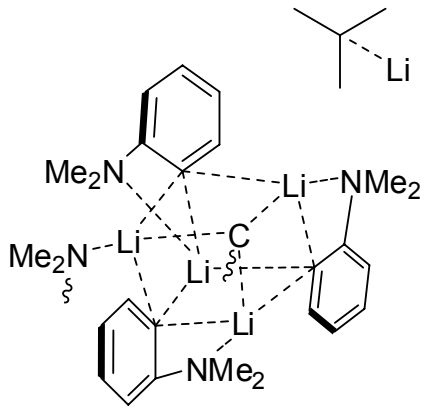

15: one phenyl ring has been omitted for clarity

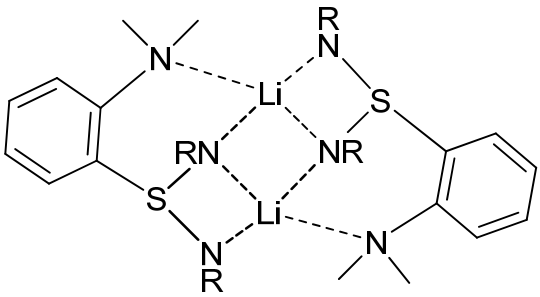

16: R = $SiMe_3$

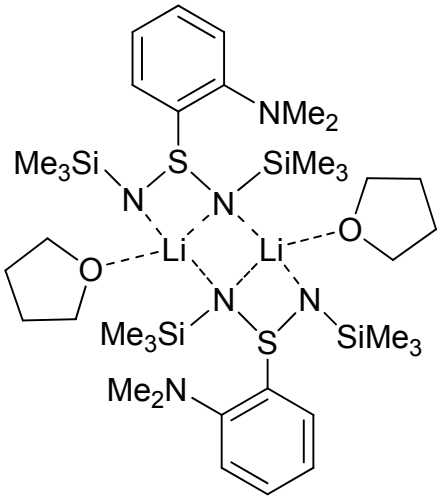

17

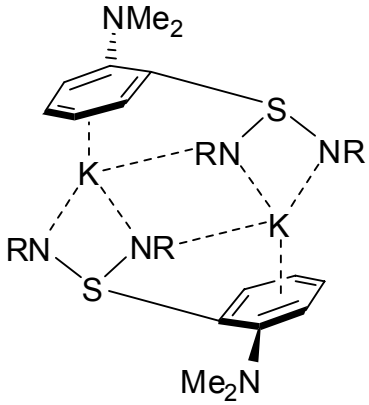

18: R = $SiMe_3$

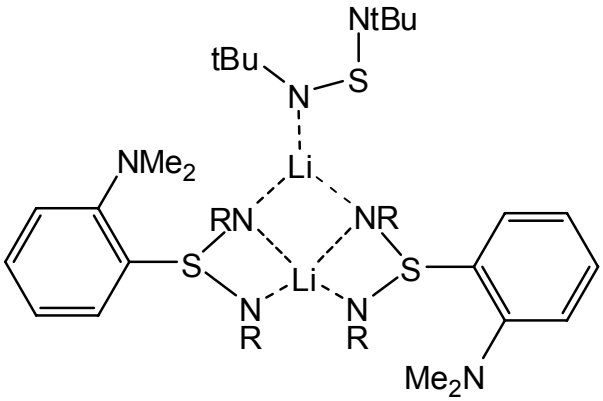

19: R = *t*Bu

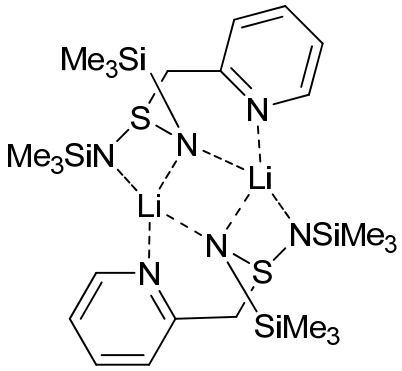

20

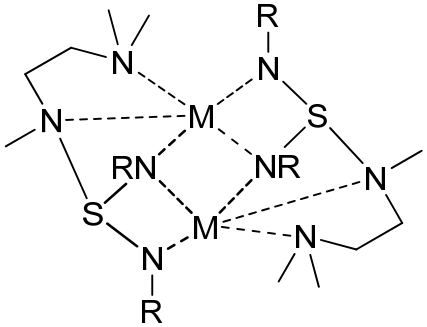

21: R = $SiMe_3$, M = Li; **22**: R = $SiMe_3$, M = Na

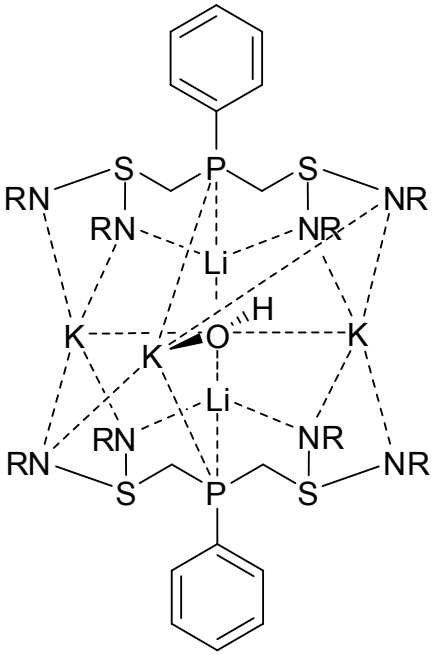

23: R = $SiMe_3$

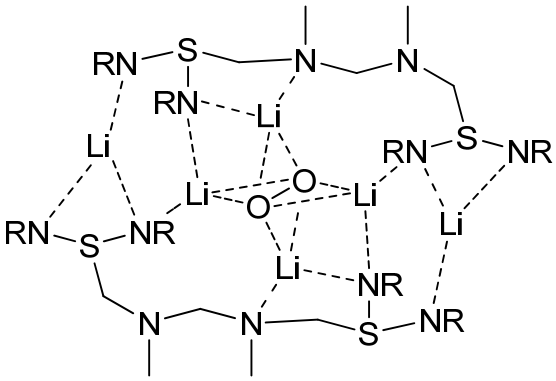

24: R = *t*Bu

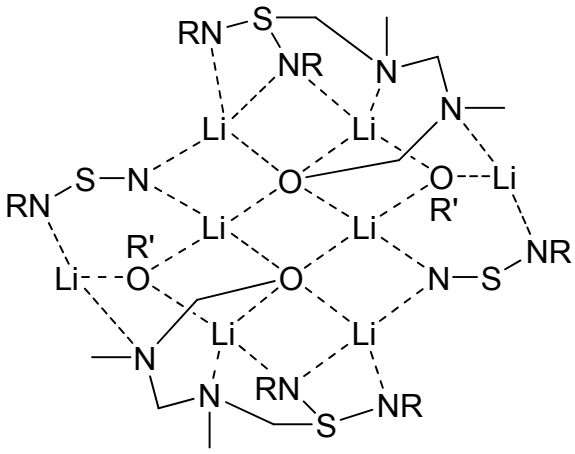

25: R = $SiMe_3$, R' = *t*Bu

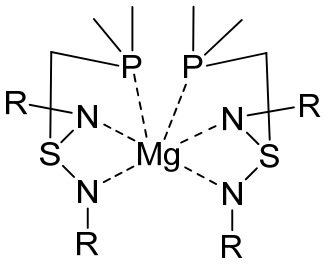

26: R = *t*Bu; **27**: R = $SiMe_3$

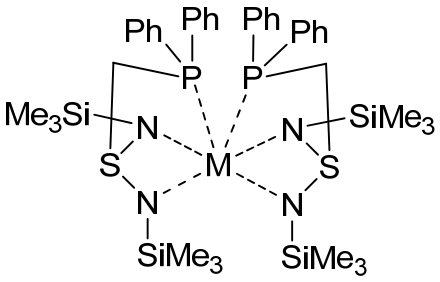

28: M = Ca^{2+}; **29**: M = Sr^{2+}; **30**: M = Co^{2+}; **31**: M = Fe^{2+}

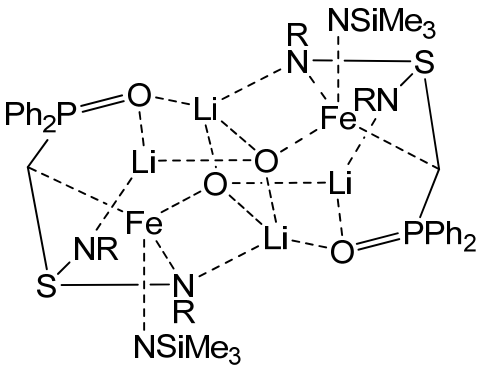

32: R = $SiMe_3$

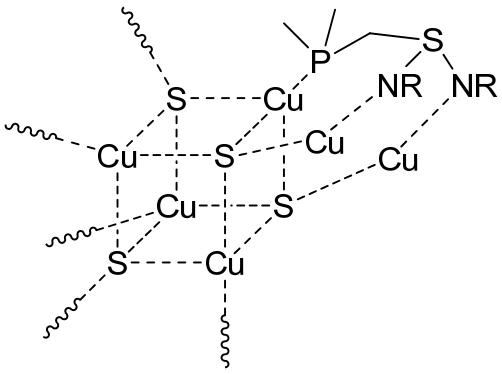

33: R = $SiMe_3$

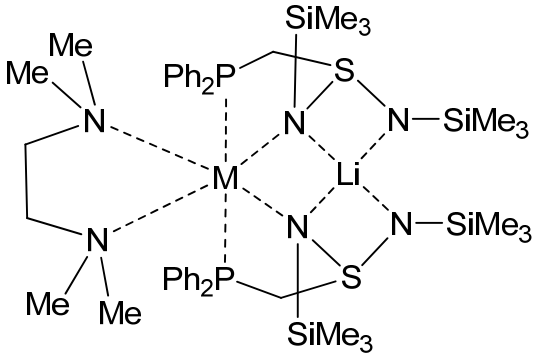

34: M = Rb^+; **35**: M = K^+

1 INTRODUCTION

A prominent example for ligand design are poly(pyrazolyl)borates which *Trofimenko* introduced in 1966 as a new class of chelating ligands (Figure 1-1).[1] They are prepared by heating an alkali metal borohydride with pyrazole at different temperatures, thus adding subsequent equivalents of pyrazole to the boron atom. Their stability towards air and moisture increases with the number of pyrazolyl groups bonded to the central boron atom. Tris(pyrazolyl)borate for instance is storable for years in the solid state even if exposed to air and light. Most of the poly(pyrazolyl)borate transition metal complexes are stable in water and air as well.[2]

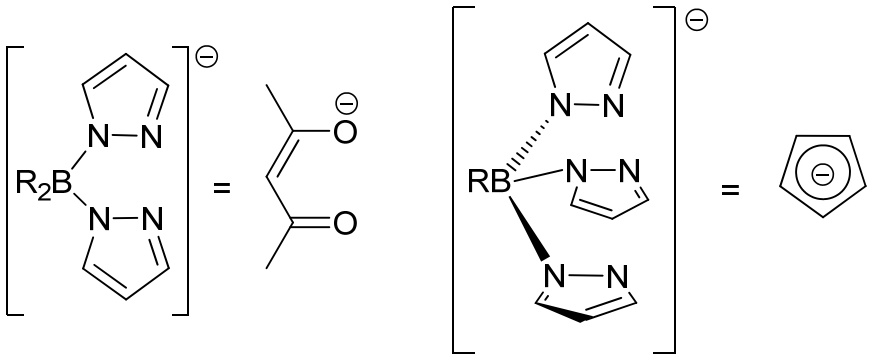

Figure 1-1: Analogies between bis(pyrazolyl)borate and β-diketonates (left); tris(pyrazolyl)borates and cyclopentadienyl (right); R = H, alkyl, aryl, … .

The tris(pyrazolyl)borates in particular show very interesting complexation properties. They are often described as being analogues to Cp or Cp^* (Figure 1-1) as they are also six-electron donors, monoanionic and coordinate in a facial way, but this description does not take into account their unique complexation behaviour.[3,4] With this ligand it was even possible to synthesise a homologue series of complexes with the hapticity of the ligand changing from κ^3 to κ^0.[5] A κ^5 Ir-complex[6] and a η^5 compound[7], where one of the pyrazole rings is coordinating a potassium cation, were described, too. However, these are special cases.

In general, the most important features of poly(pyrazolyl)borates are:

- formation of a six-membered, boat-shaped ring with a coordinated metal (Figure 1-2)
- tridentate, tripodal
- monoanionic
- facial coordinating
- “spectator ligands” (do not take part in reactions at the metal centre)

The two pz groups (pz = 1-pyrazolyl or substituted 1-pyrazolyl) that are in plain chelate the metal in a bidentate way. The third pseudoaxial pz group acts as a side-arm that bends towards the metal. Therefore, the term “scorpionates” was coined with the two in-plane pyrazolyl groups being the claws and the third pz group being the sting of the scorpion.

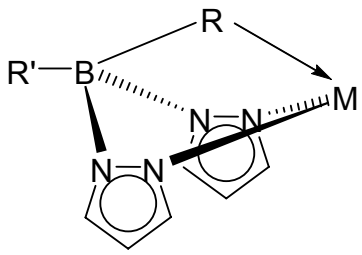

Figure 1-2: Boat conformation in metal complexes of poly(pyrazolyl)borates. R’ = H, alkyl, aryl, …; R = H, NR_2, pz, OR, SR, agostic C–H, … .

Over the years, the poly(pyrazolyl)borates triggered significant development in terms of ligands design and shaping of the complexation properties. Until today, there are four generations of poly(pyrazolyl)borate ligands. The first generation has been described above, where each donor site is a pz group.

The second generation came up in the 1980s and was developed by *Trofimenko* and co-workers as well.[8] In this ligand type, the pyrazole rings bear bulky substituents at the 3-position and thus increased control is gained on the coordination behaviour. By choice of the substituents (*t*Bu, Ph, …), a coordination pocket of desired size can be created to fit certain metals. To be precise, it was then possible to synthesise monomeric complexes of transition metals (ML(X), L = scorpionate, X = monodentate ligand) rather than dimeric octahedral complexes (ML_2). In terms of catalytic applications, the ML(X) form is preferred as it is more reactive. Additionally, the second generation scorpionate ligands prevent dissociation into ML_2 and MX_2[9] and access of substrates can be controlled by the size of the coordination pocket.[8a]

The third generation scorpionates are tuned by substituting the non-coordinating ligand R’ (Figure 1-2).[10] This leads to different packing of the molecules in the crystal structure and can alter the spin state of the coordinated metal. In addition, the introduction of a further donor site paves the way for heterobimetallic complexes. Finally, the term "fourth generation scorpionates" was introduced in 2010 for linked pyrazolylborates that can bind in a meridional way to metal ions.[11,12,13] Consequently, they offer different coordination modes in comparison to the classical

scorpionate ligands, however their stability is sometimes limited. Examples for the four generations of scorpionate ligands are depicted in Figure 1-3.

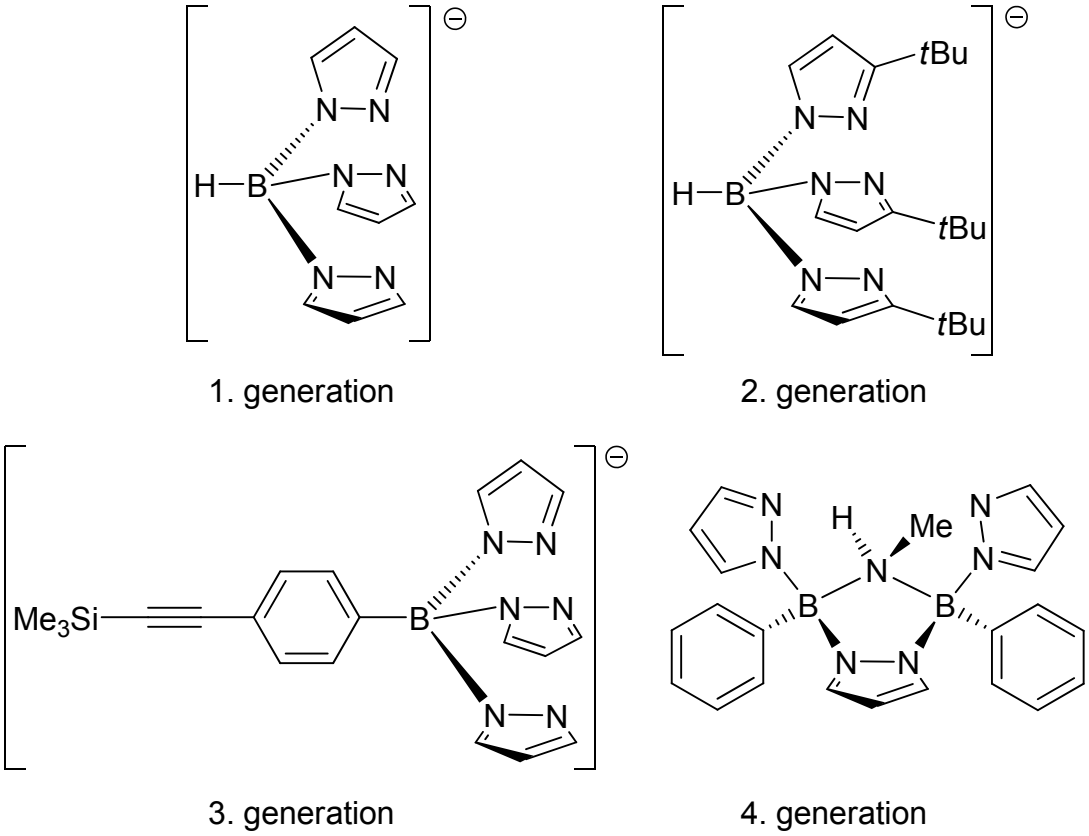

Figure 1-3: Four generations of scorpionate ligands.

Further classification into two different classes of scorpionate ligands is possible. Homoscorpionates have three identical coordinating groups, usually pyrazole. Heteroscorpionates consist of two identical chelating claws (pyrazole) and a sting that is different from pyrazole. Thus, it is possible to introduce softer donor sites into the ligand periphery. Alternatively, all pz groups can be replaced by substituents with other donor atoms like sulphur, selenium or phosphorus. Interesting examples can be found in the phosphinoborate family, namely $[PhB(CH_2P\textit{i}Pr_2)_3]^-$ [14] or $[PhB(CH_2PPh_2)_3]^-$ [15]. The boron atom can also be replaced by carbon, leading to poly(pyrazolyl)methanes[16] which are neutral analogues of poly(pyrazolyl)borates and are also important in coordination chemistry.[17]

One of the most important features of scorpionate ligands is their applicability in biomimetical complexes as the pyrazole group is histidine-like. By the introduction of other donor atoms in the side-arms, the coordination by different amino-acids can be modelled. Important examples come from the group of *Lippard* who succeeded in

modelling the diiron centre of the oxygen transport protein hemerythrin.[18] This dinuclear oxo-bridged iron complex contains histidine and oxygen donors around the iron atoms and could be modelled with the complex $[Fe_2O(O_2CCH_3)_2(HBpz_3)_2]$ (Figure 1-4).

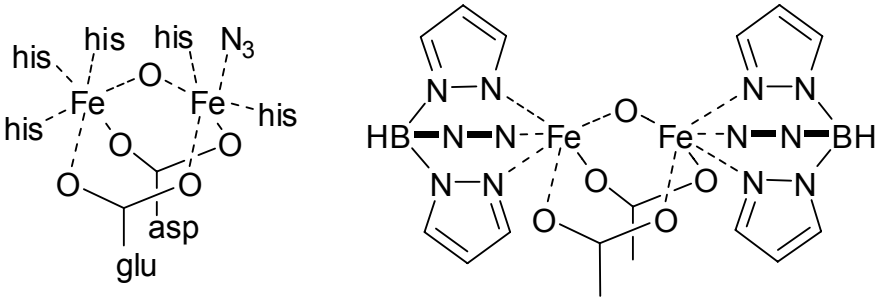

Figure 1-4: Diiron site of hemerythrin (a, his = histidine, glu = glutamate, asp = aspartate) and structural model (b, B-N-N = pyrazole).

Kitajima et al. worked on dinuclear copper complexes which could serve as models for the oxygen binding in hemocyanin which also is an oxygen transport protein.[19] The compound $[Cu(HB(3,5\text{-}i\text{Pr}_2pz)_3)]_2(O)_2$ is a dimer where both copper atoms are coordinated facially by the tris(pyrazolyl)borate ligands and are bridged side-on by a peroxide molecule. The steric bulk of the employed second generation scorpionate made this dinuclear complex feasible.

In 1997 *Higgs* and *Carrano* introduced (2-hydroxyphenyl)-bis(pyrazolyl)methanes as biomimetically relevant heteroscorpionates.[20] These ligands can stabilise cobalt(II) in an octahedral or a tetrahedral environment thereby showing their flexibility.

A heteroditopic approach was undertaken by *Holthausen*, *Wagner* and co-workers.[21] They wanted to model the coordination environment of the copper atoms in dopamine β-monooxygenase and peptidylglycine α-hydroxylating monooxygenase which catalyse the stereo specific hydroxylation of C–H bonds in certain peptides. In the dinuclear reactive centre of the enzymes one copper atom is surrounded by three histidine ligands (Cu_A), the other one by two imidazolyl and one methionine-thioether group (Cu_B).[22] Therefore, two scorpionates with pyrazolyl and thioether substituents were linked together *via* a *p*-phenylene bridge (Figure 1-5). Thus, both copper atoms would be held at a distance of 11 Å, which had also been found in the enzymes mentioned above.

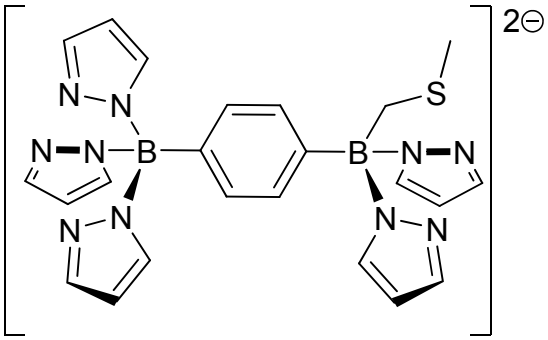

Figure 1-5: Structural model of the active site in dopamine β-monooxygenase and peptidylglycine α-hydroxylating monooxygenase.

In general, the steric demand, ligand field strength and the complexation behaviour of scorpionate ligands can nowadays be controlled. Scorpionate ligands are used in polymerisation reactions[23], chemical vapour deposition (CVD)[24] and bioinorganic chemistry, just to name a few applications. They have one drawback, though: it is very difficult to synthesise homogeneous series of heteroscorpionate ligands because of selectivity problems and substituent scrambling on the borate ion.[11] This is important, however, if the ligand properties are to be reliably tuned.

Instead of a boron atom as bridgehead, other elements can be used in order to create scorpionate-like tripodal ligands. One example, which was already mentioned above, is the carbon atom in poly(pyrazolyl)methanes. However, softer elements like silicon[25] and phosphorus[26] or even metals like germanium[27], tin[27] and lead[28] can serve as bridgehead atoms.

In our group, the sulphurimide chemistry is a well investigated field. Therefore, the idea of using sulphur as a bridgehead atom was obvious. It is well known that in sulphur diimides $S(NR)_2$, the S–N bonds can be described as $S^{\delta+}$–$N^{\delta-}$ polar bonds, which has been proven by theoretical and experimental charge density studies.[29,30]

$$2\ S(NtBu)_2 + 4\ [Li(HNtBu)] \xrightarrow{\text{hexane, rt}} [Li_4\{(NtBu)_3S\}_2] + 2\ H_2NtBu$$

$$[Li_4\{(NtBu)_3S\}_2] + 2\ Br_2 \xrightarrow[\text{-78 °C}]{\text{hexane/thf}} S(NtBu)_3 + 4\ LiBr$$

Equation 1-1: Preparation of $S(NtBu)_3$.

Therefore, it is possible to add nucleophiles to the central sulphur atom in order to synthesise potentially tripodal ligands. One very interesting example which has been extensively studied is tris(*tert*-butyl)sulphur triimide, $S(NtBu)_3$.

The third coordinating imido group is added *via* reaction of S(N*t*Bu)$_2$ with [Li(HN*t*Bu)] and subsequent oxidation with bromine (Equation 1-1).[31] However, there are certain disadvantages in the synthesis and the final product. The intermediate [Li$_4${(N*t*Bu)$_3$S}$_2$] is highly oxygen sensitive and immediately turns blue if it is not handled with the greatest care.[32] In addition, the tris(*tert*-butyl)sulphur triimide is not very flexible regarding its coordination properties. The S–N bonds are rather short and rigid and the substituents on the nitrogen atoms are bulky. This could be overcome, however, by the introduction of an additional, more flexible side-arm. As the molecule is planar, the attack of a nucleophile from above or beneath the N–S–N plane seems feasible.

However, this is hindered by electronic reasons, because exactly in these positions there is an accumulation of electron density (Figure 1-6). The attack of a nucleophile is only possible directly between two N*t*Bu groups, where a charge depletion can be found.[29] Therefore, only reagents that are quite slim *i. e.* small and planar can be used because of the bulky *tert*-butyl groups that shield the sulphur atom. In another approach, *Schulz* employed *Grignard* reagents that are softer and thereby more reactive towards the sulphur atom.[33] He succeeded in bonding phenyl and benzyl groups to the central atom. However, these substituents do not have additional donor functionalities.

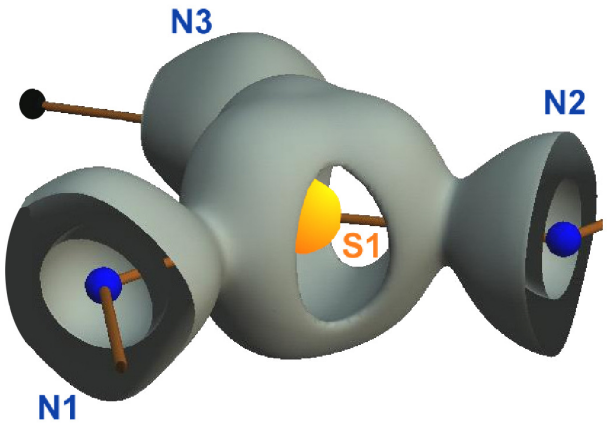

Figure 1-6: Laplacian of S(N*t*Bu)$_3$.[29]

For those reasons, the functionalization of sulphur diimides seemed more rewarding as they already show a great variety of coordination motives[34] (Figure 1-7) and the introduction of a side-arm is straightforward. Thus, heteroscorpionate type ligands can be created.

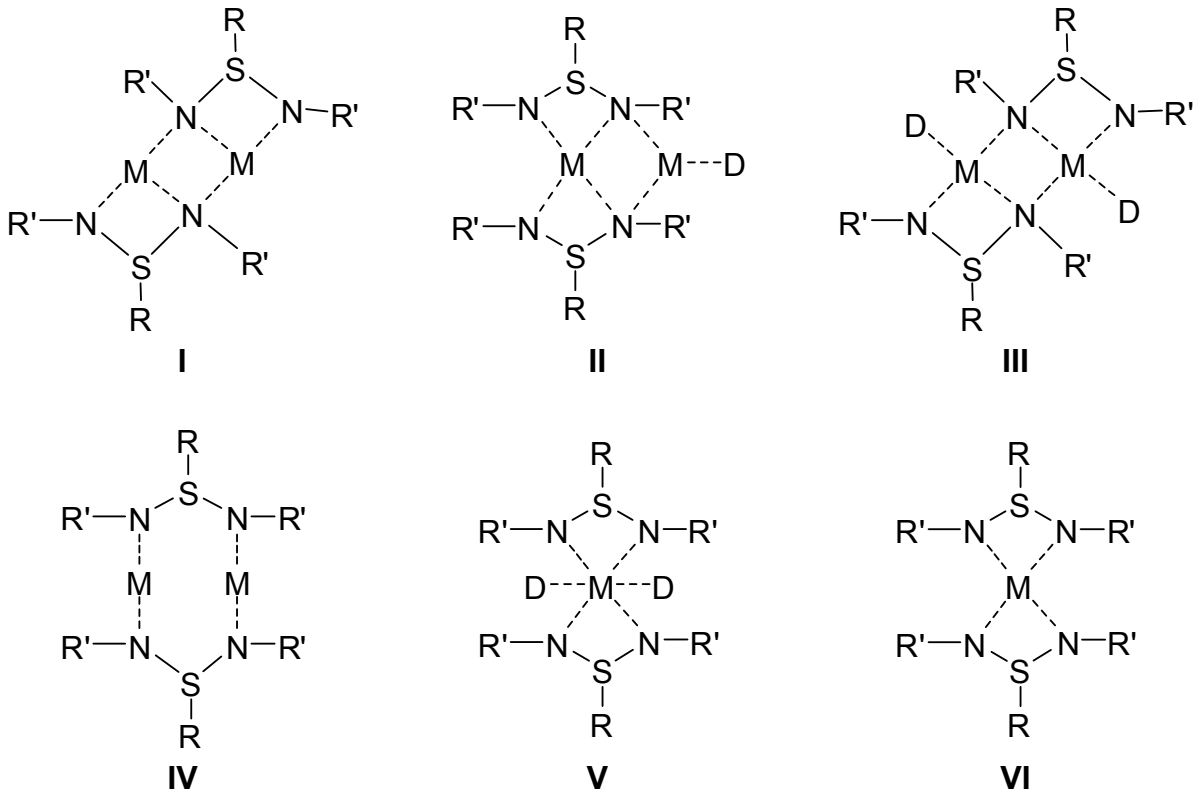

Figure 1-7: Coordination motives of diimidosulfinates (M = metal, D = donor, R/R' = organic group).

Side-arms that have already been added to sulphur diimides include carbon, silicon, nitrogen and sulphur functionalities.[35,36,37]

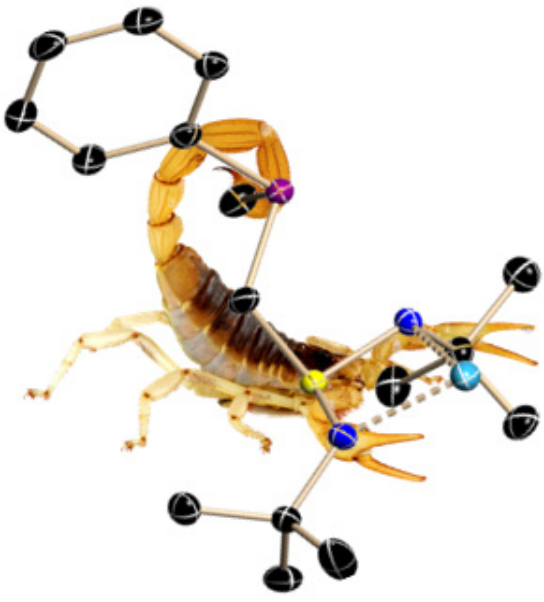

Figure 1-8: The scorpion is ready to sting.

In 2007 *Deuerlein* presented the synthesis of the phosphorus-functionalized sulphur diimide $[Li\{Me_2PCH_2S(NtBu)_2\}]_2$ (**1**).[38,39] This molecule is reminiscent of heteroscorpionates which also have the (*N,N,P*) form.[40]

Its claws are the two diimido groups (dark blue) whereas the sting is represented by the phosphorus side-arm (purple) which can swing out and coordinate to the metal (Figure 1-8). Thereby potentially tridentate ligands with different donor sites can be created. This is of great

importance for the synthesis of heterobimetallic complexes with metals of different HSAB hardness.[41]

Heterobimetallic complexes gain ever increasing attention in preparative chemistry, above all in deprotonation reactions. Usually, lithium organic reagents like BuLi or LDA are used for such purposes. However, they suffer from insufficient functional group tolerance, low selectivity and the reactions have to be conducted at low temperatures (usually below 0 °C) to avoid side-reactions. This is where so-called complex metalators consisting of two or more metal components are used. In these compounds the metal atoms interact synergistically because they are held in close spatial proximity. Thereby, unusual (for lithium organics) deprotonation reactions are feasible and selectivities can greatly be enhanced. Prominent examples are the LiCKOR superbases of *Lochmann* and *Schlosser*[42], zincate complexes[43], turbo-*Grignard* reagents[44] or inverse crown reagents for alkali metal mediated metalations (AMMMs)[45]. These four types of metalating agents will be described briefly and some examples are presented (Figure 1-9). A more detailed discussion can be found in the literature and partly in upcoming chapters of this thesis.

In the 1960's, *Lochmann* and *Schlosser* observed independently, that the interaction of a lithium organic reagent (LiC) and a potassium alkoxyde (KOR) lead to a more reactive species (LiCKOR). Therefore, these systems were called superbases, as their reactivity is enhanced in comparison to *n*BuLi although is below that of pure *n*BuK. Until today, however, the structures of most of these superbases are not clear.

Zincate complexes have been investigated by *Kondo* and *Uchiyama* since 1999. They paired lithium-TMP (TMP = tetramethylpiperidine) with $Zn(tBu)_2$ to produce a TMP-zincate.[43a] This reagent proved to be highly reactive in the ortho-metalation of arenes. Also the metalation of heteroaromatic systems was possible with excellent selectivity. By the change of the substituents on the zinc atom, the stereo selectivity can be controlled.[43b] However, again no crystal structure was presented. *Stalke et al.* studied the aggregation and deaggregation of parent lithium trimethylzincate with different donor bases and presented crystal structures of a contact ion pair and a solvens separated ion pair.[46]

Turbo-*Grignard* reagents are linked to the name of *Knochel* and obey the general formula RMgCl·LiCl (R = alkyl). Such mixed lithium/magnesium complexes are more reactive than the original, monometallic *Grignard* reagents (RMgX). When an equimolar amount of LiCl is added to *i*PrMgCl, its reactivity in Br/Mg exchange reactions is greatly increased.[44a,47] The reagent was prepared for the first time by adding *i*PrCl to magnesium turnings and LiCl in THF and was used as this solution. Today it is even commercially available.[48] *Knochel* suggested that the high reactivity of this turbo-*Grignard* base was due to the fact that LiCl breaks up the oligomeric $(i\text{PrMgCl})_n$ aggregates.

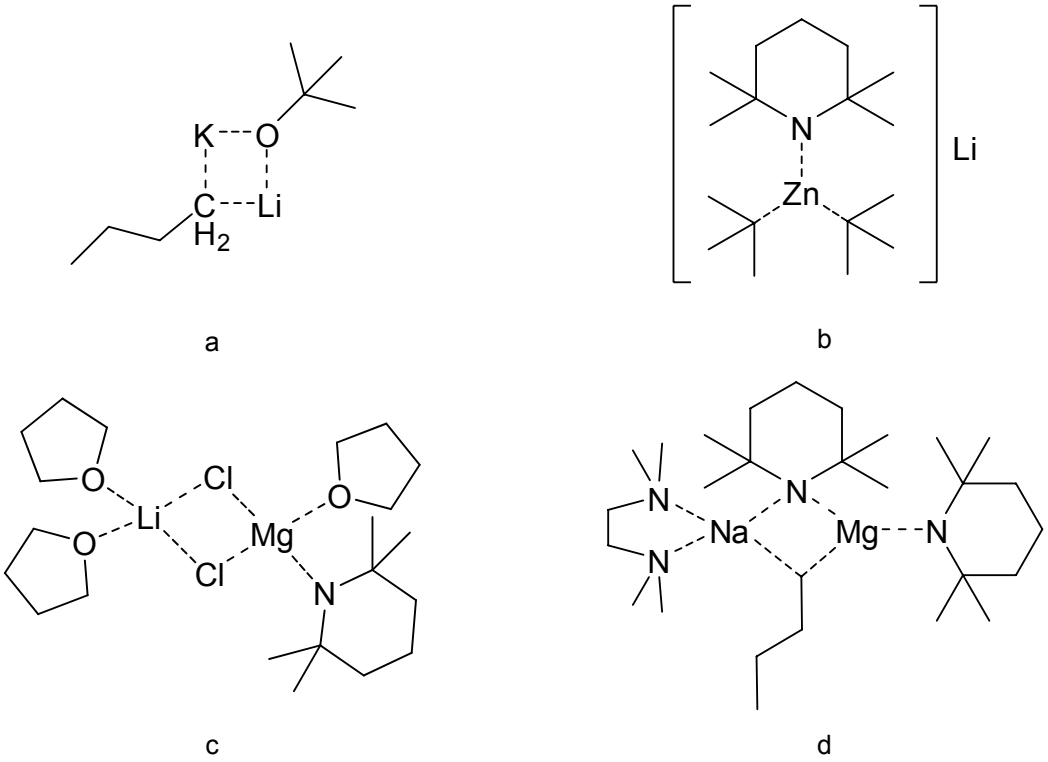

Figure 1-9: Heterobimetallic complexes for metalation reactions; a: LiCKOR, b: Zincate, c: turbo-*Grignard*, d: AMMM.

In subsequent reactions it became evident that derivatives of *i*PrMgCl·LiCl display an enhanced stereo selectivity in the magnesiation of arenes and heteroarenes.[49] The turbo-*Grignard* reagents for this reactions were prepared by mixing *i*PrMgCl·LiCl with an amine (TMP, HN*i*Pr$_2$) and the resulting turbo-*Hauser*[50] base (which can be regarded as a special case of turbo-*Grignards*) was then reacted with an arene or heteroarene (Equation 1-2).

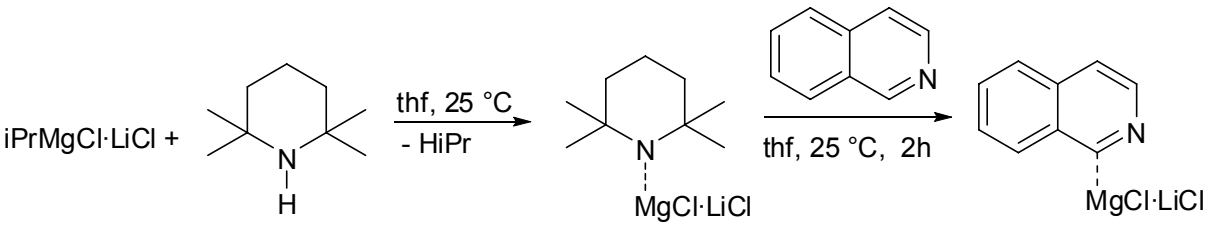

Equation 1-2: Preparation and reaction of turbo-*Grignard* reagents.

Recently, the structure of one of these reagents has been elucidated (Figure 1-9, **c**).[51] This is very important because with the knowledge of the structure, deductions regarding the reactivity can be made. In turn, this could lead to a better understanding of the mechanism of these deprotonation reactions and the development of tailor-made bases.

In another approach, *Mulvey* and co-workers put considerable effort into the research of alkali metal mediated metalations (AMMMs). For these reactions an alkali metal is combined with another divalent metal in a heterobimetallic organometallic compound. To achieve this, a metal amide, a metal alkyl reagent and a donor base are mixed. It is, however, the divalent metal which effects the deprotonation in the end. This is surprising as the alkali metal is usually more reactive but there seems to be a strong synergistic effect when both metals are in close spatial proximity. Thus, the meta-deprotonation of toluene was achieved with a mixed sodium/magnesium reagent (Figure 1-9, **d**).[45,52]

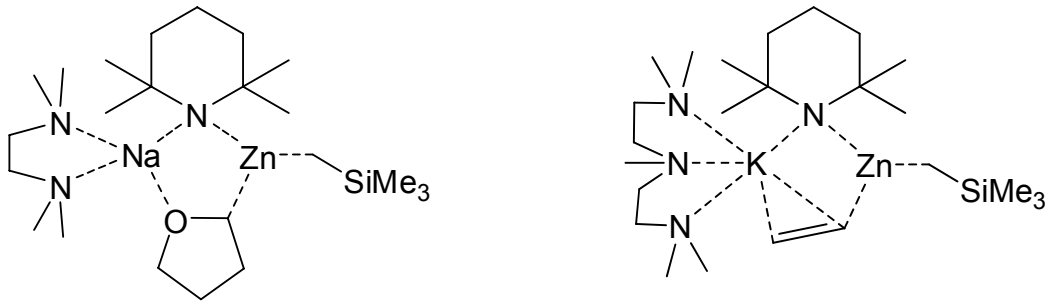

Figure 1-10: Products of the deprotonation of THF (right) and ethene (left) with heterobimetallic bases.

In another approach, ferrocene was fourfold deprotonated with a similar reagent.[53] Apart from unusual stereoselectivities, those compounds can even deprotonate THF, THP (tetrahydropyrane) or ethene.[54] The abstraction of a hydrogen atom adjacent to oxygen in cyclic ethers usually leads to ether cleavage reactions. However, with the heterobimetallic base [(tmeda)Na(μ-tmp)(μ-CH_2SiMe_3)Zn(CH_2SiMe_3)], the

α-deprotonation of THF is possible and the reaction product has been characterised by X-ray crystallography. Likewise, the deprotonation of ethene was achieved with the mixed potassium/zinc complex [(pmdeta)K(μ-tmp)(μ-CH_2SiMe_3)Zn(CH_2SiMe_3)] and the product was structurally characterised (Figure 1-10).

Scope of this Thesis

As the introduction of nucleophiles at the sulphur atom in sulphur diimides has been well established over the years, the goal of this thesis was to develop new sulphur diimido ligands with functionalized side-arms in order to generate potentially tripodal ligands. As it is also established so far that the sulphur atom does not take part in metal coordination, an additional donor site should be soft. With this approach, potentially hemilabile ligands are accessible that are reminiscent of heteroscorpionates. Hemilability means, that in one coordination compound, some metal-donor bonds are weaker than others and can easily be cleaved.[55] In lithium complexes of (*N,N,P*) ligands for example, this would be the P–Li bond because of the unsuitable soft/hard interaction.

Furthermore, a side-arm should be flexible enough to bind small and large metal atoms and make the synthesis of heterobimetallic complexes feasible. Phosphorus was chosen as an additional donor site, because of the good availability of the starting materials and the already established synthesis.[38,39] The resulting ligands were called NSCP ligands because a sulphur diimide (NS) is linked to a phosphane *via* a carbon-bridge (CP). As the side-arm of a ligand should be flexible in order to achieve variable binding modes, phosphanes with methyl groups were to be employed. These represent potential CH_2-bridges between the sulphur and the phosphorus atom. For comparison, the corresponding nitrogen analogues of the NSCP-ligands were to be synthesised as well. It would be interesting to elucidate the differences between the period one and two elements in their coordination behaviour and compare their binding modes.

The development of a whole set of building blocks (*i. e.* sulphur diimides on the one hand – nucleophile side-arms on the other hand) that may be combined in many different ways was the main goal. Thereby, a modular synthesis of side-arm donating, tripodal ligands for the desired application would become possible. It should be feasible to alter the ligand at need for the complexation of the metals of choice and to change the steric and electronic properties in a straightforward way. In

addition, it should be possible to complex both hard and soft metals and stabilise them in low oxidation states.

First, a set of ligands had to be synthesised that differed on the one hand in their sulphur diimido moiety and on the other hand in the coordinating side-arm. Second, the complexation of various metal cations was to be tested. Thereby, different oxidation states, coordination modes as well as transition and main group metals could be employed in metalation reactions and the behaviour of the ligand could be analysed. It was also of interest to compare different starting materials for transmetalation reactions regarding their reactivity. In the end, it should be possible to synthesise heterobimetallic complexes as well.

To fully understand and characterise the new compounds in the solid state as well as in solution, X-ray crystallography and NMR spectroscopy should become the analytical methods of choice.

2 LIGANDS WITH PHOSPHORUS SIDE-ARM

2.1 Introduction

As the sulphur atom in the sulphur diimides does not take part in metal coordination, a different soft donor site in the ligand would be of great interest. Therefore, a phosphorus containing side-arm was connected to the sulphur atom. Such a side-arm donation has the advantage of increased flexibility and complexation versatility.

In upcoming chapters, the exchange of the phosphorus side-arm by a nitrogen containing one in order to compare the different possible coordination modes is described. In addition, the connection of two sulphur diimides by donor containing bridges is shown. Thus, even more diverse coordination modes are gained. In the end, metal exchange reactions were carried out to fully explore the complexation properties of the new ligand system. Therefore, main group and transition metals were employed in different oxidation states.

In this chapter, the design of different sulphur diimide centred lithium complexes is described. Additionally, the access to a metal free derivative is shown as well as the synthesis of an ideal starting material for metal exchange reactions.

In 2007, *Deuerlein* reported the synthesis of a novel diimidosulfinate with phosphorus side-arm.[38] In a first attempt, he reacted the lithiated sulphur ylide $[(thf)Li\{H_2CS(NtBu)_2\}]_2$ with Me_2PCl, $Me(Ph)PCl$ or Ph_2PCl in a salt elimination reaction. Unfortunately, this route led to decomposition of the ligand with unpredictable products as Equation 2-1 points out. A similar reaction had also earlier been described by *Hänssgen et al.* in 2001.[56]

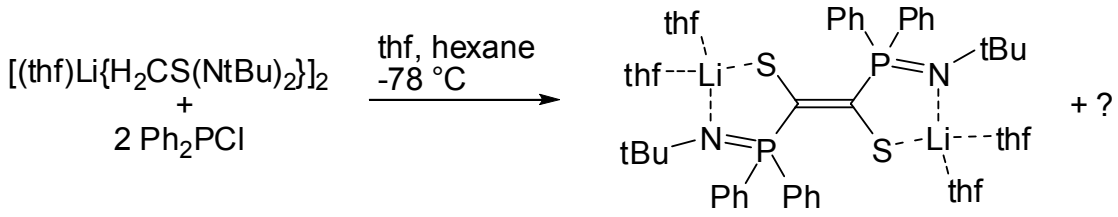

Equation 2-1: Reaction of $[(thf)Li\{H_2CS(NtBu)_2\}]_2$ with Ph_2PCl.

The sulphur ylides and other similar sulphur nitrogen compounds are too redox active[38,57,58] and the addition of metal halogenides leads to S–N and S–C bond cleavage reactions. This phenomenon had already been reported by *Hänssgen* and *Steffens* for sulphur diimide derivatives in the 1980's.[59] Therefore, the reaction

had to be conducted differently. PMe_3 was lithiated – a procedure that has been well described in the literature [60,61,62] – and reacted with $S(NtBu)_2$ (general Equation 2-2). The structure of the obtained lithium complex is shown in Figure 2-1.

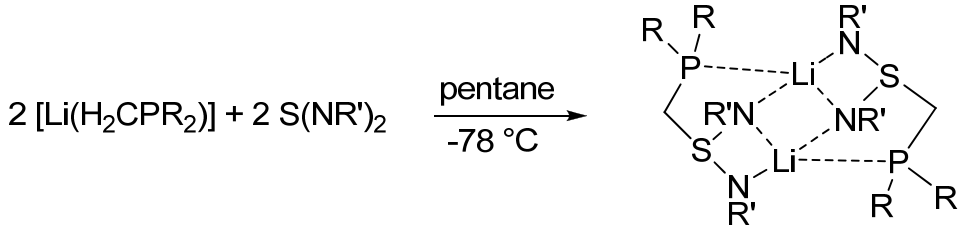

Equation 2-2: Preparation of $[Li\{R_2PCH_2S(NR')_2\}]_2$.

There exists a patent of a nickel complex with the related ligand $\{tBu_2PCH_2S(NSiMe_3)_2\}^-$ for olefin polymerization [63] and *Deuerlein* started to pursue this topic. He was able to show that the phosphane-functionaliziation of a sulphur diimide is easily possible. This reaction – which was mentioned above – should in principle be applicable to any phosphane with a methyl group.

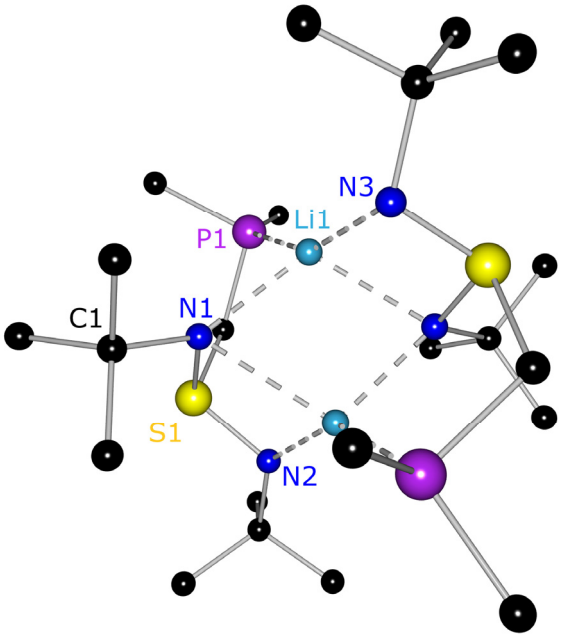

Figure 2-1: Molecular structure of $[Li\{Me_2PCH_2S(NtBu)_2\}]_2$ (**1**). Hydrogen atoms are omitted for clarity.

2.2 Di(*tert*-butyl)sulphur diimide

As already mentioned above, the linkage of sulphur diimide and phosphane was achieved by an equimolar reaction of lithium dialkyl phosphanyl methanide and di(*tert*-butyl)sulphur diimide, $S(NtBu)_2$. This reaction had to be improved further, as the lithiation of PMe_3 by the mentioned literature methods was not satisfying because

the yield was too low and the instructions contradictory.[60,61,62] Eventually, a modified procedure was established: a solution of *t*BuLi in pentane (1.5 M) was reduced to approx. half of its volume and the phosphane was added drop wise at room temperature. After 30 min a white precipitate could be observed. After stirring over night, the reaction was complete, the white powder was filtered off and thoroughly washed with pentane. With this rather drastic method a yield of up to 75 % [Li(H_2CPMe_2)] can be obtained.

Deuerlein had also reacted S(N*t*Bu)$_2$ with [(tmeda)Li(H_2CPPh_2)] in pentane and observed a beige powder which he characterised by ^{1}H and ^{31}P{^{1}H} NMR spectroscopy. A full characterisation of [Li{$Ph_2PCH_2S(NtBu)_2$}]$_2$ (**2**) including the crystal structure is given in this thesis. Different to PMe_3, Ph_2PMe can only be deprotonated by *t*BuLi in moderate yield. Therefore, a 1:1 equimolar mixture of *n*BuLi/TMEDA has to be used. This gives [(tmeda)Li(H_2CPPh_2)] as a white powder in 80 % yield.[64,65,66] Complex **2** was synthesised by equimolar reaction of lithio(diphenylphosphino)methane-tetramethylethylenediamine with S(N*t*Bu)$_2$ in pentane, according to Equation 2-2.

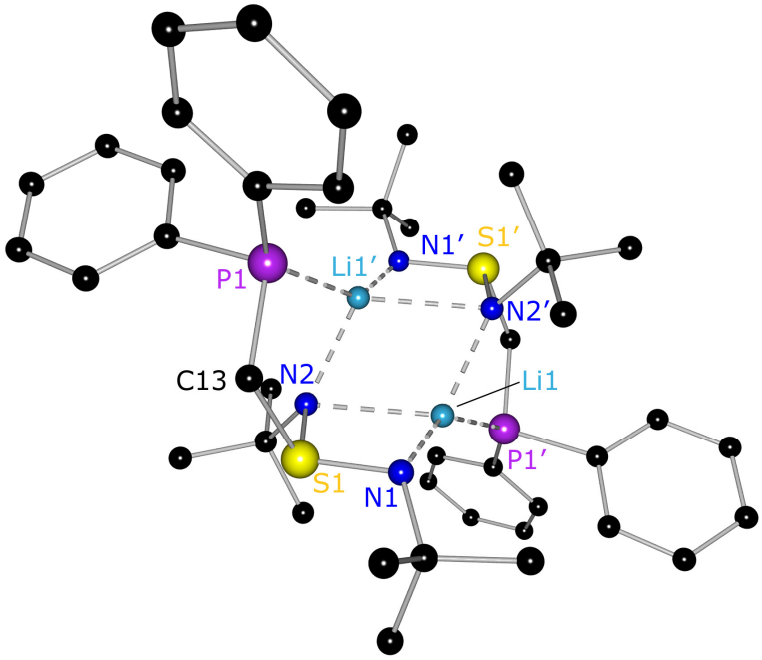

Figure 2-2: Molecular structure of [Li{$Ph_2PCH_2S(NtBu)_2$}]$_2$ (**2**). Hydrogen atoms are omitted for clarity.

The resulting beige powder was dissolved in toluene and stored at -25 °C, yielding colourless crystals in the space group $P\bar{1}$ after several days with half a dimer in the asymmetric unit. The inadequate bite of the tridentate ligand with respect to the small lithium cation in addition to a missing donor solvent results in a dimeric complex (Figure 2-2). The main core of the system is consisting of a (LiN)$_2$

heteroatomic ring in which both the lithium cations are fourfold coordinated by the donor atoms of each ligand. The structural characteristics of **2** are thus akin to complex **1**. The bond lengths and angles of **2** are within the expected range, being not very different to **1**. One nitrogen atom of each ligand unit (N2 and N2') is coordinating to both lithium atoms while the other nitrogen atoms coordinate to the lithium atom of just one half (Li1–N1/Li1'–N1'). It is important to note that the phosphorus atom coordinates to the lithium atom of the other half of the dimer (Li1–P1'/Li1'–P1). This arrangement is responsible for the good stability of the system. All S–N distances (1.6120(14) Å -1.6295(14) Å) are marginally shorter than an average sulphur-nitrogen single-bond (1.69 Å).[67] However, these S–N bond lengths are in the range of other alkyl diimidosulfinates (1.598-1.657 Å).[29]

Table 2-1: Selected bond lengths [Å] and angles [°] of **2** and **5**

	2	**5**		**2**	**5**
S1–N1	1.6120(14)	1.6238(15)	N1–S1–N2	104.15(7)	106.34(8)
S1–N2	1.6295(14)	1.6060(15)	S1–C13–P1	113.51(9)	114.43(9)
S1–C13	1.8412(17)	1.8381(18)	S1–N1–Li1	98.12(11)	83.35(10)
P1–C13	1.8404(17)	1.8402(19)	C13–P1–Li1’	102.33(8)	90.73(9)
P1–Li1’	2.657(3)	2.588(3)	N1–Li1–N2	72.88(10)	73.93(12)
N1–Li1	1.959(3)	2.303(4)	Li1–N2–Li1’/Li1–N1–Li1’	69.88(13)	77.27(14)
N2–Li1	2.318(3)	1.974(3)	N2–Li1–N2’/N1–Li1–N1’	110.12(13)	102.72(14)
Li1’–N2/N1	2.044(3)	2.028(4)	P1–Li1’–N2/N1	76.78(9)	79.97(11)
N1–C14/Si1	1.485(2)	1.7394(16)	S1–N1–C14/Si1	114.75(11)	118.40(9)

The longer Li–N2 distances (Li1–N2 2.318(3) Å and Li1'–N2 2.044(3) Å) compared to Li1–N1 (1.959(3) Å) are due to the shared lithium coordination of N2. Li1–N1 and Li1'–N2 are in the typical range of Li–N bonds (1.905-2.202 Å),[68] but Li1 seems to be weakly coordinated to N2. The Li1’–P1 distance of 2.657(3) Å is in the normal range for Li(P–C–C=N) systems (2.365-2.824 Å) which are similar to the ligand described here.[34,69] The N1–S1–N2 (104.15(7)°), N1–S1–C13 (106.45(8)°) and N2–S1–C13 (101.29(7)°) bond angles are more acute than the ideal tetrahedral angle of 109.5°. This is a result of the stereochemically active lone pair of the sulphur atom which takes up more space than a normal substituent. The acute N2–Li1'–P1 angle of 79.63(7)° is typical for Li(P–C–C=N) systems though (73.10-87.35°).[69]

Selected bond lengths and angles of **2** and its silicon analogue **5** can be found in Table 2-1.

From the NMR spectra of **2** in solution it is obvious that the complex shows a dynamic behaviour different to the solid state. The $^{7}Li\{^{1}H\}$ NMR spectrum reveals a coupling between one lithium atom and two phosphorus atoms (triplet in the $^{7}Li\{^{1}H\}$ NMR, $^{1}J_{P-Li}$ = 12.8 Hz). This can only be rationalized with a flipping Li–P-bond and on average the contact of a single phosphorus atom to two lithium atoms and *vice versa* in solution (Figure 2-3). This phenomenon was as well observed by *Izod et al.* for $[MeP(C_6H_4\text{-}2\text{-}CH_2NMe_2)\{C_6H_4\text{-}2\text{-}CH(Li)NMe_2\}]_2$.[70]

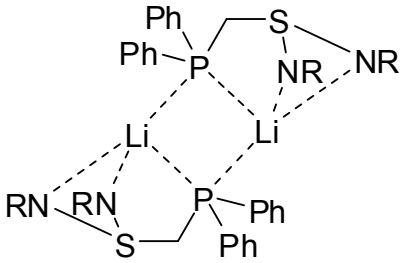

Figure 2-3: Proposed average structure of **2** in solution, R = *t*Bu.

This hypothesis can also be proven by the $^{13}C\{^{1}H\}$ NMR spectra of **2** (Figure 2-4). The phenyl carbon atoms show various multiplets whit structures that can only be explained if both phosphorus atoms are coupled to each other over the bridging lithium atom and thereby influence the carbon atoms in the rings. With phosphorus decoupling, those multiplets change into singlets. The solution structure according to Figure 2-3 gets even more plausible by simulation of the spin system (Figure 2-4).

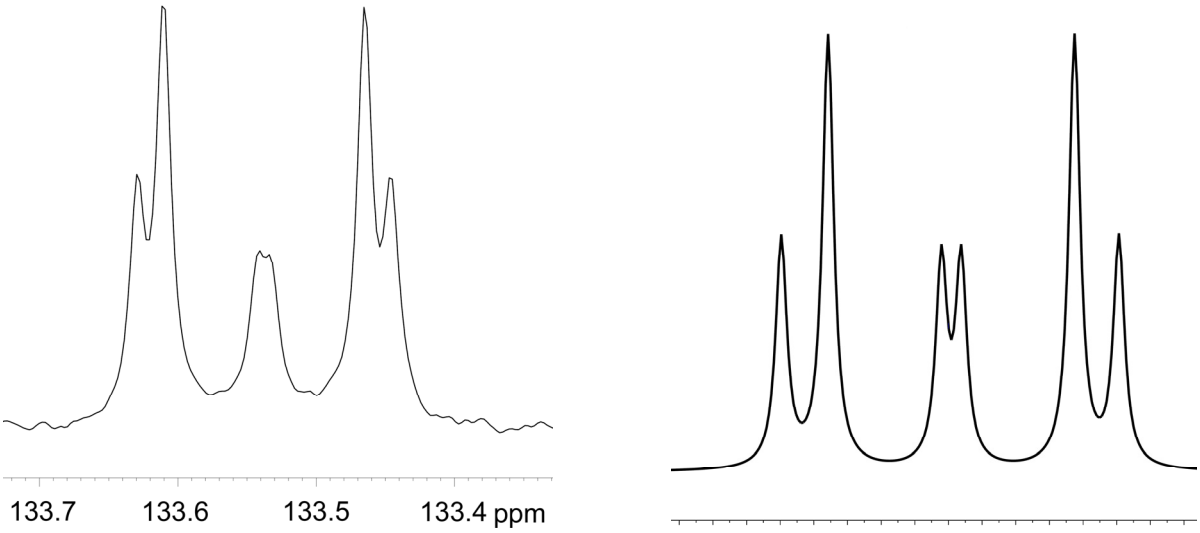

Figure 2-4: $^{13}C\{^{1}H\}$ NMR signal of the meta carbon atom in **2** (right, no ^{31}P decoupling); simulation of the signal (left) [71].

As a part of the strategy to create a structural variety of new multidentate ligands, modifications in the phosphane moiety were made to get [Li{Me(Ph)PCH$_2$S(N*t*Bu)$_2$}]$_2$ (**3**). It crystallises from pentane in the monoclinic space group $P2_1/c$. **3** is also obtained as a dimer and the main core of the system is the known (LiN)$_2$ four-membered ring with both lithium atoms being fourfold coordinated by the nitrogen and phosphorus atoms of each ligand. Most of the overall structural features are like in **1** and **2**, but differently to them, chirality is introduced at the phosphorus atoms P1 and P1' of the donating side-arm. Due to the centre of inversion in the middle of the (LiN)$_2$ four-membered ring, **3** crystallizes as a centrosymmetric structure. Consequently, both phosphorus atoms have different absolute configurations. The solid state structure is shown in Figure 2-5.

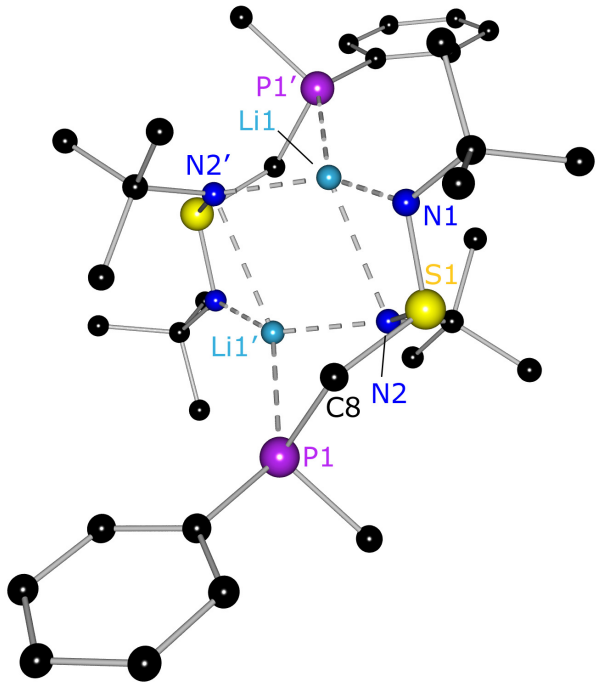

Figure 2-5: Molecular structure of [Li{Me(Ph)PCH$_2$S(N*t*Bu)$_2$}]$_2$ (**3**). Hydrogen atoms are omitted for clarity.

The S–N bond distances are almost equal and lie in the range of 1.6107(11)-1.6278(11) Å. The two (SN$_2$) units are tilted by 134.4° with respect to the (LiN)$_2$ ring with the phosphane moiety residing on opposite sides of the (SN$_2$) planes. The N1–S1–N2 (105.68(6)°) and N1–S1–C8 (104.97(6)°) angles are almost in the same range as for compounds **1** and **2**. However, the N2–S1–C8 angle of 98.81(6)° is slightly more acute than in **1** and **2**. The Li1–P1 distance is 2.644(2) Å, which is slightly longer than the average (2.520 Å) of the Li–P bonds.[68] The acute N2–Li1–P1 angle of 76.66(7)° is known for such systems (73.10-87.35°),[72] however, this angle

is the most acute among the compounds **1**-**3**. Selected bond lengths and angles are compared to the silicon analogue [Li{Me(Ph)PCH$_2$S(NSiMe$_3$)$_2$}]$_2$ (**6**) in Table 2-3.

The NMR spectra show a signal doubling that is due to two diastereomers which are present. In solution the phenyl rings can be arranged '*trans*' to each other like in the solid state or '*cis*'. The resulting diastereomers have very similar chemical shifts and their NMR signals are therefore overlapping. Thus, it is impossible to assign specific shifts to one specific diastereomer. Nevertheless, it can be conjectured that the '*trans*' isomer prevails as it is also the preferred arrangement in the solid state and displays the least steric strain. Integration of the PC*H*$_3$ signals shows a ratio of 1 to 0.75 for '*trans*' to '*cis*'. To get a rough estimate of the conversion times from the '*trans*' to the '*cis*' isomer, a NOESY spectrum was recorded. With the knowledge of the mixing time τ_{mix} (d_8 = 0.5 s) the velocity constants k_1/k_{-1} can be calculated: k_1 = 0.34 s^{-1} (*trans* to *cis*) and k_{-1} = 0.49 s^{-1} (*cis* to *trans*).

As in compounds **1** and **2** a P–Li–P system seems to be present. It is obvious not only through the ^{31}P{^{1}H} and ^{7}Li{^{1}H} spectra but as well through the ^{13}C{^{1}H} spectrum. The nuclei are coupled to both phosphorus atoms over the Li-bridge. Thus the resulting multiplets can be explained. In ^{31}P decoupled spectra the couplings disappear just like in **2**. The P–CH$_2$–S signal in the ^{1}H NMR spectrum (Figure 2-6) is a good example for this.

In the upper half of the figure a rather complicated coupling pattern can be seen. This is due to the two diastereomers and the coupling of the protons to the neighbouring phosphorus atom as well as the phosphorus atom on the other side of the bridging lithium ion. When the ^{1}H spectrum is recorded with ^{31}P decoupling, the picture gets somewhat clearer. It can now be distinguished between two sets of signals which are expected for two diastereomers A and B. In addition, the protons in the CH$_2$ bridge are coupled to each other because they are diastereotopic ($^2J_{H–H}$ = 13.3 Hz (A), $^2J_{H–H}$ = 13.4 Hz (B)) and a roof effect becomes visible. This phenomenon always occurs if two atoms that are coupling to each other differ very little in their chemical environment.[73]

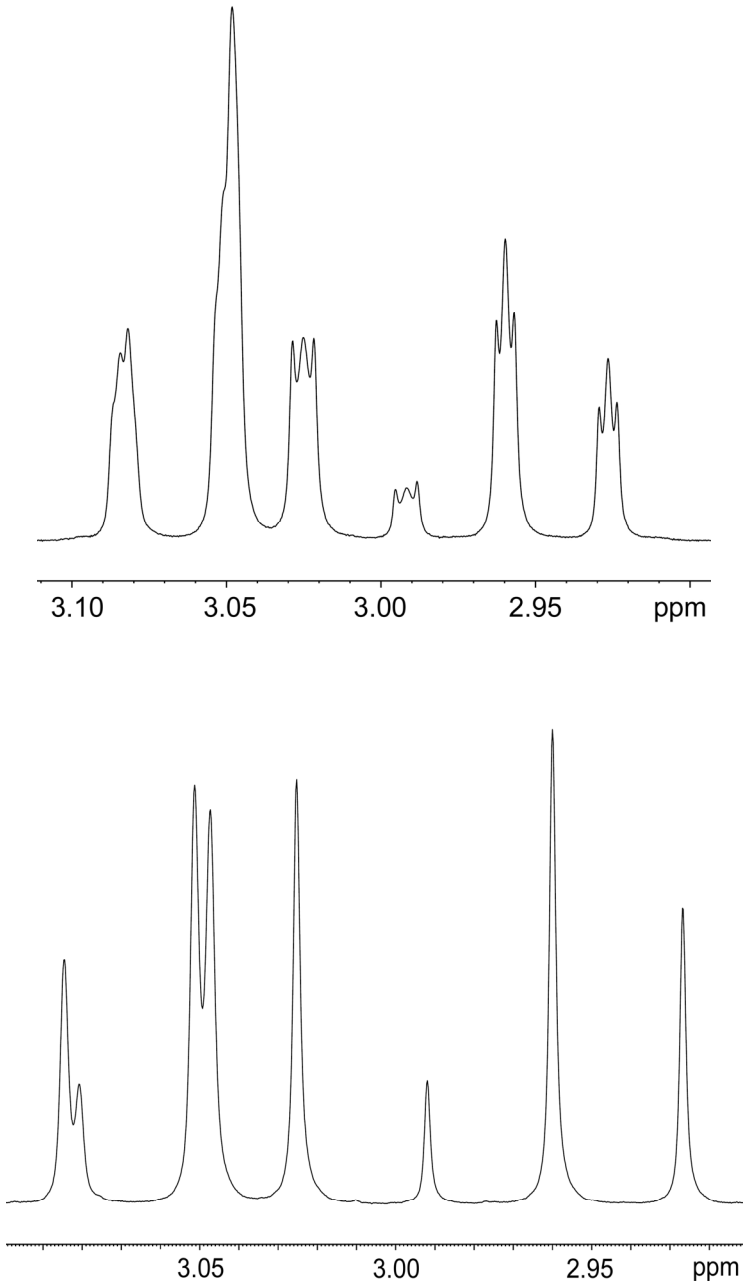

Figure 2-6: ^{1}H NMR signals of P–C*H*$_2$–S in [Li{Me(Ph)PCH$_2$S(N*t*Bu)$_2$}]$_2$ (**3**); above: ^{31}P coupled, below: ^{31}P decoupled.

2.3 Bis(trimethylsilyl)sulphur diimide

For ligand design, it is desirable to modify not only the substituents on the phosphorus atom but also the imido groups at the sulphur atom. S(NSiMe$_3$)$_2$ is easily accessible by the reaction of SOCl$_2$ with [Li{N(SiMe$_3$)$_2$}].[74] It was chosen because it only differs from S(N*t*Bu)$_2$ in one atom bound to nitrogen. Silicon is softer and larger than carbon and has lower electronegativity, giving rise to a different electronic

situation. The reaction of [Li(CH_2PMe_2)] with $S(NSiMe_3)_2$ in pentane gave [Li{$Me_2PCH_2S(NSiMe_3)_2$}]$_2$ (**4**) as a white powder. Crystallization from pentane at -25 °C yielded colourless crystals in the space group $P\bar{1}$. The structural characteristics are the same as in compounds **1**-**3** (Figure 2-7). A comparison with [Li{$Me_2PCH_2S(NtBu)_2$}]$_2$ (**1**) can be found in Table 2-2.

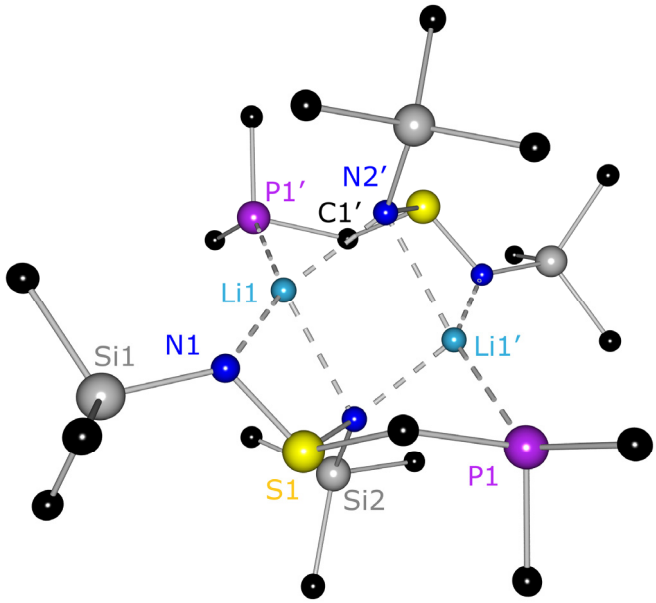

Figure 2-7: Molecular structure of [Li{$Me_2PCH_2S(NSiMe_3)_2$}]$_2$ (**4**). Hydrogen atoms are omitted for clarity.

The introduction of the silicon atom does not change the overall structural characteristics of the complex. However, the bond angles – especially around the sulphur atom – are affected.

Table 2-2: Selected bond lengths [Å] and angles [°] of **1** and **4**

	1	**4**		**1**	**4**
S1–N1	1.6144(9)	1.6031(10)	N1–S1–N2	104.74(5)	105.89(5)
S1–N2	1.6351(9)	1.6221(10)	S1–C9–P1/S1–C1–P1	116.24(6)	113.96(6)
S1–C9/C1	1.8406(11)	1.8286(12)	S1–N1–Li1	100.05(7)	95.76(8)
P1–C9/C1	1.8403(11)	1.8406(13)	C9–P1–Li2/C1–P1–Li1’	96.36(5)	86.45(6)
N1–Li1	1.939(2)	1.989(2)	N1–Li1–N2	71.93(7)	73.00(8)
N2–Li1	2.398(2)	2.315(2)	Li1–N2–Li2/Li1’	69.23(7)	80.96(9)
N2–Li2/Li1’	2.059(2)	2.029(2)	N2–Li1–N3/N2’	103.61(9)	99.04(9)
P1–Li2/Li1’	2.6425(19)	2.655(2)	P1–Li2–N2/P1–Li1’–N2	76.79(6)	79.63(7)
N1–C1/Si1	1.4792(13)	1.7138(10)	S1–N1–C1/Si1	116.43(7)	119.57(6)

The N1–S1–N2 angle is wider by approx. one degree; on the other hand the S1–C1–P1 angle of 113.96(6)° is considerably more acute and approaches the value for an ideal tetrahedron. The angles inside the $(LiN)_2$ heteroatomic ring are also closer to 90°, which is the expected value for a square planar environment. The bond lengths are not affected much by the different electronic situation in the ligand and only deviate slightly from the values reported for **1**. It seems obvious that an electronic change in the ligand causes structural changes as well. This indicates a different reactivity of the di(*tert*-butyl)sulphur diimides compared to the bis(trimethylsilyl)sulphur diimides which might become useful for future work.

In order to synthesise a lithium complex with $S(NSiMe_3)_2$ similar to **2**, Ph_2PMe was deprotonated with *t*BuLi to give $[Li(CH_2PPh_2)]$. When this lithiated phosphane was reacted with $S(NSiMe_3)_2$ (Equation 2-3) and the solution stored at -25 °C for several days, $[Li\{Ph_2PCH_2S(NSiMe_3)_2\}]_2$ (**5**) crystallised as colourless needles in the monoclinic space group $P2_1/n$.

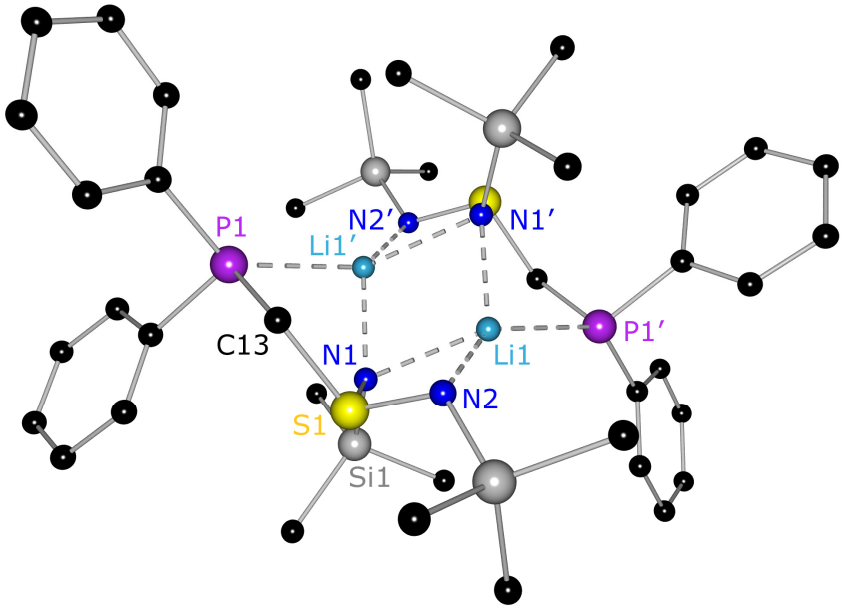

Figure 2-8: Molecular structure of $[Li\{Ph_2PCH_2S(NSiMe_3)_2\}]_2$ (**5**). Hydrogen atoms are omitted for clarity.

The structural features are similar to those of **2**. There is a centre of inversion in the middle of the structure and the bond lengths are virtually the same. However, the angles differ notably, as could be observed for **1** and **4** already. The structure is shown in Figure 2-8, selected bond lengths and angles of **2** and **5** can be found in Table 2-1.

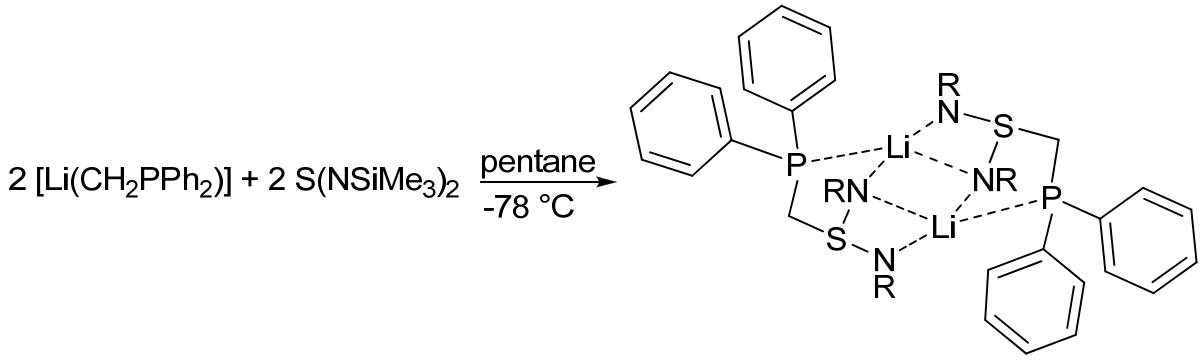

Equation 2-3: Preparation of $[Li\{Ph_2PCH_2S(NSiMe_3)_2\}]_2$ (**5**); R = $SiMe_3$.

The analogue to **3**, $[Li\{Me(Ph)PCH_2S(NSiMe_3)_2\}]_2$ (**6**), was prepared according to Equation 2-2 and crystallises in the triclinic space group $P\bar{1}$ with one half of the dimer in the asymmetric unit. Due to poor data quality the residual electron density of 1.32 eA^{-3}) cannot be assigned sensibly. The structure is shown and discussed nevertheless for comparison reasons although the bond lengths and angles might have bigger standard deviations.

The geometrical features are similar to $[Li\{Me(Ph)PCH_2S(NtBu)_2\}]_2$ (**3**). Both have an inversion centre in the middle of the $(LiN)_2$ ring, the bond lengths are almost the same and the angles differ a little. The molecular structure of **6** is shown in Figure 2-9. Selected bond lengths and angles in comparison to **3** can be found in Table 2-3.

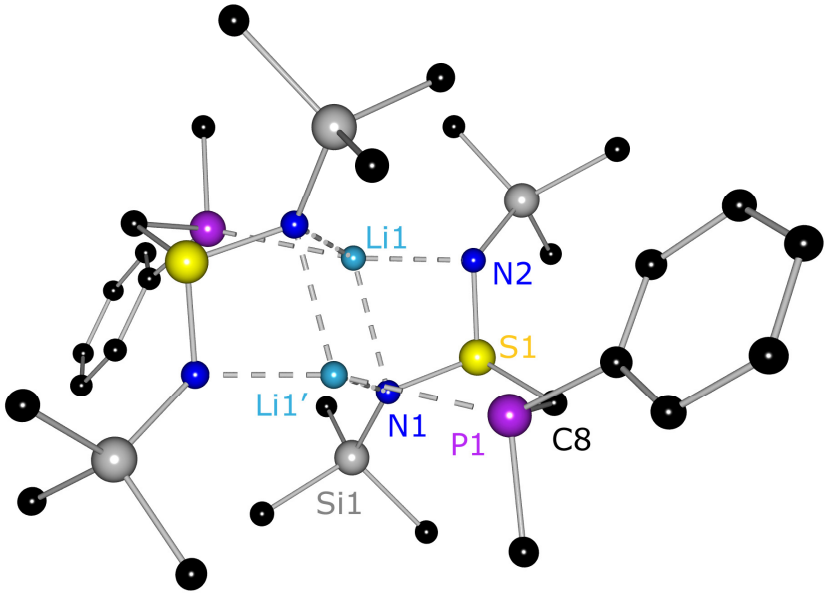

Figure 2-9: Molecular structure of $[Li\{Me(Ph)PCH_2S(NSiMe_3)_2\}]_2$ (**6**). Hydrogen atoms are omitted for clarity.

Table 2-3: Selected bond lengths [Å] and angles [°] of **3** and **6**

	3	**6**		**3**	**6**
S1–N1	1.6107(11)	1.626(3)	N1–S1–N2	105.68(6)	104.59(14)
S1–N2	1.6278(11)	1.594(3)	S1–C8–P1	114.41(7)	112.94(19)
S1–C8	1.8398(13)	1.814(4)	S1–N1–Li1	101.81(9)	85.55(19)
P1–C8	1.8463(14)	1.840(4)	C8–P1–Li1’	89.37(7)	101.80(17)
N1–Li1	1.957(3)	2.224(7)	N1–Li1–N2	69.41(8)	74.3(2)
N2–Li1	2.506(3)	1.984(6)	Li1–N2–Li1’/Li1–N1–Li1’	76.86(11)	69.2(3)
Li1’–N2/N1	2.008(3)	2.049(6)	N2–Li1–N2’/N1–Li1–N1’	103.14(11)	110.8(3)
P1–Li1’	2.644(2)	2.591(6)	P1–Li1’–N2/N1	76.66(8)	80.4(2)
N1–C9/Si1	1.4820(17)	1.741(3)	S1–N1–C9/Si1	116.96(9)	112.73(15)

2.3.1 A Stereocentre on the connecting Carbon Atom

When PEt_3 was lithiated with *t*BuLi, [Li(HCP(Me)Et_2)] was produced. The CH_2 group was rather deprotonated than the CH_3 group because of the higher acidity of the hydrogen atoms as the electron-withdrawing phosphorus atom is in closer proximity. Thus, is could be shown that the deprotonation does not take place at the sterically unprotected methyl group. When this lithiated phosphane was reacted with $S(NSiMe_3)_2$, chirality was introduced at the connecting carbon atom and the resulting product has the formula $[Li\{Et_2PCH(Me)S(NSiMe_3)_2\}]_2$ (**7**).

Due to the centre of inversion in the $(LiN)_2$ four membered ring both connecting carbon atoms have different absolute configurations (Figure 2-10). The S–N bond distances are almost equal to **4** and lie at 1.5906(10) Å for S1–N1 and 1.6235(10) Å for S1–N2, respectively. The two (SN_2) units are inclined by 116.9° with respect to the $(LiN)_2$ ring and the ethyl phosphane moieties reside on opposite sides of the (SN_2) planes. Thus, the steric strain between the trimethylsilyl groups is minimized. It is worthy to note that the Li–N bond distances in **7** differ less from each other than in **4**. The N2–Li1'–P1 angle of 83.25(7)° is less acute in **7** compared to **4** due to the bulkier groups on the phosphorus atom. Selected bond lengths and angles can be found in Table 2-4.

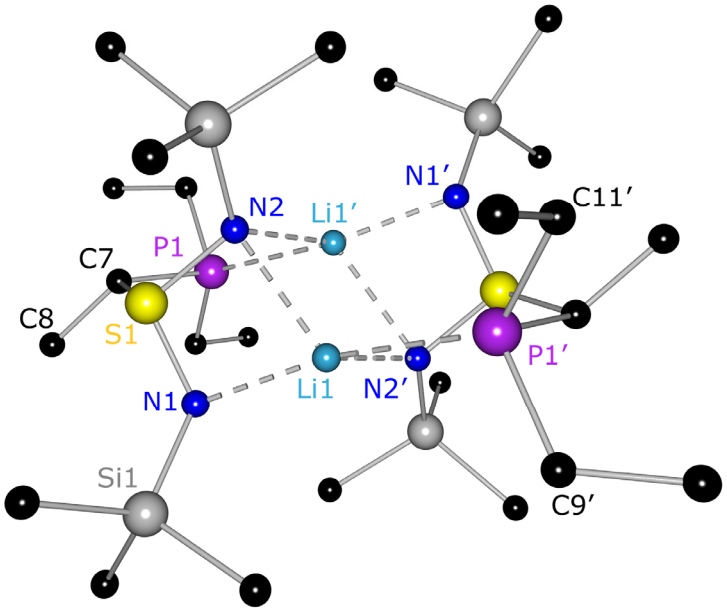

Figure 2-10: Molecular structure of $[Li\{Et_2PCH(Me)S(NSiMe_3)_2\}]_2$ (**7**). Hydrogen atoms are omitted for clarity.

Table 2-4: Selected bond lengths [Å] and angles [°] in **7**

S1–N1	1.5906(10)	N1–S1–N2	104.22(5)
S1–N2	1.6235(10)	S1–C7–P1	111.63(6)
S1–C7	1.8300(12)	S1–N1–Li1	94.40(8)
P1–C7	1.8682(13)	C7–P1–Li1’	99.18(6)
P1–Li1’	2.622(2)	N1–Li1–N2	73.19(8)
N1–Li1	2.028(2)	Li1–N2–Li1’	69.46(10)
N2–Li1	2.219(2)	N2–Li1–N2’	110.54(10)
N2–Li1’	2.037(2)	P1–Li1’–N2	114.22(9)
N1–Si1	1.7122(11)	S1–N1–Si1	123.87(6)

From the NMR spectra, the presence of two diastereomers due to the stereocentre on C7 becomes obvious. This observation is comparable to complex **3**. However, in the case of **7**, the two compounds are clearly separated in the $^{31}P\{^1H\}$ spectrum (δ(A) = -30.74, δ(B) = -27.34 ppm, see Figure 2-11), showing two septets due to the coupling of one phosphorus atom to two lithium atoms as discussed in chapter 2.2. Again, it can be speculated that the ‘trans’ isomer is the preferred arrangement in solution (*i. e.* the methyl groups are on opposite sides of the $(LiN)_2$ plane).

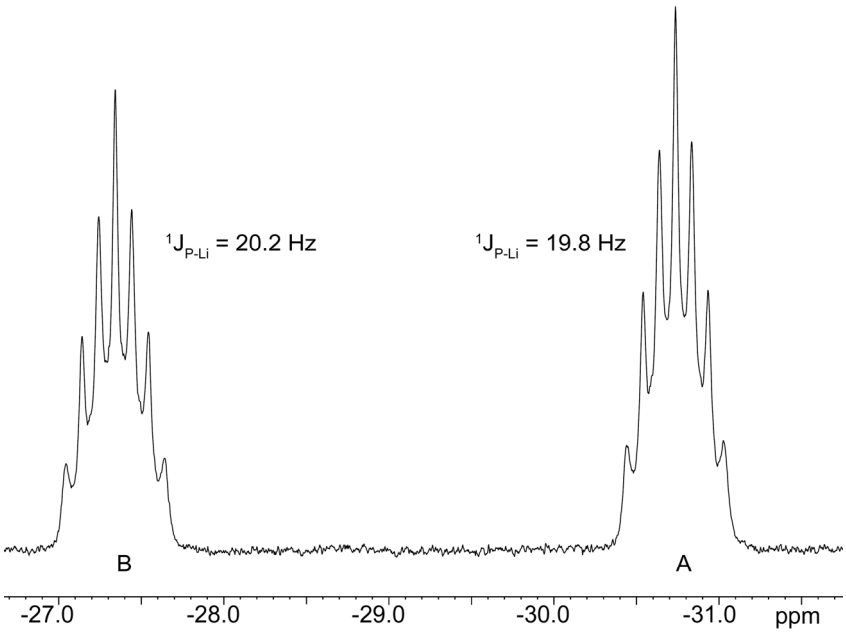

Figure 2-11: $^{31}P\{^1H\}$ NMR spectrum of **7** showing the signals for two diastereomers A and B.

The formation of the equilibrium between the two diastereomers seems to be very fast. Even a frozen sample which is allowed to warm up in the spectrometer shows the same ratio of A to B which does not change during the measurement. In the ^1H spectrum, the signals are not as clearly separated as in the $^{31}P\{^1H\}$ spectrum and complicate the interpretation.

2.3.2 Extending the Side-Arm

In order to further enhance the flexibility and adaptability of the new ligand system, the length of the side-arm can be changed. One way would be to use a phosphane with longer alkane substituents like ethane or butane. It is a problem though, that those groups are deprotonated at the CH_2 group next to the phosphorus atom as those hydrogen atoms are the most acidic. This was clearly demonstrated by the synthesis of $[Li\{Et_2PCH(Me)S(NSiMe_3)_2\}]_2$ (**7**). Therefore, another synthetic route had to be explored. *Morrow et al.* reported the preparation of the diphenyl-1-alkinylphosphane Ph_2PCCCH_3 in 1969 (Equation 2-4), which should be a good starting material.[75] The absence of CH_2 groups should prevent side-reactions.

In order to lithiate the phosphane, a solution of *t*BuLi in pentane was reduced in volume and Ph_2PCCCH_3 added drop wise at room temperature. The orange precipitate was filtered and washed with pentane. Although the substance was poorly soluble, the NMR spectra showed to expected signals. The equimolar reactions with

$S(NtBu)_2$ or $S(NSiMe_3)_2$ did not yield crystals or other uniform products even after months, therefore this route was abandoned.

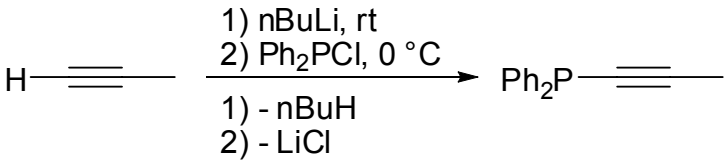

Equation 2-4: Preparation of Ph_2PCCCH_3.

Another way to elongate the donating side-arm would be to oxidise the phosphorus atom. This reaction is well known in our work group from the field of phosphanyl anthracenes. This substance class can be oxidised at the phosphorus atom with $[H_2O_2 \cdot (NH_2)_2CO]$, elemental sulphur and selenium.[76] The reaction is of importance because some of the resulting phosphoryl anthracenes show solid state fluorescence when aromatic guest molecules are present in the crystal lattice and can therefore be employed as chemosensors.

For the oxidation of $[Li\{Me_2PCH_2S(NSiMe_3)_2\}]_2$ (**4**) elemental sulphur was suspended in pentane and a solution of **4** in pentane was added slowly at -78 °C.

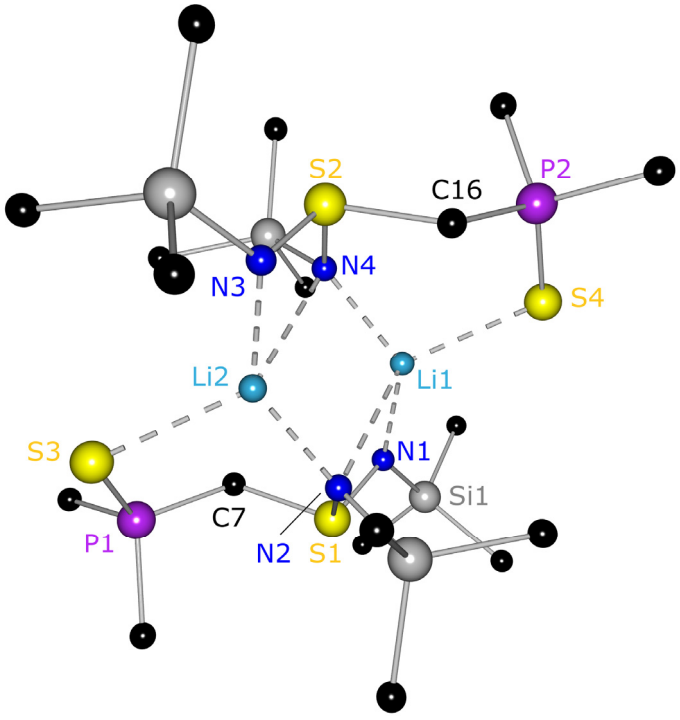

Figure 2-12: Molecular structure of $[Li\{Me_2P(S)CH_2S(NSiMe_3)_2\}]_2$ (**8**). Hydrogen atoms are omitted for clarity.

After warming to room temperature and stirring over night, insoluble material was filtered off, the solution reduced in volume and stored at -25 °C for

crystallization. The product $[Li\{Me_2P(S)CH_2S(NSiMe_3)_2\}]_2$ (**8**) crystallises in the monoclinic space group $P2_1/n$ as colourless blocks (Figure 2-12). There is one dimer in the asymmetric unit which displays the same geometrical characteristics as all the other structures of that type. The lithium atoms are coordinated by three nitrogen and one sulphur atom, thus the side-arm is indeed elongated. The S4–Li1 bond length is 2.495(7) Å which is slightly shorter than the P1–Li1' length of 2.665(2) Å in **4**. First of all this is due to the fact that the sulphur atom is not as sterically hindered as the phosphorus atom because of the missing methyl groups. Second, it is the better donor for lithium because of its greater HSAB hardness.[41] In addition, it can get in closer proximity because of the greater flexibility of the side-arm. The side-arm in **8** forms a six-membered ring in a boat conformation when it is coordinating to the lithium cation *vs.* a five-membered ring in **4**, thereby reducing the steric strain in the system. It can also be seen that the central $(LiN)_2$ ring and the diimido moieties intersect at a much smaller angle (42.2°) than all other structures of this type.

The P1–S3 bond of 1.9526(14) Å matches that of related structures like $[(thf)Li\{SP(N\textit{i}Pr)(NH\textit{i}Pr)_2\}]_2$ (P–S: 1.9927(8) Å)[77], $[(tmeda)Li\{\textit{t}BuN(S)P(\mu\text{-}N\textit{t}Bu)_2P(S)NH\textit{t}Bu\}]$ (P–S: 1.978(2) Å)[78] and the predicted value of 1.92 Å.[67] However it is slightly elongated due to the coordination of the lithium atom. Selected bond lengths and angles can be found in Table 2-5.

Table 2-5: Selected bond lengths [Å] and angles [°] in **8** and **9**

	8	**9**		**8**	**9**
S1–N1	1.599(3)	1.595(2)	N1–S1–N2	107.56(16)	107.49(12)
S1–N2	1.602(3)	1.614(2)	S1–C7–P1	118.6(2)	119.80(16)
S1–C7	1.828(4)	1.831(3)	S3–P1–C7/Se1–P1–C7	116.29(14)	114.75(10)
P1–C7	1.819(4)	1.822(3)	P1–S3–Li2/P1–Se1–Li1	94.30(16)	91.28(11)
P1–S3/Se1	1.9526(14)	2.1196(8)	N1–Li1–N2/N1–Li2–N2	67.9(2)	68.25(16)
Li1–N1/N3	1.982(7)	1.994(5)	N2–Li1–N4	132.7(4)	99.0(2)
N2–Li1	2.560(7)	2.018(5)	Li1–N2–Li2	82.5(3)	80.8(2)
N2–Li2	1.989(7)	2.554(5)	S3–Li2–N2/Se1–Li1–N2	104.7(3)	105.6(2)
S3–Li2/Se1–Li1	2.470(7)	2.614(5)	S3–Li2–N3/Se1–Li1–N3	115.4(3)	115.0(2)

All signals in the ^{1}H NMR spectrum of **8** show a downfield shift of approx. 0.4 ppm in comparison to the starting material **4**. This could be due to the electron withdrawing effect of the sulphur atom at the phosphorus atom and the resulting

deshielding of the hydrogen atoms. Interestingly, a $^{2}J_{Li-P}$ coupling is not detected. The $^{31}P\{^{1}H\}$ shift of 27.05 ppm is in the expected region for oxidised phosphorus atoms although not very near to the reported value of 83 ppm for the olefin polymerisation catalyst $[(C_3H_5)Ni\{tBu_2PCH_2S(NSiMe_2)\}]$ which was already mentioned in the introduction of this chapter.[63] Regarding the chemical shift of this catalyst, it is thinkable that is was oxidised during the reaction. This finding will be discussed in more detail in chapter 2.4.

The selenium analogue of **8** was synthesised in the same way, using grey selenium as a starting material. $[Li\{Me_2P(Se)CH_2S(NSiMe_3)_2\}]_2$ (**9**) also crystallises in the monoclinic space group $P2_1/n$ with the whole molecule in the asymmetric unit (Figure 2-13). The structure is isostructural to **8**. The coordination of the lithium cations is similar to **8**, with the selenium atoms taking part in the coordination.

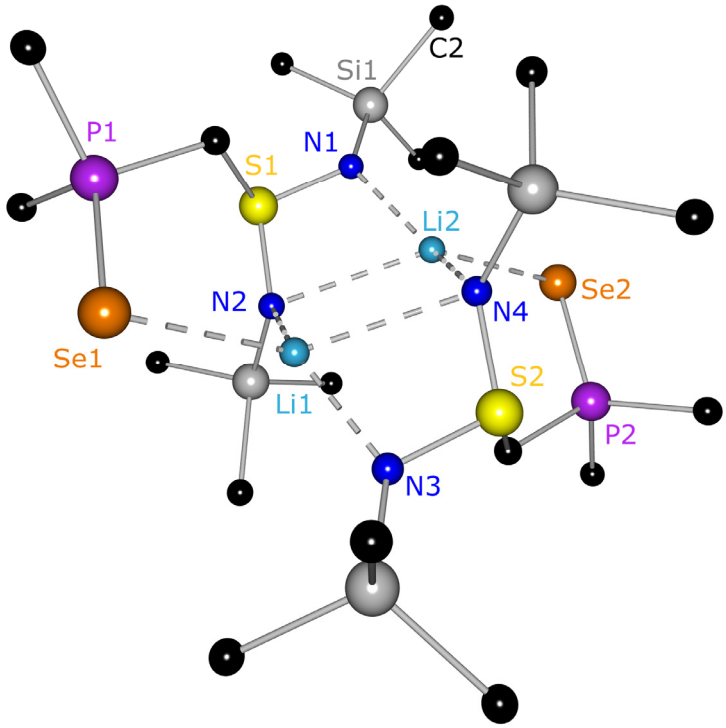

Figure 2-13: Molecular structure of $[Li\{Me_2P(Se)CH_2S(NSiMe_3)_2\}]_2$ (**9**). Hydrogen atoms are omitted for clarity.

The central $(LiN)_2$ four-membered ring shows similar values for the bond lengths and angles. Nevertheless, the coordination of the $SePCH_2$ side-arm is even weaker than in the corresponding sulphur compound with Li–Se bond lengths of 2.614(5) Å (Se1–Li1) and 2.593(5) Å (Se2–Li2) which are quite similar to the values found for $[(thf)_2Li\{tBuN(Se)P(\mu\text{-}NtBu)_2PNHtBu\}]$ (Se–Li: 2.605(10) Å)[78]. Interestingly,

these bond distances are almost the same as the P1–Li1' bond of 2.655(2) Å in the non-oxidised starting material [Li{$Me_2PCH_2S(NSiMe_3)_2$}]$_2$ (**4**).

The $^{31}P\{^1H\}$ signal of 6.23 ppm is shifted less downfield in comparison to **8** because of the lower electronegativity of selenium compared to sulphur. On the contrary this effect is not visible in the ^1H spectrum where the signals are shifted to even lower fields.

By oxidizing the phosphorus atom it was possible to extend the side-arm by one atom. It could be shown that the oxidation of phosphorus in the NSCP ligands with elemental sulphur or selenium is possible if the right conditions are chosen, which represents an additional possibility for ligand design. By this synthesis the coordinating side-arm can be lengthened which is essential if larger metal atoms are to be coordinated.

2.3.3 Obtaining the free Ligand

The reaction of [(tmeda)Li(H_2CPPh_2)] and S(N*t*Bu)$_2$ in toluene proceeded to give [Li{$Ph_2PCH_2S(N$*t*$Bu)_2$}]$_2$ (**2**) as a lithium dimer. However, when the same reaction was carried out with $S(NSiMe_3)_2$ in toluene, protonation of the ligand occurred, resulting in the formation of $Ph_2PCH_2S(NSiMe_3)(HNSiMe_3)$ (**10**) in nearly quantitative yield. Currentyl it is proposed that this is due to the C–H bond activation reaction described in Equation 2-5. Thus, a TMEDA molecule is deprotonated, resulting in the formation of **10** and lithiated TMEDA. This lithium organic compound has already been described by *Strohmann et al.* [79] but could until now not be accounted for in the present reaction.

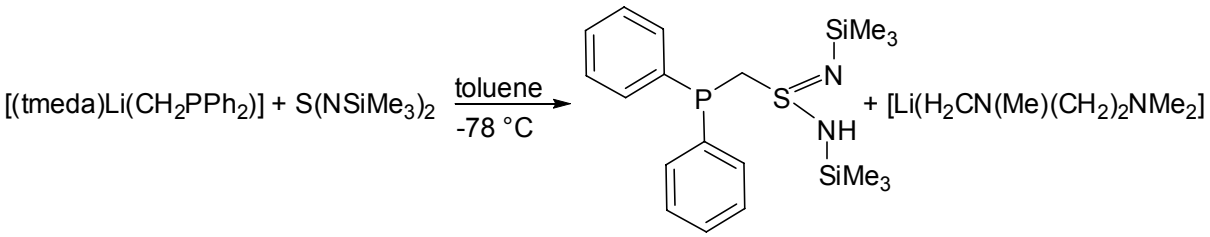

Equation 2-5: Preparation of $Ph_2PCH_2S(NSiMe_3)(HNSiMe_3)$ (**10**).

Compound **10** crystallises from toluene layered with pentane in the monoclinic space group $P2_1/n$ as a monomer. The solid state structure is shown in Figure 2-14. The bond distances for P1–C1 (1.8404(13) Å) and P1–C13 (1.8526(11) Å) are similar to those of **1**-**6**. The S1–C13 bond distance of 1.8092(12) Å is also slightly shorter

than in complexes **1**-**6**. The N1–S1–N2 (109.26(5)°) as well as the S1–C13–P1 angle (113.54(6)°) are widened compared to the lithiated species. The S–N bond distances of 1.6520(9) Å (S1–N1) and 1.5698(10) Å (S1–N2) are very close to the predicted values for a single and a double bond.[67] They also match the bond lengths of methyl(diimido)sulfinic acid H(N*t*Bu)$_2$SMe and methylene-bis(triimido)sulfonic acid H$_2$C{S(N*t*Bu)$_2$(NH*t*Bu)}$_2$, which have S–N bond distances of 1.52 and 1.68 Å.[30,80] Both six-membered rings are inclined by 99.1° with respect to each other. In addition, two molecules are linked with each other *via* a hydrogen bond between H1 and N2. This behaviour is similar to PhS(HNSiMe$_3$)(NSiMe$_3$), where the protonated nitrogen atom has a trigonal planar environment.[81] In **10**, the nitrogen atom N1 only deviates by 7.2° from the H1–S1–Si1 plane which is in accordance with PhS(HNSiMe$_3$)(NSiMe$_3$) where the corresponding angle is 7.3°. The S–N bond lengths of 1.662(1) Å and 1.572(1) Å are also very similar to **10**. Selected bond lengths and angles can be found in Table 2-6.

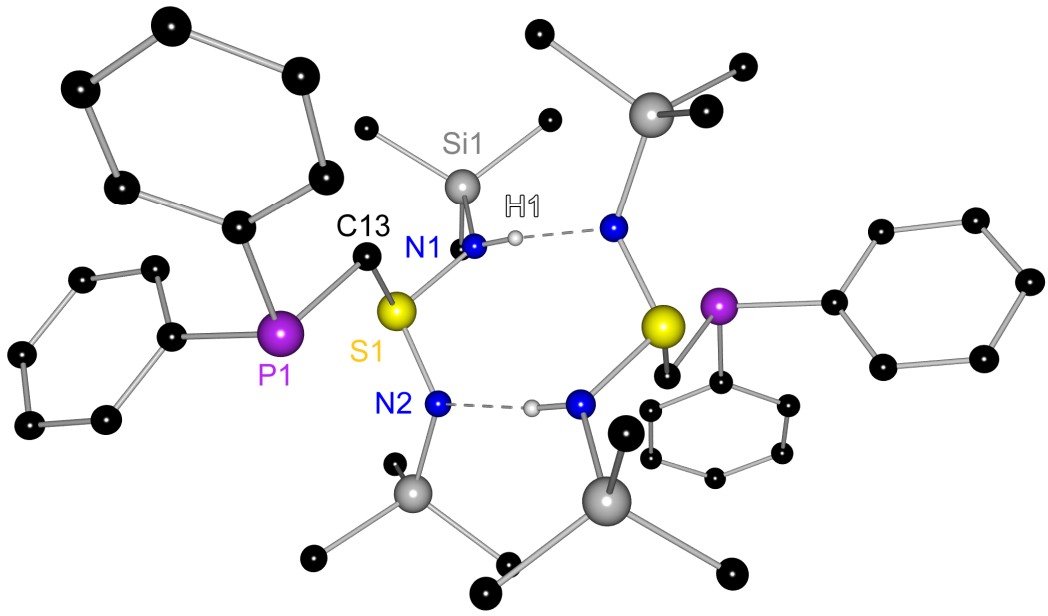

Figure 2-14: Molecular structure of Ph$_2$PCH$_2$S(NSiMe$_3$)(HNSiMe$_3$) (**10**) including the connecting hydrogen bonds. Hydrogen atoms (except H1) are omitted for clarity.

2.3.4 A monomeric Complex

To identify the source of the hydrogen atom, several experiments were carried out. They show that toluene cannot be the source of the hydrogen atom. After stirring the reaction mixture for 20 h, there was evidence of a compound which gave a very broad signal at -39 ppm in the ^{31}P{^{1}H} NMR spectrum. From this intermediate compound the reaction to the final product (δ_{31P} = -28.8 ppm) proceeded very slowly

at -25 °C. From the NMR spectrum it was concluded that the intermediate compound probably is some kind of lithium complex. When the same reaction (according to Equation 2-5) was carried out in pentane instead of toluene it was possible to crystallise the intermediate lithium complex [(tmeda)Li{$Ph_2PCH_2S(NSiMe_3)_2$}] (**11**) (Equation 2-6). The $^{31}P\{^1H\}$ NMR spectrum of the crystals shows a very broad signal at -39 ppm. This indicates **11** to be the intermediate in the synthesis of **10**.

These results were unexpected regarding the strategy and are probably due to the different electronic situation in the $S(NSiMe_3)_2$ moiety. Compound **11** crystallises from pentane as a monomer in the monoclinic space group *C*2/*c* with half a pentane molecule in the asymmetric unit (Figure 2-15). A comparison of the bond lengths and angles with $Ph_2PCH_2S(NSiMe_3)(HNSiMe_3)$ (**10**) can be found in Table 2-6.

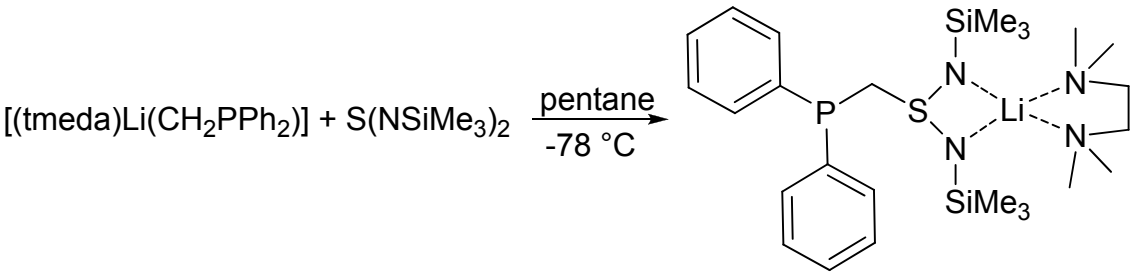

Equation 2-6: Preparation of [(tmeda)Li{$Ph_2PCH_2S(NSiMe_3)_2$}] (**11**).

The coordination mode in this compound is new compared to the complexes **1**-**8**. The lithium cation is fourfold N-coordinated and the phosphorus atom is not taking part in the coordination as the Li–P distance of 3.23 Å is too long to be regarded a bond. Nevertheless, an orientation towards the lithium ion can be observed which is due to electrostatic attraction. Furthermore, the S1–C13–P1 angle of 108.79(9)° indicates the inclination of the phosphorus atom towards the lithium cation. This finding is confirmed by the $^{31}P\{^1H\}$ NMR spectrum which shows a very broad signal at -39 ppm. The line broadening can only be explained with a (weak) Li–P contact in solution. The significant quadropolar moment of the lithium nucleus broadens the phosphorus signal. This long-range interaction might also be the reason for the protonation of the ligand when the reaction is conducted in toluene.

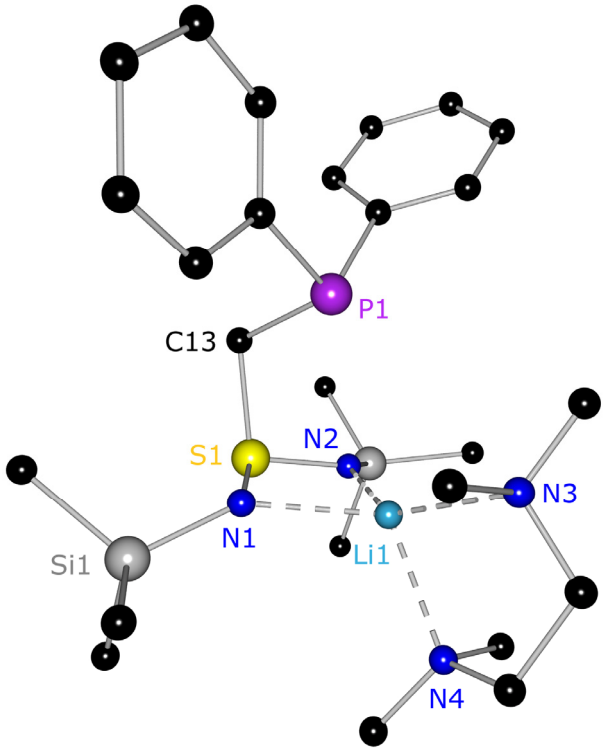

Figure 2-15: Molecular structure of [(tmeda)Li{$Ph_2PCH_2S(NSiMe_3)_2$}] (**11**). Hydrogen atoms are omitted for clarity.

In the solid state both phenyl rings are twisted by 90° with respect to each other, facilitating close packing of the molecules in the crystal. The central (SN_2Li) ring is almost perfectly planar with the phosphorus atom residing above this plane. It is aligned with C13, S1, Li1 and both nitrogen atoms of the TMEDA molecule with respect to the N1–S1–N2 bisection.

Table 2-6: Selected bond lengths [Å] and angles [°] in **10** and **11**

	10	**11**		**10**	**11**
S1–N1	1.6520(9)	1.6070(15)	N1–S1–N2	109.26(5)	103.72(8)
S1–N2	1.7184(10)	1.6032(16)	S1–C13–P1	113.54(6)	108.79(9)
S1–C13	1.8092(12)	1.8338(18)	S1–N1–Li1	---	89.41(12)
P1–C13	1.8526(11)	1.8557(18)	S1–N2–Li	---	90.63(12)
N1–Si1	1.7421(10)	1.7150(16)	S1–N1–Si1	123.18(6)	117.55(9)
N1–Li1	---	2.071(4)	N1–Li1–N2	---	75.80(12)
N2–Li1	---	2.039(4)	N3–Li1–N4	---	83.19(13)
N3–Li1	---	2.150(4)	N1–Li1–N3	---	132.61(18)
N4–Li1	---	2.129(4)			

The N1–S1–N2 angle of 103.72(8)° is slightly more acute than in the lithium complexes **1**-**8**. The Li–N distances range from 2.039(4) Å (Li1–N2) to 2.150(4) Å (Li1–N3) with the bonds from the TMEDA molecule being marginally longer than the bonds from the diimido moiety. As the phosphorus side-arm is not donating to the Li cation, it is free for binding to any other soft metal, thus providing the opportunity to generate heterobimetallic complexes just like the earlier reported $[(thf)_2Li\{(N\textit{t}Bu)_3SMe\}ZnMe_2]$.[82]

To check whether or not the solvent toluene was the source of the hydrogen atom in **10**, a sample of crystalline $[(tmeda)Li\{Ph_2PCH_2S(NSiMe_3)_2\}]$ (**11**) was dissolved in toluene-d^8 and the NMR tube was melted off. The idea behind this was that the incorporation of deuterium into $Ph_2PCH_2S(NSiMe_3)(HNSiMe_3)$ (**10**) would be detectable in the NMR spectra. Curiously, the spectra did not change at all, *i. e.* pure **11** could not be converted into **10** by this method. Consequently, it could not be resolved why the deprotonation of TMEDA only occurs in toluene and not in pentane. The different polarity of the two solvents and therefore a distinct activation of the lithium complex **11** could be a reason. When the synthesis of $[Li\{Ph_2PCH_2S(NSiMe_3)_2\}]_2$ (**5**) is carried out in toluene, the outcome is the same as with pentane. However, if **5** is dissolved in pentane together with two equivalents of TMEDA and stored at room temperature for several weeks, the protonated species $Ph_2PCH_2S(NSiMe_3)(HNSiMe_3)$ (**10**) is isolated.

Conclusion

With the free ligand at hand, it should now be easily possible to obtain a great variety of mono- and bimetallic complexes directly rather than following the metathesis or salt elimination route. This can be problematic as some sulphur diimido compounds undergo ligand scrambling with metal halogenides as was already discussed at the beginning of this chapter. Now the reaction of **10** with metal amides or metal hydrides will hopefully give new metal complexes. **10** would be an excellent starting material for such reactions as it can be prepared in nearly quantitative yield and great purity. However, the reaction has to be further investigated to prove the source of the hydrogen.

However, **11** could also be a very good starting material for metal exchange reactions. As the phosphorus atom does not take part in the complexation of lithium, it is free to coordinate to other metals. Thereby, a precoordination is possible that

brings the metal in close proximity to the nitrogen atoms. Lithium could then leave the complex as a TMEDA/ligand adduct and the metal exchange would be complete.

In conclusion, it can be stated that the phosphorus side-arm on the sulphur diimide can be modified in a straightforward way. The NSCP ligands are indeed tridentate, containing hard nitrogen and soft phosphorus donor sites. Although the bite of the ligand system is not optimized for lithium cations, the complexes formed are quite stable. Even the softer phosphorus site coordinates the hard lithium cation, yet in solution. It seems that the $\{R_2PCH_2S(NR')_2\}^-$ anions are indeed the ligands which are complexing as good as envisaged. Further, the formation of dimers seems to be favoured as it helps to balance the electron deficiency of the metal cations.

There is a wide range of methyl phosphanes which can be deprotonated and reacted with a sulphur diimide. Thus, the steric properties of the obtained lithium complexes can be tuned. It is even possible to introduce a stereocentre at the phosphorus atom (**3**, **6**) or at the carbon atom (**7**) of the connecting CH_2 bridge. In addition, different sulphur diimides can be used which are responsible for the distinct electronic properties of the compounds. In addition, the side-arm can be extended by oxidation of the phosphorus atom without loosing the soft donor site.

It has been shown, that it is possible to generate a complex of choice by choosing the appropriate phosphane, diimide and solvent. Thereby, a metal-free ligand (**10**) and a monomeric complex (**11**) were synthesised. There is now a library of different building blocks that can be combined in order to synthesise the appropriate compound for the desired application. The yields are good and **10** and **11** are excellent starting materials for subsequent metalation or metal exchange reactions. The new ligand system can thereby be fitted to the needs of the synthetic chemist, giving the opportunity to choose from a variety of possible derivatisations.

Besides, the phosphorus side-arm is in general flexible in solution and can bind to both lithium atoms. This process is fast on the NMR time scale and cannot be frozen out even at very low temperatures (120 K).

2.4 Complexes with the di(*tert*-butyl)phosphanyl Side-Arm

As already mentioned above, in 2005 a patent was granted for $[(C_3H_7)Ni\{tBu_2PCH_2S(NSiMe_3)_2\}]$ which was said to be a catalyst for the polymerization of olefins.[63]

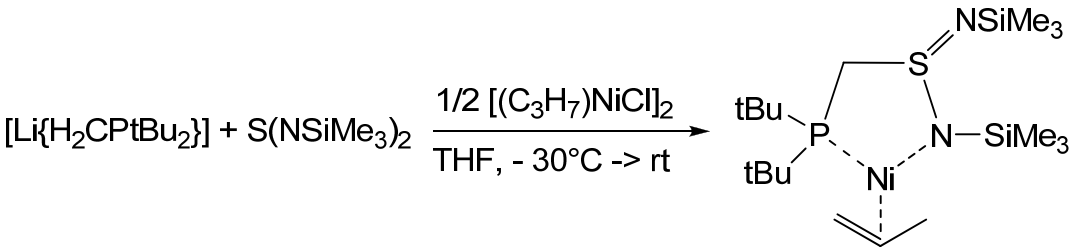

Equation 2-7: Preparation of $[(C_3H_7)Ni\{tBu_2PCH_2S(NSiMe_3)_2\}]$.[63]

The only analysis given was a ^{31}P NMR spectrum of δ = +83 ppm chemical shift. This is quite striking when we take into account that all the other lithium dimers of that type described in this thesis show ^{31}P signals between -68 and -27 ppm. Although one might argue this shift difference could be due to the different central metal or the substituents on the phosphorus atom this is highly doubtful. It is much more probable that the compound described in the patent was oxidised during the reaction or a chlorine substituent of the transmetalation reagent $[(C_3H_7)NiCl]_2$ was present in the molecule. The described reaction pathway also suggests that. In order to prove this hypothesis it was tried to synthesise the complex $[(C_3H_7)Ni\{tBu_2PCH_2S(NSiMe_3)_2\}]$. The first step is the lithiation of tBu_2PMe which is quite difficult and has to be conducted under harsh conditions.[60,83,84] The product $[Li(H_2CPtBu_2)]$ is even more reactive than $[Li(H_2CPMe_2)]$ and has to be handled with great care.

After the reaction with $S(NSiMe_3)_2$, three different products from three different reaction flasks could be structurally characterized. Two of them were indeed oxidised. As it proved impossible to get a uniform product in reasonable yield, the transmetalation with $[(C_3H_7)NiCl]_2$ was not attempted.

The compound from the first experiment has the formula $[Li\{tBu_2P(O)CH_2S(NSiMe_3)_2\}]_2$ (**12**) and crystallises in the triclinic space group $P\bar{1}$ with half a dimer in the asymmetric unit. The centre of the structure is a $(LiO)_2$ heteroatomic ring with both lithium atoms being additionally coordinated by two nitrogen atoms of one diimido moiety. Therefore two six-membered rings are connected to the central four-membered ring and are perfectly aligned and planar. The phosphorus side-arms are in that plane but point to opposite sides of the

molecule. The sulphur atoms are in that plane as well with the nitrogen atoms bent somewhat downwards/upwards by 7.5° to either side. The structure is depicted in Figure 2-16.

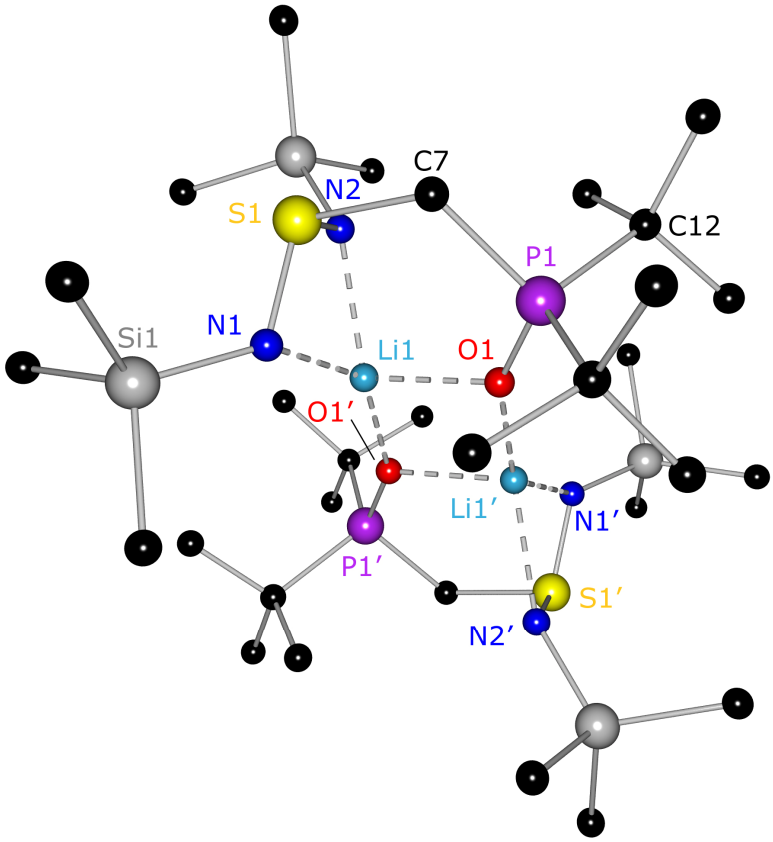

Figure 2-16: Molecular structure of $[Li\{tBu_2P(O)CH_2S(NSiMe_3)_2\}]_2$ (**12**). Hydrogen atoms are omitted for clarity.

The S–N bonds have almost the same length and are slightly shorter than a typical S–N single bond. The Li–O distances are shorter than the Li–N distances which is expected because oxygen is the better donor for the hard lithium cation.

Table 2-7: Selected bond lengths [Å] and angles [°] in **12**

S1–N1	1.5985(17)	N1–S1–N2	105.71(9)
S1–N2	1.5951(6)	S1–C7–P1	117.60(10)
S1–C7	1.860(2)	O1–Li1–O1'	95.04(15)
C7–P1	1.8314(19)	Li1–O1–Li1'	84.96(15)
N1–Li1	2.065(4)	O1–Li1–N1	99.10(15)
N2–Li1	2.075(4)	N1–Li1–N2	75.88(13)
O1'–Li1	1.884(4)	S1–N1–Li1	86.73(12)
O1–Li1	1.983(3)	P1–O1–Li1	120.87(12)
P1–O1	1.5067(13)	Li1–N2–Si2	140.54(13)

The P–O bond length of 1.5067(13) Å is slightly elongated, a phenomenon that was already observed for the P–S bond in $[Li\{Me_2P(S)CH_2S(NSiMe_3)_2\}]_2$ (**8**). From the angles Li1–O1–Li1' (84.96(15)°) and O1–Li1–O1' (95.04(15)°) it is obvious that the central four-membered ring is almost planar but slightly distorted in direction of the oxygen atoms. The bond lengths and angles can be found in Table 2-8.

The crystal structure of **13** (Figure 2-17) contains a tBu$_2$P(O)Me molecule as free donor emphasising yet again that the starting material is easy to oxidise. The lithium cations are additionally coordinated by two $\{t$Bu$_2$PCH$_2$S(NSiMe$_3$)$_2\}^-$ ligands.

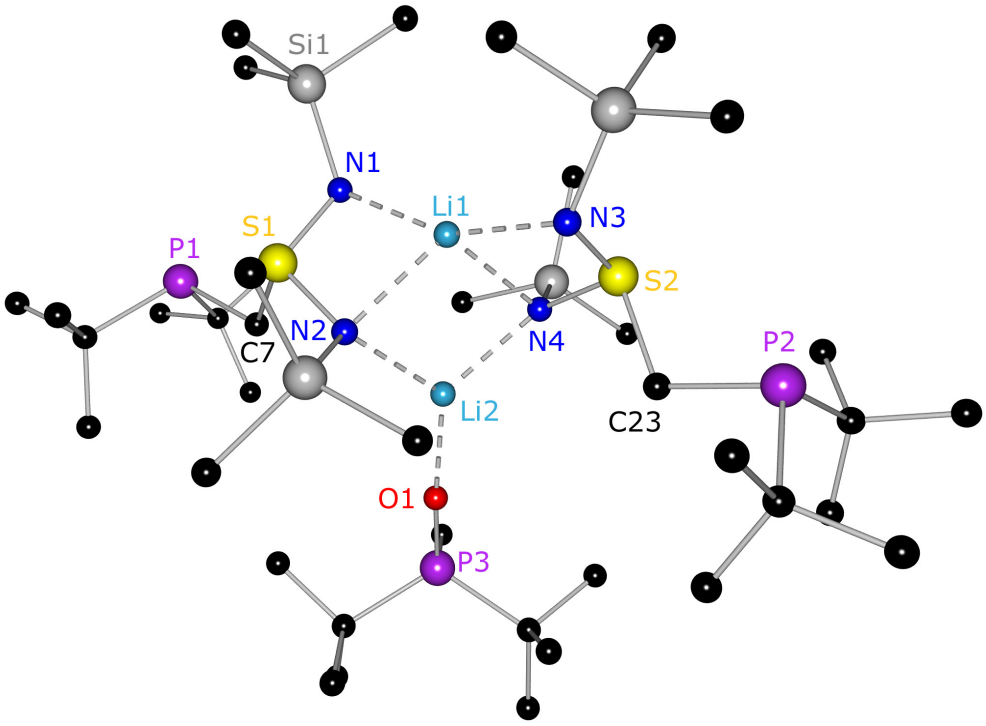

Figure 2-17: Molecular structure of $[Li_2\{t$Bu$_2$PCH$_2$S(NSiMe$_3$)$_2\}_2(t$Bu2P(O)Me)] (**13**). Hydrogen atoms are omitted for clarity.

It is remarkable that the phosphorus atoms do not take part in the coordination at all because the binding site is blocked by tBu$_2$P(O)Me. Both lithium atoms rather have different coordination environments. Li1 is distorted tetrahedrally surrounded by four nitrogen atoms of the diimido moieties. Li2 is trigonal planar coordinated by the two nitrogen atoms N2 and N4 and the oxygen atom of the tBu$_2$P(O)Me molecule which is not aligned with the lithium atoms but bent slightly to one side. The phosphane side-arms point to opposite sides of the complex, thereby reducing the steric strain. They are free to rotate about the P–CH$_2$ bond and could bind another metal atom, thus opening the way to heterobimetallic complexes. It might also be

possible to exchange the tBu$_2$P(O)Me ligand to generate heterotrimetallic complexes. The major problem for the preparative use of this compound is the uncertain outcome of the reaction. Selected bond lengths and angles can be found in Table 2-8. They do not show any unusual values and the bond lengths in both halves of the dimer a virtually the same. **13** still shows a low electron density peak which can not be accounted for and which is probably due to insufficient crystal quality.

The binding motif of a dimeric sulphur-nitrogen lithium complex with a fourfold/threefold mixed nitrogen/oxygen coordination is well known in the literature and has been reported *e. g.* for [(thf)Li$_2${(H$_3$CCNC$_4$H$_3$)S(NtBu)$_2$}$_2$],[35] [(Et$_2$O){Li(C$_6$H$_5$)S(NSiMe$_3$)$_2$}$_2$] or [(Et$_2$O){Li(C$_6$H$_5$)S(NtBu)(SNiMe$_3$)}$_2$].[85] It is also a typical structural feature in organolithium compounds with side-arm donation.[86] tBu$_2$P(O)Me has so far only once been reported as a donor molecule in dichlorobis(di-*tert*-butylmethylphosphineoxide-κO)diphenyltin(IV) which was just structurally characterised but not further investigated.[87]

Table 2-8: Selected bond lengths [Å] and angles [°] in **13** and **14**

	13	**14**		**13**	**14**
S1–N1	1.599(2)	1.628(2)	N1–S1–N2	104.06(11)	104.73(13)
S1–N2	1.632(2)	1.605(2)	N3–S2–N4	104.03(10)	---
S1–C7	1.832(3)	1.831(3)	S1–C7–P1	114.50(14)	115.06(16)
P1–C7	1.856(3)	1.851(3)	N1–Li1–N2	74.67(15)	74.39(19)
N1–Li1	2.076(4)	2.183(5)	N3–Li1–N4	74.75(15)	---
N1–Li1’	---	2.062(6)	N1–Li1–N3/N1’	155.5(2)	110.8(2)
N2–Li1	2.123(5)	2.048(6)	P1’–Li1–N2	---	153.8(2)
P1–Li1’	---	2.887(5)	N2–Li2–N4/N1’–Li1–N2	107.5(2)	123.2(3)
N2–Li2	2.063(5)	---	N2–Li2–O1	125.2(2)	---
O1–Li2	1.831(4)	---	Li2–O1–P3	168.7(2)	---
O1–P3	1.4913(19)	---	Li2–N2–Li1	75.54(17)	---
N1–Si1	1.717(2)	1.741(2)			

After several attempts, it was finally possible to crystallise the non-oxidised form of the lithium complex [Li{tBu$_2$PCH$_2$S(NSiMe$_3$)$_2$}]$_2$ (**14**). It is a dimer with the well known (LiN)$_2$ four-membered ring in the centre. The geometry of **14** is therefore the same as in all the other complexes of this type which have been described in the preceding

chapters. The structure is depicted in Figure 2-18, selected bond lengths and angles in comparison with **13** can be found in Table 2-8.

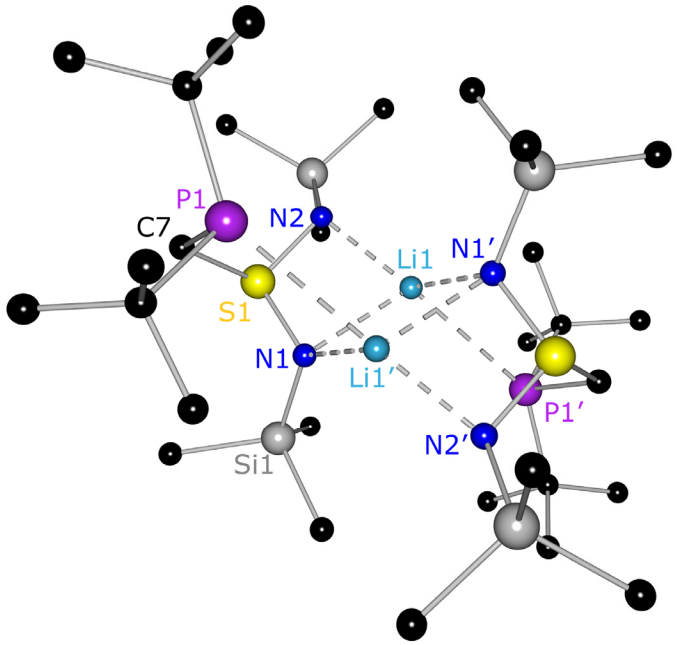

Figure 2-18: Molecular structure of [Li{*t*Bu$_2$PCH$_2$S(NSiMe$_3$)$_2$}]$_2$ (**14**). Hydrogen atoms are omitted for clarity.

The Li–P bond length of 2.887(5) Å is considerably longer than in the other dimeric structures **1**-**8**, where values of about 2.60 Å were found. This observation can be explained with the *tert*-butyl groups at the phosphorus atom which exhibit a considerable steric strain, although they are good σ-donors that increase the negative charge on the phosphorus atom which should strengthen the Li–P bond. Thus, steric reasons seem to be more important. This finding is very interesting in terms of ligand design. It could be shown that the substituents at the phosphorus atom have an influence on the bond lengths and therefore could as well have an influence on the structure of the complex. With even more sterically shielding groups it would be possible to synthesise complexes which are not dimeric but form larger aggregates. **14** could also be a good starting material for transmetalation reactions as the phosphorus side-arm seems to be bonding even weaker than in the other complexes discussed so far.

The sensitivity towards oxygen is a problem. Therefore, the synthesis of **14** should probably be conducted in an argon glove box and the starting material *t*Bu$_2$PMe should be thoroughly dried. Due to these obstacles, an application for this type of ligand in homogenous catalysis does not seem very likely. The ^{31}P{^{1}H} chemical shift of **14** is +8.75 ppm and the signal is shifted to higher field when the ligand is oxidised (around 65 ppm, from the reaction solution). Therefore, it is even

more likely that the supposed polymerization catalyst [(C_3H_7)Ni{*t*$Bu_2PCH_2S(NSiMe_3)_2$}] with a reported chemical shift of +83 ppm was oxidised as well.

3 Ligands with Nitrogen Side-Arm

3.1 Metalation and Reaction of Dimethylaniline

Since the reactions of sulphur diimides with lithiated phosphanes proceeded smoothly and give very good yields the analogous lithium amides were employed in the synthesis. Although the softer coordination site is sacrificed other binding modes become more important. It also was of interest to compare the complexes that only differ in one heteroatom. For these reasons and also because it is analogous to Me_2PPh, dimethylaniline became the first starting material. In addition, its deprotonation is well established in the literature.[88] However, refluxing the *in situ* reaction mixture for 20 h with *n*BuLi as described was modified to a lithiation with *t*BuLi just like for the phosphanes mentioned above. The advantages are that the lithiated product precipitates partly from pentane, it can be obtained very pure and the yield can be determined unequivocally.

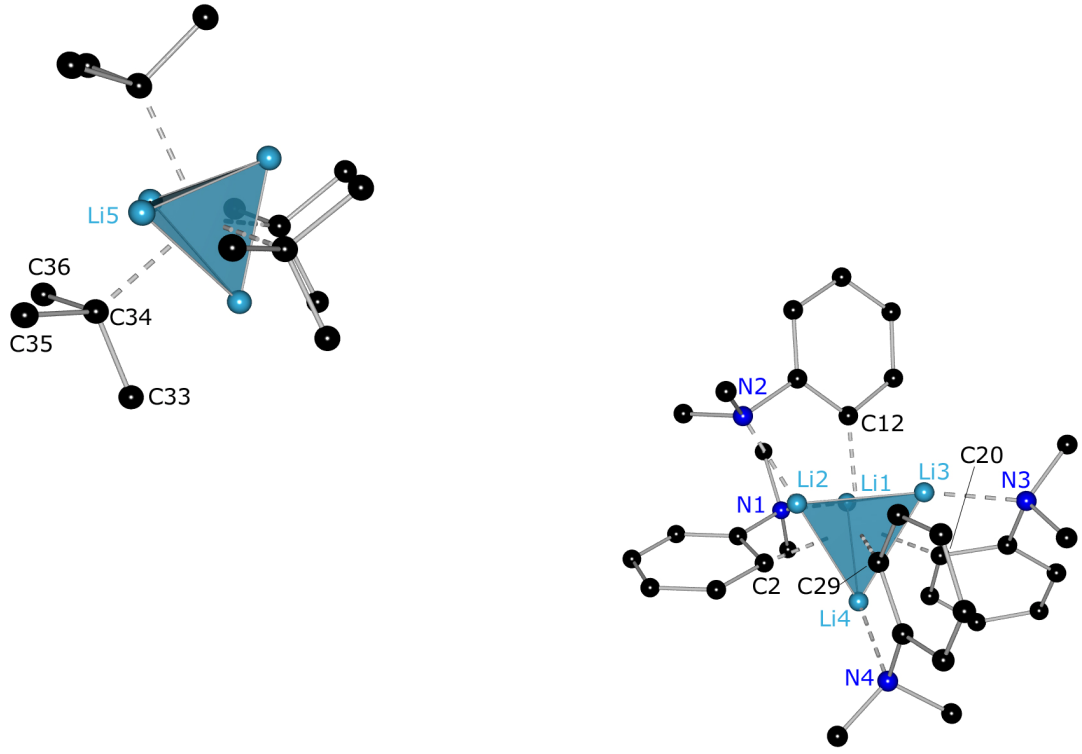

Figure 3-1: Molecular structure of [Li{(C_6H_4)NMe_2}]$_4$[*t*BuLi] (**15**). Hydrogen atoms are omitted for clarity and two Me_2NPh moieties are shown transparent; the *t*BuLi tetramer is shown completely.

When the orange filtrate was stored at room temperature for one day, colourless needles crystallised. Unexpectedly, they were quite stable and could be

mounted onto the diffractometer without cooling and haste. The structure of **15** is shown in Figure 3-1, selected bond lengths and angles can be found in Table 3-1.

Surprisingly, the unit cell contains two different lithium organic molecules which is quite rare. One is a tetrameric $[Li\{(C_6H_4)NMe_2\}]_4$ cluster, the other one is a *t*BuLi molecule that is part of a tetramer as well. This structural motif is quite unique. There is only one other example in the literature.[89] In 2007 *Mitzel et al.* crystallised 2-lithio-1,3-dimethyl-1,3-diazacyclohexane as a tetramer with one *t*BuLi molecule in the unit cell. The structural motif is similar to **15** and both compounds crystallise in the tetragonal space group $I\bar{4}$. The $[t\text{BuLi}]_4$ units are located on four edges of the unit cell as well as on two faces. Eight $[Li\{(C_6H_4)NMe_2\}]_4$ tetramers fill the spaces in between. The remarcable stability of the crystals probably has its origin in the good shielding of the lithium cations by the ligand periphery. In both tetramers the lithium cations form triangles which are μ_3-capped by a carbanionic C_α atom. This arrangement is the most efficient structure building principle in lithium organic chemistry and can further be aggregated to build different lithium deltahedra. The Li_4 tetrahedron is found in various lithium organic tetramers while the Li_6 octahedron is present in many hexamers.[86,90]

The nature of the Li–C bond was an issue of constant research and was debated to be predominantly ionic [91] or mainly covalent.[92] Currently, the Li–C bond nature again is revisited, mainly by theoretical investigations.[93] However, the presence of a direct Li–Li metal bond has never been proven in the tetrameric or hexameric aggregates. Assuming a covalent contribution, the Li_3C_α moieties should be held together by 4c-2e bonds.[72] The tetrameric lithium organics $[MeLi]_4$,[94] $[EtLi]_4$,[95] and $[t\text{BuLi}]_4$,[96] are white pyrophoric powders. While methyllithium is soluble only in polar solvents like diethyl ether, the two others are soluble in non-polar hydrocarbons like hexane. Even in the solid-state none of the three tetrameric structures adopts ideal T_d symmetry, but the Li···Li distances fit reasonably well. While they are 284 pm in $[LiF]_\infty$, they cover the range from 241 to 256 pm in the $[RLi]_4$ tetramers. The crystallographically independent Li···Li distances of the individual tetramers are similar within the estimated standard deviations. They decrease from 256 pm in $[MeLi]_4$, to 253 pm in $[EtLi]_4$, and 241 pm in $[t\text{BuLi}]_4$. Interestingly, the Li–C_α bond lengths are almost the same at 226±2 pm and close to the mean Li–C bond distance of 230 pm.[68] In addition, $[EtLi]_4$ and $[t\text{BuLi}]_4$ display relatively short Li···C_β distances. In the latter they are only 10 pm longer than the Li–C_α bonds.

Addition of neutral donor bases like Et_2O, THF, DME, TMEDA or PMDETA to aggregated lithium organics usually decreases their degree of aggregation.[97] Multiple Li–C_α and additional Li···C_β interactions are partly substituted by N→Li or O→Li donor bonds. This deaggregation commonly results in increased reactivity because the rate determining step in deprotonation reactions is normally the reaction of the monomer.[98]

In lithium aryls like $[Li\{(C_6H_4)NMe_2\}]_4$ two structure building principles are opperating: (i) the haptotropic η^6-coordination of the lithium cation to the π charge density of the aromatic carbanion and (ii) the Li_2C_2 four-membered ring built upon donorbase-induced dimer formation. On the addition of donorbases or implementation of donating side-arms it is the π-bonding that is given up first. It is the predetermined breaking point of the infinite solid-state structure if molecular fractions are cut out in the deaggregation process.

Table 3-1: Selected bond lengths [Å] and angles [°] in **15**

Li1–N1	2.042(4)	N1–Li1–C2	68.70(13)
Li3–N3	2.051(4)	N1–Li1–C20	131.17(19)
Li1–C2	2.274(4)	C12–Li1–C20	107.04(17)
Li1–C12	2.277(4)	C2–Li1–C12	103.84(15)
Li1–C20	2.254(4)	N3–Li3–C29	117.23(17)
Li3–C12	2.244(4)	N3–Li3–C12	132.70(19)
Li3–C20	2.218(4)	C12–Li3–C20	109.53(17)
Li3–C29	2.234(4)	C12–Li3–C29	108.65(16)
Li5–C34	2.267(5)	Li1–C20–Li3	69.15(14)
Li1···Li2	2.630(6)		
Li1···Li4	2.499(6)		

In $[Li\{(C_6H_4)NMe_2\}]_4$ a single dimethylamino group in *ortho*-position to the *ipso*-carbon atom causes a structural motif reminiscent to the $[(Et_2O)LiPh]_4$[99] tetramer. The amino nitrogen atoms act as the diethyl ether molecules at the apexes of the metal deltahedron. In addition, each of the four Li_3 triangles is μ_3-capped by a C_α atom above the center of the equilateral metal triangle. Thus **15** is comparable to $[(tmeda)\{(LiC_6H_4OMe)_4\}_2]$ [100] and $[Li\{(C_6H_3)(NMe_2)_2\}]_3$.[101] The Li–$C_\alpha$ bond lengths in **15** range from 2.218 Å (Li3–C20) to 2.277 Å (Li1–C12) compared to 2.30 Å in $[(tmeda)\{(LiC_6H_4OMe)_4\}_2]$. The average Li–N bond lengths of 2.14 Å and 2.12 Å are

slightly elongated in comparison to **15** (on average 2.040 Å). The average Li···Li distance in **15** is 2.562(6) Å and is closer to the reported value for [(tmeda){($LiC_6H_4OMe)_4$}$_2$] (2.64 Å). The corresponding distance in [Li{(C_6H_3)(NMe_2)$_2$}]$_3$ is 3.08 Å .

It is worthy to note that the coordination angles for Li1/Li2 and Li3/Li4 are different. Li3 is almost in plane with C29, N3 and C12 resulting in a distorted trigonal pyramidal coordination. The N3–Li3–C29 and C29–Li3–C12 planes only deviate by 11.9° from each other. Li1 on the other hand is distorted tetrahedrally coordinated (C2–Li1–C20: 109.59(16)°, C12–Li1–N1: 120.99(17)°). As a result, two $(LiC)_2$ rhombuses that are turned by 90° against each other make up the centre of the structure. The methyl groups of two neighbouring Me_2NPh moieties point into opposite directions and the phenyl rings are inclined by 64.3° although this is only the case for the pairs Li1/Li2 and Li3/Li4.

The [*t*BuLi]$_4$ subunit in **15** has the same structural features as the donor-free parent material in the solid state.[96] The methyl groups are arranged ecliptically with respect to the lithium atoms of the capped metal triangle. The Li–C_α bond length of 2.267(5) Å is in the expected range. The average Li–C_β distance is 2.410(8) Å while the Li···Li distance is 2.424(8) Å.

The NMR spectra of the complex are very interesting and illustrative about the equilibriae present in solution. In the 400 MHz ^{7}Li{^{1}H} spectrum in toluene-d^8, twelve signals with different intensities can be identified in the region from approx. 0 to 4 ppm (Figure 3-2).

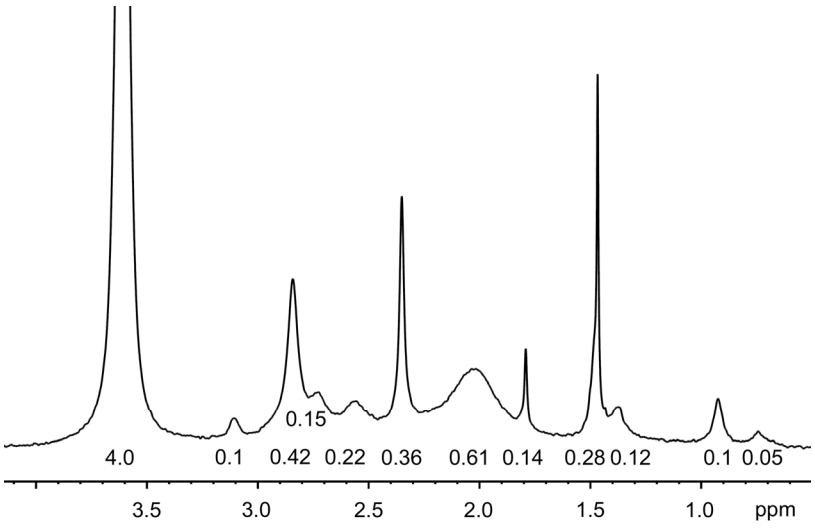

Figure 3-2: ^{7}Li{^{1}H} NMR spectrum of [Li{(C_6H_4)NMe_2}]$_4$[*t*BuLi] (**15**) in toluene-d^8, including integrals.

However, if the complexes would have the same composition in solution as in the solid state, one would expect only two signals – one for the almost T_d-symmetric [*t*BuLi]$_4$ and one for [Li{$(C_6H_4)NMe_2$}]$_4$. Therefore, the conclusion can be drawn that probably different aggregates exist in solution. With the stochiometry in mind, five different arrangements for tetramers can *ab initio* be envisaged: [Li{$(C_6H_4)NMe_2$}]$_4$, [Li{$(C_6H_4)NMe_2$}]$_3$[*t*BuLi], [Li{$(C_6H_4)NMe_2$}]$_2$[*t*BuLi]$_2$, [Li{$(C_6H_4)NMe_2$}][*t*BuLi]$_3$ and [*t*BuLi]$_4$. In addition, the formation of dimers and other species is also possible. Therefore, several questions arose:

- Are there mixed aggregates?
- Are there other aggregates than tetramers?
- Are the aggregates interconvertible?
- What exactly are the different aggregates?

In order to answer those questions, DOSY NMR spectra were recorded among others. DOSY is the abbreviation for **D**iffusion-**O**rdered NMR **S**pectroscop**y** and its basic principles were first introduced by *Stejskal* and *Tanner* as a one-dimensional experiment in the 1960's.[102] In 1992, *Johnson* went one step further and developed the corresponding two-dimensional experiment.[103] With this pulse gradient spin-echo (PGSE) method, the diffusion of molecules in the NMR tube can be observed and a plot of the diffusion coefficient *vs.* the chemical shift is generated. Thereby, different components of a mixture can be identified *via* their hydrodynamic radii according to the *Stokes-Einstein* equation (Equation 3-1).[104] These are correlated to their formula weights and at the same time to their degrees of aggregation. Of course, this is only strictly true, if the molecules are spherical and considerably larger than the solvent. For the discussed tetrahedra with an average diameter of 7.50 Å for [*t*BuLi]$_4$ and 10.17 Å for [Li{$(C_6H_4)NMe_2$}]$_4$ this is valid (the values are estimated from the crystal structure).

$$D = \frac{kT}{6\pi\eta R_H}$$

D = diffusion coefficient
k = *Boltzmann* constant
T = temperature
η = viscosity
R_H = hydrodynamic radius

Equation 3-1: *Stokes-Einstein* equation.

The individual spectra of every component can also be obtained from the DOSY experiment. Thus, DOSY represents an excellent method for the analysis of complex mixtures (*e. g.* enzymes), systems containing different aggregates or for polymer analysis. In addition, the molecular masses of the distinct molecules can be extrapolated if an internal reference is present.[105]

In 2000, *Williard et al.* used DOSY spectroscopy for the first time for the analysis of different THF/*n*BuLi aggregates in solution.[106] From such an experiment, lots of information can be drawn:[107]

- determination of the aggregation number of organometallic compounds
- determination of the solvation state
- identification of new aggregates in solution (*i. e.* which are not present in the solid state)
- extrapolation of the molecular weight of the different components by using an internal reference with known weight
- determination of relative diffusion coefficients
- individual 1D spectra of every component that is present in the mixture (if the spectrum is not too complex)

To take full advantage of the method it is vital that the signals are well separated. Relative diffusion coefficients can either be directly read from the spectrum or the peak areas are fitted to the *Stejskal-Tanner* equation (Equation 3-2).[102]

$$\ln\frac{I}{I_0} = -(\gamma^2\delta^2G^2(\Delta - \frac{\delta}{3}))D$$

I = peak area, I_0 = peak area in the absence of gradients

γ = gyromagnetic ratio

δ = gradient duration

G = strength of the gradient pulse

Δ = diffusion time, D = diffusion coefficient

Equation 3-2: *Stejskal-Tanner* equation.

In the resulting plots, the slope of the straight line is directly proportional to the diffusion coefficient and thereby the particle size.[106]

The ^{1}H DOSY [108] spectrum of **15** shows four to five different tetrameric aggregates in the aromatic region (Figure 3-3) which are associated to the peaks between 7.8 and 8.2 ppm. The *t*BuLi tetramer can be identified as well because it has a similar diffusion coefficient to the solvent toluene.

The largest peak at 8.22 ppm belongs to the ring-proton next to the lithium cation in the $[Li\{(C_6H_4)NMe_2\}]_4$ tetramer which is believed to be the main isomer in solution. The smaller signals at 7.89, 7.96, 8.01 and 8.08 ppm belong to other tetramers which contain the $[Li\{(C_6H_4)NMe_2\}]$ moiety. Most likely, the broad singlet at 8.08 ppm is just the result of exchange between different aggregates. The same could be observed in the $^{7}Li\{^{1}H\}$ spectrum (Figure 3-2).

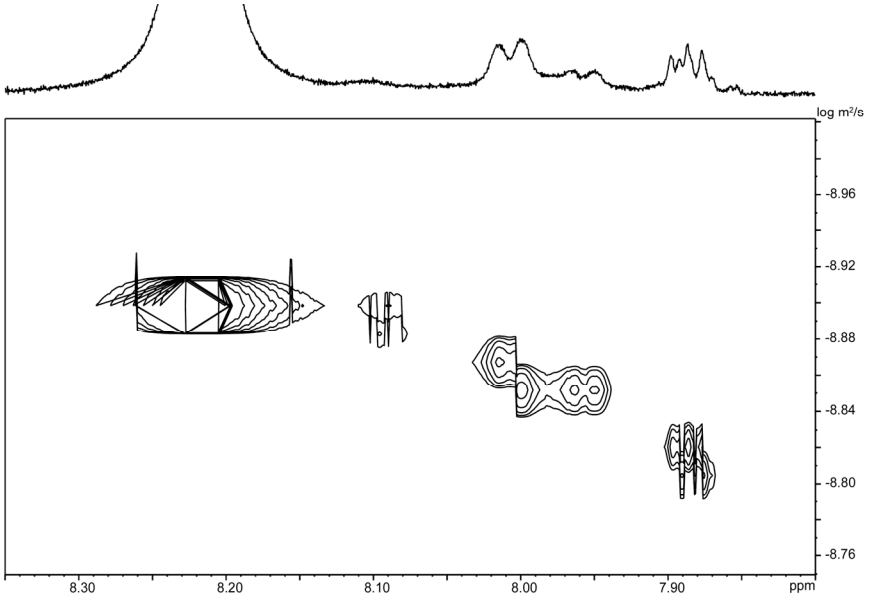

Figure 3-3: ^{1}H DOSY spectrum of $[Li\{(C_6H_4)NMe_2\}]_4[t\text{BuLi}]$ (**15**) in toluene-d^{8}.

Because of the exchange of the different molecules in solution, the aggregates contain chemically inequivalent lithium ions. Thus, the sharp peaks would belong to defined aggregates and the broad peaks are exchange peaks which are not visible in a 300 MHz spectrum but become sharper when the sample is cooled to -50 °C. Upon cooling of the sample to -80 °C, only two peaks at 3.61 and 1.47 ppm remain, which are associated to $[Li\{(C_6H_4)NMe_2\}]_4$ and $[t\text{BuLi}]_4$, respectively. Thus, the arrangement of the solid state is also achieved in solution at very low temperatures.

With this knowledge, one problem arises for the assignment of the aggregates in the ^{1}H DOSY spectrum: because the spectrum has an acquisition time of approx. one hour, peaks for exchange products are visible that can be mistaken for additional

aggregates. As a consequence, a ^{7}Li DOSY spectrum was recorded because the exchange peaks can be determined easier in the ^{7}Li spectrum (broad peaks).

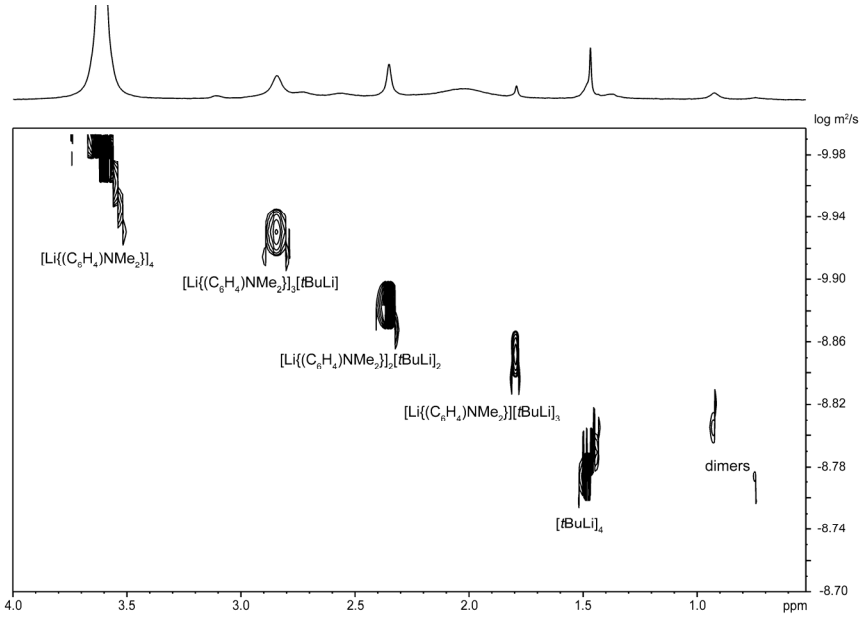

Figure 3-4: ^{7}Li DOSY spectrum of [Li{$(C_6H_4)NMe_2$}]$_4$[*t*BuLi] (**15**) in toluene-d^{8}.

In Figure 3-4 clearly separated diffusion peaks for the five main aggregates in solution (see above) are visible. From left to right the diffusion coefficient (as well as the molecular weight) of the tetramers decreases stepwise by the same amount because one [Li{$(C_6H_4)NMe_2$}] moiety is consecutively substituted with a *t*BuLi molecule. Two additional peaks at around 1.00 ppm could be dimers their composition, however, is unresolved. From the diffusion coefficient a mixed [Li{$(C_6H_4)NMe_2$}]/*t*BuLi dimer could be rationalised.

The exchange between the five tetramers was further verified with ^{1}H and ^{7}Li NOESY spectra that show definite exchange peaks between *t*Bu and aromatic signals. In the ^{7}Li NOESY spectrum the exchange between [Li{$(C_6H_4)NMe_2$}]$_4$ and the other [Li{$(C_6H_4)NMe_2$}]-containing tetramers (and *vice versa*) is clearly visible (Figure 3-5).

The assignment of peaks to the two main aggregates [*t*BuLi]$_4$ and [Li$(C_6H_4)NMe_2$}]$_4$ was achieved by a combination of HSQC, HMBC, ^{7}Li HOESY as well as ^{13}C{^{1}H} room temperature and low temperature spectra. In [Li$(C_6H_4)NMe_2$}]$_4$, all lithium ions are chemically equivalent. A shift of 3.61 ppm is assigned to them because of a cross peak between that signal and the signal of the neighbouring H-atom. The shifts for [*t*BuLi]$_4$ were compared to the literature.[109] When the sample is cooled to -50 °C, a coupling between the lithium atoms and the CH_3 groups in [*t*BuLi]$_4$ becomes visible

($^2J_{Li-C}$ = 14.22 Hz). As the resolution is not high enough, it can be speculated if ten or thirteen lines are present, corresponding to a coupling of the carbon atom with three or four ^{7}Li cores. This fluxionality of *t*BuLi tetramers in solution was already observed by *Thomas et al.* in 1986 for [*t*Bu^{6}Li]$_4$. Depending on the temperature, the carbon atom can couple to four lithium atoms, when the temperature is high, or only three lithium ions when the temperature is lower because the movement is frozen.[110]

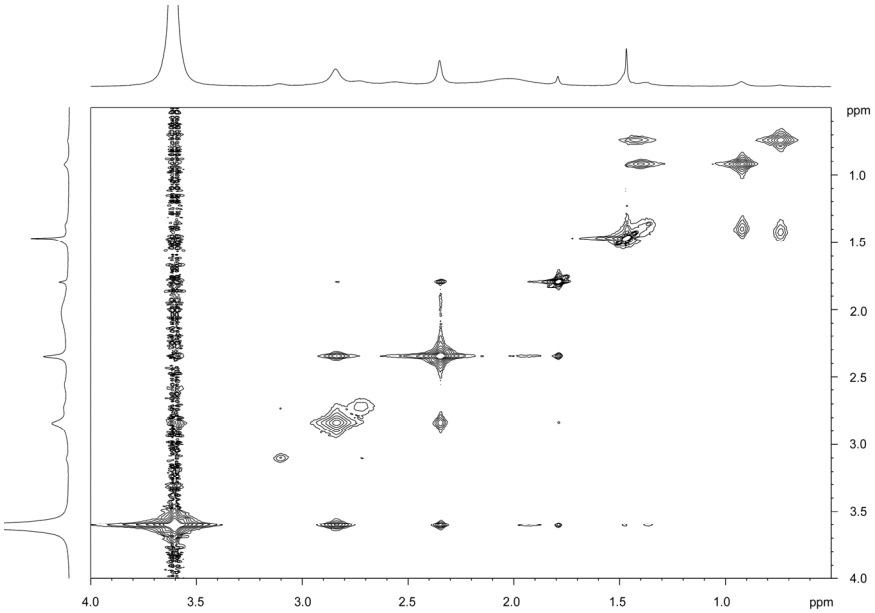

Figure 3-5: ^{7}Li NOESY spectrum of [Li{(C$_6$H$_4$)NMe$_2$}]$_4$[*t*BuLi] (**15**) in toluene-d^8.

To summarize, the questions posed above can be answered as follows:

- Are there mixed aggregates?: Yes. There definitely is exchange between *t*Bu and Ph signals as well as different lithiated species (^{1}H and ^{7}Li NOESY) therefore there are mixed aggregates. The different species in the aromatic region of the ^{1}H DOSY spectrum also suggest that.
- Are there other aggregates than tetramers?: Most probable yes. All species that contain the Me$_2$NPh moiety seem to be tetrameric (^{1}H DOSY), the [*t*BuLi]$_4$ tetramer is also visible. In the ^{7}Li DOSY two peaks are visible that could be mixed dimers.
- Are the aggregates interconvertible?: Yes. There is exchange between different aggregates (^{1}H and ^{7}Li NOESY).
- What exactly are the different aggregates?: The tetramers are [Li(C$_6$H$_4$)NMe$_2$}]$_4$, [Li{(C$_6$H$_4$)NMe$_2$}]$_3$[*t*BuLi], [Li{(C$_6$H$_4$)NMe$_2$}]$_2$[*t*BuLi]$_2$, [Li{(C$_6$H$_4$)NMe$_2$}][*t*BuLi]$_3$ and [*t*BuLi]$_4$. This can be rationalized by the ^{7}Li DOSY as well as ^{1}H DOSY, NOESY, HSQC, HMBC and ^{1}H spectra. The exact nature of the dimeric aggregates is still under investigation.

Interestingly, deprotonation of Me_2NPh does not occur at one of the methyl groups but at the phenyl ring in *ortho* position to the dimethylamino group. This effect is known as 'directed *ortho* metalation' (DoM) and has been thoroughly explored by *Snieckus*.[111] According to this concept, *t*BuLi is precoordinated by the dimethylamino side-arm and gets in close spatial proximity to the ortho-hydrogen atom, facilitating deprotonation at that position.

The case of Me_2PPh is different because deprotonation is only possible at the methyl groups. Strangely, when considering the electronegativities of nitrogen (3.0) and phosphorus (2.1) [112], methyl deprotonation should be favoured in the nitrogen compound as the protons are thermodynamically more acidic.

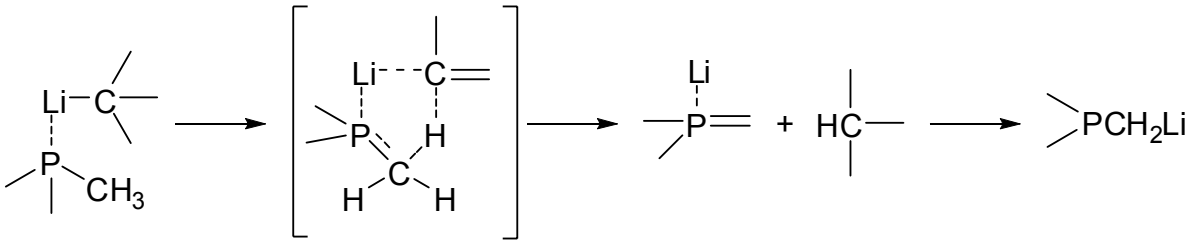

Figure 3-6: Suggested mechanism of the methyl-metalation in tertiary phosphanes.

The phenomenon is well known in the literature[113] and can be rationalized with the different stabilization of the intermediate carbanion. *Peterson et al.* [113c] suggested d-orbital resonance stabilization of the carbanion *via* a cyclic transition state in tertiary phosphanes (Figure 3-6).

Unlike phosphorus, nitrogen does not have a high polarizability or empty orbitals of low energy to stabilise the transition state. In addition, the lone pair at the nitrogen atom would have a repulsive force on the carbanion at the methyl group and deprotonation of the ring is therefore favoured. Deuterium exchange studies have also shown that the relative kinetic acidity of α-C hydrogen atoms in nitrogen containing compounds is much lower than in the corresponding phosphorus or sulphur analogues.[114]

Generation of unactivated or unstabilised lithiomethyl(amines) can only be achieved by metal-lithium exchange (where the metal predominantly is tin) [113c,115], reductive carbon-sulphur [116] or carbon-tellurium bond cleavage [117]. Another alternative is the precoordination of the lithium organyl by a donor site which is in close proximity to the α-C hydrogen atoms. Known examples are the lithiation of TMEDA,[79,118] PMDTA,[119] TMCDA [120] or TMMDA [121]. Generally speaking, it is not

possible to α-deprotonate tertiary amines without carbanion stabilizing groups or an additional chelating site.

Upon reaction of an equimolar amount of **15** with $S(NSiMe_3)_2$ a dimer with the formula $[Li\{Me_2N(C_6H_4)S(NSiMe_3)_2\}]_2$ (**16**) was formed. There had obviously been no reaction with *tert*-butyllithium although one could argue that only one product crystallised. Compound **16** crystallises as a dimer in the monoclinic space group $P2_1/c$ with the whole dimer in the asymmetric unit. It shows the already well known $(LiN)_2$ four-membered planar ring with bond distances similar to the corresponding phosphorus compound (**6**). Due to the different deprotonation of the starting material, **16** shows different connectivity from **6**, though. The sulphur diimide moiety is directly bonded to the phenyl ring and not to the methyl group of the dimethylamino substituent. Thereby, a larger bite angle of the nitrogen side-arm is created. Nevertheless, the coordination of the lithium ion is the same. One lithium atom is coordinated by one sulphur diimide moiety (Li1) whereas the other lithium atom is complexed by the Me_2N side-arm (Li2) of the same ligand, providing the dimeric link (see Figure 3-7).

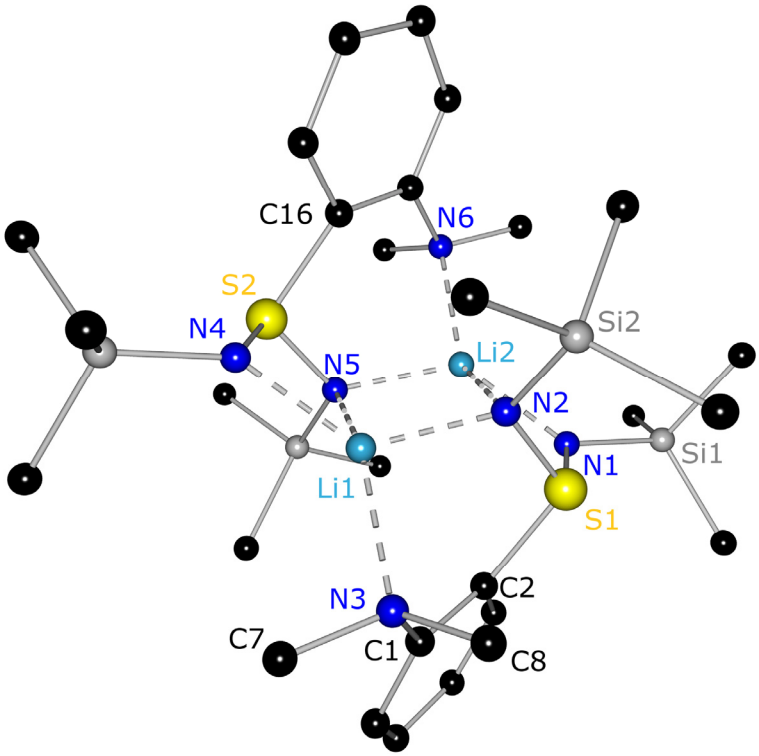

Figure 3-7: Molecular structure of $[Li\{Me_2N(C_6H_4)S(NSiMe_3)_2\}]_2$ (**16**). Hydrogen atoms are omitted for clarity.

The N–S–N angle is widened compared to the phosphorus compound **6** (106.54(4)° *vs.* 105.68(6)°). This is due to the sterically slightly more demanding

nitrogen side-arm. The methyl groups of the dimethylamino substituent are not aligned with the phenyl ring but are pointing away from the centre of the molecule, thus reducing steric strain and bringing the lone pair in the right position to coordinate the metal. The bond lengths and angles are all in the expected range. Selected bond lengths and angles for $[Li\{Me(Ph)PCH_2S(NSiMe_3)_2\}]_2$ (**6**) and **16** can be found in Table 3-2.

Table 3-2: Selected bond lengths [Å] and angles [°] in **6** and **16**

	6	**16**		**6**	**16**
S1–N1	1.6107(11)	1.6053(10)	N1–S1–N2	105.68(6)	106.54(5)
S1–N2	1.6278(11)	1.6139(10)	S1–C8–P1/S1–C2–C1	114.41(7)	126.70(9)
S1–C8/C2	1.8398(13)	1.8431(12)	Li1–N2–Li1'/Li2	76.86(11)	85.74(9)
C7–P1/C1–N3	1.8330(15)	1.4388(15)	N1–Li1–N2/N1–Li2–N2	69.41(8)	72.53(7)
N1–Li1/Li2	1.957(3)	2.068(2)	N2–Li1–N2'/N5	103.14(11)	94.38(9)
N2–Li1'/Li1	2.008(3)	1.968(2)	N2'–Li1–N1/N2–Li1–N4	138.96(14)	129.89(12)
N2–Li1/Li2	2.506(3)	2.284(2)	P1'–Li1–N2/N3–Li1–N5	122.84(10)	136.21(11)
P1–Li1'/N3–Li1	2.644(2)	2.193(2)			

To further test if the Me_2N side-arm is as flexible and easily cleavable in solution as the R_2P side-arm in corresponding complexes, two equivalents of THF were added to $[Li\{Me_2N(C_6H_4)S(NSiMe_3)_2\}]_2$ (**16**). As expected, the Me_2N side-arm coordination was replaced by one THF donor molecule each as the oxygen atom in THF is a better donor for lithium than nitrogen. Thereby the lability of the Li–NMe_2 bond could be proved. The dimethylamino group should now be easily approached by a second metal to give heterobimetallic complexes. The structure of $[(thf)Li\{Me_2N(C_6H_4)S(NSiMe_3)_2\}]_2$ (**17**) is depicted in Figure 3-8.

The structure shows the typical four-membered $(LiN)_2$ ring and the overall structural features are similar to other compounds of this type, *e. g.* $[(thf)Li(C_6H_5)S(NSiMe_3)_2]_2$.[85] The lithium cations are each coordinated by three nitrogen atoms of the two ligands and one oxygen atom of the THF molecule. Both phenyl rings are on opposite sides of the central N_2Li-plane and are arranged almost parallel to each other with the NMe_2 groups pointing away from the centre. Therefore, the coordination of a second metal seems feasible, as the nitrogen atoms N1 and N1' are sterically not protected.

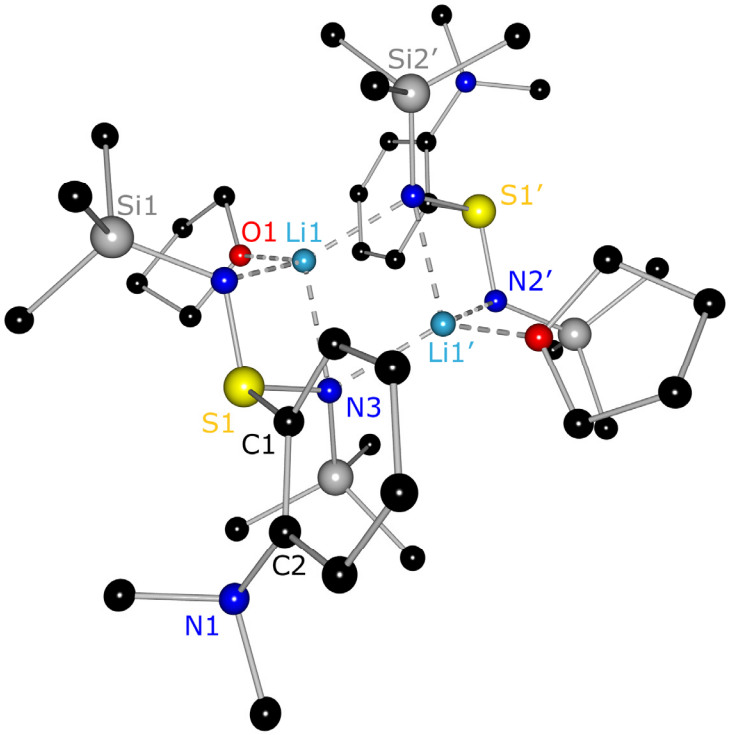

Figure 3-8: Molecular structure of $[(thf)Li\{Me_2N(C_6H_4)S(NSiMe_3)_2\}]_2$ (**17**). Hydrogen atoms are omitted for clarity.

The S–N, S–C and C–N bond lengths are all quite similar to **16**. The N–Li contacts differ very little, too. Nevertheless, the angles vary. The N–S–N angle is more acute as well as the S1–C1–C2 angle (120.28(10)°, 126.70(9)° in **16**). This is clearly due to the non-coordinating side-arm. The oxygen atoms of the THF molecules deviate by 40.6° from the central $(LiN)_2$ plane. The NSN moiety is located at an angle of 91.6° to the N3–Li1–O1 plane. Selected bond lengths and angles can be found in Table 3-3.

Table 3-3: Selected bond lengths [Å] and angles [°] in **17**

S1–N2	1.5994(10)	N2–S1–N3	103.19(5)
S1–N3	1.6252(10)	C1–S1–N3	104.21(6)
S1–C1	1.8325(13)	N1–C2–C1	119.16(12)
C2–N1	1.4263(18)	S1–C1–C2	120.28(10)
O1–Li1	1.946(2)	N2–Li1–N3	72.33(8)
N3–Li1	2.231(2)	N2–Li1–N3'	121.16(11)
N2–Li1	2.043(2)	N3–Li1–O1	115.10(11)
N3–Li1'	2.091(2)	Li1–N3–Li1'	72.55(10)

The NMR spectra of 16 and 17 differ only slightly. The signals for the ring hydrogen atoms in 17 are shifted to lower field because of the missing Li-coordination. Interestingly, this does not seem to influence the NMe_2 shift. The signal just gets very broad, probably because the group can rotate freely due to the missing coordination.

3.1.1 A Potassium Complex

In the 1960s *Lochmann* and *Schlosser* presented an excellent method for the deprotonation of unacidic substances.[42] Following this concept, *Ott* was able to synthesise a homologues series of alkaline metal functionalized picolines; he even succeeded to crystallise the first Cs-picolines.[122] In 2007 *Izod et al.* successfully employed NaO*t*Bu and KO*t*Bu for the transmetalation of lithium amino phosphanide complexes.[123]

With these successes in mind, KO*t*Bu was used for the deprotonation of Me_2NPh. KO*t*Bu and the amine were suspended in hexane und *t*BuLi was added drop wise with stirring at room temperature. After several hours, the brown slurry was filtered, thoroughly washed with hexane to remove LiO*t*Bu and dried *in vacuo*. The resulting powder is highly pyrophoric and even in an argon glove box it was only storable for about one week before it degraded into a white powder. NMR spectroscopy clearly showed that $[K\{(C_6H_4)NMe_2\}]$ was the obtained product. Thereby, the transmetalation step had already been effected during the synthesis of the starting material, thus omitting the difficult metal exchange in the final compound.

When $[K\{(C_6H_4)NMe_2\}]$ was reacted with an equimolar amount of $S(NSiMe_3)_2$ at -78 °C and the solution stored at -20 °C, colourless crystals were obtained after one week (Equation 3-3). The complex $[K\{Me_2N(C_6H_4)S(NSiMe_3)_2\}]_2$ (**18**) crystallises in the monoclinic space group *C*2/*c* with two dimers in the asymmetric unit. The potassium ions are bonded by two nitrogen atoms of one diimido moiety (N1/N2, N1'/N2'), one nitrogen atom of the other diimido moiety (N1'/N1) and η^6 by the phenyl ring of that half.

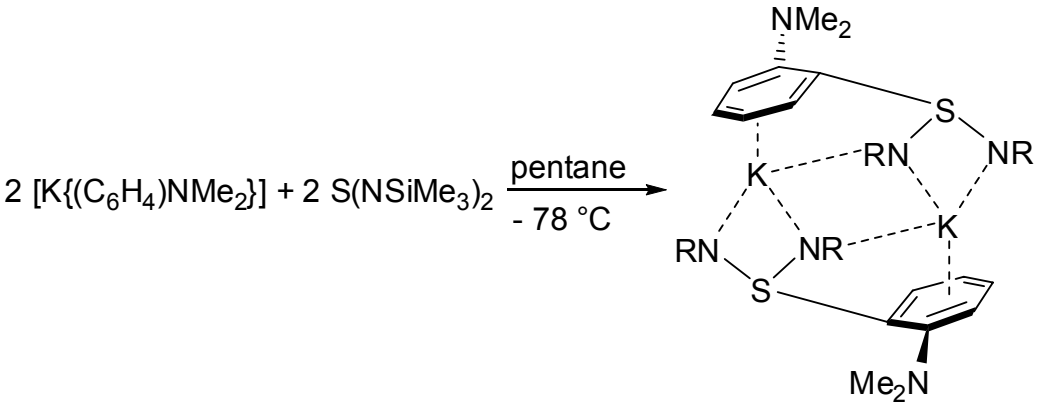

Equation 3-3: Preparation of $[K\{Me_2N(C_6H_4)S(NSiMe_3)_2\}]_2$ (**18**), R = $SiMe_3$.

This is very different in comparison to the corresponding lithium complex **16** (Figure 3-7) and is due to the lower HSAB hardness of potassium. In the case of lithium, the dimethylamino group takes part in the coordination rather than the C_6-perimeter. Despite of the η^6-coordination of the phenyl ring, the connecting S–C bond is virtually not affected (1.832(2) Å in **18** *vs.* 1.8431(12) Å in **16**).

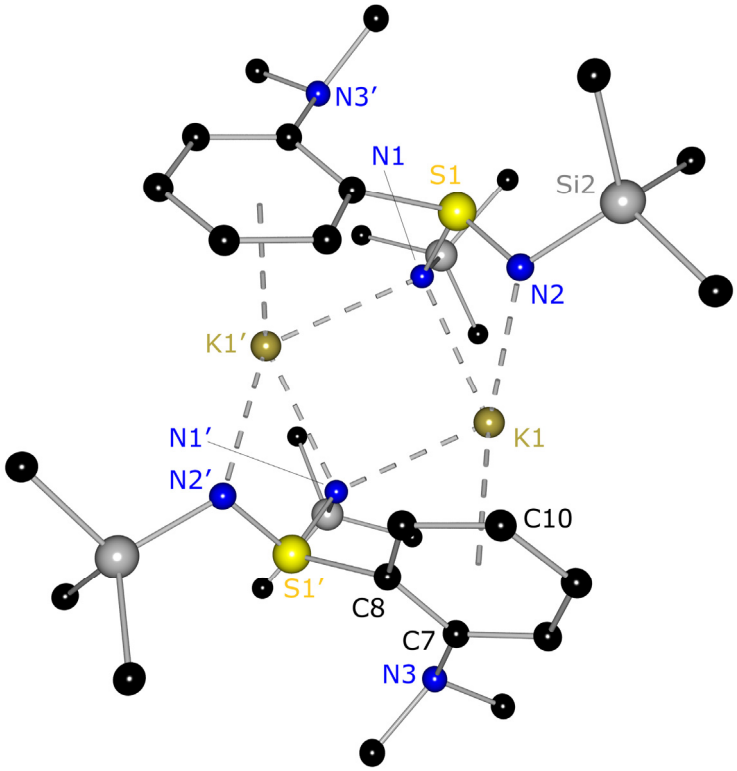

Figure 3-9: Molecular structure of $[K\{Me_2N(C_6H_4)S(NSiMe_3)_2\}]_2$ (**18**). Hydrogen atoms are omitted for clarity.

In **18**, the amino arm is free to rotate and may bind to other metal atoms. The N–K bond lengths range from 2.7656(18) Å (N2–K1) to 2.8923(17) Å (N1–K1') and are therefore in the expected range.[68] They are similar to the diimido potassium complex $[(dme)K\{(Me_3SiN)_2SPh\}]_2$ which displays N–K distances of 2.725(2) Å and

2.823(2) Å.[81] The distance of the potassium cation from the coordinating phenyl ring is on average 3.3 Å which is in the usual range [124] and comparable to [{(*t*BuO)$_2$Sb$_3$(μ-NCy)$_3$(μ^3-NCy)}K(η^6-C$_6$H$_5$Me)] [125] [Ph$_3$CK(thf)(pmdta)],[126] [PyPh$_2$CK(thf)(pmdta)] [127] or (η^3-(PN*t*Bu)$_2$(N*t*Bu)$_2$)[η^2-(N*t*Bu)$_2$P]ZrCl [128]. The phenyl rings are oriented 95.5° with respect to each other (Figure 3-9). Important bond lengths and angles of **18** and **16** are compared in Table 3-4.

Table 3-4: Selected bond lengths [Å] and angles [°] in **18** and **16**

	16	**18**		**16**	**18**
S1–N1	1.6053(10)	1.6140(17)	N1–S1–N2	106.54(5)	107.55(9)
S1–N2	1.6139(10)	1.6067(17)	S1–C2–C1/S1'–C8–C7	126.70(9)	119.76(16)
S1–C2/C8'	1.8431(12)	1.832(2)	Li1–N2–Li2/K1–N1–K1'	85.74(9)	85.39(5)
N3–C1/C7	1.4388(15)	1.419(3)	N1–Li2–N2/N1–K1–N2	72.53(7)	55.95(5)
N1–Li2/K1	2.068(2)	2.7726(17)	N2–Li1–N5/N1–K1–N1'	94.38(9)	88.23(5)
N2–Li1/K1	1.968(2)	2.7656(18)	N2–Li1–N4/N2–K1–N1'	129.89(12)	125.93(5)
N2–Li2/N1–K1'	2.284(2)	2.8923(17)	N2–K1–C7	---	127.71(5)
N3–Li1/C10–K1	2.193(2)	3.375(2)	N3–Li1–N5	136.21(11)	---
C7–K1	---	3.361(2)			

With the complexation of potassium by the {Me$_2$N(C$_6$H$_4$)S(NSiMe$_3$)$_2$}$^-$ ligand, compounds with softer metals come into focus and the versatility of the ligand system is displayed. Not only the nitrogen atoms can act as donors but the phenyl ring as well because it is in spatial proximity to the diimido moiety.

3.1.2 S(N*t*Bu)$_2$ as a Donor Solvent

As the reaction of lithiated dimethylaniline and S(NSiMe$_3$)$_2$ proceeded smoothly and in excellent yield, S(N*t*Bu)$_2$ was employed to generate a ligand analogous to **16** but with different substituents at the sulphur atom. Surprisingly, the conversion is not equimolar and proceeds according to Equation 3-4. It is striking that [(*t*BuN)$_2$S·{LiMe$_2$N(C$_6$H$_4$)S(N*t*Bu)$_2$}$_2$] (**19**) always crystallises with one equivalent of S(N*t*Bu)$_2$ as a donor solvent, even when the reaction is conducted with equimolar amounts of S(N*t*Bu)$_2$ and [Li{(C$_6$H$_4$)NMe$_2$}]. This behaviour is not observed when S(NSiMe$_3$)$_2$ is used instead.

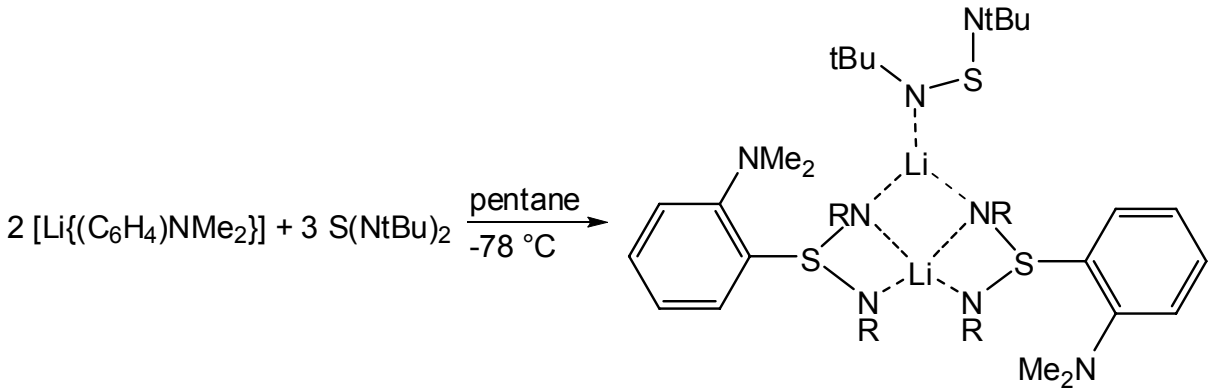

Equation 3-4: Preparation of [(*t*BuN)$_2$S·{LiMe$_2$N(C$_6$H$_4$)S(N*t*Bu)$_2$}$_2$] (**19**), R = *t*Bu.

The reaction product crystallises in the monoclinic space group $P2_1/n$ with the whole molecule in the asymmetric unit (Figure 3-10). One lithium atom (Li1) is tetrahedrally coordinated by four nitrogen atoms of the two {Me$_2$N(C$_6$H$_4$)S(N*t*Bu)$_2$}$^-$ ligands. Different to **16**, the dimethylamino groups do not take part in the coordination. The Li–N bond lengths are in the expected range between 1.955(3) Å (Li1–N2) and 2.338(3) (Li1–N3) Å. Two of the diimido nitrogen atoms (N3 and N5) additionally coordinate a second lithium cation, giving rise to the longer Li–N distances. Li2 has a trigonal planar coordination geometry with all N–Li2–N angles close to 120° (N3–Li2–N5: 115.74(14)°, N3–Li2–N8: 124.27(14)°, N5–Li2–N8: 119.73(14)°). The third coordination site is occupied by a free, non-disordered S(N*t*Bu)$_2$ molecule, acting as a donor solvent.

The diimide molecule is almost perfectly aligned which can be rationalized with the torsion angle C37–N8–S3–N7 of 0.81(16)°. The S–N distances of the coordinating diimido moieties are in the expected range for diimido sulfinates. In contrast, the S–N distances in the free S(N*t*Bu)$_2$ are considerably shorter (1.5331(15) Å and 1.5396(14) Å), which is well in the range of the uncoordinating starting material.[129] The distance between S3 and N8 is slightly longer (1.5396 Å) because of the coordination to the lithium atom. All S–N bond lengths suit the concept of polar reinforced $S^{\delta+}$–$N^{\delta-}$ bonds deduced from experimental and theoretical charge density investigations.[130] Nevertheless, the centre of the structure consists of the well known (LiN)$_2$ four-membered ring with the Li–N distances being in the same range as for all the other structures. The diimido moieties are inclined by 42.7° and 44.3° from the central Li–N–Li plane. Both S(N*t*Bu)$_2$ groups are twisted by 62.0° with respect to each other, thus promoting the tetrahedral environment around Li1. Selected bond lengths and angles are shown in Table 3-5.

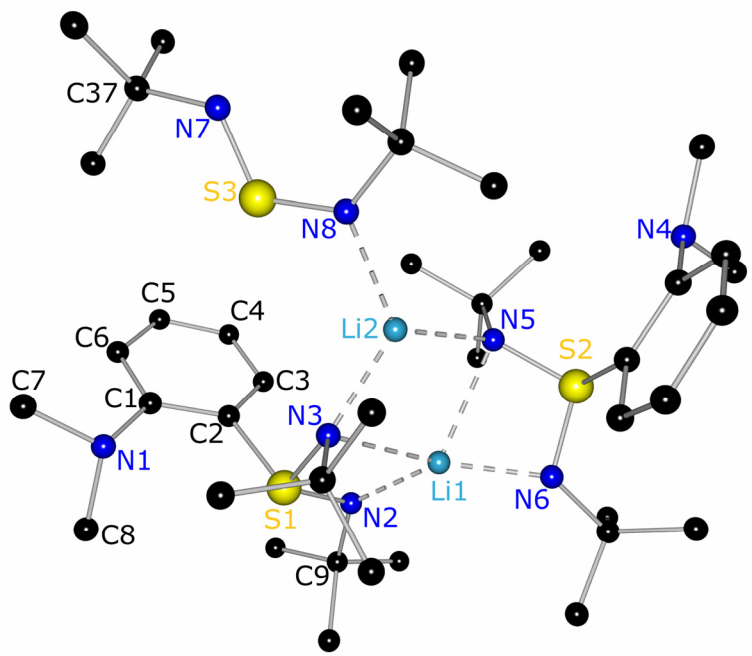

Figure 3-10: Molecular structure of $[(t\text{BuN})_2\text{S}\cdot\{\text{LiMe}_2\text{N}(\text{C}_6\text{H}_4)\text{S}(\text{N}t\text{Bu})_2\}_2]$ (**19**). Hydrogen atoms are omitted for clarity.

The threefold/fourfold binding motif of lithium is well known – not only in diimido complexes [36,131] but also with other ligands [132] and is one of the preferred coordination geometries for sulphur diimido complexes with donor solvents. It is interesting though, that the coordination is not similar to **17** and the two diimido moieties are bridging both lithium atoms. This could be due to the increased steric demand of $\text{S}(\text{N}t\text{Bu})_2$ in comparison to THF. Consequently, a control of the coordination motif seems feasible just by choosing the right solvent.

Table 3-5: Selected bond lengths [Å] and angles [°] in **19**

S1–N2	1.617(13)	N2–S1–N3	104.15(7)
S1–N3	1.6350(13)	N7–S3–N8	114.98(8)
S3–N7	1.5331(15)	C1–C2–S1	121.65(12)
S3–N8	1.5396(14)	N2–Li1–N6	143.34(16)
S1–C2	1.8267(16)	N6–Li1–N5	72.74(10)
C1–N1	1.422(2)	N2–Li1–N3	72.63(10)
N1–Li1	1.955(3)	N5–Li1–N3	96.20(11)
N3–Li2	2.051(3)	N5–Li2–N3	115.74(14)
N8–Li2	2.127(3)	N5–Li2–N8	119.73(14)
N3–Li1	2.338(3)	N3–Li2–N8	124.27(14)

Conclusion

The very different structural characteristics in **19** compared to **16** might have their origin in electronic reasons, as the silicon atom in $S(NSiMe_3)_2$ is the only difference in the reactions leading to both lithium complexes. It is striking that **19** always crystallises with one equivalent of $S(N\textit{t}Bu)_2$ as a donor solvent, even if the reaction is conducted with equimolar amounts of $S(N\textit{t}Bu)_2$ and $[Li\{(C_6H_4)NMe_2\}]$. This behaviour is not observed when $S(NSiMe_3)_2$ is used instead.

During the course of this research, it became obvious that most of the reactions proceeded much better with $S(NSiMe_3)_2$ than with $S(N\textit{t}Bu)_2$. Some do not even work at all with di(*tert*)butyl sulphur diimide. A reason for this could be the different activation of the sulphur atom by the different substituents. In both cases the S–N bond is polarized in direction of the nitrogen atom. However, the better polarizability and lower electronegativity of silicon compared to carbon allows for a better distribution of the negative charge into the ligand. Consequently, the positive charge at the sulphur atom is augmented. For nucleophiles (just like the employed carbanions), the addition becomes easier *i. e.* faster. It can be speculated that the complete addition of $S(N\textit{t}Bu)_2$ to $[Li\{(C_6H_4)NMe_2\}]$ to form $[(\textit{t}BuN)_2S{\cdot}\{LiMe_2N(C_6H_4)S(N\textit{t}Bu)_2\}_2]$ proceeds slowly, so that **19** is already being formed in the reaction flask and complete conversion cannot be achieved. This effec is likely to be minimal, as it has no influence on the S–N bond lengths.

3.2 The Picolyl Side-Arm

As has already been discussed in chapter 3.1, dimethylaniline can only be deprotonated with *tert*-butyllithium directly at the ring. In order to synthesise a compound that has a nitrogen-functionalized side-arm which is connected to the sulphur atom *via* a CH_2 bridge 2-picoline was employed in the synthesis. The deprotonation and reactivity of this heterocycle has been extensively studied by *Ott* in our workgroup.[122] One of the most convenient ways is the deprotonation with *n*BuLi and TMEDA at -78 °C.[133] [(tmeda)Li(2-Pic)] crystallises as dark red needles that can be filtered, washed and stored in an argon drybox without being too reactive.

The equimolar reaction with $S(NSiMe_3)_2$ yields colourless crystals of space group $P\bar{1}$. Compound **20** is a dimer (see Figure 3-11) which is isosteric to the

previously reported [Li{2-PicS(N*t*Bu)$_2$}]$_2$ which crystallises in the monoclinic space group *C*2/*c*.[36] There are no unusual bond lengths and angles. A selection is shown in Table 3-6.

Table 3-6: Selected bond lengths [Å] and angles [°] in **20** and [Li{2-PicS(N*t*Bu)$_2$)}]$_2$

	20	**[Li{2-PicS-(N*t*Bu)$_2$)}]$_2$**		**20**	**[Li{2-PicS-(N*t*Bu)$_2$)}]$_2$**
S1–N3	1.6140(9)	1.6253(17)	N2–S1–N3	106.66(5)	103.48(9)
S1–N2	1.6018(9)	1.6101(17)	C6–C1–N1	116.21(10)	115.96(19)
S1–C6	1.8442(11)	1.859(2)	S1–C6–C1	114.01(8)	113.26(15)
C1–C6	1.4901(15)	1.487(3)	Li1–N3–Li1'	81.09(9)	81.54(16)
Li1–N1’	2.052(2)	2.118(4)	N3–Li1–N3’	98.91(9)	98.46(16)
Li1–N2	2.046(2)	1.979(4)	N2–Li1–N3	74.69(7)	126.8(2)
Li1–N3	2.201(2)	2.281(4)	N1–Li1’–N3	94.44(9)	94.55(16)
Li1–N3’	2.091(2)	2.074(4)	C1–N1–Li1’	114.58(9)	110.43(17)

The compound shows the same structural features as [Li{2-PicS(N*t*Bu)$_2$)}]$_2$. In the centre of the structure is the typical (LiN)$_2$ four-membered heteroatomic ring. Both lithium atoms are coordinated by four nitrogen atoms in a distorted tetrahedral manner. The N2–S1–N3 angle of 106.66(5)° is wider than in the corresponding complex [Li{2-PicS(N*t*Bu)$_2$)}]$_2$ (N–S–N: 103.48(9)°). As a consequence, the corresponding Li–N bond distances are elongated: N2–Li1 2.046(2) Å in **20** *vs.* 1.979(4) Å and N3'–Li1 2.091(2) Å *vs.* 2.074(4) Å. The C6–C1–N1 (116.21(10)°) and S1–C6–C1 (114.01(8)°) angles are also widened compared to [Li{2-PicS(N*t*Bu)$_2$)}]$_2$ (115.96(19)° and 113.26(15)°, respectively). Interestingly, this larger bite of the ligand brings the two lithium cations into closer proximity. They are 2.791 Å apart in **20**, compared to 2.848 Å in the di(*tert*-butyl)sulphur diimido complex.

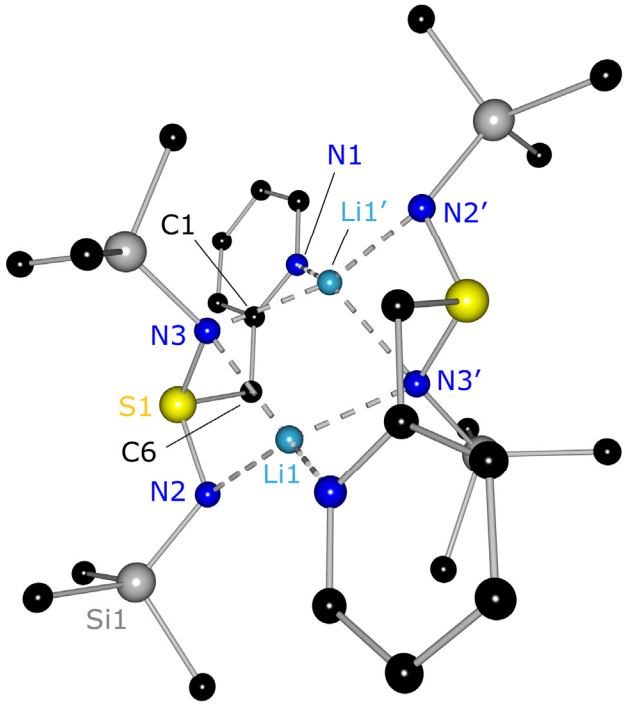

Figure 3-11: Molecular structure of $[Li\{2\text{-}PicS(NSiMe_3)_2\}]_2$ (**20**). Hydrogen atoms are omitted for clarity.

3.3 A Ligand of higher Denticity

To generate a ligand with more than three binding sites, trimethylethylenediamine (TrMEDA) was lithiated and reacted with bis(trimethylsilyl)sulphur diimide in a one pot synthesis. This particular amine was chosen because it can be metalated very easily, it has two additional donor sites and should have the required flexibility.[134] In addition, it is already being used as a bidentate ligand in many metal complexes [135] and should therefore have the desired properties.

After lithiation of the amine, the reaction mixture was stirred for two hours and the diimide was added. The solution was then stirred for several hours, reduced in volume and stored at -25 °C for crystallization. The molecular structure of $[Li\{Me_2N(CH_2)_2N(Me)S(NSiMe_3)_2\}]_2$ (**21**) is shown in Figure 3-12.

All four nitrogen atoms of one ligand take part in the coordination, proving the anticipated flexibility. Consequently, the lithium cations are fivefold coordinated in a very distorted way and the coordination polyhedron seems arbitrary to assign.

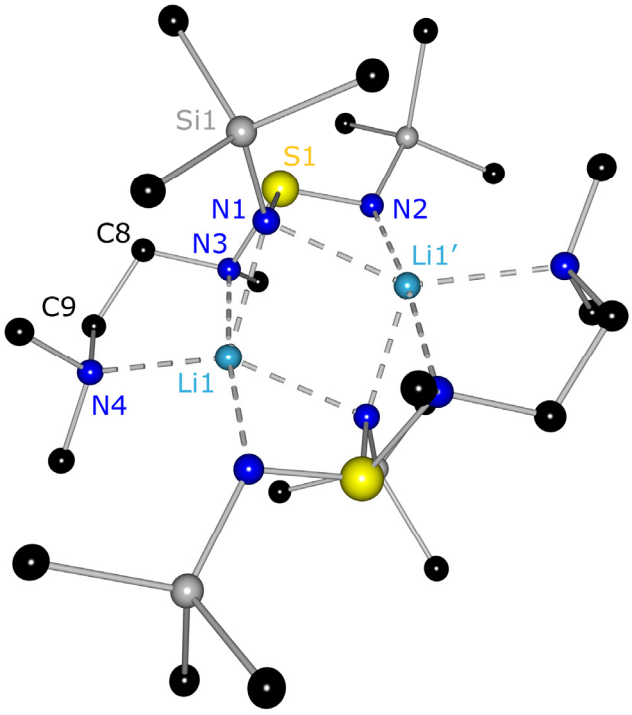

Figure 3-12: Molecular structure of $[Li\{Me_2N(CH_2)_2N(Me)S(NSiMe_3)_2\}]_2$ (**21**). Hydrogen atoms are omitted for clarity.

If the two largest bond angles around Li1 (N3–Li1–N2': 171.77(9)° and N4–Li1–N1': 143.11(9)°) are taken into account, the geometry index τ_5 can be calculated, where the angle β is larger than the angle α (Equation 3-5).[136]

$$\tau_5 = \frac{\beta - \alpha}{60}$$

Equation 3-5: Definition of τ_5.

This value was introduced by *Addison* and *Reedijk* in 1984 and represents an easy method to distinguish between a square pyramidal and a trigonal bipyramidal coordination geometry. This is especially handy for cases where the geometry is not clearly visible. Thus, for a square pyramidal coordination $\tau_5 = 0$ and for a trigonal bipyramid $\tau_5 = 1$. In the case of **21** it is optically almost impossible to discern the coordination geometry around the lithium atoms. The value of $\tau_5 = 0.48$ proves this but hints to a probably heavily distorted square pyramid.

It could be stated that in the ligand the nitrogen side-arm acts as an intramolecular TMEDA molecule. The N–Li distances range from 2.0989(19) Å (N1–Li1) to 2.442(2) Å (N3–Li1) and are comparable to the other structures with nitrogen side-arm although N3–Li1 is near to the upper limit for N–Li bonds.[68] The N1–S1–N2 angle of 107.75(4)° is somewhat wider than in the other structures reported so far. This is due to the third nitrogen atom bonded to the diimido moiety and the arising

fivefold coordination of the lithium cation. The trigonal bipyramidal environment could only be achieved if N1 and N2 were further apart from each other. The S–N distances of 1.6009(8) Å (S1–N1) and 1.5847(8) Å (S1–N2) are on average shorter than in similar complexes but S1–N3 (1.7770(9) Å) is even longer than an average S–N single bond. This is due to the complexation of Li1. Selected bond lengths and angles, compared with the corresponding sodium complex, can be found in Table 3-7.

There seems to be a certain dynamic in solution. The N(CH_2)$_2$N signals in the ^{1}H NMR spectrum are very broad at room temperature, indicating that the whole side-arm is moving. This is only possible if the N4–Li bond is cleaved and the side-arm is free to rotate.

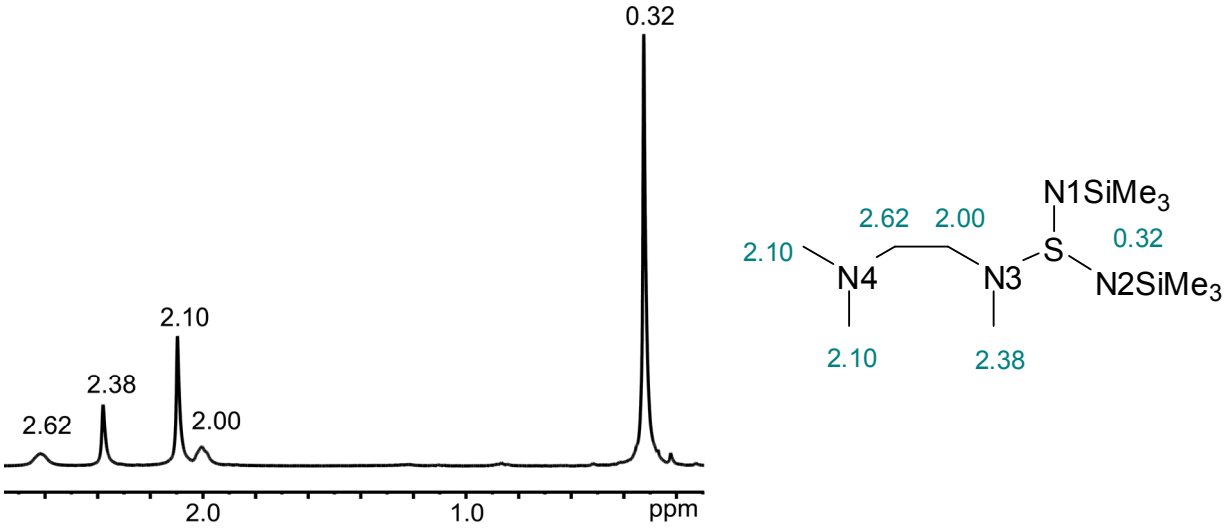

Figure 3-13: ^{1}H NMR spectrum of **21** in C_6D_6.

The fivefold N-coordination of lithium is not very common. Li^+ rather prefers the coordination numbers four and six. When coordinated by a matching hemiporphyrizinato ligand however, a donor solvent can occupy the fifth coordination site, leading to a square pyramidal geometry around lithium.[137] There are also amidinate complexes that show the fivefold coordination motif.[138] Amidinates of the general form [R^1NC(R^2)NR^3]$^-$ have nearly the same complexation potential as sulphur diimides resulting from the same geometry. Nevertheless, their coordination modes are limited.

3.3.1 From Lithium to Sodium

When deprotonating TrMEDA with *n*BuLi in the presence of NaO*t*Bu, the sodium intermediate is obtained which forms the dimer **22** upon reaction with $S(NSiMe_3)_2$ which is analogous to **21** (see Equation 3-6). The structure of **22** is shown in Figure 3-14.

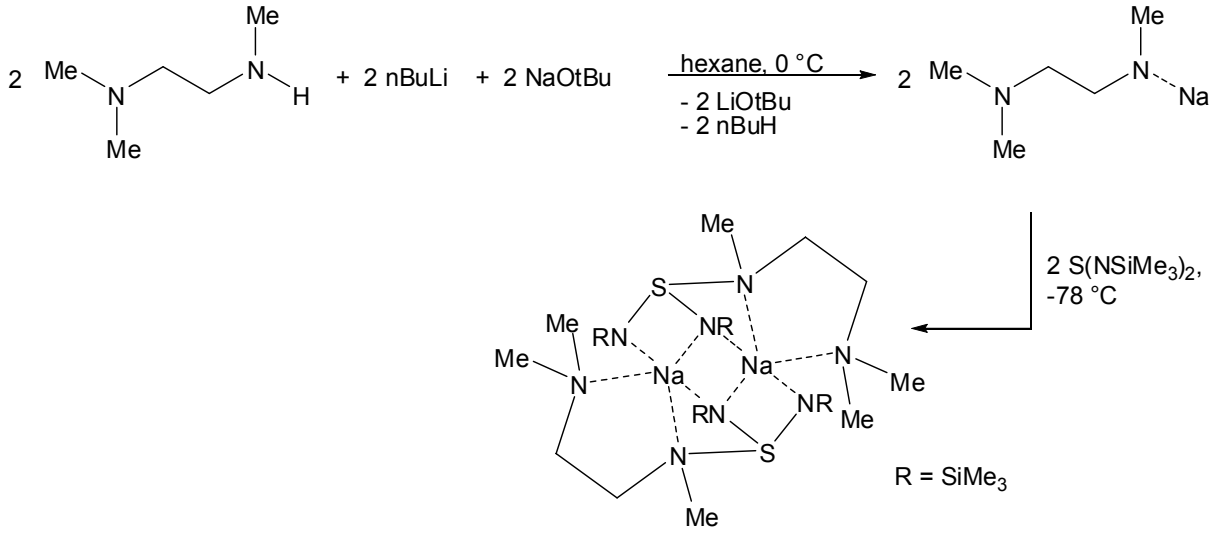

Equation 3-6: Preparation of $[Na\{Me_2N(CH_2)_2N(Me)S(NSiMe_3)_2\}]_2$ (**22**).

The sodium cation is fivefold coordinated by nitrogen atoms, similar to the lithium atom in the related complex. The resulting trigonal bipyramidal environment of the sodium atoms is more distorted than in the corresponding lithium complex (N1–Na1–N3: 167.53(4)° *vs.* N2'–Li1–N3: 171.77(9)°). This is also evident if the geometry index τ_5 is calculated. The two largest angles around Na1 are N1–Na1–N3 (167.53(4)°) and N4–Na1–N2' (144.69(4)°) and $\tau_5 = 0.38$. Therefore, it can be deduced that **22** has a rather distorted square pyramidal geometry around the sodium cations. This is probably due to the fact that sodium is larger than lithium and the ligand in **22** is moved further away from the metal. Thereby, the coordinating nitrogen atoms can easier get into the plane of Na1 and Na1'.

Selected bond lengths and angles of **22** compared to the lithium complex **21** can be found in Table 3-7.

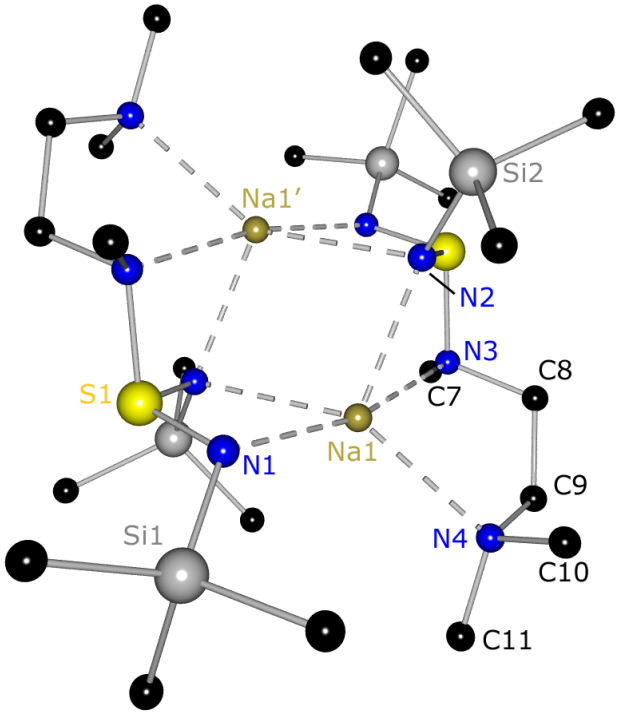

Figure 3-14: Molecular structure of $[Na\{Me_2N(CH_2)_2N(Me)S(NSiMe_3)_2\}]_2$ (**22**). Hydrogen atoms are omitted for clarity.

Table 3-7: Selected bond lengths [Å] and angles [°] in **21** and **22**

	21	**22**		**21**	**22**
S1–N1	1.6009(8)	1.5836(11)	N1–S1–N2/N2'	107.75(4)	108.69(6)
S1–N2/N2'	1.5847(8)	1.5889(11)	N1–S1–N3/N3'	96.08(4)	102.37(5)
S1–N3/N3'	1.7770(9)	1.7892(11)	C8–N3–S1/S1'	108.17(6)	107.95(8)
N1–Li1/Na1	2.0989(19)	2.4256(12)	N1–Li1'–N2/N1–Na1–N2'	114.89(8)	62.83(4)
N1–Li1'/N2–Na1	2.2768(19)	2.4173(12)	N1–Li1–N1'/N2–Na1–N2'	98.81(7)	100.06(4)
N2–Li1'/Na1'	2.1934(19)	2.5173(12)	Li1–N1–Li1'/	81.19(7)	
N3–Li1/Na1	2.442(2)	2.5784(12)	Na1–N2–Na1'		79.95(4)
N4–Li1/Na1	2.2534(19)	2.5051(12)	N1–Li1–N3/N2–Na1–N3	66.76(6)	60.68(4)
N1–Si1	1.7268(8)	1.7208(11)	N3–Li1–N4/N3–Na1–N4	78.89(6)	74.46(4)
C8–C9	1.5201(14)	1.5244(18)	N2'–Li1–N3/N1–Na1–N3	171.77(9)	167.53(4)
			N3–C8–C9	110.11(8)	111.68(1)

The S1–N1 and S1–N2 bond lengths are in the expected range for diimido sulfinates. The S1–N3' bond of 1.7892(11) Å, on the other hand, is considerably elongated in comparison to a standard S–N single bond of 1.69 Å. This is due to the complexation of Na1' and the complexing TrMEDA side-arm. The ligands are less strained and occupy more space around the central metals in comparison to **21**. This

is also obvious if the angles around the sulphur atoms are taken into account. The TrMEDA sidearm is not bent inwards as much (N1–S1–N3': 102.37(5)° *vs.* 96.08(4)° in **21**). As a result, all nitrogen-metal bond lengths are on average 0.3 Å longer than in the lithium derivative. This is of course also due to the fact that sodium has a larger ionic radius. All Na–N bonds are in the expected range for diimido-sodium compounds.[139,140] Interestingly, the N3–Na1–N4 angle of 74.46(4)° is more acute than the corresponding angle in the lithium complex (78.89(6)°). That is only possible because the ligand in **22** is bonding weaker to the metal, thereby leaving more space at the centre of the structure where the TrMEDA side-arm can get closer. The distances in the central four-membered ring support this observation: Li1···Li1': 2.851 Å and Na1···Na1': 3.171 Å.

The ^{1}H NMR spectrum also shows a dynamic behaviour which is even more pronounced than in the corresponding lithium complex. The N(CH_2)$_2$N signals only become visible at -30 °C. Thus, the presumption that the whole side-arm moves in solution is confirmed. As the N4–Na1 bond is longer than the N4–Li1 bond, it can be cleaved easier and the movement of the side-arm becomes faster. Consequently, the signals get broader and eventually disappear.

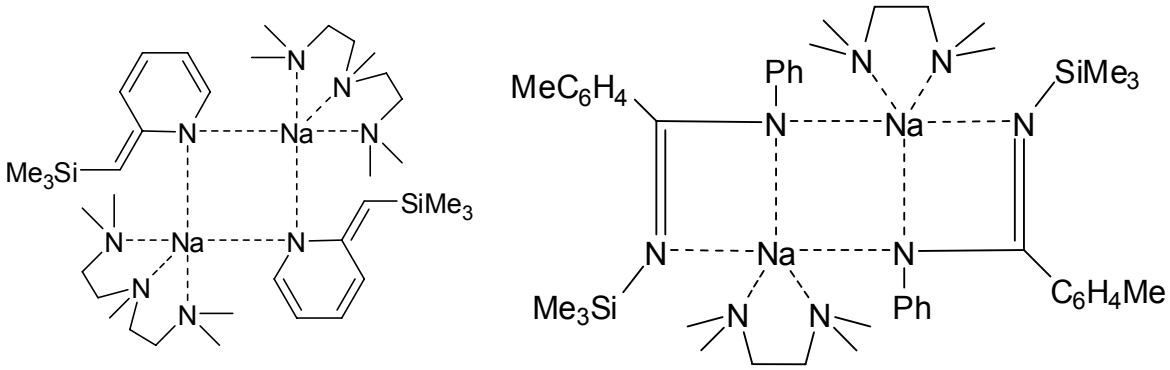

Figure 3-15: Examples for fivefold N-coordinated sodium cations.

The coordination number five is also not preferred by sodium as is the same case for lithium. There are only a few examples reported in the literature. *Raston et al.* synthesised a dimeric sodium complex with a monosilylated picolyl ligand and PMDETA with the formula [(pmdeta)Na{2-Pic(SiMe$_3$)CH}]$_2$ (Figure 3-15, left).[140] The sodium cation is fivefold coordinated by nitrogen atoms resulting in the formation of a central planar (NaN)$_2$ four-membered ring which is similar to complex **22**. *Lappert et al.* reported on fivefold coordinated sodium in a benzamidinato/TMEDA complex (Figure 3-15, right) in 2007 that also shows the central (NaN)$_2$ ring.[141] Apparently,

this is a preferred arrangement with such a bidentate ligand which is quite similar to sulphur diimides.

Conclusion

To summarize the results, it can be stated that the functionalization of sulphur diimides with metalated amines is a straightforward method to generate a great variety of new ligands. They show flexibility just like the corresponding phosphorus compounds, although the amine backbone in **16** and **19** is more rigid than the SCH_2P bridge in chapter **1**-**12**. This slight disadvantage is compensated by the introduction of the TrMEDA side-arm in **21** which has an additional binding site for metal cations and provides a bigger coordination claw than $S(NR)_2$. This result should be encouraging for the use of similar phosphorus compounds to regain the advantage of a softer donor site. The donor exchange reaction at the lithium cation in **16** leaves it very clear that the nitrogen side-arm is – like the phosphorus side-arms – bonding weakly. It can therefore easily be replaced by better donors for lithium metal. Thus, a free donor site in the ligand is generated, opening up the route to further coordination compounds and heterobimetallic complexes. In addition, the THF molecule itself may also be interchangeable. Interestingly, the addition of THF to a solution of $[Li\{Me_2PCH_2S(N\textit{t}Bu)_2\}]_2$ (**1**) does not lead to the replacement of the phosphorus side-arm.[38] This is indeed surprising as the phosphorus-lithium bond in **1** (2.6425(19) Å) is significantly longer than the N3–Li bond in **16** (2.193(2) Å). It has to be further investigated what the reason might be, hence the role of the substituents on the nitrogen atoms of the sulphur diimido moiety has not been determined yet.

It has also been shown that a transmetalation step does not necessarily have to be carried out with the final lithium complexes. A more elegant way is to metalate the starting materials and subsequently react them with a sulphur diimide. It has been proven that alkali metal complexes of the different ligands can be obtained by this route. It has to be further investigated now, which other metals can be introduced *via* this reaction pathway. Finally, it was also possible to synthesise $[Li\{2\text{-}PicS(NSiMe_3)_2\}]_2$ (**20**), the analogue of $[Li\{2\text{-}PicS(N\textit{t}Bu)_2\}]_2$. This ligand preserves the CH_2 bridge between the sulphur atom and the side-arm.

4 COMPLEXES WITH TWO SULPHUR DIIMIDO MOIETIES

A ligand with two donating diimido groups would be a beneficial addition to this new class of compounds because it would exhibit even more donor atoms and increased flexibility as well as complexation versatility. Me_2PPh was chosen as a starting material because it offers two possible CH_2 bridges. However, direct metalation of both methyl groups is difficult which is due to the fact that deprotonation at one methyl group deactivates the second methyl group and the reaction gets too slow.[142] Usually, metal-lithium exchange reactions are conducted in order to obtain $[RE(CH_2Li)_2]$ compounds (E = main group element). By this method $[MeN(CH_2Li)_2]$ and $[Me_2C(CH_2Li)_2]$ [143] have been prepared *via* tin-lithium and mercury-lithium exchange, respectively. $[S(CH_2Li)_2]$ can be synthesised by tellurium-lithium exchange but is highly explosive.[144] *Strohmann et al.* reported in 2010 the double deprotonation of dimethylphenylphosphine borane with *t*BuLi and (*R,R*)-TMCDA.[145] This reaction readily proceeds at -30 °C which is due to stabilizing Li–H interactions with the borane that lower the barrier for the second deprotonation to only 92 kJ/mol.

Considering all this, it was obvious that a stronger base than *t*BuLi had to be used if the hazardous organo-tin and organo-mercury compounds were to be avoided. *Lochmann* and *Schlosser* presented independently in the late 1960s the use and preparation of so-called superbasic mixtures.[42] They consist of an alkali metal alkoxyde (*e. g.* KOR) and a lithium organic reagent (Li–C) and were therefore called LiCKOR.

To facilitate dual metalation of Me_2PPh, the phosphane was mixed with KO*t*Bu and *t*BuLi was slowly added drop wise at room temperature. Thereby, a superbase formed *in situ*, promoting deprotonation of both methyl groups. The precipitated powder was filtered, washed, suspended in pentane and $S(NSiMe_3)_2$ was slowly added at -78 °C. After some time several crystals, suitable for structural analysis, were obtained. Unfortunately, the yield was very low, so that no NMR spectra could be recorded. The double deprotonation probably had not completed or the ligand was partly decomposed by the superbase. The molecular structure of **23** is shown in Figure 4-1. The compound crystallises in the monoclinic space group $P2_1/c$ with the whole molecule and one equivalent of pentane in the asymmetric unit.

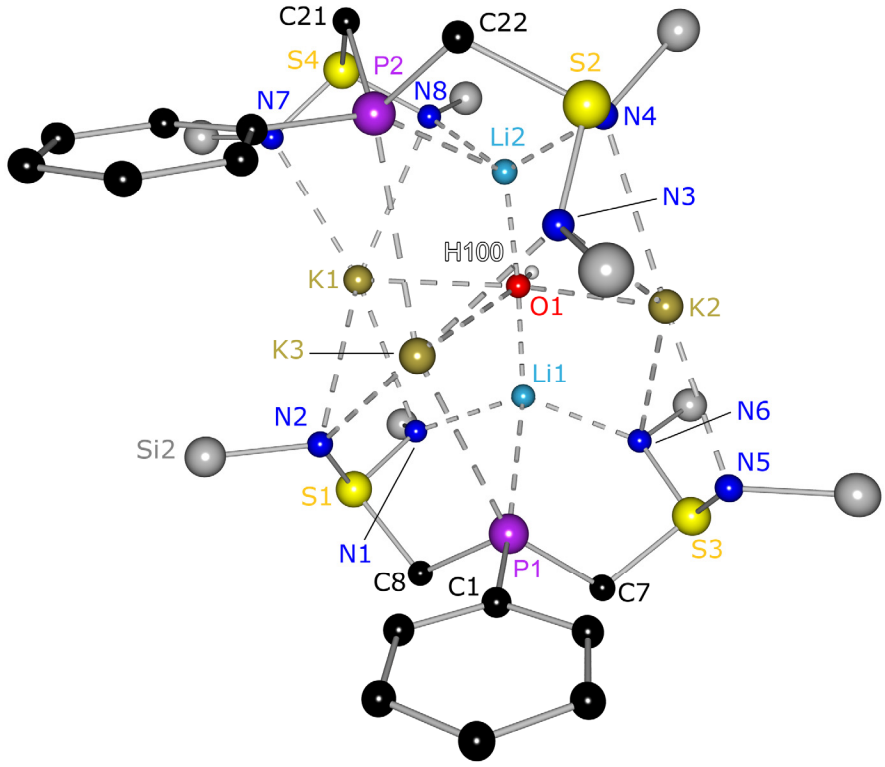

Figure 4-1: Molecular structure of $[Li_2K_3\{PhP(CH_2S(NSiMe_3)_2\}_2OH]$ (**23**). Hydrogen atoms and the methyl groups of the trimethylsilyl substituents are omitted for clarity.

The complex is a dimer formed by two $\{PhP\{CH_2S(NSiMe_3)_2)\}_2\}^{2-}$ ligands, two lithium atoms, three potassium cations and one hydroxide ion. The hydrogen position was taken from the difference *Fourier* map and refined freely. The two lithium monocations have the same coordination sphere. They are bound to two nitrogen atoms of two different diimido moieties, one phosphorus atom of the same ligand and the central $(OH)^-$ ion. The coordination polyhedron can be describes as distorted tetrahedron with angles of 120.54(17)° (P1–Li1–O1) and 133.08(19)° (N1–Li1–N6).

The potassium cations have different coordination geometries. K1 and K2 are fivefold coordinated by four nitrogen atoms of two diimido moieties of both ligands and the $(OH)^-$ ion in a distorted square pyramidal manner (N2–K1–O1: 88.77(5)°, N1–K1–N7: 168.82(5)°) with the oxygen atom at the apex of the pyramid. The N5–K2–N6 and N4–K2–N3 planes are inclined by 49.6°, thereby promoting the distortion. K3 is complexed by two nitrogen atoms, both phosphorus atoms and the hydroxide ion in a distorted square pyramidal manner. The N2–K3–N3 (167.90(6)°) and N2–K3–O1 (84.80(5)°) angles point that out. The oxygen atom is bridging all the metal ions in the structure with bond lengths of O1–Li1 1.920(4) Å, O1–K1 2.7438(16) Å and O1–K3 3.2473(18) Å. The bond to K3 is rather long and is in the upper range for such distances.[68] Selected bond lengths and angles can be found in Table 4-1.

The two ligands act as pentadentate chelates with all four nitrogen and the phosphorus atom taking part in the metal coordination. Interestingly, both the hard and the soft donor sites coordinate the lithium and the potassium ions at the same time. Just N2/N7 and N3/N5 bind to potassium cations only, with bond lengths of N2–K1 3.0646(18) Å and N2–K3 2.7638(18) Å. N1, which is bonding to Li1 and K1, has bond lengths of 2.110(4) Å (Li1–N1) and 2.8888(18) Å (K1–N1), respectively. As expected, the N–Li bond is considerably shorter than the N–K bond. The phosphorus atoms P1 and P2 are connected to one lithium and one potassium cation, each showing bond distances of 2.655(4) Å (P1–Li1) and 3.3326(8) Å (P1–K3). Both ligand units are only slightly strained as can be seen from the angles around C8 and P1, which do not deviate much from the ideal tetrahedral angle, for example S1–C8–P1: 110.69(11)° and C8–P1–C1: 103.58(10)°.

Table 4-1: Selected bond lengths [Å] and angles [°] in **23**

S1–N1	1.6182(18)	N1–S1–N2	108.22(9)
S1–N2	1.6110(17)	S1–C8–P1	110.69(11)
S1–C8	1.817(2)	C8–P1–C1	103.58(10)
P1–C7	1.841(2)	C1–P1–Li1	151.41(10)
P1–C8	1.849(2)	N1–Li1–P1	85.18(13)
N1–K1	2.8888(18)	N6–Li1–O1	114.08(18)
N2–K1	3.0646(18)	P1–Li1–O1	120.54(17)
N2–K3	2.7638(18)	N1–K1–N2	52.03(5)
N1–Li1	2.110(4)	N2–K1–O1	88.77(5)
N6–Li1	2.094(4)	N1–K1–N7	168.82(5)
O1–Li1	1.920(4)	P1–K3–P2	148.72(2)
P1–Li1	2.655(4)	N2–K3–N3	167.90(6)
P1–K3	3.3326(8)	N2–K3–O1	84.80(5)
O1–K3	3.2473(18)	K1–O1–K2	153.95(7)
O1–K1	2.7438(16)	Li1–O1–Li2	173.52(18)
N2–Si2	1.7250(18)	Li1–O1–K3	86.59(12)

It can be concluded that it is indeed possible to deprotonate Me_2PPh twice with the help of the superbase *t*BuLi/KO*t*Bu. This reaction still has to be investigated further to make use of it on a preparative scale. In addition, a donor base should probably be added for the crystallization in order to obtain monomeric complexes and

to make the hydroxide ion dispensable as a crystallization template. It seems plausible that the discussed complex was only stable because of that capping ligand, which probably originates from traces of water or $(O\textit{t}Bu)^-$. This would also explain the very low yield in crystals. Nevertheless, a compound like $[PhP(CH_2S(NSiMe_3)_2M)_2]$ (with M = any alkali metal) is only feasible if donor bases are present to saturate the coordination sphere of the metal.

Known complexes in the literature with different alkaline metals in the same crystal structure are usually approaches towards novel superbases and therefore contain the $(O\textit{t}Bu)^-$ ligand.[146,147]

In an attempt to synthesise other ligands with two diimido moieties like **23** with better yields, TMMDA (**t**etra**m**ethyl**m**ethylen**e**d**i**amine) was deprotonated with *t*BuLi according to a published procedure.[121] The double α-lithiation of this tertiary amine is possible because of the precoordination of *t*BuLi by the substrate as already discussed in chapter 3.1. The lithiated product was suspended in pentane and two equivalents of $S(N\textit{t}Bu)_2$ were slowly added at -78 °C (Equation 4-1).

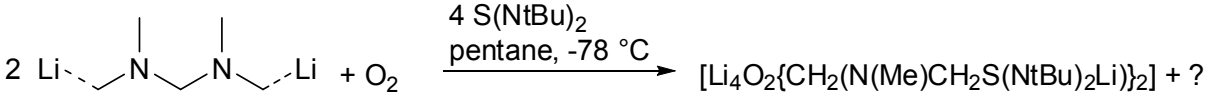

Equation 4-1: Possible preparation of $[Li_4O_2\{CH_2(N(Me)CH_2S(N\textit{t}Bu)_2Li)\}_2]$ (**24**).

After stirring over night, the suspension was filtered and the resulting light yellow solution stored at -25 °C for crystallization. The molecular structure of **24** is shown in Figure 4-2. Interestingly, there was oxygen incorporated into the compound. Most likely it was O_2 which was still dissolved in the TMMDA as the starting material was only shortly degassed prior to use. With the same batch of amine and diimide the structure was successfully reproduced. The presence of water would probably have led to the incorporation of OH^- rather than O_2^{2-}. However, the exact source of the oxygen remains uncertain.

The compound crystallises in the monoclinic space group $P2_1/c$ as a dimeric structure with an O_2^{2-} anion in the centre. The anticipated ligand $\{(CH_2(N(Me)CH_2S(N\textit{t}Bu)_2)_2\}^{2-}$ has formed, with six nitrogen atoms as possible donor sites. Interestingly, there was no formation of lithium oxide, which could have been expected when O_2 or moisture are present.

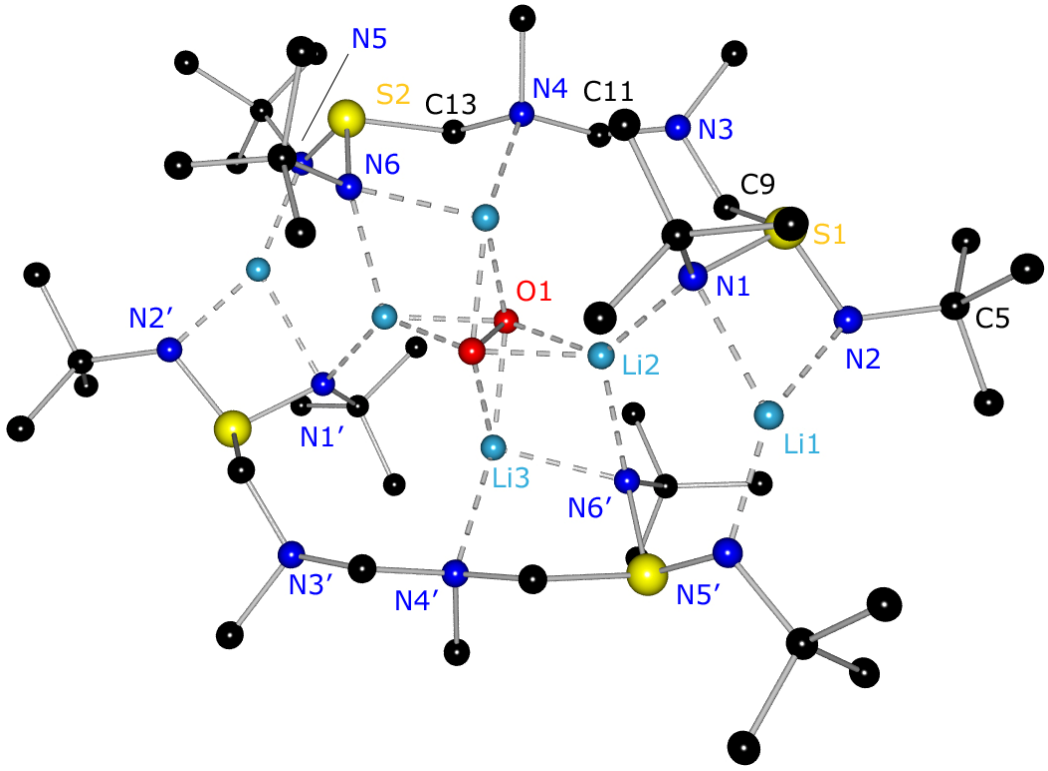

Figure 4-2: Molecular structure of $[Li_4O_2\{CH_2(N(Me)CH_2S(N\mathit{t}Bu)_2Li)\}_2]$ (**24**). Hydrogen atoms are omitted for clarity.

The oxygen molecule in the centre of the structure has a bond length of 1.559(3) Å and can therefore be regarded as a peroxide anion.[148] Both oxygen atoms are connected to four lithium cations and form a star in the centre of the structure which is surrounded by two ligands and two additional lithium ions. Li2, Li2', Li3 and Li3' are coordinated by both oxygen donors with an average bond length of 1.936(4) Å. This matches the value reported for $[Ph_4Si_2O(OLiPy)_2]_2$ which displays Li–O bonds of 1.943 Å.[149] Li2 and Li2' are additionally coordinated by two nitrogen atoms (N1/N1', N6/N6') of two diimido substituents in two ligands. Li3 is also coordinated by N6' and by N4' which is part of the TMMDA bridge. The third lithium atom, Li1, at the edge of the complex, is only threefold coordinated by N1, N2 and N3'. There is no interconnection to neighbouring molecules. All Li–N bond lengths range from 1.961(5) Å to 2.175(9) Å which is in the expected range.[68] Thus **24** is yet another example of threefold/fourfold lithium coordination in the same structure. The N1–S1–N2 angle of 102.21(11)° is more acute than in the other structures described in this thesis. In addition, the tetrahedral angle N1–S1–C9 of 100.13(11)° is quite acute. Selected bond lengths and angles in comparison with the similar complex **25** can be found in Table 4-2.

Table 4-2: Selected bond lengths [Å] and angles [°] in **24** and **25**

	24	**25**		**24**	**25**
S1–N1	1.643(2)	1.6004(16)	N1–S1–N2	102.21(11)	104.61(8)
S1–N2	1.620(2)	1.6158(15)	N5–S2–N6	---	114.51(9)
S2–N5	---	1.5551(16)	N1–S1–C9/N1–S1–C7	100.13(11)	105.23(9)
S2–N6	---	1.4924(16)	N3–C11–N4/N3–C9–N4	112.36(18)	112.16(14)
S1–C9/S1–C7	1.845(3)	1.8337(19)	N1–Li1–N2/N1–Li4'–N2	75.57(16)	75.37(12)
O1–O1‘	1.557(5)	---	Li1–N1–Li2/Li1–N2–Li4'	76.82(19)	75.09(13)
C11–O2	---	1.388(2)	N4–Li3'–N6/N2–Li1–N3	90.60(17)	90.42(13)
Li1–O1	---	1.865(3)	O1–Li2–N1/O1–Li2–N5	131.0(2)	136.80(18)
Li2–O1	1.922(5)	1.886(3)	Li2–O1–Li2‘/Li3–O2–Li3'	131.9(2)	80.65(13)
Li3–O1	1.987(5)	1.942(3)	O1–Li2–O1'/O1–Li1–O2	48.08(13)	94.19(14)
Li1–N1/Li4'–N1	2.175(9)	2.019(3)	Li2–O1–Li3'	86.8(2)	---
Li1–N2/Li4'–N2	1.961(5)	2.141(3)	Li2–N6'–Li3/Li3–N6–Li4	67.62(16)	79.68(13)
Li1–N5'/Li1–N3	1.965(5)	2.101(3)	S1–C9–N3/S1–C7–N3	112.46(15)	113.89(12)
Li2–N1/Li2–N4	2.021(4)	2.146(3)	S2–C13–N4/N4–C11–O2	114.43(15)	112.86(14)
Li3–N4'/Li3–O2	2.119(5)	1.999(3)	S1–N2–C5/S2–N6–Li4	117.86(17)	130.31(13)
Li3–N6'/Li3–N6	2.128(4)	2.084(3)			

The coordination of O_2^{2-} by four metal cations in a star formation is not unknown in the literature. In 1998, *Mulvey et al.* presented a mixed lithium/magnesium hexamethyldisilazid that can stabilise peroxide in the centre of a four-membered ring.[150] The resulting structural motif is the same as in **24**, nevertheless the yield of 1-5 % was very poor. In addition, the peroxide ion was disordered with an oxide ion. Compounds of that sort were dubbed ‘inverse crown complexes’ in comparison to crown ethers.[151] These molecules contain various oxygen donor sites and are cyclic ethers which can accommodate metal cations of the appropriate shape in the centre. **24** as well as the lithium/magnesium hexamethyldisilazide act with inverted sign. They are cyclic compounds with metal ions bonded in the ring periphery which can coordinate matching anions like peroxide, oxide,[150] hydrides [152] or even larger molecules like ferrocene.[53] In essence, the *Lewis* basic sites have been exchanged for *Lewis* acids. With this substance class, the stabilization of unusual anions as well as deprotonation reactions are feasible that are otherwise thermodynamically hindered. One example is the 2,5-deprotonation of toluene to form $(C_6H_3CH_3)^{2-}$ where the more acidic methyl group is left intact (Figure 4-3).[153]

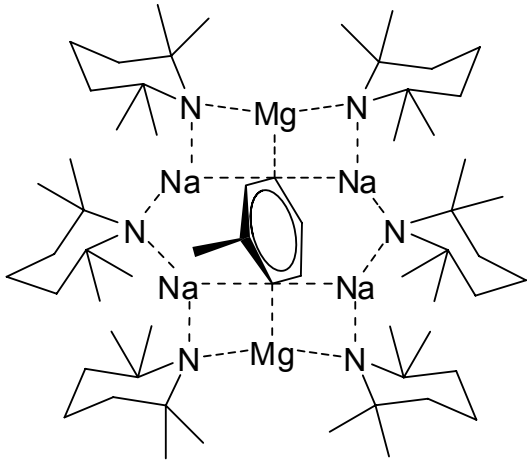

Figure 4-3: Structure of $[Na_4Mg_2(tmp)_6(C_6H_3CH_3)]$, (tmp = 2,2,6,6-tetramethylpiperidine).[153]

This phenomenon is probably due to the position of the magnesium atoms in the ring and presents a great advantage over *n*BuLi/TMEDA. This mixture is only able to deprotonate toluene twice in a random and unpredictable way.[154] It has to be considered, however, that most of the reported structures of 'inverse crowns' so far contain two different metals in the ring which leads to synergistic effects and the ring itself is only held together by amides.

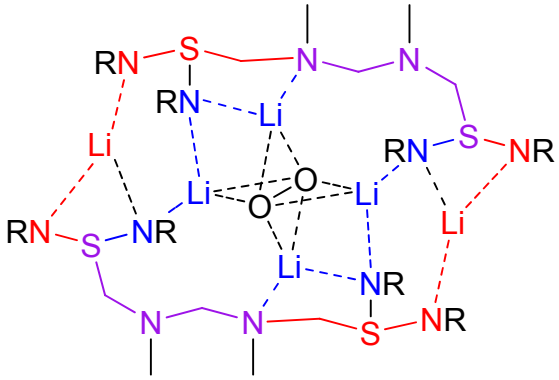

Figure 4-4: 'Ring in the ring' structure; blue: inner ring, red: outer ring, purple: part of both rings.

With this concept in mind it is noteworthy that **24** contains different heteroatoms in the ring and can be regarded as a 'ring in the ring' system. There is an outer 20-membered ring of the two ligands which are connected by two lithium atoms, Li1 and Li1'. The inner ring is consisting of 18 atoms and is directly coordinating the peroxide dianion (Figure 4-4).

In analogy to **24,** the reaction of lithiated TMMDA with $S(NSiMe_3)_2$ was performed to yield $[Li_4\{(NSiMe_3)_2SCH_2N(Me)CH_2N(Me)CO\}\{NSN(SiMe_3)\}(O\textit{t}Bu)]_2$ (**25**). In this

reaction, the desired ligand was only formed in small yield as heavy ligand scrambling occurred. One ligand can be described with the formula $\{(Me_3SiN)_2SCH_2N(Me)CH_2N(Me)CH_2(O)\}^{2-}$ (**L1**). Another ligand is $\{Me_3SiNSN\}^-$ (**L2**) which originates from a sulphur diimide after N–Si bond cleavage. The third ligand is $\{O\textit{t}Bu\}^-$ (**L3**) which is disordered with $\{OSiMe_3\}^-$ (27 % *vs.* 73 %), with the trimethylsilyl group originating from the cleaved diimide and the *tert*-butyl group from the utilized *t*BuLi. It becomes clear with this structure in mind that the starting material was indeed contaminated with oxygen (see Figure 4-5).

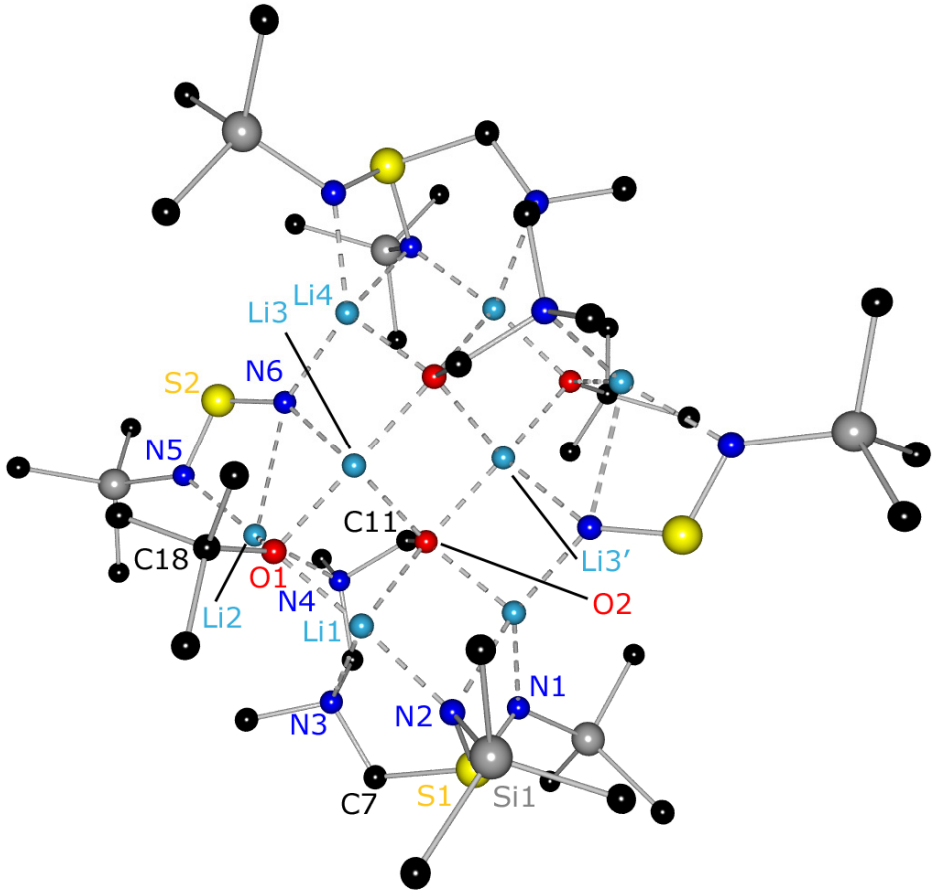

Figure 4-5: Molecular structure of $[Li_4\{(NSiMe_3)_2SCH_2N(Me)CH_2N(Me)CO\}\{NSN(SiMe_3)\}(O\textit{t}Bu)]_2$ (**25**). Hydrogen atoms are omitted for clarity.

In addition, the reactivity of the lithiated amine seems to be too high for $S(NSiMe_3)_2$ as it is partially cleaved during the reaction. Even lower temperatures than -78 °C should be employed during the synthesis to avoid this.

There are eight lithium cations in the structure that are coordinated in four different ways. Li1 is distorted tetrahedrally coordinated by two nitrogen atoms and one oxygen atom of **L1** as well as by the $O\textit{t}Bu^-$ anion. The N–Li and O–Li bonds do not show any unusual values. Both the N2–Li1–N3 (90.42(13)°) and O1–Li1–O2

(94.19(14)°) angles are close to 90°. The coordination geometry of Li2 can be described as a trigonal pyramid. The base is formed by O1, N4 and N5 (O1–Li2–N5: 136.80(18)°) with N6 at the apex. Li3 is distorted tetrahedrally coordinated by three oxygen atoms O1, O2 and O2' and by N6. Consequently, it is interconnecting both halves of the dimer. Li4 on the other hand is coordinated by the diimido nitrogen atoms N1' and N2' of **L1**, N6 and O2' in a distorted tetrahedral manner. In that way, the centre of the structure is consisting of seven four-membered rings which are interconnected.

The bond lengths in the two diimido ligands **L1** and **L2** differ considerably. While N1–S1 (1.6004(16) Å) and N2–S1 (1.6158(15) Å) are in the typical range for diimido sulfinates, N5–S2 (1.5551(16) Å) and N6–S2 (1.4924(16) Å) are significantly shorter. Generally speaking, the bond lengths and angles in **L1** are almost the same as in the corresponding ligand in **24**.

To summarize the results, it has to be acknowledged that it is possible to link two sulphur diimides by a diamino bridge. Nevertheless, if the synthetic route according to Equation 4-1 is employed, anions are needed to balance the electron deficiency. Especially **24** seems to be an excellent oxygen scavenger as even the degassing of the reactants leads to high yields of the peroxide containing complex. However, these new ligands show the versatility of the sulphur diimido moiety and its value in ligand design.

Conclusion

All new complexes that have been presented so far, arranged in their different categories, are depicted in Figure 4-6. The functionalization of sulphur diimides with donor-containing side-arms was achieved. These can be modified regarding their steric bulk and the HSAB hardness of the donor. The electronic properties of the ligand can be tuned by the choice of the sulphur diimide. Thus, the different building units can be combined to synthesise the ligand of choice. Through this modularity different coordination modes can be achieved, *e. g.* $[Li\{Me_2N(C_6H_4)S(NSiMe_3)_2\}]_2$ (**16**) and $[(t\text{BuN})_2S{\cdot}\{LiMe_2N(C_6H_4)S(Nt\text{Bu})_2\}_2]$ (**19**). Additionally, the phosphorus atom can be oxidised with oxygen (**12**, **13**), sulphur (**8**) or selenium (**9**) in order to modify the coordination claw. By choice of the right reaction conditions, the free ligand (**10**) and a monomeric complex (**11**) can be synthesised which are promising precursors for metalation reactions. It could also be shown that the side-arms are weakly

bonding in solution and can be exchanged by better donors (**17**), proving the hemilability of the system.

The connection of two sulphur diimides with TMMDA yields multidentate complexes that are reminiscent of inverse crown complexes.

Metal exchange reactions of the lithiated amines with alkali metal *tert*-butoxides give access to interesting coordination compounds. It seems that the adaption of the ligands to different ionic radii is unproblematic and stable complexes of lithium, sodium and potassium are formed.

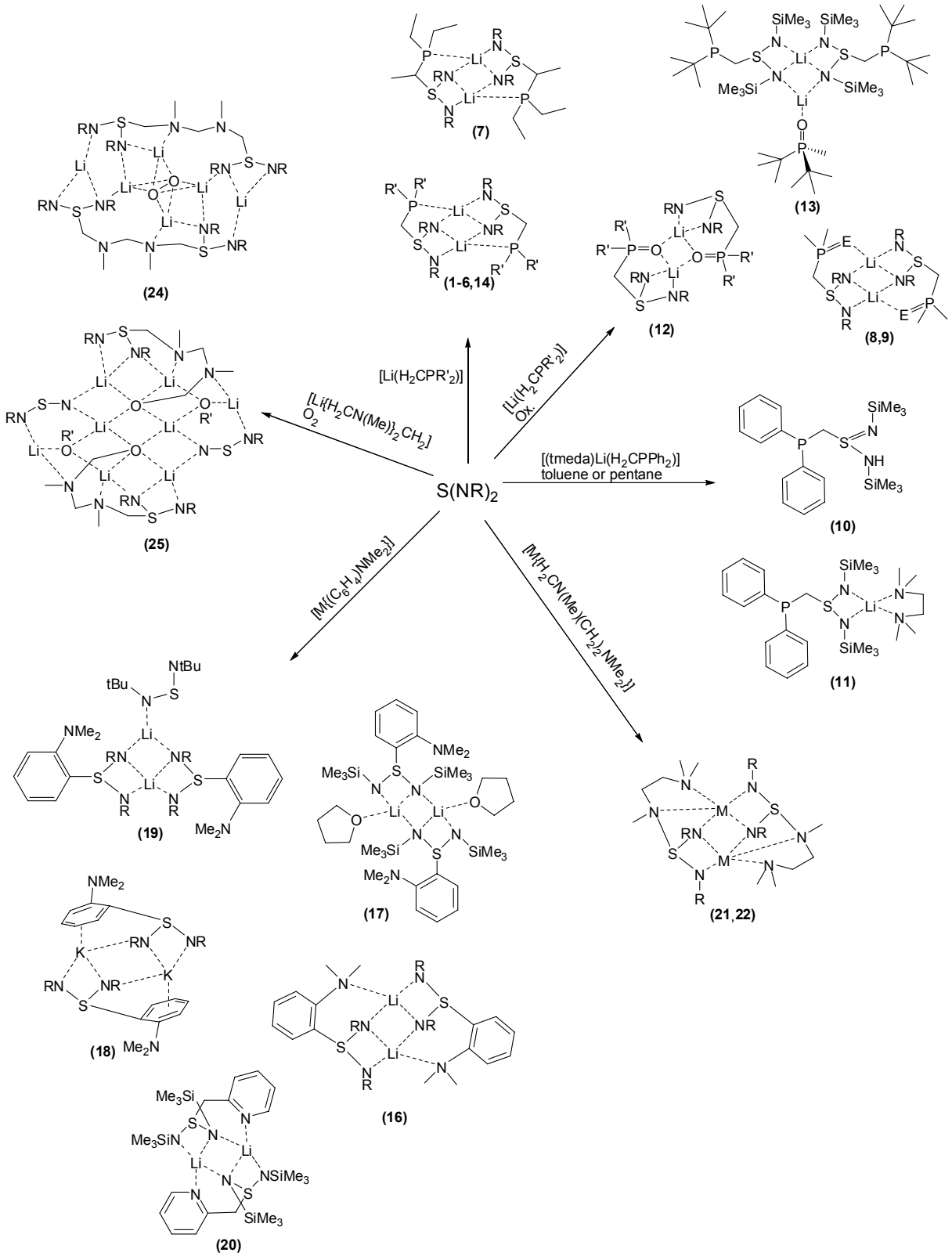

Figure 4-6: Novel sulphur diimido complexes with (potential) side-arm donation; R = *t*Bu, $SiMe_3$; R' = Me, Ph.

5 FROM MAIN GROUP TO TRANSITION METALS

5.1 Monometallic Complexes

The lithium complexes discussed in the previous chapters have demonstrated the flexibility and versatility of this class of new hemilabile *Janus* head ligands. It would now be of interest to promote metal exchange reactions to explore their full complexation potential. Cations, dications as well as main group and transition metals were employed in order to get a broad overview.

Direct transmetalation of the lithium dimers with metal halides was successful in the case of $MgCl_2$ only. The ineptness for metal halides in general for such reactions with sulphur diimido compounds has already been discussed above. The use of $MgCl_2$ was probably successful because of the diagonal relationship to lithium.

Unfortunately, $Ph_2PCH_2S(NSiMe_3)(HNSiMe_3)$ has a long crystallization time of months rather than weeks. Therefore, it is not a good starting material. A substance would be preferred that can be synthesised in reasonable time. Therefore, another method or starting material had to be found. As already discussed concerning the NSCP ligands, another reaction to obtain the desired metal-free ligands is not feasible – transmetalation is inevitable. It should be possible to transmetalate lithium diimido complexes if the lithium metal is already precoordinated by another donor. This principle is quite intuitive as the lithium cation is not coordinated as firmly and can be removed easier. With this in mind, [(tmeda)Li{$Ph_2PCH_2S(NSiMe_3)_2$}] (**11**) should be a good starting point, as the lithium atom is not only complexed by the diimido nitrogen atoms but as well by a TMEDA molecule. In addition, **11** can be prepared in high purity as well as in reasonable yield and time.

5.1.1 Alkaline Earth Metals

Because of the diagonal relationship to lithium, magnesium was the first metal to be employed in a salt elimination reaction. Although the use of metal halides for such syntheses is sometimes problematic with sulphur diimide derivatives because of their redox-activity,[58] the reaction of **1** with $MgCl_2$ in a 1:1 molar ratio afforded the spirocyclic species [Mg{$Me_2PCH_2S(NtBu)_2$}$_2$] (**26**) according to Equation 5-1.

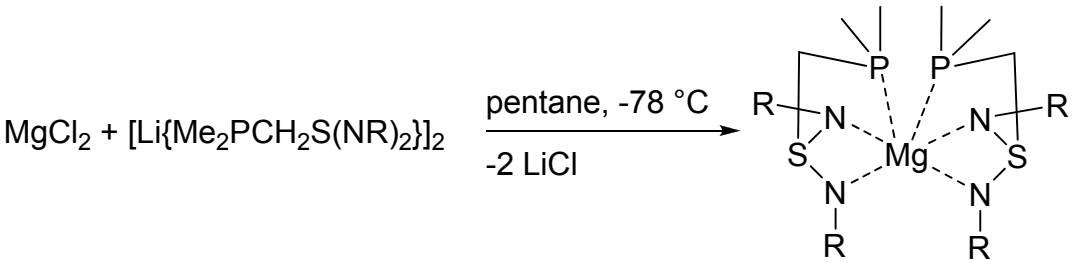

Equation 5-1: Preparation of [Mg{$Me_2PCH_2S(NR)_2$}$_2$]; R = *t*Bu (**26**), R = $SiMe_3$ (**27**).

The formation of this magnesium complex demonstrates that the new *Janus* head ligands are valuable multidentate chelating ligands due to the intramolecular phosphane donor site held in close spatial proximity to the functional imido groups. Complex **26** crystallises at 4 °C from pentane as colourless plates in the orthorhombic space group *Fdd*2 (Figure 5-1) with half a molecule in the asymmetric unit.

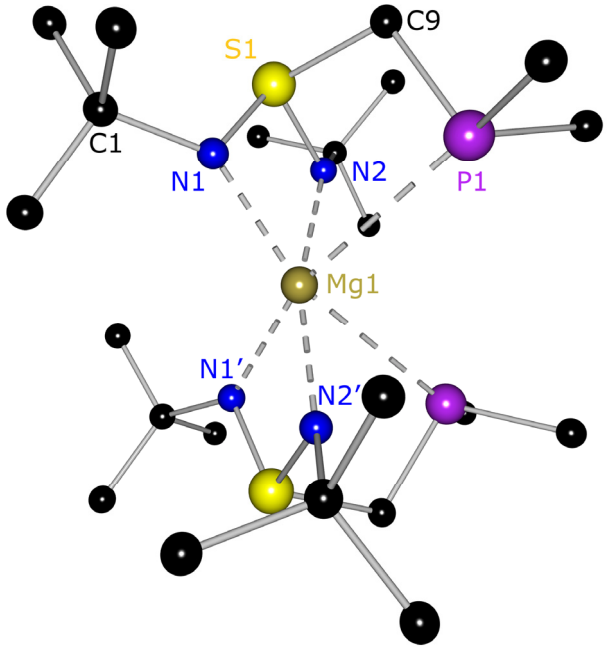

Figure 5-1: Molecular structure of [Mg{$Me_2PCH_2S(NtBu)_2$}$_2$] (**26**). Hydrogen atoms are omitted for clarity.

As the compound undergoes a destructive phase transition at about 220 K the X-ray data set had to be collected at -23 °C (Figure 5-2). The marked reflex clearly indicates a splitting of the crystal between 219 and 207 K. In order to get a data set that would be resolved better, it should be tried to crystallise the compound at a temperature which lies below the phase transition barrier.

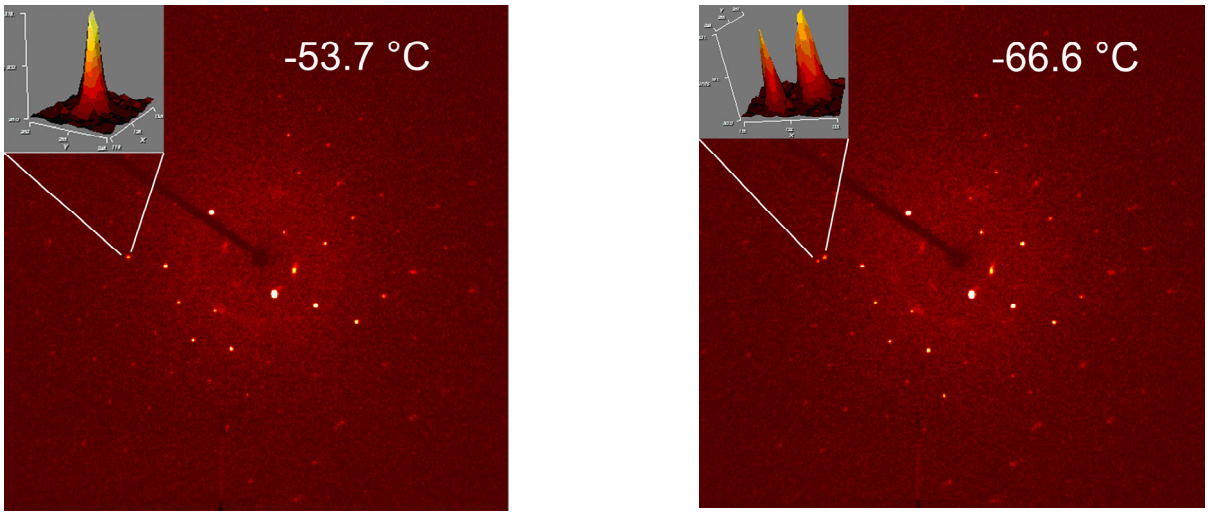

Figure 5-2: Diffraction pattern of a single crystal of [Mg{$Me_2PCH_2S(NtBu)_2$}$_2$] (**26**) at different temperatures and in the same orientation.

The monomeric structure shows a distorted octahedral geometry at the central magnesium dication. The molecule has a crystallographically imposed twofold symmetry with the magnesium atom located at the twofold axis. It is coordinated by two nitrogen atoms and one phosphorus atom of each phosphane side-arm as a five membered chelating ring with bite angles of 74.24(8)° (N1–Mg1–P1) to 70.82(8)° (N2–Mg1–P1). This means that the NSCP ligand behaves in a tridentate manner, thus demonstrating tripodal donation by means of two terminal nitrogen atoms and side-arm donation by the phosphorus atom.

Coordination of the magnesium atom shows Mg–N distances in the range of 2.102(2) Å to 2.138(2) Å. These values are similar to those reported for compounds containing a sulphur-bonded imido nitrogen donor (2.035-2.295 Å).[34,69] The Mg–N bond distances are marginally longer than in [Mg{$(NSiMe_3)_2SN(SiMe_3)_2$}$_2$] (2.0592(6) Å), probably because in that complex side-arm donation is hindered due to steric reasons.[155] The Mg–P bond length is not consistent with the predicted covalent value (2.65 Å). The distance of 2.9855(13) Å is elongated in comparison to Mg–P distances in mononuclear and dinuclear magnesium phosphanides *e. g.* [BuMg{$P(CH(SiMe_3)_2)(C_6H_4$-2-OMe)}]$_2$ (2.5760(8) Å and 2.5978(8) Å) or [Mg{$P(CH(SiMe_3)_2)(C_6H_4$-2-CH_2NMe_2)}]$_2$ (2.556(1) Å).[156] This elongation of the Mg–P bond distance is attributed to the side-arm donation of a phosphane rather than coordination of a phosphanide. **26** is therefore closer related to [Mg{$(C_6H_3)(H_2CPMe_2)_2$}$_2$] which displays Mg–P bond lengths of 2.770(1) Å and 2.761(1) Å.[157] With a different central metal, it would be possible to reversibly cleave the metal-phosphorus-bond to generate a pendent donor site for other softer metal

cations. The N–S–N bond angle (97.43(12)°) is more acute than in **1** and those in alkali metal derivatives (104.2-110.7°), but covers almost the same range as in comparable compounds with Mg^{2+} or other dicationic metals (97.6-98.9°).[82,155,158] This can be attributed to the higher charge of the magnesium dication, leading to a stronger repulsion between the positively charged sulphur atom and the metal ion. Selected bond lengths and angles of **26** compared to [Mg{$Me_2PCH_2S(NSiMe_3)_2$}$_2$] (**27**) can be found in Table 5-1.

Table 5-1: Selected bond lengths [Å] and angles [°] in **26** and **27**

	26	**27**		**26**	**27**
S1–N1	1.617(2)	1.6123(8)	N1–S1–N2	97.43(12)	100.44(4)
S1–N2	1.622(2)	1.6111(8)	S1–C9/P1–C7	108.24(16)	107.75(5)
P1–C9/C7	1.838(4)	1.8481(10)	N1–Mg1–N2	70.07(9)	70.81(3)
S1–C9/C7	1.838(4)	1.8263(10)	N1–Mg1–P1	74.24(8)	72.54(2)
Mg1–N1	2.102(2)	2.1481(8)	N1–Mg1–P1'/P2	163.71(8)	100.47(2)
Mg1–N2	2.138(2)	2.1276(8)	N2–Mg1–P1'/P2	98.35(8)	163.15(2)
Mg1–P1	2.9855(13)	2.8570(4)	N2–Mg1–N2'	164.93(17)	---
N1–C1/Si1	1.481(4)	1.7237(8)	N1–Mg1–N4	---	169.95(3)

The magnesium complex [Mg{$Me_2PCH_2S(NSiMe_3)_2$}$_2$] (**27**) was equally isolated from a transmetalation reaction of **4** with $MgCl_2$ in equimolar ratio. Unlike compound **26** which undergoes a phase transition at about 220 K, **27** is stable when cooled to 100 K. The complex crystallises at -25 °C from pentane as colourless blocks in the monoclinic space group $P2_1/n$ and the structure is monomeric. The phosphane diimido moiety is attached to the magnesium atom in a tripodal fashion involving donation from two terminal nitrogen atoms and the side-arm donation from the phosphorus atom (Figure 5-3). In the solid state the central magnesium atom in **27** approximately adopts an octahedral coordination polyhedron, consisting of two phosphorus and four nitrogen atoms of two ligands. The structural motif is the same as in the magnesium compound **26**. Selected bond lengths and angles in comparison with the latter can be found in Table 5-1.

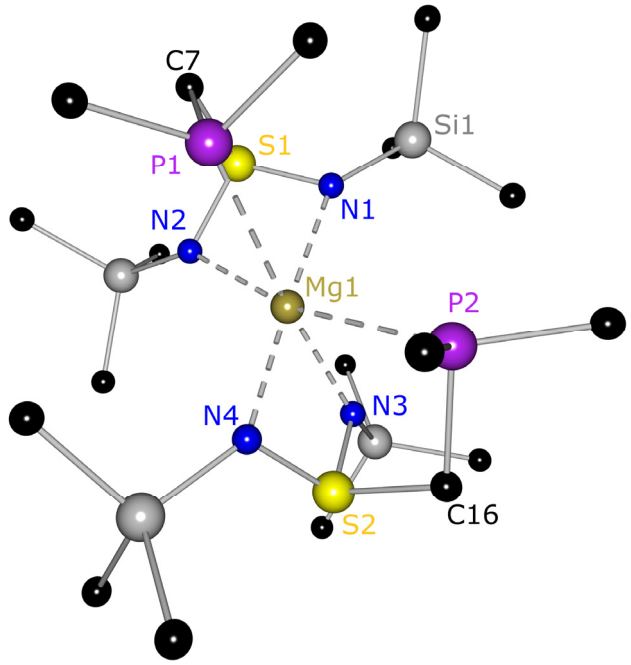

Figure 5-3: Molecular structure of [Mg{$Me_2PCH_2S(NSiMe_3)_2$}$_2$] (**27**). Hydrogen atoms are omitted for clarity.

The synthesis of the magnesium complexes **26** and **27** has proven that two NSCP ligands have the ability to complex small dications in a hexadentate manner. Consequently, it was of interest what coordination geometry would be adapted by a larger dication. For comparison reasons, the heavier homologues calcium and strontium were employed. Unfortunately, it was only possible to obtain crystals of the two magnesium complexes *via* the salt elimination route. The use of other metal halides did not yield the desired products. Therefore the second route – transmetalation of **11**, where the lithium atom is already precoordinated – was pursued.

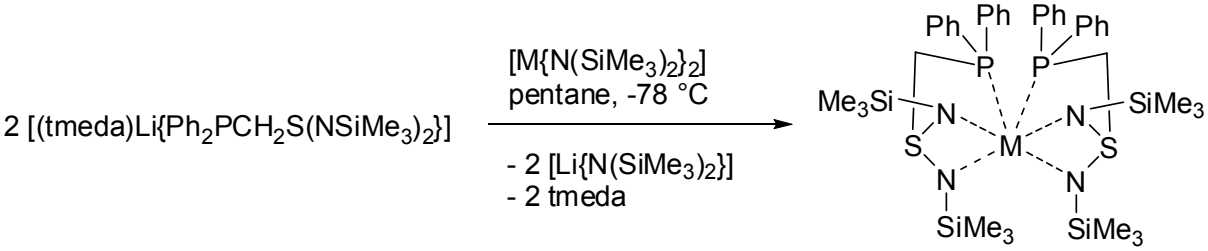

Equation 5-2: Preparation of metal complexes [M{$Ph_2PCH_2S(NSiMe_3)_2$}$_2$], M = Ca, Sr, Co, Fe.

β-diketiminato-calcium complexes are known to catalyse hydroamination and hydrophosphination reactions of alkenes and alkynes or carbodiimides.[159] This addition of the P–H bond of a primary or a secondary phosphane can also be promoted by trivalent lanthanide catalysts or transition metals. The catalytic activity of alkaline earth metals is thus not unknown in the literature. Benzyl alkaline earth

metals are precatalysts for the hydrosilylation of alkenes.[160] Calcium has the advantage over many other metals to be readily available, cheap and non-toxic which is most advantageous if it is to be used in polymerization reactions. This has *e. g.* been studied by *Souter et al.* for 2-vinylpyridine.[161]

The reaction of $[Ca\{N(SiMe_3)_2\}_2]$ with $[(tmeda)Li\{Ph_2PCH_2S(NSiMe_3)_2\}]$ (**11**) proceeded with a complete metal exchange according to Equation 5-2. It could have been speculated that the large calcium atom would be coordinated by the pendent phosphorus side-arm and the smaller lithium cation would remain between the nitrogen atoms yielding a heterobimetallic complex. This was not observed; a dimer of formula $[Ca\{Ph_2PCH_2S(NSiMe_3)_2\}_2]$ (**28**) was formed instead, with the calcium dication being coordinated by the four nitrogen and two phosphorus atoms of two ligands (Figure 5-4) in a tridentate, cap-shaped manner. The coordination of the SNCP ligand resembles the coordination of $S(NtBu)_3^{2-}$ in $[(thf)_2Li_2Ca\{(NtBu)_3S\}_2]$ [58] and **28** could be regarded as a monometallic analogue of that complex. The coordination cannot be described as an octahedron as it is too distorted. One could rather speak of two NNPCa tetrahedra that are linked *via* their apexes over the central calcium dication.

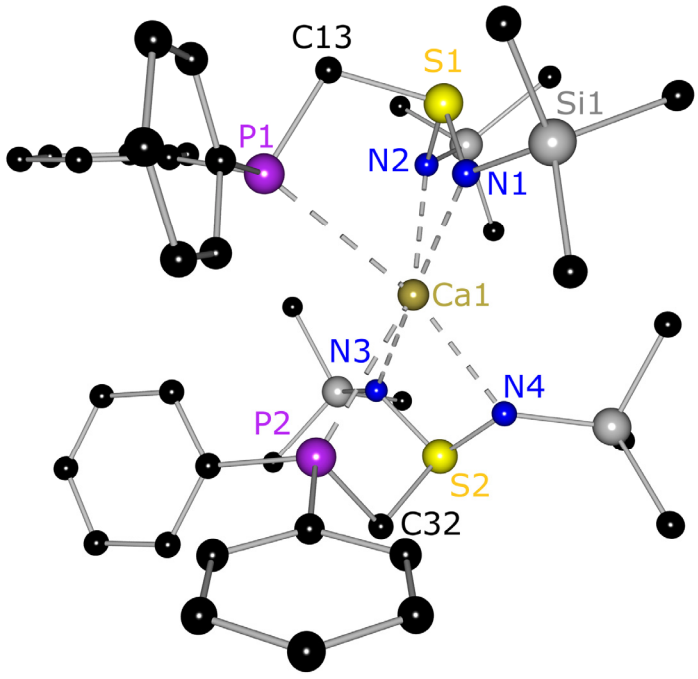

Figure 5-4: Molecular structure of $[Ca\{Ph_2PCH_2S(NSiMe_3)_2\}_2]$ (**28**). Hydrogen atoms are omitted for clarity.

The angles of N1–Ca1–N2 63.47(6)° and N2–Ca1–P1 71.20(5)° around the calcium atom make that clear. Both tetrahedra are twisted by 55° with respect to each other, inhibiting an alignment of the two phosphorus donor atoms. Despite of

the different ligand, the structure is very similar to the magnesium complexes **26** and **27**. Selected bond lengths compared with other metal complexes can be found in Table 5-2, angles in Table 5-3.

Table 5-2: Selected bond lengths [Å] in **28** to **31**

	28 (Ca)	**29 (Sr)**	**30 (Co)**	**31 (Fe)**
S1–N1	1.6078(19)	1.6056(12)	1.6051(17)	1.606(2)
S1–N2	1.6076(17)	1.6013(13)	1.6177(17)	1.6151(19)
N1–Si1	1.7223(18)	1.7138(13)	1.7251(16)	1.7276(19)
S1–C13	1.831(2)	1.8254(15)	1.834(2)	1.836(2)
P1–C13	1.847(2)	1.8454(15)	1.849(2)	1.846(2)
N1–M1	2.4198(18)	2.5495(12)	2.1228(16)	2.1523(18)
N2–M1	2.3909(19)	2.5517(14)	2.1402(16)	2.1697(19)
N3–M1	2.4378(18)	2.5374(13)	2.1245(15)	2.1785(19)
N4–M1	2.3960(18)	2.5698(12)	2.1429(16)	2.1475(18)
P1–M1	3.0815(7)	3.1804(5)	2.8421(6)	2.7569(7)
P2–M1	3.0219(7)	3.1608(5)	2.7409(6)	2.8279(7)

Table 5-3: Selected angles [°] in **28** to **31**

	28 (Ca)	**29 (Sr)**	**30 (Co)**	**31 (Fe)**
N1–S1–N2	103.80(9)	104.73(7)	99.75(8)	99.95(10)
S1–C13–P1	107.70(11)	108.20(8)	105.95(10)	105.68(12)
S1–N1–Si1	121.71(11)	122.93(8)	121.80(10)	122.12(11)
C1–P1–C7	105.86(10)	106.36(7)	102.65(9)	101.22(10)
N1–M1–N2	63.47(6)	59.71(4)	70.63(6)	69.59(7)
N2–M1–P1	71.20(5)	66.70(3)	70.60(5)	71.19(5)
N3–M1–N4	63.37(6)	59.77(4)	70.18(6)	69.88(7)
N4–M1–P2	71.88(4)	60.91(3)	71.66(5)	77.33(5)
P1–M1–Nx	158.40(5) (N4)	154.03(3) (N3)	172.27(4) (N3)	170.87(5) (N4)
N1–M1–Nx	175.82(6) (N3)	176.82(4) (N4)	110.39(6) (N3)	109.86(7) (N3)

It is striking that the phosphorus atoms are on the same side of the molecule and not on opposite sides as one could expect to reduce steric strain. When taking a closer look this assumption is not the case. If the phenyl rings would be arranged on opposite sides of the molecule the hydrogen atoms of the trimethylsilyl groups and

the rings would come too close to each other. In the arrangement that exists in the crystal, the four phenyl rings are twisted by approximately 90° with respect to each other, thereby evading that problem. In addition, it has already been established by theoretical investigations that the heavier alkaline earth metals show not only ionic but also covalent bonding properties. This is achieved by contribution of the d-orbitals and the high polarisability of the sub-valence shells, making the atom non-spherical.[162] Therefore, the heavier alkaline earth metal halides and hydrides have bent rather than linear structures.

It is thinkable that the arrangement of the phosphorus atoms in **28** is also controlled by these facts, which is underlined by the geometry of the complex. Thus, σ-bonding character between the phosphorus p-orbital and the calcium d-orbital could be responsible for the *cis*-arrangement of the phosphorus side-arms as well as the polarisation of Ca^{2+} by the ligand. A similar *cisoid* arrangement of ligands was found in $[(thf)Ca\{(NSiMe_3)_2PPh_2\}_2]$ [163] and $[(N\text{-carbazolyl})_2Ba(dme)_3]$ [164] and discussed accordingly.

The bond lengths in **28** are all in the expected range and are comparable to other similar phosphorus-calcium or nitrogen-calcium complexes, although the phosphorus-calcium bonds are somewhat elongated.[165]

The reaction of **11** with $[Sr\{N(SiMe_3)_2\}_2]$ afforded the strontium complex **29** as colourless crystals. The structure which is depicted in Figure 5-5 is isosteric to the calcium complex **28**.

The nitrogen-strontium and phosphorus-strontium bond distances are elongated in comparison to the calcium complex which is due to the larger ionic radius of strontium. They are in the range of the bis(diphosphanylamido) complex $[(thf)_3Sr\{(Ph_2P)_2N\}_2]$ [165b] and aminotroponiminate complexes [165c] that have comparable steric requirements. The N1–S1–N2 angle is slightly widened in comparison to the calcium complex (104.73(7)° *vs.* 103.80(9)°) as well as the S1–C13–P1 angle (108.20(8)° *vs.* 107.70(11)°).

On the other hand, the angles around the strontium dication are considerably more acute than in the calcium complex. This could be due to the fact that the bond lengths to the donor atoms are longer because of the increased ionic radius and the ligand is located further away from the central metal. Consequently the angles have to become more acute. The arrangement of the phosphorus side-arms is the same as in the corresponding calcium complex, however the bending of the ligand is

reduced (S1–Ca1–S2: 158.103(19)°, S1–Sr1–S2: 162.896(10)°) which might be due to the larger cation size.

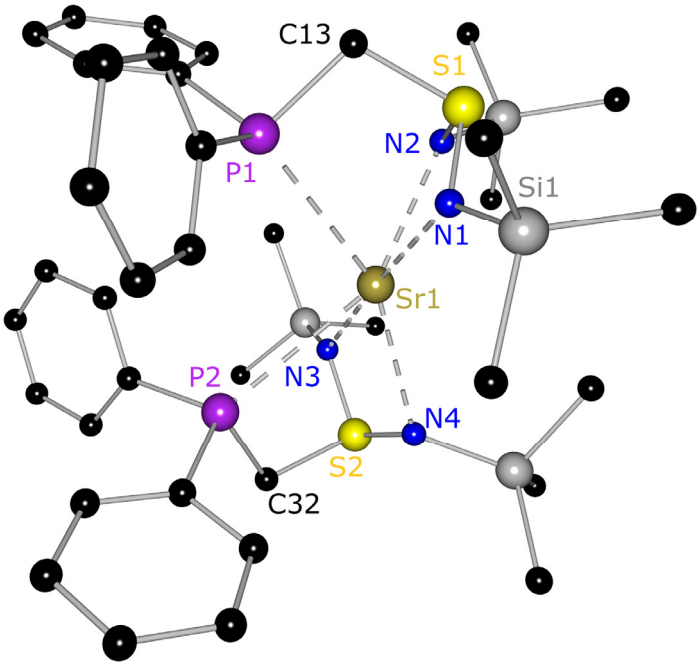

Figure 5-5: Molecular structure of $[Sr\{Ph_2PCH_2S(NSiMe_3)_2\}_2]$ (**29**). Hydrogen atoms are omitted for clarity.

In essence, it could be shown that the new ligand $\{R_2PCH_2S(NSiMe_3)_2\}^-$ is indeed very flexible and versatile as it can form stable complexes of the lower and higher homologues of the alkaline earth metals. In the cases described here the ionic radii range from 72 pm (Mg^{2+}) to 121 pm (Sr^{2+}) for the coordination number six. The connectivity is always the same with all nitrogen and phosphorus atoms taking part in the coordination, regardless of the HSAB hardness of the central metal. There is no formation of aggregates, which usually is a known property of the heavier alkaline earth metals because of their very large ionic radii.[166] It can be concluded that the ligand employed is sterically demanding enough to block certain coordination sites and prevent the formation of aggregates. This is a great advantage regarding possible catalytic applications as it ensures the complex to remain intact during and after the reaction.

It is also known that the coordination behaviour and the chemistry of the alkaline earth metals is comparable to certain lanthanides.[167] This becomes evident if the ionic radii of Ca^{2+} and Sr^{2+} are contrasted with those of Yb^{2+} and Sm^{2+} or Eu^{2+}: 106 and 121 *vs.* 108, 122 and 120 pm (for coordination number six).[168,169] For the future it would therefore be very interesting to employ metal amides of some lanthanides in

the metal exchange reactions discussed above and compare them to their alkaline earth metal counterparts.

5.1.2 Transition Metals

To further investigate the complexation potential of the new ligand, bivalent transition metals were employed in the synthesis. Cobalt was chosen as a central metal because it is easily accessible and has two stable oxidation states that should be well interconvertible. It would be of great interest to compare the coordination of the same metal in different oxidation states by the same ligand. Cobalt complexes are being employed as catalysts for the release of hydrogen from ammonia borane, NH_3BH_3, which is a very good hydrogen storage material.[170] This is desirable because the combustion of hydrogen produces no toxic by-products and thus is a favourable source of energy. In contrast to methane, there is no formation of CO_2 after release of the hydrogen from ammonia borane. It contains a high hydrogen percentage (19.6 wt%) and possesses good stability because it is solid at room temperature and therefore does not have to be stored under pressure like hydrogen gas.[171]

Cobalt(II) compounds with tridentate bispyridyl-based nitrogen ligands are highly active catalysts for the oligomerization of ethylene.[172] There also exists an application of Co(II) phosphane complexes in the hydrovinylation of styrene with excellent chemoselectivity.[173]

From the experience gained with the alkaline earth metal complexes it was clear that bivalent metals form very stable compounds with the ligand $\{Ph_2PCH_2S(NSiMe_3)_2\}^-$. Therefore $[Co\{N(SiMe_3)_2\}_2]$ was reacted with **11** according to the general reaction scheme (Equation 5-2). After storing the solution at 4 °C for several hours, blue to purple crystals suitable for X-ray crystallography could be obtained. The structure crystallises in the orthorhombic space group *Pna*2_1. It has the same characteristics as the other complexes discussed above and is shown in Figure 5-6. The bond lengths and angles can be found in Table 5-2 and Table 5-3, respectively.

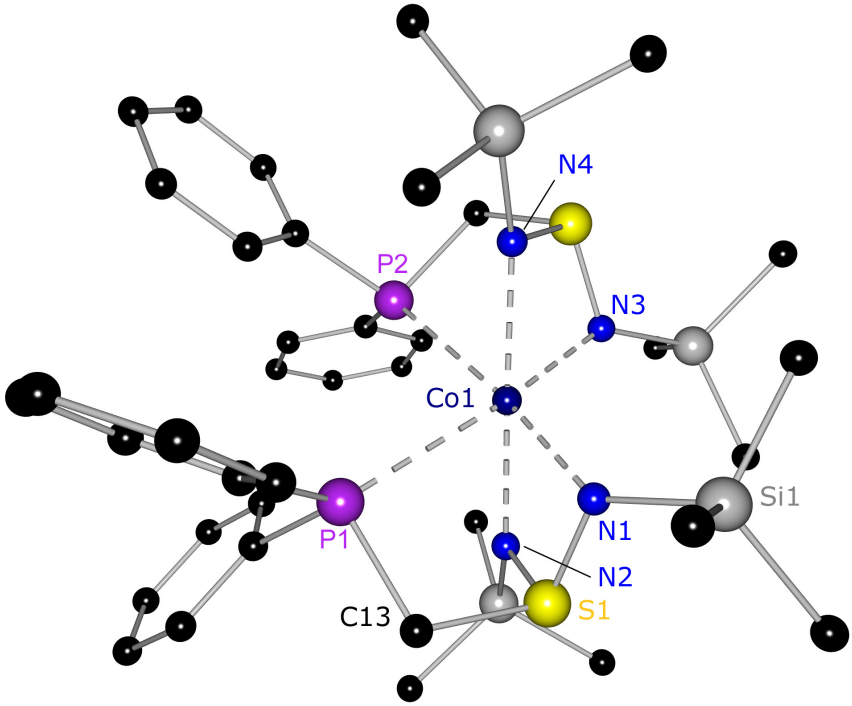

Figure 5-6: Molecular structure of [Co{$Ph_2PCH_2S(NSiMe_3)_2$}$_2$] (**30**). Hydrogen atoms are omitted for clarity.

Interestingly, the coordination of the central cobalt dication can be described as a distorted octahedron which is in contrast to the calcium and the strontium complexes. N3 and P1 can be regarded as the apexes of the polyhedron. The N3–Co1–N4 and N1–Co1–N2 angles of 70.18(6)° and 70.63(6)°, respectively underline that view. They are not very close to 90° but closer than the corresponding values of the strontium complex (63.37(6)° and 59.71(4)°). P1 and N3 are almost aligned straight which is demonstrated by the P1–Co1–N3 angle of 172.27(4)°. The corresponding value in the strontium complex is 154.03(3)° and therefore much smaller. It is remarkable that the N1–S1–N2 angle of 99.75(8)° is much more acute than in the two complexes described earlier. It is comparable to the magnesium complexes **26** and **27** that show values of 97.43(12)° and 100.44(4)°. This decrease of the N–S–N angle could be due to the small cation size of Co(II) (65 pm low-spin, 74.5 pm high-spin) which is comparable to Mg(II) (72 pm).[169]

The ligand is able to get closer to the central metal, getting twisted stronger as a result. The S–C–P angle (105.95(10)°) is reduced as well. The Co–N and Co–P bond lengths range from 2.1228(16) Å (N1–Co1) to 2.1429(16) Å (N4–Co1) and 2.7409(6) Å to 2.8421(6) Å (P2/P1–Co1). Particularly the cobalt-phosphorus bonds are much longer than in comparable octahedral structures of cobalt(III).[174,175] In 2006, *Salem* and co-workers presented a hexadentate P_3N_3 ligand which forms an

octahedral complex with cobalt(III).[176] The Co–P and Co–N bond lengths in those complexes are around 2.2067 Å and 2.024 Å. The question remains wether **30** is a high-spin or a low-spin complex. PR_3 is known to be a strong σ-donor ligand and a good π-acceptor so that the ligand field splitting is large. Co^{2+} probably is in a low-spin state and the phosphorus side-arms form σ-bonds with the d_{z2} and the d_{x2-y2} orbitals. Consequently, their *cisoid* arrangement gets obvious. However, the spin-state has still to be further investigated.

A search for similar cobalt(II) complexes in the CCDC clearly shows that there are none. There is a great variety of cobalt(III) compounds involving the NioxH or similar ligands ($NioxH_2$ = 1,2-cyclohexanedione dioxime). The coordination sphere is then widened to six by PPh_3 ligands, resulting in an octahedral geometry of the complexes.[177] Another class of nitrogen and phosphorus bonded cobalt complexes is made with PNNP pincer ligands like $\{Ph_2P(CH_2)_2N(CH_2)_2N(CH_2)_2PPh_2\}$ or derivatives thereof. These are closely related to the ligand employed during this work. However, cobalt(II) complexes of this type are very rare which is probably due to the easy oxidation to cobalt(III). This brings the new ligand presented here into the focus as it is able to stabilise that oxidation state and paves the way to metal complexes that are in general not easily accessible.

As a second example for transition metals, iron(II) was chosen. It is known to catalyse all sorts of reactions, *e. g.* hydrogenations [178], hydrosilylations [179], olefin-polymerizations [180], cross-couplings [181], bond-cleavages [182] and many more.[183] Catalysts based on iron are desirable because of their low cost and low toxicity in comparison to other transition metals. *Morris et al.* described in 2008 an iron(II) complex with a tetradentate PNNP ligand for the asymmetric hydrogenation of polar bonds with hydrogen at relatively low temperatures.[184] Their goal was to synthesise enantiopure alcohols and amines from prochiral molecules which was only efficiently possible with ruthenium and rhodium catalysts until that time.[185]

In 2010, *Morris et al.* presented iron(II) complexes with tridentate phosphorus/nitrogen based ligands that could be active in hydrogenation reactions.[186] These ligands form octahedral complexes with Fe(II) where iron is complexed by two ligands and coordinated by two phosphorus and four nitrogen atoms or *vice versa*. Unfortunately, those compounds could not be characterised by X-ray crystallography due to poor solubility. NMR spectra were recorded however,

showing no paramagnetism. These PNP or NPN ligands therefore seem to generate a strong ligand field, leading to low-spin iron(II). Other examples for NPN ligands come from the group of *Braunstein*. They used bis(2-picolyl)phenylphosphane and related systems for the complexation of divalent transition metals.[187] Fe(II) is coordinated as well by two ligands with all three donor atoms taking part in the coordination to form a distorted octahedral coordination geometry. *Kirchner et al.* use similar ligands of the PNP form on the basis of N-heterocyclic diamines.[188] Some tridentate ligands which have already been employed in the complexation of Fe(II) are depicted in Figure 5-7 and Figure 5-10 [189].

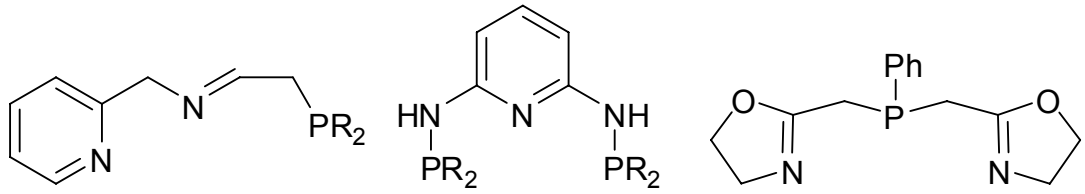

Figure 5-7: Examples for tridentate phosphorus/nitrogen ligands: a[186], b[188], c[187].

$[Fe\{Ph_2PCH_2S(NSiMe_3)_2\}_2]$ (**31**) was synthesised just like the cobalt complex **30**. After storing the reaction solution for two weeks at 4 °C, colourless crystals could be obtained. The complex crystallises in the orthorhombic space group $Pna2_1$ with the whole molecule in the asymmetric unit. A picture of compound **31** can be found in Figure 5-8. The structure is analogous to $[Co\{Ph_2PCH_2S(NSiMe_3)_2\}_2]$ (**30**) which is due to the similar ionic radii of Co(II) and Fe(II). The angles in the ligand as well as around the iron dication have almost the same values as in the cobalt analogue. The bond lengths are also very similar. Selected bond lengths and angles, compared to the calcium, strontium and cobalt complexes can be found in Table 5-2 and Table 5-3. The similarity of the structures **26** to **31** is certainly due to the flexibility of the ligand which is able to accommodate ions of very different radii. In addition, all the metal complexes presented here so far show excellent solubility in all sorts of hydrocarbons.

Unfortunately, it was not possible until now to gather enough substance for NMR spectroscopic measurements or other analytics because the complex seemed to decompose partially. It would be of great interest to confirm if the iron(II) dication is low-spin as well (like in *Morris'* case) because this would allow to draw conclusions about the behaviour of the ligand.

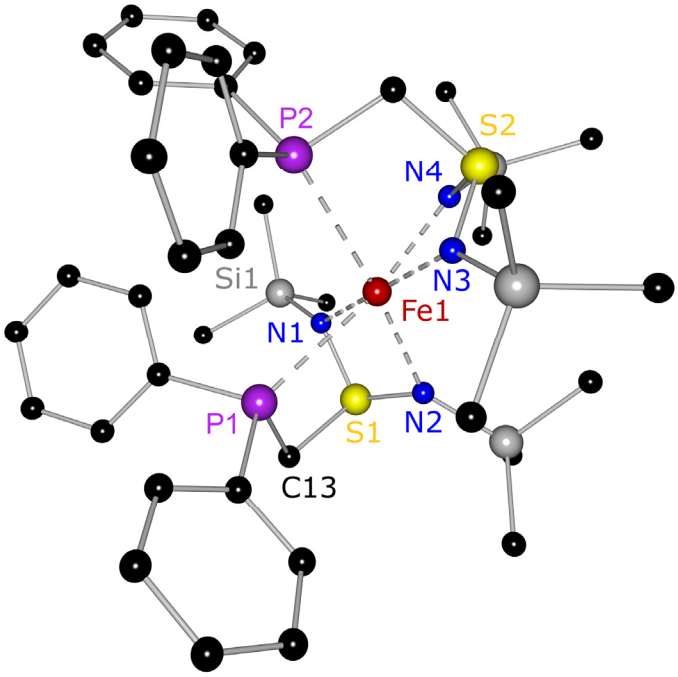

Figure 5-8: Molecular structure of [Fe{$Ph_2PCH_2S(NSiMe_3)_2$}$_2$] (**31**). Hydrogen atoms are omitted for clarity.

It is possible that the iron complex [Fe{$Ph_2PCH_2S(NSiMe_3)_2$}$_2$] can promote H_2 hydrogenation reactions as well. The phosphorus side-arm seems to be bonded weakly and could easily dissociate to form an amine-hydrido complex. The synthesis of $Ph_2PCH_2S(NSiMe_3)(HNSiMe_3)$ (**10**) shows, that the nitrogen atoms can be protonated. A possible reaction mechanism is described in the literature for a related Ru system.[185b,190,191]

The reaction of [(tmeda)Li{$Ph_2PCH_2S(NSiMe_3)_2$}] (**11**) with [Fe{$N(SiMe_3)_2$}$_2$] afforded a second product from the same reaction vessel which was obtained as red plates. The molecular structure is shown in Figure 5-9.

The phosphorus atom in the starting material **11** was oxidised and two O^- ions were incorporated into the structure. There was no metal exchange but the formation of a heterobimetallic complex of Li^+ and Fe^{2+} instead. A similar case was described by *Kempe et al.* when they tried to transmetalate lithiated 4-methyl-2[(trimethylsilyl)amino]pyridine with $FeCl_2$.[192] They obtained a mixed metal lithium/iron(II) complex with a central O^{2-} dianion (Figure 5-10, right).

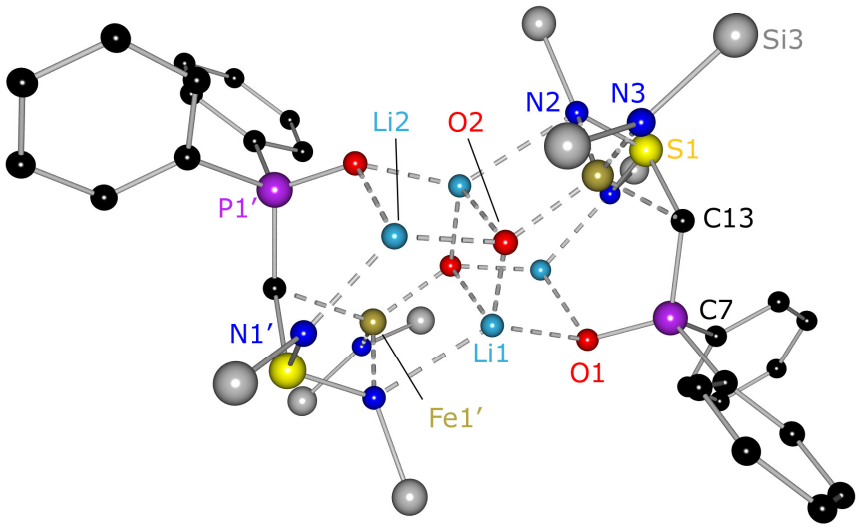

Figure 5-9: Molecular structure of $[\{FeN(SiMe_3)_2\}\{Li(NSiMe_3)_2SCHP(O)Ph_2\}(LiO)]_2$ (**32**). Hydrogen atoms and the methyl substituents of the $SiMe_3$ groups are omitted for clarity.

In **32**, the PCH_2S bridge was deprotonated by the iron bis(hexamethyl)silylamide, creating a carbocation which is taking part in the coordination of Fe(II). The reaction could be described according to Equation 5-3.

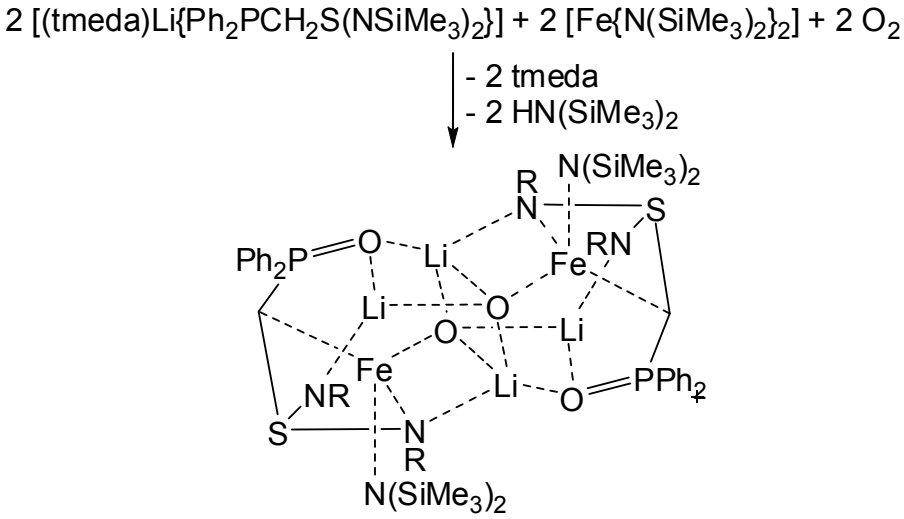

Equation 5-3: Possible formation of **32**, R = $SiMe_3$.

The structure is dimeric with a four-membered planar $(LiO)_2$ ring in the centre. This central ring is connecting four six-membered rings which are as well interconnected. There are four lithium and two iron cations in the complex. The nitrogen atoms of the diimido moieties coordinate two lithium atoms (Li1 and Li2') of different halves of the dimer and one iron atom (Fe1) of the same half. The oxygen atoms on the phosphorus coordinate two lithium cations of both halves (Li1 and Li2').

The iron(II) dication is additionally coordinated by the carbocation C13, one oxygen atom of the central four-membered ring (O2) and a bis(trimethylsilyl)amido ligand.

Li1 is bonding to three oxygen atoms and one nitrogen atom. It adopts a distorted tetrahedral coordination geometry with angles between 101.46(11)° (O2–Li1–O2') and 130.03(12)° (N2'–Li1–O1). The nitrogen-lithium and oxygen-lithium bonds are in the expected range with the O–Li bonds being slightly shorter. Li2 is threefold coordinated by two oxygen atoms of different halves of the dimer and one nitrogen atom of a diimido moiety. The coordination around Li2 is not planar and can rather be described as trigonal pyramidal with Li2 being at the apex of the pyramid. The O2–Li2–O1' angle of 97.45(11)° is closer to 90° than to 120°. This is due to the fact that Li2, O2, Li1' and O1' form a square that is connected to the central four-membered ring and encloses an angle of 110.4°.

Fe1 is distorted tetrahedrally coordinated by N2, N3, O2 and C13. The bond lengths are in accordance with the HSAB concept with Fe1–O2 (1.7850(10) Å) being the shortest and Fe1–C13 (2.1601(13) Å) the longest bond. Fe1–N2 however is rather short (2.0352(12) Å). This is probably due to the fact that the negative charge on C13 is partly delocalised into the diimido moiety. That explains the long Fe1–C13 as well as the short Fe1–N2 bond. This finding is further supported by the fact that the S1–C13–P1 angle of 117.41(7)° is widened in comparison to the ideal tetrahedral angle and points to a sp^2-hybridised carbon atom. The S–N bond lengths in the diimido moieties show an elongation of S1–N2 (1.6722(12) Å *vs.* 1.5961(12) Å for S1–N1) which is due to the coordination of two metals by N2. Selected bond lengths and angles in **32** can be found in Table 5-4.

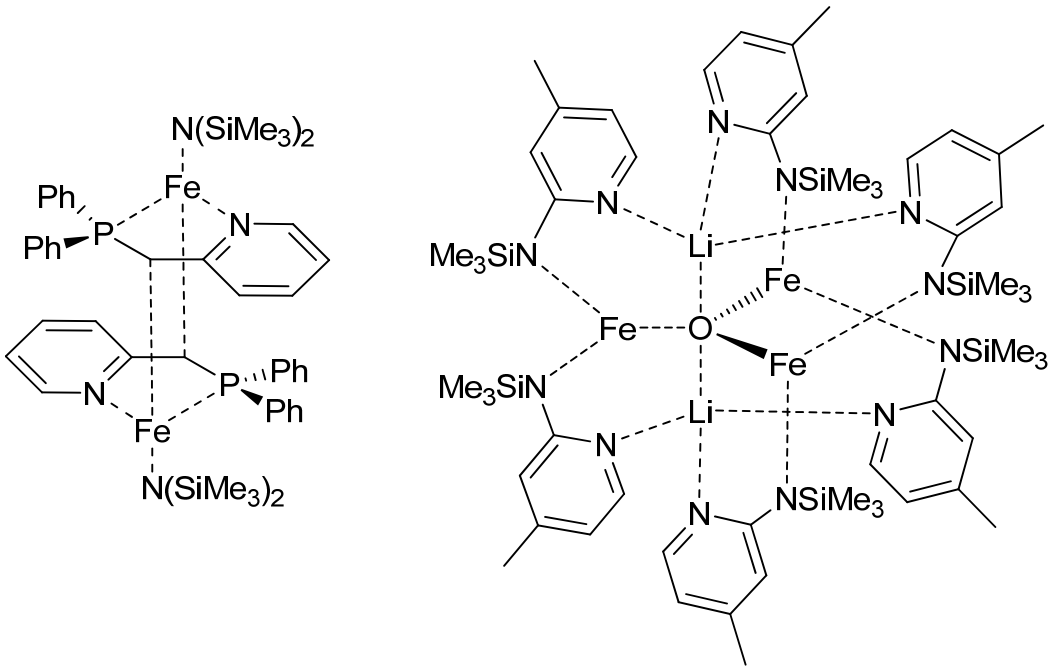

Figure 5-10: Iron(II) complexes related to [{FeN(SiMe$_3$)$_2$}{Li(NSiMe$_3$)$_2$SCH$_2$P(O)Ph$_2$}(LiO)]$_2$ (**32**).

Table 5-4: Selected bond lengths [Å] and angles [°] in **32**

S1–N1	1.5961(12)	N1–S1–N2	110.03(6)
S1–N2	1.6722(12)	S1–C13–P1	117.41(7)
S1–C13	1.8110(14)	C13–P1–O1	113.40(6)
P1–C13	1.7645(14)	O1–Li1–O2	109.34(13)
P1–O1	1.5148(10)	N2'–Li1–O1	130.03(12)
N1'–Li2	1.994(3)	O2–Li1–O2'	101.46(11)
N2'–Li1	2.372(3)	N1'–Li2–O1'	105.05(12)
N2–Fe1	2.0352(12)	O2–Li2–O1'	97.45(11)
N3–Fe1	1.9343(12)	O2–Li2–N1'	128.99(14)
C13–Fe1	2.1601(13)	N2–Fe1–N3	125.11(5)
O2–Fe1	1.7850(10)	N2–Fe1–C13	75.88(5)
O1–Li1	1.942(3)	N3–Fe1–O2	115.28(5)
O2–Li1	1.882(3)	O2–Fe1–C13	111.41(5)
N1–Si1	1.7345(12)	C7–P1–C13	115.07(7)

The coordination of iron(II) by oxygen, carbon and nitrogen in a fourfold geometry is not unknown. One example is [{(Ph$_2$CN)$_2$C$_2$H$_4$}Fe(CH$_2$SiMe$_3$)(thf)][BPh$_4$] where the oxygen atom belongs to a coordinating THF molecule.[193] Therefore the Fe–O bond of 2.055(2) Å is considerably longer than in **32** where the O-donor is part of the ligand

itself. *Murso* reported on the deprotonation of Ph_2PCH_2Py with $[Fe\{N(SiMe_3)_2\}_2]$ at the PCH_2 bridge yielding $[Fe\{Ph_2PC(H)Py\}\{N(SiMe_3)_2\}]_2$.[189] In this complex, the Fe(II) dication is fourfold coordinated by two nitrogen and one phosphorus donor atoms as well as by a carbanion (Figure 5-10, left). Although there is no oxygen present, the coordination is quite similar to **32** and there is a $N(SiMe_3)_2$ ligand from the starting material as well. The reported average Fe–C bond length of 2.201(3) Å is almost the same as in **32**.

5.1.3 Metal Exchange *via* a Lithium Dimer

Metal exchange reactions with metal amides were conducted with the lithium dimer $[Li\{Me_2PCH_2S(NSiMe_3)_2\}]_2$ (**4**), too. The equimolar reaction of **4** and $[Cu\{N(SiMe_3)_2\}]$ yielded colourless crystals after several days. The crystal structure revealed that the metal exchange did indeed proceed completely. Nevertheless, S^{2-} ions are incorporated in the structure (Figure 5-11).

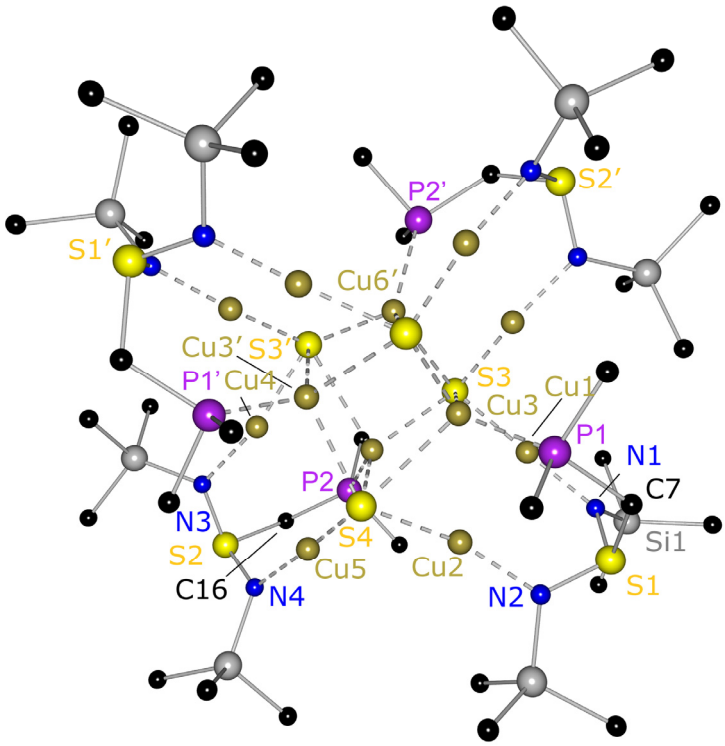

Figure 5-11: Molecular structure of $[\{Cu(Me_2PCH_2S(NSiMe_3)_2)\}_4\{Cu_2S\}_4]$ (**33**). Hydrogen atoms are omitted for clarity.

The compound crystallises in the monoclinic space group *C*2/*c* with half of the cluster in the asymmetric unit. It consists of four $\{Me_2PCH_2S(NSiMe_3)_2\}^-$ ligands which are bonding to two copper(I) ions each and a central $(Cu(I)S)_4$ distorted cube. Selected bond lengths and angles can be found in Table 5-5.

It is remarkable that copper(I) exhibits two different coordination geometries in the same complex. In sulphur diimido compounds the twofold linear coordination would usually be favoured.[81,35,194] However, the formation of cubes or prisms between copper(I) and chalcogens is a known coordination motif in cluster chemistry.[195] Usually, the cluster formation can be controlled by varying the employed phosphane ligands and/or reaction conditions.[196] The formation of such compounds according to the general reaction scheme (Equation 5-4) is very interesting. If the formation of clusters between copper(I) and chalcogens is a stable and preferred arrangement, the source of S^{2-} in **33** thus could be explained as it is known that the S–N and N–Si bonds in $S(NSiMe_3)_2$ are easily cleaved. It could therefore act analogues to $E(SiMe_3)_2$ according to Equation 5-4, releasing the S^{2-} dianion. This does not mean, however, that $S(SiMe_3)_2$ is formed in the reaction that leads to **33**.

$$CuX + PR_2R' \xrightarrow[\text{- } SiMe_3X]{\text{1. org. solvent}\\ \text{2. } E(SiMe_3)_2} [Cu_{2n}E_n(PR_2R')_m] \qquad \begin{matrix} X = Cl, OAc \\ R, R' = \text{org. group} \\ E = S, Se \end{matrix}$$

Equation 5-4: General preparation of copper(I) chalcogen clusters; n,m = integers.[197]

Probably because of the mixed linear/tetrahedral coordination, the Cu1···Cu3 distance of 2.563 Å is very short. However, this seems to be induced by the complex geometry and is not regarded a bond due to closed shell d^{10}-d^{10} interactions.[198]

In contrast, Cu1 and Cu2 are 3.014 Å apart, which is due to the wide bite of the sulphur diimido moiety and the coordination of the central S^{2-} ions to Cu1 and Cu2. Consequently, the N1–Cu1–S3 angle of 168.76(6)° deviates considerably from 180°. This is different to other sulphur diimido copper complexes like $[Cu\{(SC_8H_5)S(N\textit{t}Bu)_2\}]_2$ (Cu···Cu: 2.7852(6) Å) [35] and has its origin in the central $(CuS)_4$ cube which influences the coordination angles of the outer ligands.

Each ligand is binding to three different copper atoms. N1 and N2 are coordinating Cu1 and Cu2 in an almost linear fashion. The N1–Cu1–S3 and N2–Cu2–S4 angles of 168.76(6)° and 162.08(6)°, respectively, underline this very clearly. The N1–Cu1 (1.8902(17) Å) and N2–Cu2 (1.9077(17) Å) bond lengths are comparable to the average values found in $[(thf)_2Cu_3Li_2I\{(N\textit{t}Bu)_3S\}_2]$ (Cu–N: 1.876(5) Å) [194] and $[Cu\{PhS(NSiMe_3)_2\}]_2$ (av. Cu–N: 1.874(2) Å).[81] The Cu1–S3 bond of 2.1299(5) Å is somewhat longer which is expected as sulphur is larger and easier to polarize than nitrogen.

Table 5-5: Selected bond lengths [Å] and angles [°] in **33**

S1–N1	1.6089(19)	N1–S1–N2	109.59(10)
S1–N2	1.6131(19)	S1–C7–P1	118.46(12)
S1–C7	1.809(2)	N3–S2–N4	110.65(10)
P1–C7	1.864(2)	N1–Cu1–S3	168.76(6)
Cu1–N1	1.8902(17)	N2–Cu2–S4	162.08(6)
Cu1–S3	2.1299(5)	S3–Cu3–S4	112.471(17)
Cu2–N2	1.9077(17)	S4–Cu3–S4’	85.44(2)
Cu2–S4	2.1630(5)	P1–Cu3–S3	124.94(2)
Cu3–P1	2.2950(6)	P1–Cu3–S4’	102.98(2)
Cu3–S3	2.4384(6)	Cu2–S4–Cu3’	131.82(2)
Cu3–S4	2.7265(6)	Cu5–S4–Cu3	125.92(2)
Cu3–S4’	2.3390(5)	S1–N1–Si1	121.20(11)
N1–Si1	1.7323(19)		

The copper(I) ions in the central $(CuS)_4$ cube are fourfold coordinated by three S^{2-} ions and one phosphorus atom of the ligand side-arm in a distorted tetrahedral manner. The angles around Cu3 for instance range from 85.44(2)° to 124.94(2)°. The distortion is partly due to the different bond lengths inside the central cube; *e. g.* Cu3–S4 (2.7265(6) Å) is considerably longer than Cu3–S4’ (2.3390(5) Å). The bonds around Cu3, Cu3’, Cu6 and Cu6’ are also longer than the Cu–S bonds outside the cube.

$$2\ [Li\{Me_2PCH_2S(NSiMe_3)_2\}]_2 + 12\ [Cu\{N(SiMe_3)_2\}] + 4\ S$$

$$\downarrow\ -\ 4\ [Li\{N(SiMe_3)_2\}]$$

$$[\{Cu(Me_2PCH_2S(NSiMe_3)_2)\}_4\{Cu_2S\}_4] + 4\ (Me_3Si)_2NN(SiMe_3)_2$$

33

Equation 5-5: Possible formation of **33**.

Sulphur is always a minor contamination of the diimides employed in the reactions and could be the origin of the S^{2-} ions. Otherwise, sulphur can be generated by decomposition of the ligand. Therefore, only a very small amount of crystals could be grown which were – apart from the X-ray structure and some NMR spectra – not further analysed. The reaction can probably be described according to Equation 5-5 although none of the by-products was verified.

In summary, it has been shown in this work that copper(I) complexes of the new *Janus* head ligands are feasible even if the very stable lithium dimers are employed in the synthesis. For the future there are two possible routes: care must be taken to purify the starting materials even more thoroughly to prevent the formation of the copper/sulphur cluster **33**. Alternatively, elemental sulphur could be added to the reaction in a stochiometric amount to synthesise **33** deliberately.

5.2 Heterobimetallic Complexes

As the copper complex **33** demonstrated, metal exchange with monovalent metals is possible, too. It was now of interest to prepare complexes of the ligand $\{Ph_2PCH_2S(NSiMe_3)_2\}^-$ and the heavier alkali metals to investigate the possible changes in coordination.

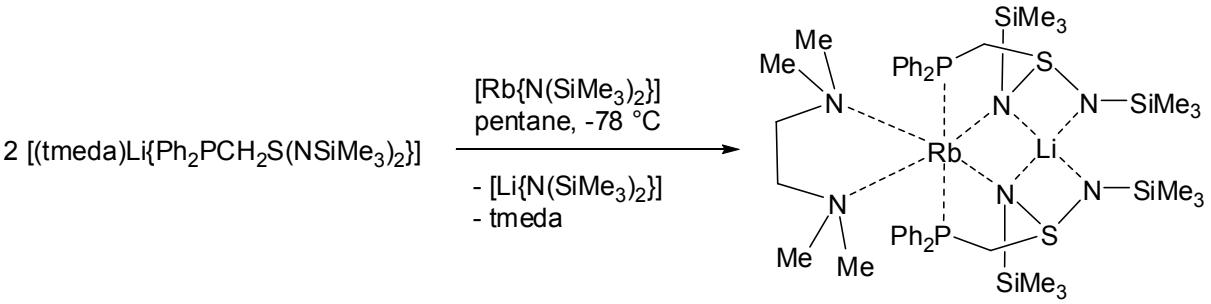

Equation 5-6: Preparation of $[(tmeda)Rb\{Ph_2PCH_2S(NSiMe_3)_2\}_2Li]$ (**34**).

Compound **34** was prepared from reacting equimolar amounts of $[(tmeda)Li\{Ph_2PCH_2S(NSiMe_3)_2\}]$ (**11**) and $[Rb\{N(SiMe_3)_2\}]$ at -78 °C in pentane (Equation 5-6). Interestingly, the metal exchange was not complete. Only half an equivalent of lithium was exchanged with rubidium, resulting in the formation of a heterobimetallic dimeric complex with the molecular structure shown in Figure 5-12. As could have been expected, the lithium cation coordinated to four nitrogen atoms is persistent in the complex. In contrast, the rubidium cation is complexed by two nitrogen atoms of the diimido moieties, each of the phosphorus side-arms and the TMEDA molecule which completes the coordination. Consequently, both alkali metals have different coordination geometries and environments. The structure is bisected by a mirror plane which includes both metal ions.

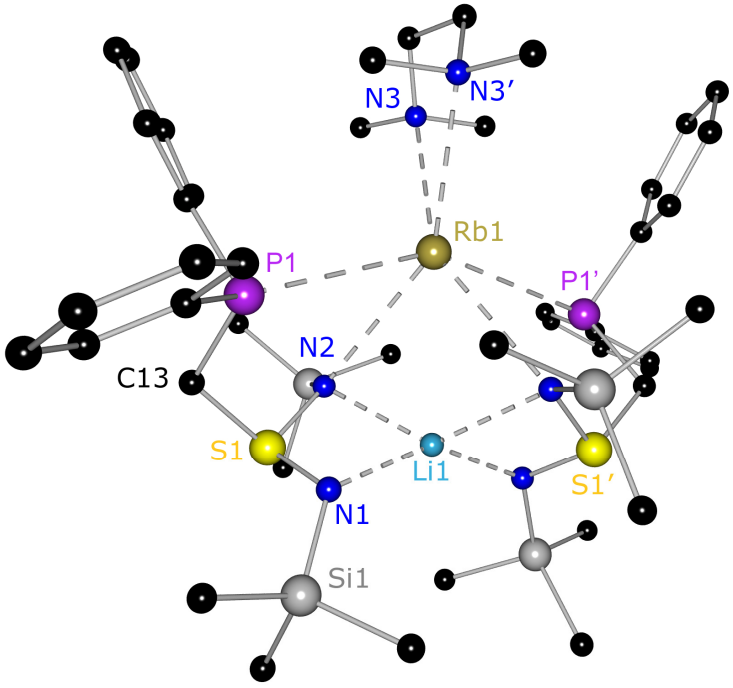

Figure 5-12: Molecular structure of [(tmeda)Rb{$Ph_2PCH_2S(NSiMe_3)_2$}$_2$Li] (**34**). Hydrogen atoms are omitted for clarity.

Li1 has a distorted tetrahedral geometry with Li–N bond lengths between 2.053(2) Å (Li1–N1) and 2.262(2) Å (Li1–N2). The Li1–N2 bond is slightly elongated because N2 is also coordinating Rb1. The rubidium atom Rb1 is six fold coordinated in a severely distorted octahedral manner. It is interesting that one of the TMEDA molecules remains in the complex but has switched its coordination to rubidium. The Rb–N and Rb–P bonds are longer than 3.0 Å which is normal and can be found in other complexes like [$Rb(thf)P(SiMe_3)_2]_\infty$ [199], [RbP(H)(dmp)] [200] (dmp = 2,6-dimesitylphenyl) or [$Rb\{((Me_3Si)_2C)P(C_6H_4\text{-}2\text{-}CH_2NMe_2)_2\}]_n$ [201]. Bond lengths and angles can be found in Table 5-6.

A CCDC search reveals that heterobimetallic complexes of lithium and rubidium are virtually unknown. There are only five examples of structurally characterised compounds of which three should be discussed. *Mulvey et al.* describe a heptalithium tetrarubidium mixed alkoxide peroxide wherein the clusters are linked by Rb–(TMEDA)–Rb bridges.[202] The reported mean N–Rb bond length of 3.197 Å is close to the value for Rb1–N3 (3.0458(16) Å). Another compound with the constitution [(tBuO)$_8$Li$_4$Rb$_4$] contains neither nitrogen nor phosphorus atoms.[203] This is also the case in the third complex where lithium and rubidium are bridged by oxygen donors.[204]

Table 5-6: Selected bond lengths [Å] and angles [°] in **34** and **35**

	34	**35**		**34**	**35**
S1–N1	1.6024(15)	1.602(2)	N1–S1–N2	103.69(8)	103.62(12)
S1–N2	1.6076(15)	1.604(2)	S1–C13–P1	113.78(9)	113.92(15)
S1–C13	1.8272(18)	1.827(3)	N1–Li1–N2	71.43(6)	71.07(9)
P1–C13	1.8515(18)	1.853(3)	N1–Li1–N1’	143.1(3)	144.0(6)
N1–Li1	2.053(2)	2.063(4)	N2–Li1–N2’	130.4(2)	128.2(5)
N2–Li1	2.262(2)	2.263(5)	N2–M1–P1	59.15(3)	60.43(5)
N2–M1	3.0646(15)	2.934(2)	N2–M1–P1’	97.97(3)	101.35(5)
N3–M1	3.0458(16)	2.936(3)	N2–M1–N2’	84.11(6)	87.87(9)
P1–M1	3.5996(5)	3.5613(7)	N3–M1–N3’	59.03(6)	62.83(12)
N1–Si1	1.7106(16)	1.712(2)	P1–M1–P1’	150.818(18)	156.23(4)

Interestingly, there are two signals in the $^{7}Li\{^{1}H\}$ NMR spectrum of **34**. The signal at 1.81 ppm can be associated with the Rb/Li heterobimetallic complex **34**; the other one at 1.02 ppm seems to belong to the starting material [(tmeda)Li{$Ph_2PCH_2S(NSiMe_3)_2$] (**11**). This is certainly not due to contamination of the sample as crystals of **34** were dissolved for the NMR spectra and the sample was sealed airtight. In addition, the signal for the starting material is quite high. An impurity of such a high concentration should have been detected in the elemental analysis. However, this was not the case. When looking at the $^{31}P\{^{1}H\}$ spectrum the presence of the starting material in the sample gets even more obvious. There is a small broad signal at -39 ppm, whereas the heterobimetallic complex **34** shows a signal at -33 ppm. The integration reveals a ratio of 1 to 0.2. All these analytical results indicate that the Rb/Li complex is not retained completely in solution. Part of it seems to loose the rubidium. However, this is impossible because the charges would not be balanced anymore. Thus, another possibility has to be taken into account. The whole system is flexible in solution like the other structures discussed so far. Therefore, the TMEDA molecule is switching positions in solution and is also binding to the lithium cation. The shift of this new compound would then be very similar to **11**.

In essence, **34** represents the first heterobimetallic lithium/rubidium complex with nitrogen and phosphorus donor atoms. The coordination of phosphorus in such complexes is unprecedented. The compound is soluble in polar and unpolar organic solvents which is a great advantage and is due to the ligand periphery. Complexes of

the heavier alkali metals usually tend to form larger aggregates which are poorly soluble. However, in the case of **34** this is averted by the ligand.

A reaction according to Equation 5-6 with [K{N(SiMe$_3$)$_2$}] yielded colourless crystals in the space group *C*2/*c*. The compound is the heterobimetallic lithium/potassium complex [(tmeda)K{Ph$_2$PCH$_2$S(NSiMe$_3$)$_2$}$_2$Li] (**35**) with the same structural features as **34**. The molecular structure is shown in Figure 5-13.

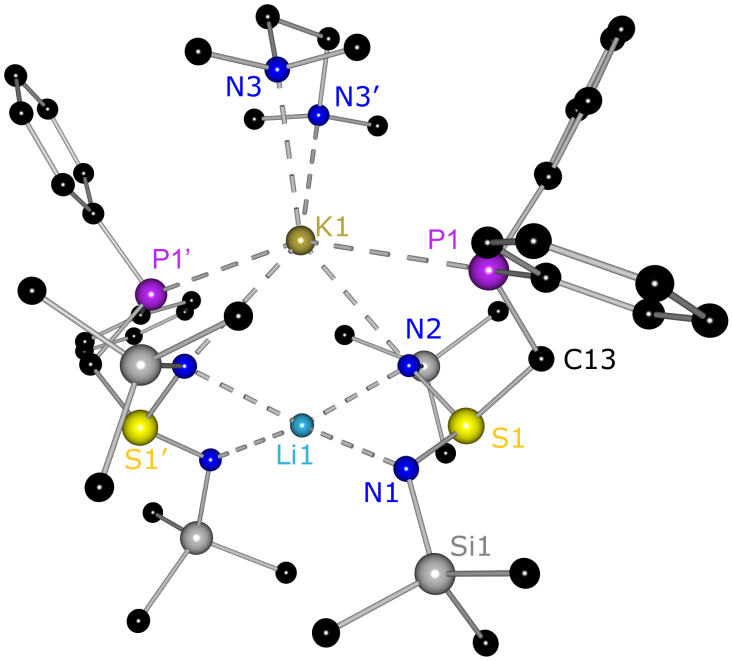

Figure 5-13: Molecular structure of [(tmeda)K{Ph$_2$PCH$_2$S(NSiMe$_3$)$_2$}$_2$Li] (**35**). Hydrogen atoms are omitted for clarity.

Unfortunately, the crystals were of poor quality and there still was some electron density unaccounted for in the refined model. The structure is shown here nevertheless for comparison reasons. Bond lengths and angles are discussed to give a general idea of their magnitude and the difference to [(tmeda)Rb{Ph$_2$PCH$_2$S(NSiMe$_3$)$_2$}$_2$Li] (**34**).

The Li–N bond lengths are 2.069(4) Å (Li1–N1) and 2.254(4) Å (Li1–N2). The K1–P1 bond of 3.5613(7) Å is almost the same as in the rubidium derivative (3.5996(5) Å). This is probably due to the fact that the coordination of the lithium cation as a structural anchor already predetermines the position of the phosphorus side-arm. The potassium-nitrogen bond lengths almost have the same value (K1–N2: 2.933(2) Å, K1–N3: 2.937(2) Å). The angles differ very little from the rubidium derivative. It is

striking though, that the P1–K1–P1' angle of 156.23(4)° is almost six degrees wider than in **34**.

There are only a few examples of lithium/potassium heterobimetallic complexes. Several examples with butoxy ligands are supposed to be novel superbases; there are even Li/Na/K heterotrimetallic compounds.[146,147] *Westerhausen et al.* synthesised mixed phosphanediide/silanolate heterotrimetallic aggregates with Li/K/Sr or Li/K/Ba.[205] The average K–P bond length of 3.365 Å is shorter than in **35** though the structural features are also not very alike.

In 1998, our group presented a lithium/potassium heterobimetallic complex based on the $\{S(N\textit{t}Bu)_3\}^{2-}$ ligand.[206] The compound $[(thf)_2Li_4K_2(O\textit{t}Bu)_2\{(N\textit{t}Bu)_3S\}_2]$ was the first example of such a complex with a triazasulfite dianion. The metal ions are sandwiched between two $\{S(N\textit{t}Bu)_3\}^{2-}$ caps with different coordination geometries. Thus, the arrangement is very different to **35** because there is no side-arm donation.

It would be interesting to see the results from metal exchange with $[Na\{N(SiMe_3)_2\}]$ as it is not clear if this reaction would also be incomplete or if a monometallic compound could be obtained due to the smaller cation size.

6 CONCLUSION AND OUTLOOK

In this thesis a new synthetic access to side-arm functionalized sulphur diimide ligands was developed. They can be tuned in their steric demand as well as in their electronic properties. Thus, this new ligand class shows outstanding performance in terms of ligand design. It can be adapted to accommodate the metal of choice and can stabilise metal cations like Co(II) and Fe(II) in low oxidation states. It became evident, that the side-arm has not as much influence on the coordination motif as the sulphur diimide moiety. As the SN_2-chelating group is the structural anchor, the variation of the side-arm is almost without limits.

The coordination pattern can be changed by choosing the appropriate substituents or altering the sulphur diimido moiety. This became especially clear in $[Li\{Me_2N(C_6H_4)S(NSiMe_3)_2\}]_2$ (**16**) and $[(t\text{BuN})_2S{\cdot}\{LiMe_2N(C_6H_4)S(Nt\text{Bu})_2\}_2]$ (**19**) which show a $(LiN)_2$ four-membered central ring (**16**) or a threefold/fourfold coordination (**19**) of the lithium ions. It would be of great interest to further investigate this phenomenon and tune the electronic properties in **16**. For example the sulphur diimido moiety could be exchanged with $S(NSiMe_3)(Nt\text{Bu})$ [207]. Thus, an intermediate compound between **16** and **19** would be synthesised. To compare its coordination pattern to those of **16** and **19** would be of great interest because it is not clear which geometry would be favoured. In general, the introduction of different diimides into the complexes should be studied in order to gain more insight into the adaptability of the ligands which will be valuable for future work. The electronic and steric properties of the ligands were further altered by oxidising the phosphorus atom of the coordinating side-arm with oxygen (**12**), sulphur (**8**) and selenium (**9**). Thereby, the bite-angle of the ligand can be increased as well which will become important for the complexation of large metal cations in the future.

On the other hand, the choice of the diimide and the right reaction conditions yielded the metal-free ligand $Ph_2PCH_2S(NSiMe_3)(HNSiMe_3)$ (**10**). **10** represents an excellent starting material to introduce various metals because a salt elimination is no longer required. Thus, unwanted metal salts that could interfere with the final product are not formed. In addition, the versatility of possible metalating agents is greatly increased. The formation of **10** should be further investigated in order to fully understand the reaction. Unequivocally, a fast and more efficient access to this

valuable starting material is required. It would be the basis of a vast range of various products. Not only bivalent metals but also metals with higher (or lower) valency could be coordinated by the ligand. If metal hexamethylsilylamides are used, the only by-product would be $HN(SiMe_3)_2$ which is easily removed. With the protonated ligand **10**, one of the key compounds of this thesis and for future reactions was synthesised.

The sulphur diimides with amine side-arm could be protonated as well in order to increase the choice of free ligands, which will play an important role in the synthesis of heterobimetallic complexes. This could be done by using either stochiometric amounts of water or *t*$BuNH_3Cl$, a reaction that has already been successfully employed with sulphur diimide derivatives.[30,80]

Protonation of the oxidised complexes $[Li\{Me_2P(S)CH_2S(NSiMe_3)_2\}]_2$ (**8**) and $[Li\{Me_2P(Se)CH_2S(NSiMe_3)_2\}]_2$ (**9**) should be tried as well. The unoxidised compounds of this type are not stable enough in hydrolysis reactions with water or *t*$BuNH_3Cl$. However, the oxidation of the phosphorus atom probably stabilises the ligand.

During the course of this thesis it became obvious, that the precoordination of the lithium atom seems to be essential for transmetalation reactions. The dimeric complexes that are formed are too stable and undergo ligand scrambling in most cases, when they are reacted with metal halogenides, hydrides or amides. However, transmetalations were achieved with $[(tmeda)Li\{Ph_2PCH_2S(NSiMe_3)_2\}]$ (**11**). **11** is an excellent starting material for such reactions because the phosphorus side-arm is not coordinating to the lithium atom. It is therefore free to bind other metals and bring them into close spatial proximity of the two nitrogen chelating 'claws'. Lithium can then leave the complex as a stable TMEDA/ligand adduct. *Via* this route, a great variety of complexes with divalent metals was synthesised (**26**-**31**). The tripodal heteroscorpionate-like ligand is able to stabilise *s*- and *d*-block metals in low oxidation states. When monovalent metals are employed, heterobimetallic complexes (**34**, **35**) are generated, showing the great potential of this ligand class.

Another starting material for such reactions could be $[(thf)Li\{Me_2N(C_6H_4)S(NSiMe_3)_2\}]_2$ (**17**) which contains a free NMe_2 side-arm. It would be very interesting to compare the metal complexes of the amino side-arm donating ligand with the phosphorus containing one.

Alternatively, the transmetalation of the starting materials should be further pursued. The metal exchange with alkoxides works well which could be demonstrated by the synthesis of $[Na\{Me_2N(CH_2)_2N(Me)S(NSiMe_3)_2\}]_2$ (**22**) and $[K\{Me_2N(C_6H_4)\text{-}S(NSiMe_3)_2\}]_2$ (**18**). By means of this method, the synthesis of a homologues series of alkali metal complexes is thinkable. Even a Cu(I) complex seems feasible as the syntheses of $[Cu\{(C_6H_4)NMe_2\}]$ [208] and Cu*O*t*Bu* [209] have already been described in the literature.

More effort has also to be put into the transition metal complexes that were presented in this thesis. First of all, the yield has to be improved in order to make further analysis possible. Therefore, the whole reaction should probably be conducted in an argon glovebox. Especially the Fe(II) complex is of great interest because it can give insight into the donating properties of the ligand. By analysis of the spin state – which could be done *via Mößbauer* spectroscopy – the ligand field strength could be determined. In addition, the corresponding Fe(III) complex should be synthesised in order to compare the binding modes of the ligand.

For the future, the impact of the side-arm on the binding modes of the ligand should be further investigated. 3- and 4-picoline could yield different coordinations with a pendent side-arm. With such building blocks, the synthesis of polymeric structures would be possible. The use of side-arms with various donor sites is also intriguing. Thereby, the assembly of multimetallic systems or three-dimensional networks is feasible. These donor sites could be different in order to adapt to the coordination of various metals.

7 EXPERIMENTAL SECTION

7.1 General

All experiments were carried out either in an atmosphere of purified dry nitrogen or argon, using modified *Schlenk* techniques [210] or in an argon glovebox. Glassware was dried for several hours at 130 °C, assembled hot and cooled under vacuum. The solvents were freshly distilled from sodium-potassium alloy (Et_2O, pentane), sodium (toluene) or potassium (THF, hexane) and degassed prior to use. *t*BuLi in pentane and *n*BuLi in hexane were supplied by Chemetall GmbH. The reactants were commercially available or synthesised according to published procedures ($S(NtBu)_2$ [211], $S(NSiMe_3)_2$ [212], $[(tmeda)Li(H_2CPPh_2)]$ [64,65,66]).

7.2 Analytical Methods

7.2.1 Mass spectrometry

Mass spectra were recorded by electron ionization (EI-MS: 75 eV) on a Finnigan MAT 95 spectrometer. The mass-to-charge ratios (m/z) of the fragment ions are based on the molecular masses of the isotopes with the highest natural abundance. The molecular peak M is defined as the compound without coordinating solvent.

7.2.2 NMR spectroscopy

All NMR spectra were recorded on Bruker Avance DPX 300 or DRX 500 spectrometers using TMS (^1H, ^{13}C and ^{29}Si), H_3PO_4 (^{31}P) and LiCl (^7Li) as external reference and the protons of the deuterated solvents as internal standard. If not otherwise stated the spectra were recorded at room temperature and with ^1H or ^{13}C decoupling. The chemical shifts δ are given in ppm. Multiplicities are denominated s (singlet), d (doublet), tr (triplet), hept (heptet), br (broad signal).

7.2.3 Elemental analysis

Elemental analyses were performed by the "Mikroanalytisches Labor des Instituts für Anorganische Chemie der Universität Göttingen" with an elementar Vario EL3 apparatus. The inclusion of argon, from canning in an argon drybox, led to systematic errors.

7.3 Syntheses and Characterizations

7.3.1 General preparation of lithiated phosphanes

A solution of *t*BuLi in pentane (1.5 M, 1.1 eq.) was reduced to half of its volume and the corresponding phosphane (PMe_3, Me_2PPh, Ph_2PMe, PEt_3, tBu_2PMe; 1.0 eq.) was added very slowly at rt. The solution was stirred over night and in the cases of PEt_3 and tBu_2PMe refluxed for 1 h. The white to light yellow precipitate was filtered and thoroughly washed with pentane several times.

a) [Li(H_2CPMe_2)]:

Yield: 75 %

^{1}H-NMR (200.13 MHz, d_8-THF): δ = -0.91 (s, 2 H, PCH_2Li), 0.76 (d, 6 H, $^2J_{P-H}$ = 1.64 Hz, P(CH_3)$_2$) ; **^{31}P-NMR (81.01 MHz, d_8-THF)**: δ = -42.64

b) [Li($H_2CP(Ph)Me$)]:

Yield: 78 %

^{1}H-NMR (200.13 MHz, d_8-THF): δ = -0.65 (d, 2 H, $^2J_{P-H}$ = 0.90 Hz, PCH_2Li), 1.02 (d, 3 H, $^2J_{P-H}$ = 2.41 Hz, PCH_3), 6.82-6.89 (m, 1 H, *p*-H), 7.19-7.34 (m, 4 H, *o*-H, *m*-H); **^{31}P-NMR (81.01 MHz, d_8-THF)**: δ = -20.48

c) [Li(H_2CPPh_2)]:

Yield: 61 %, further analysis see [64,65,66]

d) [Li{$HC(CH_3)PEt_2$}]:

Yield: 30 %

^{1}H-NMR (200.13 MHz, d_8-THF): δ = -0.60-(-0.43) (m, 1 H, PCHLi), 0.11 (s, 3 H, PCH_3), 0.95-1.09 (m, 6 H, PCH_2CH_3), 1.29-1.40 (m, 4 H, PCH_2CH_3); **^{31}P-NMR (81.01 MHz, d_8-THF)**: δ = -2.15

e) [Li(H_2CPtBu_2)]:

Yield: 64 %, for further analysis see [60,84]

7.3.2 $[Li\{Me_2PCH_2S(NtBu)_2\}]_2$ (1)

The product was synthesised according to *Deuerlein* [38] and fully characterised.

Empirical formula: $C_{22}H_{52}Li_2N_4P_2S_2$ **Molecular weight**: 512.64 g/mol

Elemental analysis (found (calc.) [%]): C 51.6 (51.6), H 10.9 (10.2), N 10.8 (10.9), S 12.3 (12.5)

^{1}H-NMR (500.13 MHz, C_6D_6): δ = 0.896 (d, 6 H, $^2J_{P-H}$ = 0.55 Hz, P(CH_3)$_2$), 0.898 (d, 6 H, $^2J_{P-H}$ = 0.55 Hz, P(CH_3)$_2$), 1.44 (s, 36 H, C(CH_3)$_3$), 2.676 (d, 2 H, $^2J_{P-H}$ = 0.92 Hz, PCH_2S), 2.678 (d, 2 H, $^2J_{P-H}$ = 0.92 Hz, PCH_2S)

^{7}Li-NMR (194.37 MHz, C_6D_6): δ = 2.22 (tr, $^1J_{P-Li}$ = 18.79 Hz, P*Li*P)

^{13}C-NMR (125.76 MHz, C_6D_6): δ = 13.70 (d, $^1J_{P-C}$ = 1.67 Hz, P*C*H$_3$), 13.73 (d, $^1J_{P-C}$ = 1.62 Hz, P*C*H$_3$), 33.76 (C(*C*H$_3$)$_3$), 54.02 (*C*(CH$_3$)$_3$), 64.83 (d, $^1J_{P-C}$ = 2.98 Hz, P*C*H$_2$S), 64.92 (d, $^1J_{P-C}$ = 3.00 Hz, P*C*H$_2$S)

^{31}P-NMR (202.46 MHz, C_6D_6): δ = -67.00 (hept, $^1J_{P-Li}$ = 18.17 Hz, Li*P*Li)

EI-MS m/z [%]: 235 ({$Me_2PCH_2S(NtBu)_2$}, 51), 178 ({$Me_2PCH_2S(NtBu)$}, 44), 162 ({$MePCH_2S(NtBu)_2$}, 30), 122 ({$PCH_2S(NtBu)_2$}, 37), 75 (Me_2PCH_2, 100), 57 (*t*Bu)

7.3.3 $[Li\{Ph_2PCH_2S(NtBu)_2\}]_2$ (2)

The product was synthesised according to *Deuerlein* [38] and fully characterised.

Empirical formula: $C_{42}H_{60}Li_2N_4P_2S_2$ **Molecular weight**: 760.93 g/mol

Elemental analysis, EI-MS see [38]

^{1}H-NMR (500.13 MHz, C_6D_6): δ = 1.37 (s, 36 H, C(CH_3)$_3$), 3.64 (s, 4 H, PCH_2S), 6.98-7.01 (m, 4 H, *p*-H), 7.04-7.07 (m, 8 H, *o*-H), 7.56-7.59 (m, 8 H, *m*-H)

^{7}Li-NMR (194.37 MHz, C_6D_6): δ = 2.63 (tr, $^1J_{P-Li}$ = 12.80 Hz, P*Li*P)

^{13}C-NMR (125.76 MHz, C_6D_6): δ = 33.60 (C(*C*H$_3$)$_3$), 54.31 (*C*(CH$_3$)$_3$), 62.26 (d, $^1J_{P-C}$ = 17.49 Hz, P*C*H$_2$S), 128.63-128.76 (m, *o*-C), 128.92 (*p*-C), 133.45-133.63 (m, $^3J_{P-C}$ = 18.30 Hz, *m*-C), 137.79-137.82 (m, $^1J_{P-C}$ = 3.76 Hz, *i*-C)

^{31}P-NMR (202.46 MHz, C_6D_6): δ = -32.57 (s br, Li*P*Li)

7.3.4 $[Li\{Me(Ph)PCH_2S(NtBu)_2\}]_2$ (3)

To a suspension of [Li{H_2CP(Ph)Me}] (1.50 g, 11.4 mmol, 2.0 eq.) in pentane (30 mL) was added S(N*t*Bu)$_2$ (1.98 g, 11.4 mmol, 2.0 eq.) very slowly at -78 °C. After 20 min at -78 °C the suspension was allowed to warm to rt and stirred for 24 h. The yellow-

orange solution was reduced to 2/3 of its volume and stored at -25 °C. After 3 d colourless crystals suitable for structural analysis were obtained.

Empirical formula: $C_{32}H_{56}Li_2N_4P_2S_2$ **Molecular weight**: 636.78 g/mol

Yield: 2.65 g, 4.16 mmol, 73 % **Melting point**: 125.5 °C (decomp.)

Elemental analysis (found (calc.) [%]): C 59.33 (60.36), H 8.75 (8.86), N 8.79 (8.80), S 10.26 (10.07)

^{1}H-NMR (500.13 MHz, C_6D_6): δ = 1.20 (s, 3 H, PCH_3), 1.32 (s, 3 H, PCH_3), 1.37 (s, 9 H, C(CH_3)$_3$), 1.38 (s, 9 H, C(CH_3)$_3$), 1.43 (s, 9 H, C(CH_3)$_3$), 1.45 (s, 9 H, C(CH_3)$_3$), 2.96-3.12 (m, 4 H, PCH_2S), 7.02-7.05 (m, 2 H, *p*-H), 7.08-7.12 (m, 4 H, *o*-H), 7.47-7.51 (m, 4 H, *m*-H)

^{7}Li-NMR (194.37 MHz, C_6D_6): δ = 2.41 (tr, $^1J_{P-Li}$ =13.43 Hz, P*Li*P)

^{13}C-NMR (125.76 MHz, C_6D_6): δ = 13.43 (dd, $^1J_{P-C}$ = 4.73 Hz, $^3J_{P-C}$ = 3.01 Hz, PLiP*C*H$_3$), 13.60 (dd, $^1J_{P-C}$ = 5.02 Hz, $^3J_{P-C}$ = 2.44 Hz, PLiP*C*H$_3$), 33.51-33.67 (m, C(*C*H$_3$)$_3$), 53.94-54.40 (m, *C*(CH$_3$)$_3$), 64.10-64.27 (m, P*C*H$_2$S), 128.56-128.70 (m, *o*-C), 131.89-132.27 (m, *p*-C), 139.65 (dd, $^3J_{P-C}$ = 3.49 Hz, $^5J_{P-C}$ = 1.99 Hz, *m*-C), 139.97 (dd, $^1J_{P-C}$ = 3.16 Hz, $^3J_{P-C}$ = 2.24 Hz, *i*-C)

^{31}P-NMR (202.46 MHz, C_6D_6): δ = -51.77 (s br, Li*P*Li)

EI-MS m/z [%]: 312 ({Me(Ph)PCH$_2$S(N*t*Bu)$_2$}, 7), 297 ({PhPCH$_2$S(N*t*Bu)$_2$}, 93), 240 ({Me(Ph)PCH$_2$S(N*t*Bu)}, 72), 184 ({Me(Ph)PCH$_2$SN}, 39), 137 ({Me(Ph)PCH$_2$}, 100), 109 (PPh, 47), 77 (Ph, 7), 57 (*t*Bu, 18)

7.3.5 [Li{Me$_2$PCH$_2$S(NSiMe$_3$)$_2$}]$_2$ (4)

To a suspension of [Li(H$_2$CPMe$_2$)] (0.60 g, 7.32 mmol, 2.0 eq.) in pentane (40 mL) S(NSiMe$_3$)$_2$ (1.51 g, 7.32 mmol, 2.0 eq.) was added very slowly at -78 °C. After 20 min at -78 °C the suspension was allowed to warm to rt and stirred for 24 h. The green-yellow solution was filtered, reduced to 1/2 of its volume and stored at -25 °C. Colourless crystals, suitable for structural analysis were obtained after two days.

Empirical formula: $C_{18}H_{52}Li_2N_4P_2S_2Si_4$ **Molecular weight**: 576.93 g/mol

Yield: 1.64 g, 2.85 mmol, 78 % **Melting point**: 147.3 °C (decomp.)

Elemental analysis (found (calc.) [%]): C 37.21 (37.47), H 9.00 (9.08), N 9.92 (9.71), S 11.14 (11.12)

^{1}H-NMR (500.13 MHz, C_6D_6): δ = 0.32 (s, 36 H, NSi(CH_3)$_3$), 0.83 (s, 12 H, P(CH_3)$_2$), 2.65 (s, 4 H, PCH_2S)

^{7}Li-NMR (194.37 MHz, C_6D_6): δ = 2.19 (tr, $^1J_{P-Li}$ = 21.25 Hz, P*Li*P)

^{13}C-NMR (125.77 MHz, C_6D_6): δ = 2.92 (NSi(*C*H$_3$)$_3$), 12.92 (d, $^1J_{P-C}$ = 3.31 Hz, P(*C*H$_3$)$_2$), 66.51 (d, $^1J_{P-C}$ = 10.94 Hz, P*C*H$_2$S)
^{29}Si-NMR (99.36 MHz, C_6D_6): δ = -2.71
^{31}P-NMR (202.46 MHz, C_6D_6): δ = -67.87 (hept, $^1J_{P-Li}$ = 20.84 Hz, Li*P*Li)

7.3.6 [Li{Ph$_2$PCH$_2$S(NSiMe$_3$)$_2$}]$_2$ (5)

S(NSiMe$_3$)$_2$ (0.22 g, 1.06 mmol, 2.0 eq.) was slowly added to a slurry of [Li(H$_2$CPPh$_2$)] (0.22 g, 1.06 mmol, 2.0 eq.) in pentane (15 mL) at -78 °C. After stirring overnight at rt the clear solution was reduced in volume and kept at -30 °C for four days, yielding colourless crystals.
Empirical formula: $C_{38}H_{60}Li_2N_4P_2S_2Si_4$ **Molecular weight**: 825.21 g/mol
Yield (crystals): 0.25 g, 0.30 mmol, 29 %
Elemental analysis (found (calc.) [%]): C 54.79 (55.31), H 7.32 (7.33), N 7.36 (6.79), S 8.02 (7.77)
^{1}H-NMR (500.13 MHz, C_6D_6): δ = 0.28 (s, 36 H, NSi(C*H*$_3$)$_3$), 3.61 (s, 4 H, PC*H*$_2$S), 6.97-7.06 (m, 12 H, *o*-H, *p*-H), 7.47-7.50 (m, 8 H, *m*-H)
^{7}Li-NMR (194.37 MHz, C_6D_6): δ = 2.62
^{13}C-NMR (125.76 MHz, C_6D_6): δ = 2.74 (NSi(*C*H$_3$)$_3$), 64.99 (d, $^1J_{P-C}$ = 11.80 Hz, P*C*H$_2$S), 128.84 (pseudo tr, *o*-C), 129.21 (*p*-C), 133.42-133.67 (m, $^3J_{P-C}$ = 18.09 Hz, *m*-C), 136.57 (*i*-C)
^{29}Si-NMR (99.36 MHz, C_6D_6): δ = -1.78
^{31}P-NMR (202.46 MHz, C_6D_6): δ = -33.19 (s br)

7.3.7 [Li{Me(Ph)PCH$_2$S(NSiMe$_3$)$_2$}]$_2$ (6)

To a suspension of [Li{H$_2$CP(Ph)Me}] (0.33 g, 2.5 mmol, 2.0 eq.) in pentane (15 mL) was added S(NSiMe$_3$)$_2$ (0.52 g, 2.5 mmol, 2.0 eq.) very slowly at -78 °C. After 20 min at -78 °C the suspension was allowed to warm to rt and stirred for 24 h. The cleared yellow solution was reduced to 2/3 of its volume and stored at -25 °C. After two weeks, colourless crystals suitable for structural analysis, were obtained.
A: first diastereomer, **B**: second diastereomer, ratio 1:0.8
Empirical formula: $C_{28}H_{56}Li_2N_4P_2S_2Si_4$ **Molecular weight**: 701.07 g/mol
^{1}H-NMR (300.13 MHz, C_6D_6): δ = 0.27 (s, 9 H, NSi(C*H*$_3$)$_3$ (**B**)), 0.28 (s, 9 H, NSi(C*H*$_3$)$_3$ (**A**)), 0.33 (s, 9 H, NSi(C*H*$_3$)$_3$ (**A**)), 0.36 (s, 9 H, NSi(C*H*$_3$)$_3$ (**B**)), 1.13 (s br,

3 H, PCH_3 (**A**)), 1.26 (s br, 3 H, PCH_3 (**B**)), 2.91-3.09 (m, 4 H, PCH_2S), 6.99-7.15 (m, 6 H, *o*-H, *p*-H), 7.34-7.43 (m, 4 H, *m*-H)

^{7}Li-NMR (116.6 MHz, C_6D_6): δ = 2.02 (tr, $^{1}J_{P-Li}$ = 17.62 Hz, P*Li*P)

^{13}C-NMR (75.47 MHz, C_6D_6): δ = 2.74 (NSi(*C*H_3)$_3$), 2.78 (NSi(*C*H_3)$_3$), 2.81 (NSi(*C*H_3)$_3$), 2.84 (NSi(*C*H_3)$_3$), 12.60-12.68 (m, PLiP*C*H_3), 12.83-12.90 (m, PLiP*C*H_3), 66.11-66.35 (m, P*C*H_2S), 128.70-128.82 (m, *o*-C), 128.99 (*p*-C), 131.70-132.13 (m, *m*-C), 138.00 (*i*-C), 138.42 (*i*-C)

^{29}Si-NMR (59.63 MHz, C_6D_6): δ = -3.67, -2.66, -2.47, -1.79

^{31}P-NMR (121.49 MHz, C_6D_6): δ = -(53.69-52.17) (m, Li*P*Li)

7.3.8 [Li{Et_2PCH(Me)S(NSiMe_3)$_2$}]$_2$ (7)

To a suspension of [Li{HC(CH_3)PEt_2}] (0.13 g, 0.81 mmol, 2.0 eq.) in pentane (10 mL) S(NSiMe_3)$_2$ (0.17 g, 0.81 mmol, 2.0 eq.) was added very slowly at -78 °C. After 20 min at -78 °C the suspension was allowed to warm to rt and stirred for 24 h. The yellow solution was reduced to 1/2 of its volume and stored at -25 °C. After one week, colourless crystals suitable for structural analysis were obtained.

A: first diastereomer, **B**: second diastereomer

Empirical formula: $C_{24}H_{64}Li_2N_4P_2S_2Si_4$ **Molecular weight**: 661.09 g/mol

Yield: 0.21 g, 0.32 mmol, 80 % **Melting point**: 138.9 °C (decomp.)

Elemental analysis (found (calc.) [%]): C 42.96 (43.60), H 9.58 (9.76), N 8.70 (8.47), S 9.83 (9.70)

^{1}H-NMR (500.13 MHz, C_6D_6): δ = 0.36-0.37 (m, 36 H, NSi(CH_3)$_3$), 0.92-1.02 (m, 12 H, PCH_2CH_3), 1.09-1.16/1.24-1.32/1.43-1.54 (m, 6 H, PCH(CH_3)S), 1.17-1.22 (m, 8 H, PCH_2CH_3)

The signals for the PCH(CH_3)S groups are overlaid by the signals of the PCH_2CH_3 groups, which is due to the two diastereomers. An unambiguous assignment is not possible.

^{7}Li-NMR (194.37 MHz, C_6D_6): δ = 2.27 (tr, $^{1}J_{P-Li}$ = 17.84 Hz, P*Li*P (**A**)), 2.37 (tr, $^{1}J_{P-Li}$ = 18.12 Hz, P*Li*P (**B**))

^{13}C-NMR (125.77 MHz, C_6D_6): δ = 3.09-3.42 (m, NSi(*C*H_3)$_3$), 10.46-11.21 (m, P*C*H_2CH_3, PCH_2*C*H_3), 13.66 (d, $^{2}J_{P-C}$ = 5.86 Hz, PCH(*C*H_3)S), 14.54 (d, $^{2}J_{P-C}$ = 5.78 Hz, PCH(*C*H_3)S), 16.96 (d, $^{2}J_{P-C}$ = 6.06 Hz, PCH(*C*H_3)S), 17.53 (d, $^{2}J_{P-C}$ = 7.19 Hz, PCH(*C*H_3)S), 63.34 (d, $^{1}J_{P-C}$ = 13.48 Hz, P*C*H(CH_3)S (**A**)), 64.87 (d, $^{1}J_{P-C}$ = 14.34 Hz, P*C*H(CH_3)S (**B**))

^{29}Si-NMR (99.36 MHz, C_6D_6): δ = -4.19, -3.65, -1.05, -0.55

^{31}P-NMR (202.46 MHz, C_6D_6): δ = -30.74 (hept, $^1J_{P-Li}$ = 19.78 Hz, Li*P*Li (**A**)), -27.34 (hept, $^1J_{P-Li}$ = 20.19 Hz, Li*P*Li (**B**))

7.3.9 [Li{$Me_2P(S)CH_2S(NSiMe_3)_2$}]$_2$ (8)

To a suspension of sulphur (0.02 g, 0.70 mmol, 2.0 eq.) in pentane (5 mL) was added [Li{$Me_2PCH_2S(NSiMe_3)_2$}]$_2$ (**4**) (0.20 g, 0.35 mmol, 1.0 eq.) in pentane (10 mL) very slowly at -78 °C. After 20 min at -78 °C the suspension was allowed to warm to rt and stirred for 24 h. The resulting white precipitate was filtered and redissolved in pentane. Colourless crystals, suitable for structural analysis were obtained after one month.

Empirical formula: $C_{18}H_{52}Li_2N_4P_2S_4Si_4$ **Molecular weight**: 641.06 g/mol

Elemental analysis (found (calc.) [%]): C 33.72 (33.72), H 7.94 (8.18), N 8.90 (8.74), S 20.87 (20.01)

^{1}H-NMR (300.13 MHz, C_6D_6): δ = 0.47 (s, 36 H, NSi(C*H*$_3$)$_3$), 1.09 (d, 12 H, $^2J_{P-H}$ = 13.03 Hz, P(C*H*$_3$)$_2$), 3.05 (d, 4 H, $^2J_{P-H}$ = 7.17 Hz, PC*H*$_2$S)

^{7}Li-NMR (194.37 MHz, C_6D_6): δ = 2.23

^{13}C-NMR (125.77 MHz, C_6D_6): δ = 3.16 (N(Si(*C*H$_3$)$_3$)), 20.74 (d, $^1J_{P-C}$ = 55.0 Hz, P(*C*H$_3$)$_2$), 66.18 (d, $^1J_{P-C}$ = 38.94 Hz, P*C*H$_2$S)

^{31}P-NMR (121.49 MHz, C_6D_6): δ = 27.05

7.3.10 [Li{$Me_2P(Se)CH_2S(NSiMe_3)_2$}]$_2$ (9)

To a suspension of selenium (0.082 g, 1.04 mmol, 2.0 eq.) in hexane (5 mL) was added **4** (0.30 g, 0.52 mmol, 1.0 eq.) in hexane (10 mL) very slowly at -78 °C. After 20 min at -78 °C the suspension was allowed to warm to rt and stirred over night. The resulting white precipitate was filtered and redissolved in toluene. Colourless crystals, suitable for structural analysis were obtained after two months.

Empirical formula: $C_{18}H_{52}Li_2N_4P_2S_2Se_2Si_4$ **Molecular weight**: 734.86 g/mol

^{1}H-NMR (300.13 MHz, C_6D_6): δ = 0.47 (s, 36 H, NSi(C*H*$_3$)$_3$), 1.24 (d, 12 H, $^2J_{P-H}$ = 13.15 Hz, P(C*H*$_3$)$_2$), 3.15 (d, 4 H, $^2J_{P-H}$ = 7.59 Hz, PC*H*$_2$S)

^{31}P-NMR (121.49 MHz, C_6D_6): δ = 6.23

7.3.11 $[Ph_2PCH_2S(NSiMe_3)(HNSiMe_3)]$ (10)

To a slurry of $[(tmeda)Li(H_2CPPh_2)]$ (0.88 g, 2.72 mmol, 1.0 eq.) in pentane (35 mL) was slowly added $S(NSiMe_3)_2$ (0.56 g, 2.72 mmol, 1.0 eq.) at -78 °C. After stirring at room temperature overnight, the solution was filtered over celite and the solvent removed *in vacuo*. The precipitate was dissolved in toluene (30 mL), layered with pentane (5 mL) and stored at -25 °C. After two months crystals suitable for structural analysis were obtained.

Empirical formula: $C_{19}H_{31}N_2PSSi_2$ **Molecular weight**: 406.67 g/mol

Yield: 1.07 g, 2.63 mmol, 97 % **Melting point**: 138.3 °C (decomp.)

Elemental analysis (found (calc.) [%]): C 55.94 (56.11), H 7.66 (7.68), N 7.00 (6.89), S 8.00 (7.88)

^{1}H-NMR (500.13 MHz, C_6D_6): δ = 0.22 (s, 18 H, NSi(CH_3)$_3$), 4.09 (d, 2 H, $^2J_{P-H}$ = 0.80 Hz, PCH_2S), 7.00-7.04 (m, 2 H, *p*-H), 7.06-7.10 (m, 4 H, *o*-H), 7.49-7.52 (m, 4 H, *m*-H)

^{13}C-NMR (125.76 MHz, C_6D_6): δ = 1.89 (NSi(CH$_3$)$_3$), 63.59 (d, $^1J_{P-C}$ = 24.61 Hz, PCH$_2$S), 128.76 (d, $^2J_{P-C}$ = 6.65 Hz, *o*-C), 129.00 (*p*-C), 133.34 (d, $^3J_{P-C}$ = 19.71 Hz, *m*-C), 138.43 (d, $^1J_{P-C}$ = 14.76 Hz, *i*-C)

^{29}Si-NMR (99.36 MHz, C_6D_6): δ = 2.59

^{31}P-NMR (202.46 MHz, C_6D_6): δ = -28.81

EI-MS m/z [%]: 406 (M, 17), 318 ({M - HNSiMe$_3$}, 14), 286 ({$Ph_2PCH_2SNSiMe_3$}, 19), 272 ({$Ph_2PCH_2SiMe_3$}, 19), 207 ({M - Ph_2PCH_2}, 15), 199 ({Ph_2PCH_2}, 100), 121 ({SN(HSiMe$_3$) + H}, 100), 73 (SiMe$_3$, 20)

7.3.12 $[(tmeda)Li\{Ph_2PCH_2S(NSiMe_3)_2\}]$ (11)

To a slurry of $[(tmeda)Li(H_2CPPh_2)]$ (3.01 g, 9.30 mmol, 1.0 eq.) in pentane (50 mL) $S(NSiMe_3)_2$ (1.92 g, 9.30 mmol, 1.0 eq.) was slowly added at -78 °C. After stirring at rt overnight the solution was filtered over celite, reduced in volume and stored at -25 °C, yielding colourless crystals after two days.

Empirical formula: $C_{25}H_{46}LiN_4PSSi_2$ **Molecular weight**: 528.29 g/mol

Yield: 4.44 g, 8.40 mmol, 90 %

Elemental analysis (found (calc.) [%]): C 56.08 (56.78), H 8.84 (8.77), N 10.37 (10.59), S 6.28 (6.06)

^{1}H-NMR (300.13 MHz, C_6D_6): δ = 0.28 (s, 18 H, NSi(CH_3)$_3$), 1.77 (s br, 4 H, N(CH_2)$_2$N), 2.07 (s, 12 H, (CH_3)$_2$N), 3.47 (s br, 2 H, SCH_2P), 6.99-7.12 (m, 6 H, *o*-H, *p*-H), 7.59-7.70 (m, 4 H, *m*-H)

^{7}Li-NMR (194.37 MHz, C_6D_6): δ = 1.00

^{13}C-NMR (125.76 MHz, C_6D_6): δ = 3.19 (NSi(*C*H$_3$)$_3$), 45.82 ((*C*H$_3$)$_2$N), 56.66 (N(*C*H$_2$)$_2$), 70.84 (d, $^{1}J_{P-C}$ = 23.99 Hz, P*C*H$_2$S), 128.46 (d, $^{2}J_{P-C}$ = 6.02 Hz, *o*-C), 132.41 (*p*-C), 132.55 (*p*-C), 133.90 (d, $^{3}J_{P-C}$ = 19.50 Hz, *m*-C), 142.04 (d, $^{1}J_{P-C}$ = 14.98 Hz, *i*-C)

^{29}Si-NMR (99.36 MHz, C_6D_6): δ = -8.29

^{31}P-NMR (121.49 MHz, C_6D_6): δ = -38.78 (s br)

7.3.13 [Li{*t*Bu$_2$P(O)CH$_2$S(NSiMe$_3$)$_2$}$_2$] (12), [(*t*Bu$_2$P(O)Me)Li$_2$-{*t*Bu$_2$PCH$_2$S(NSiMe$_3$)$_2$}$_2$] (13) and [Li{*t*Bu$_2$PCH$_2$S(NSiMe$_3$)$_2$}$_2$] (14)

S(NSiMe$_3$)$_2$ (0.72 g, 3.49 mmol, 2.0 eq.) was slowly added to a slurry of [Li(H$_2$CP*t*Bu$_2$)] (0.58 g, 3.49 mmol, 2.0 eq.) in pentane (25 mL) at -78 °C. After stirring overnight at rt the suspension was filtered and the yellow solution stored at -30 °C for eight days, yielding colourless crystals.

Empirical formula: $C_{30}H_{76}Li_2N_4O_2P_2S_2Si_4$ **Molecular weight**: 777.25 g/mol (**12**)

Empirical formula: $C_{44}H_{109}Li_2N_4OP_3S_2Si_4$ **Molecular weight**: 993.64 g/mol (**13**)

Empirical formula: $C_{30}H_{76}Li_2N_4P_2S_2Si_4$ **Molecular weight**: 745.25 g/mol (**14**)

Analysis for 14:

Elemental analysis (found (calc.) [%]): C 48.49 (48.35), H 10.80 (10.28), N 7.71 (7.52), S 8.55 (8.61)

^{1}H-NMR (300.13 MHz, C_6D_6): δ = 0.36-0.40 (m, 36 H, NSi(CH_3)$_3$), 1.11-1.19 (m, 36 H, PC(CH_3)$_3$, 2.71-2.75 (m, 4 H, PCH_2S)

^{7}Li-NMR (194.37 MHz, C_6D_6): δ = 2.32 (s)

^{13}C-NMR (125.76 MHz, C_6D_6): δ = 3.15 (NSi(*C*H$_3$)$_3$, 30.32 (PC(*C*H$_3$)$_3$), 30.49 (PC(*C*H$_3$)$_3$), 60.98 (P*C*(CH$_3$)$_3$), 61.45 (P*C*H$_2$S)

^{29}Si-NMR (99.36 MHz, C_6D_6): δ = -3.28

^{31}P-NMR (202.46 MHz, C_6D_6): δ = 8.75 (s br)

7.3.14 [Li{(C$_6$H$_4$)NMe$_2$}]$_4$[*t*BuLi] (15)

To Me$_2$NPh (3.46 g, 30.0 mmol, 4.0 eq.) was added *t*BuLi in pentane (1.5 M, 25.0 mL, 37.5 mmol, 5.0 eq.) at rt. After stirring over night the yellow solution was reduced in

volume and stored at rt. After one day colourless crystals suitable for structural analysis were obtained.

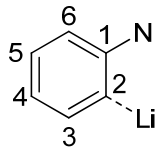

numbering scheme

Empirical formula: $C_{36}H_{49}Li_5N_4$ **Molecular weight**: 572.49 g/mol

Yield: 3.40 g, 5.94 mmol, 79 %

Elemental analysis (found (calc.) [%]): C 75.25 (75.52), H 8.99 (8.63), N 9.86 (9.79)

^{1}H-NMR (300.13 MHz, C_6D_6): δ = 0.84-1.26 (m, 9 H, C(C*H*$_3$)$_3$), 2.02-2.51 (m, 24 H, N(C*H*$_3$)$_2$), 6.77-7.04 (m, 4 H, C_6H_4), 7.18-7.28 (m, 8 H, C_6H_4), 7.91-8.26 (m, 4 H, LiCC*H*); the shifts of the main isomer [Li{(C_6H_4)NMe_2}]$_4$, [*t*BuLi]: **(400.13 MHz, tol-d^8)**: 1.01 (s, C(C*H*$_3$)$_3$), 2.06 (s br, N(C*H*$_3$)$_2$), 7.01 (m, 6-*H*), 7.22 (m, 4-*H*, 5-*H*), 8.22 (m, 3-*H*)

^{7}Li-NMR (155.51 MHz, tol-d^8): δ = 0.74 (br, 0.05 Li), 0.92 (br, 0.10 Li), 1.38 (br, 0.12 Li), 1.47 (0.28 Li), 1.79 (0.14 Li), 2.03 (br, 0.61 Li) , 2.35 (0.36 Li), 2.56 (br, 0.22 Li), 2.73 (br, 0.15 Li), 2.84 (0.42 Li), 3.11 (br, 0.10 Li), 3.61 (4 Li, [Li{(C_6H_4)NMe_2}]$_4$)

^{13}C-NMR (100.62 MHz, tol-d^8): δ = 10.94 (C(*C*H$_3$)$_3$), 32.30 (C(*C*H$_3$)$_3$), 46.85 (N(*C*H$_3$)$_2$), 118.87 (*C*6), 126.13 (*C*5), 127.97 (*C*4), 140.20 (*C*3), 166.21 (*C*1), 168.81 (br, *C*2)

7.3.15 [Li{$Me_2N(C_6H_4)S(NSiMe_3)_2$}]$_2$ (16)

To a suspension of [Li{(C_6H_4)NMe_2}] (1.00 g, 7.87 mmol, 2.0 eq.) in pentane (30 mL) was added S(N$SiMe_3$)$_2$ (1.62 g, 7.87 mmol, 2.0 eq.) very slowly at -78 °C. After 20 min at -78 °C the suspension was allowed to warm to rt and stirred for 24 h. The solution was filtered, reduced to 1/2 of its volume and stored at -25 °C. Colourless crystals, suitable for structural analysis were obtained after two days.

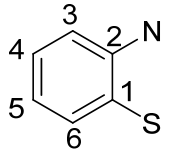

numbering scheme

Empirical formula: $C_{28}H_{56}N_6Si_4S_2Li_2$ **Molecular weight**: 667.15 g/mol

Yield (crystals): 2.21 g, 3.31 mmol, 42 %

Elemental analysis (found (calc.) [%]): C 50.25 (50.41), H 8.69 (8.46), N 12.56 (12.60), S 9.65 (9.61)

^{1}H-NMR (300.13 MHz, C_6D_6): δ = 0.27 (s, 36 H, NSi(C*H*$_3$)$_3$), 2.62 (s, 12 H, N(C*H*$_3$)$_2$), 6.77 (dd, 2 H, $^{3}J_{H-H}$ = 7.23 Hz, $^{4}J_{H-H}$ = 1.89 Hz, 6-*H*), 6.91-7.00 (m, 4 H, 4-*H*, 5-*H*), 7.94 (dd, 2 H, $^{3}J_{H-H}$ = 6.80 Hz, $^{4}J_{H-H}$ = 2.51 Hz, 3-*H*)

^{7}Li-NMR (116.64 MHz, C_6D_6): δ = 2.34 (s br)

^{13}C-NMR (75.47 MHz, C_6D_6): δ = 2.54 (NSi(*C*H$_3$)$_3$), 47.20 (N(*C*H$_3$)$_2$), 120.14 (*C*6), 124.58 (*C*5),127.43 (*C*3), 130.25 (*C*4), 149.78 (*C*1), 150.24 (*C*2); C3 is only visible in a hsqc spectrum, the signal is overlaid by C_6D_6

^{29}Si-NMR (59.63 MHz, C_6D_6): δ = -3.06

7.3.16 [(thf)Li{$Me_2N(C_6H_4)S(NSiMe_3)_2$}]$_2$ (17)

16 (0.33 g, 0.50 mmol, 1.0 eq.) was dissolved in THF (5 mL) and stirred for 15 h. The solvent was removed *in vacuo*, the residue was dissolved in pentane (20 mL) and filtered. The colourless solution was stored at 4 °C for two days, yielding colourless crystals.

Empirical formula: $C_{36}H_{72}Li_2N_6O_2S_2Si_4$ **Molecular weight**: 811.36 g/mol

^{1}H-NMR (300.13 MHz, C_6D_6): δ = 0.28 (s, 18 H, NSi(C*H*$_3$)$_3$), 0.30 (s, 18 H, NSi(C*H*$_3$)$_3$), 1.35 (m, 8 H, OCH$_2$C*H*$_2$), 2.60 (s br, 12 H, N(C*H*$_3$)$_2$), 3.45 (m, 8 H, OC*H*$_2$CH$_2$), 6.78-6.79 (m, 2 H, 6-*H*), 7.00-7.02 (m, 4 H, 4-*H*, 5-*H*), 8.20-8.28 (m, 2 H, 3-*H*)

^{7}Li-NMR (116.64 MHz, C_6D_6): δ = 1.91 (s br)

^{13}C-NMR (75.47 MHz, C_6D_6): δ = 1.35 (NSi(*C*H$_3$)$_3$), 2.13 (NSi(*C*H$_3$)$_3$), 2.75 (NSi(*C*H$_3$)$_3$), 25.56 (OCH$_2$*C*H$_2$), 45.80 (N(*C*H$_3$)$_2$), 46.44 (N(*C*H$_3$)$_2$), 67.84 (O*C*H$_2$CH$_2$), 119.88 (*C*6), 124.32 (*C*5), 130.26 (s br, *C*3, *C*4), 135.46 (*C*1), 150.69 (*C*2)

^{29}Si-NMR (99.36 MHz, C_6D_6): δ = -2.56

7.3.17 [K{$Me_2N(C_4H_4)S(NSiMe_3)_2$}]$_2$ (18)

To a suspension of [K{(C$_6$H$_4$)NMe$_2$}] (1.00 g, 6.28 mmol, 2.0 eq.) in pentane (30 mL) was added S(NSiMe$_3$)$_2$ (1.30 g, 6.28 mmol, 2.0 eq.) very slowly at -78 °C. After 20 min at -78 °C the suspension was allowed to warm to rt and stirred for 24 h. The solution was filtered, reduced to 1/2 of its volume and stored at -25 °C. Colourless crystals, suitable for structural analysis were obtained after one week.

Empirical formula: $C_{28}H_{56}N_6Si_4S_2K_2$ **Molecular weight**: 731.45 g/mol

Yield (crystals): 1.22 g, 1.66 mmol, 53 %

Elemental analysis (found (calc.) [%]): C 46.10 (45.98), H 8.01 (7.72), N 11.50 (11.49), S 8.85 (8.77)

^{1}H-NMR (300.13 MHz, C_6D_6): δ = 0.24 (s, 36 H, NSi(CH_3)$_3$), 2.66 (s, 12 H, N(CH_3)$_2$), 6.60 (dd, 2 H, $^{3}J_{H-H}$ = 7.82 Hz, $^{4}J_{H-H}$ = 1.01 Hz, 6-*H*), 7.06 (ddd, 2 H, $^{3}J_{H-H}$ = 7.82 Hz, $^{3}J_{H-H}$ = 7.30 Hz, $^{4}J_{H-H}$ = 1.73 Hz, 5-*H*), 7.37 (ddd, 2 H, $^{3}J_{H-H}$ = 7.52 Hz, $^{3}J_{H-H}$ = 7.30 Hz, $^{4}J_{H-H}$ = 1.01 Hz, 4-*H*), 8.60 (dd, 2 H, $^{3}J_{H-H}$ = 7.52 Hz, $^{4}J_{H-H}$ = 1.73 Hz, 3-*H*)

^{13}C-NMR (75.47 MHz, C_6D_6): δ = 3.31 (NSi(*C*H$_3$)$_3$), 45.16 (N(*C*H$_3$)$_2$), 117.71 (*C*6), 122.31 (*C*3), 123.15 (*C*4), 129.24 (*C*5), 150.19 (*C*1), 152.46 (*C*2)

^{29}Si-NMR (59.63 MHz, C_6D_6): δ = -7.32

7.3.18 [(*t*BuN)$_2$S·{LiMe$_2$N(C$_6$H$_4$)S(N*t*Bu)$_2$}$_2$] (19)

To a suspension of [Li{(C$_6$H$_4$)NMe$_2$}] (1.00 g, 7.87 mmol, 2.0 eq.) in pentane (30 mL) was added S(N*t*Bu)$_2$ (2.06 g, 11.8 mmol, 3.0 eq.) very slowly at -78 °C. After 20 min at -78 °C the suspension was allowed to warm to rt and stirred for 24 h. The solution was filtered, reduced to 1/2 of its volume and stored at -25 °C. Colourless crystals, suitable for structural analysis were obtained after two weeks.

Empirical formula: $C_{40}H_{74}N_8S_3Li_2$ **Molecular weight**: 777.15 g/mol

Yield (crystals): 2.08 g, 2.68 mmol, 68 %

Elemental analysis (found (calc.) [%]): C 61.63 (61.82), H 9.89 (9.60), N 14.42 (14.42), S 12.16 (12.38)

^{1}H-NMR (500.13 MHz, C_6D_6): δ = 1.36 (s br, 18 H, S(N*t*Bu)$_2$), 1.42 (s, 36 H, CS(NC(CH_3)$_3$)$_2$), 2.66 (s, 12 H, N(CH_3)$_2$), 6.77 (dd, 2 H, $^{3}J_{H-H}$ = 7.35 Hz, $^{4}J_{H-H}$ = 1.60 Hz, 6-*H*), 6.97-7.03 (m, 4 H, 4-*H*, 5-*H*), 8.33 (dd, 2 H, $^{3}J_{H-H}$ = 7.15 Hz, $^{4}J_{H-H}$ = 2.10 Hz, 3-*H*)

^{7}Li-NMR (194.37 MHz, C_6D_6): δ = 2.37 (s br)

^{13}C-NMR (125.76 MHz, C_6D_6): δ = 30.60 (S(NC(*C*H$_3$)$_3$)$_2$), 33.54 (CS(NC(*C*H$_3$)$_3$)$_2$), 46.54 (N(*C*H$_3$)$_2$), 54.46 (CS(N*C*(CH$_3$)$_3$)$_2$), 60.62 (S(N*C*(CH$_3$)$_3$)$_2$), 119.68 (*C*6), 123.84 (*C*5), 127.88 (*C*3), 139.37 (*C*4), 150.35 (*C*1), 150.43 (*C*2)

7.3.19 [Li{2-PyS(NSiMe$_3$)$_2$}]$_2$ (20)

To a solution of [(tmeda)Li(2-Py)] (0.46 g, 2.07 mmol, 2.0 eq.) in pentane (30 mL) was added S(NSiMe$_3$)$_2$ (0.43 g, 2.07 mmol, 2.0 eq.) at -78 °C and the reaction mixture stirred over night. The red suspension was filtered over celite, reduced in

volume and stored at 4 °C. After 3 h colourless crystals suitable for structural analysis were obtained.

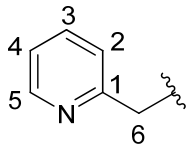

numbering scheme

Empirical formula: $C_{24}H_{48}Li_2N_6S_2Si_4$ **Molecular weight**: 611.04 g/mol

Yield (crystals): 0.46 g, 0.75 mmol, 72 %

Elemental analysis (found (calc.) [%]): C 47.06 (47.02), H 8.04 (8.22), N 14.15 (13.71), S 10.83 (10.46)

^{1}H-NMR (500.13 MHz, C_6D_6, 343 K): δ = 0.25 (s, 36 H, NSi(C*H*$_3$)$_3$)), 3.99 (s, 4 H, SC*H*$_2$C), 6.49 (ddd, 2 H, $^3J_{H–H}$ (H4/H3) = 7.60 Hz, $^3J_{H–H}$ (H4/H5) = 5.00 Hz, $^4J_{H-H}$ (H4/H2) = 1.10 Hz, 4-*H*), 6.53 (pseudo tr, 2 H, $^3J_{H–H}$ (H2/H3) = 7.70 Hz, $^4J_{H-H}$ (H2/H4) = 1.10 Hz, 2-*H*), 6.88 (ddd, 2 H, $^3J_{H–H}$ (H3/H2) = 7.70 Hz, $^3J_{H-H}$ (H3/H4) = 7.60 Hz, $^4J_{H–H}$ (H3/H5) = 1.75 Hz, 3-*H*), 8.53 (ddd, 2 H, $^3J_{H-H}$ (H5/H4) = 5.00 Hz, $^4J_{H–H}$ (H5/H3) = 1.75 Hz, $^5J_{H–H}$ (H5/H2) = 0.92 Hz, 5-*H*)

^{7}Li-NMR (116.64 MHz, C_6D_6): δ = 2.66 (s br)

^{13}C-NMR (125.48 MHz, C_6D_6): δ = 2.98 (NSi(*C*H$_3$)$_3$), 72.40 (*C*6), 121.88 (*C*4), 124.51 (*C*2), 137.38 (*C*3), 149.07 (*C*5), 154.74 (*C*1)

^{29}Si-NMR (59.63 MHz, tol-d_8, 363 K): δ = -2.57

7.3.20 [Li{$Me_2N(CH_2)_2N(CH_3)S(NSiMe_3)_2$}]$_2$ (21)

To a solution of [Li{N(Me)(CH$_2$)$_2$NMe$_2$}] (1.00 g, 9.25 mmol, 2.0 eq.) in pentane (20 mL) was added S(NSiMe$_3$)$_2$ (1.91 g, 9.25 mmol, 2.0 eq.) very slowly at -78 °C. After 20 min at -78 °C the reaction mixture was allowed to warm to rt and stirred for 24 h. The solution was reduced to 1/2 of its volume and stored at -25 °C. Colourless crystals, suitable for structural analysis were obtained after three days.

Empirical formula: $C_{22}H_{62}N_8Si_4S_2Li_2$ **Molecular weight**: 629.18 g/mol

Yield (crystals): 0.76 g, 1.20 mmol, 51 %

Elemental analysis (found (calc.) [%]): C 41.81 (42.00), H 9.84 (9.93), N 18.10 (17.81), S 10.15 (10.19)

^{1}H-NMR (300.13 MHz, C_6D_6): δ = 0.32 (s, 36 H, NSi(C*H*$_3$)$_3$), 2.00 (s br, 4 H, (CH$_3$)$_2$NCH$_2$C*H*$_2$), 2.10 (s, 12 H, N(C*H*$_3$)$_2$), 2.38 (s, 6 H, SN(C*H*$_3$)), 2.62 (s br, 4 H, (CH$_3$)$_2$NC*H*$_2$CH$_2$)

^{7}Li-NMR (116.64 MHz, C_6D_6): δ = 1.38 (s br)

^{13}C-NMR (125.76 MHz, C_6D_6): δ = 3.64 (NSi(CH$_3$)$_3$), 38.00 (N(CH$_3$)$_2$), 46.00 ((CH$_3$)$_2$NCH$_2$CH$_2$), 49.26 ((CH$_3$)$_2$NCH$_2$$CH_2$), 58.96 (SN($CH_3$))
^{29}Si-NMR (59.63 MHz, C_6D_6): δ = -3.59

7.3.21 [Na{Me$_2$N(CH$_2$)$_2$N(Me)S(NSiMe$_3$)$_2$}]$_2$ (22)

To a suspension of TrMEDA (0.25 g, 2.45 mmol, 2.0 eq.) and NaO*t*Bu (0.24 g, 2.45 mmol, 2.0 eq.) in hexane (5 mL) was added *n*BuLi (1.6 M in hexane, 1.53 mL, 2.45 mmol, 2.0 eq.) at 0 °C. After stirring at rt over night S(NSiMe$_3$)$_2$ (0.51 g, 2.45 mmol, 2.0 eq.) was added dropwise at -78 °C and the suspension stirred for 8 h. After filtration and reduction of the volume the solution was stored at 4 °C, resulting in colourless crystals after one day.

Empirical formula: $C_{22}H_{62}N_8Na_2S_2Si_4$ **Molecular weight**: 661.26 g/mol
Yield (crystals): 0.78 g, 1.18 mmol, 96 %
Elemental analysis (found (calc.) [%]): C 39.46 (39.96), H 9.33 (9.33), N 16.47 (16.95), S 10.01 (9.70)
^{1}H-NMR (500.13 MHz, tol-d$_8$, 243 K): δ = 0.36 (s, 16 H, NSi(CH_3)$_3$), 0.39 (s, 16 H, NSi(CH_3)$_3$), 1.46 (d br, 4 H, $^2J_{H–H}$ = 13.0 Hz, (CH$_3$)$_2$NCH_2CH$_2$), 1.84 (d br, 4 H, $^2J_{H-H}$ = 13.5 Hz, (CH$_3$)$_2$NCH$_2$CH_2), 2.02 (s, 12 H, N(CH_3)$_2$), 2.39 (s, 6 H, SN(CH_3))
^{13}C-NMR (125.76 MHz, tol-d$_8$, 243 K): δ = 3.10 (NSi(CH$_3$)$_3$), 3.86 (NSi(CH$_3$)$_3$), 37.55 (N(CH$_3$)$_2$), 43.34 ((CH$_3$)$_2$NCH$_2$CH$_2$), 47.88 ((CH$_3$)$_2$NCH$_2$$CH_2$), 49.77 (SN($CH_3$))
^{29}Si-NMR (99.36 MHz, tol-d$_8$, 243 K): δ = -5.35, 4.54

7.3.22 [(OH)Li$_2$K$_3${PhP(CH$_2$S(NSiMe$_3$)$_2$)$_2$}$_2$] (23)

Me$_2$PPh (1.03 mL, 8.10 mmol, 1.0 eq.) was mixed with KO*t*Bu (0.91 g, 8.10 mmol, 1.0 eq.) and *t*BuLi (1.5 M in pentane, 5.40 mL, 8.10 mmol, 1.0 eq.) was slowly added dropwise at rt. The precipitated brown powder was filtered, washed with pentane (3 x 5 mL), suspended in pentane and S(NSiMe$_3$)$_2$ (1.67 g, 8.10 mmol, 1.0 eq.) was slowly added at -78 °C. The orange-brown suspension was allowed to warm to rt and stirred over night. It was filtered over celite, washed with pentane and the solution stored at -25 °C. Colourless crystals, suitable for structural analysis were obtained after one week.

Empirical formula: $C_{45}H_{103}K_3Li_2N_8OP_2S_4Si_8$ **Molecular weight**: 1318.48 g/mol

7.3.23 $[Li_4O_2\{CH_2(N(Me)CH_2S(N\textit{t}Bu)_2Li)\}_2]$ (24)

$[Li\{H_2CN(Me)\}_2CH_2]$ (0.20 g, 1.75 mmol, 2.0 eq.) was suspended in pentane (8 mL) and $S(N\textit{t}Bu)_2$ (0.61 g, 3.50 mmol, 4.0 eq.) was slowly added at -78 °C. The solution was allowed to warm to rt over night, filtered and reduced in volume. Upon storage at -25 °C colourless crystals were obtained after several hours.

Empirical formula: $C_{42}H_{96}Li_6N_{12}O_2S_4$ **Molecular weight**: 971.20 g/mol

Yield: 0.62 g, 0.64 mmol, 73 %

Elemental analysis (found (calc.) [%]): C 51.86 (51.94), H 10.25 (9.96), N 17.34 (17.31), S 13.74 (13.21)

^{1}H-NMR (300.13 MHz, C_6D_6): δ = 1.40 (s, 72 H, NC(CH_3)$_3$), 2.10 (s, 12 H, NCH_3), 2.97 (s, 4 H, NCH_2N), 3.13 (s, 8 H, NCH_2S)

^{13}C-NMR (125.76 MHz, C_6D_6): δ = 33.95 (NC(CH_3)$_3$), 47.10 (N(CH_3)$_2$), 53.44 (C(CH_3)$_3$), 86.39 (SCH_2N), 88.15 (NCH_2N)

^{7}Li-NMR (116.46 MHz, C_6D_6): δ = 2.53

7.3.24 $[Li_4\{(NSiMe_3)_2SCH_2N(Me)CH_2N(Me)CH_2(O)\}\{NSN(SiMe_3)\}$-$(O\textit{t}Bu)]_2$ (25)

$[Li\{H_2CN(Me)\}_2CH_2]$ (0.20 g, 1.75 mmol, 2.0 eq.) was suspended in pentane (10 mL) and $S(NSiMe_3)_2$ (0.72 g, 3.50 mmol, 4.0 eq.) was slowly added at -78 °C. The solution was allowed to warm to rt over night, filtered and reduced in volume. Upon storage at -30 °C colourless crystals were obtained after four days.

Empirical formula: $C_{35.44}H_{96.02}Li_8N_{12}O_4Si_{6.57}$ **Molecular weight**: 1122.87 g/mol

7.3.25 $[Mg\{Me_2PCH_2S(N\textit{t}Bu)_2\}_2]$ (26)

$MgCl_2$ (0.17 g, 1.80 mmol, 1.1 eq.) was dissolved in THF (5 mL) and cooled to -10 °C. $[Li\{Me_2PCH_2S(N\textit{t}Bu)_2\}]_2$ (**1**) (0.84 g, 1.64 mmol, 1.0 eq.) was dissolved in pentane (20 mL), cooled with an ice bath and added dropwise to the solution of $MgCl_2$. The suspension was allowed to warm to rt and stirred overnight. The solvent was removed *in vacuo* and the resulting yellow powder suspended in 20 mL pentane. The suspension was filtered over celite and the volume of the filtrate was reduced. Colourless crystals were obtained after storing the yellow solution for three days at 4 °C.

Empirical formula: $C_{22}H_{52}MgN_4P_2S_2$ **Molecular weight**: 523.07 g/mol

Yield: 0.54 g, 1.03 mmol, 64 % **Melting point**: 165.5 °C (decomp.)

Elemental analysis (found (calc.) [%]): C 49.93 (50.52), H 9.96 (10.02), N 10.95 (10.71), S 12.21 (12.26)

^{1}H-NMR (500.13 MHz, C_6D_6): δ = 0.976 (d, 6 H, $^{2}J_{P-H}$ = 1.08 Hz, P(CH_3)$_2$), 0.978 (d, 6 H, $^{2}J_{P-H}$ = 1.10 Hz, P(CH_3)$_2$), 1.39 (s br, 36 H, C(CH_3)$_3$), 2.51 (pseudo tr, 4 H, $^{2}J_{P-H}$ = 1.65 Hz, PCH_2S)

^{13}C-NMR (125.76 MHz, C_6D_6): δ = 14.67 (d, $^{1}J_{P-C}$ = 4.06 Hz, P(*C*H$_3$)$_2$), 14.71 (d, $^{1}J_{P-C}$ = 4.06 Hz, P(*C*H$_3$)$_2$), 33.67 (C(*C*H$_3$)$_3$), 53.08 (*C*(CH$_3$)$_3$), 65.92 (d, $^{1}J_{P-C}$ = 1.85 Hz, P*C*H$_2$S), 65.94 (d, $^{1}J_{P-C}$ = 1.99 Hz, P*C*H$_2$S)

^{31}P-NMR (202.46 MHz, C_6D_6): δ = -82.69 (s br)

7.3.26 [Mg{$Me_2PCH_2S(NSiMe_3)_2$}$_2$] (27)

[Li{$Me_2PCH_2S(NSiMe_3)_2$}]$_2$ (**4**) (0.54 g, 0.94 mmol, 1.0 eq.) and $MgCl_2$ (0.13 g, 1.4 mmol, 1.5 eq.) were joined in an argon drybox and dissolved in THF (10 mL). After stirring for 24 h at rt, the solvent was evaporated *in vacuo* and the resulting powder suspended in pentane (10 mL). The suspension was filtered and reduced in volume. After storing the colourless solution at 4 °C for four days, crystals suitable for structural analysis were obtained.

Empirical formula: $C_{18}H_{52}MgN_4P_2S_2Si_4$ **Molecular weight**: 587.36 g/mol

Yield: 0.53 g, 0.90 mmol, 96 % **Melting point**: 206.5 °C (decomp.)

Elemental analysis (found (calc.) [%]): C 36.92 (36.81), H 9.27 (8.92), N 9.75 (9.54), S 11.11 (10.92)

^{1}H-NMR (500.13 MHz, C_6D_6): δ = 0.29 (s, 36 H, NSi(CH_3)$_3$), 0.91 (s, 12 H, P(CH_3)$_2$), 2.398 (d, 2 H, $^{2}J_{P-H}$ = 1.93 Hz, PCH_2S), 2.402 (d, 2 H, $^{2}J_{P-H}$ = 1.93 Hz, PCH_2S)

^{13}C-NMR (125.76 MHz, C_6D_6): δ = 2.75 (NSi(*C*H$_3$)$_3$), 13.77 (d, $^{1}J_{P-C}$ = 2.30 Hz, P(*C*H$_3$)$_2$), 13.79 (d, $^{1}J_{P-C}$ = 2.30 Hz, P(*C*H$_3$)$_2$), 67.57 (P*C*H$_2$S)

^{29}Si-NMR (99.36 MHz, C_6D_6): δ = -4.05

^{31}P-NMR (202.46 MHz, C_6D_6): δ = -84.63

7.3.27 [Ca{$Ph_2PCH_2S(NSiMe_3)_2$}$_2$] (28)

To a slurry of [Ca{N(SiMe$_3$)$_2$}$_2$] (0.10 g, 0.29 mmol, 1.0 eq.) in pentane (25 mL) a solution of [(tmeda)Li{$Ph_2PCH_2S(NSiMe_3)_2$}] (**11**) (0.30 g, 0.57 mmol, 2.0 eq.) in pentane (10 mL) was slowly added at -78 °C. After warming to rt and stirring

overnight, the light yellow suspension was filtered over celite, reduced in volume and stored at 4 °C, yielding colourless crystals after one day.

Empirical formula: $C_{38}H_{60}CaN_4P_2S_2Si_4$ **Molecular weight**: 851.40 g/mol

Yield: 0.12 g, 0.14 mmol, 48 %

Elemental analysis (found (calc.) [%]): C 53.49 (53.61), H 7.13 (7.10), N 7.19 (6.58), S 8.19 (7.53)

^{1}H-NMR (300.13 MHz, C_6D_6): δ = 0.19 (s, 36 H, NSi(CH_3)$_3$), 3.39 (d, 4 H, $^{2}J_{P-H}$ = 5.01 Hz, PCH_2S), 6.99-7.07 (m, 12 H, *o*-H, *p*-H), 7.51-7.57 (m, 8 H, *m*-H)

^{13}C-NMR (125.76 MHz, C_6D_6): δ = 2.39 (NSi(CH$_3$)$_3$), 70.09 (PCH$_2$S), 128.75 (pseudo tr, *o*-C), 128.00 (*p*-C), 133.00 (m, $^{3}J_{P-C}$ = 18.25 Hz, *m*-C), 137.29 (*i*-C)

^{29}Si-NMR (99.36 MHz, C_6D_6): δ = -3.67

^{31}P-NMR (121.49 MHz, C_6D_6): δ = -39.31

7.3.28 [Sr{$Ph_2PCH_2S(NSiMe_3)_2$}$_2$] (29)

To a slurry of [Sr{N(SiMe$_3$)$_2$}$_2$] (0.15 g, 0.37 mmol, 1.0 eq.) in pentane (5 mL) a solution of **11** (0.39 g, 0.73 mmol, 2.0 eq.) in pentane (10 mL) was slowly added at -78 °C. After warming to rt and stirring overnight, the light yellow suspension was filtered over celite, reduced in volume and stored at 4 °C, yielding colourless crystals after two days.

Empirical formula: $C_{38}H_{60}SrN_4P_2S_2Si_4$ **Molecular weight**: 898.94 g/mol

Yield (crystals): 0.15 g, 0.17 mmol, 45 %

Elemental analysis (found (calc.) [%]): C 50.73 (50.77), H 7.04 (6.73), N 6.34 (6.23), S 7.44 (7.13)

^{1}H-NMR (300.13 MHz, C_6D_6): δ = 0.21 (s, 36 H, NSi(CH_3)$_3$), 3.41 (d, $^{2}J_{P-H}$ = 5.15 Hz, PCH_2S), 6.99-7.05 (m, 12 H, *p*-H, *o*-H), 7.47-7.50 (m, 8 H, *m*-H)

^{13}C-NMR (125.76 MHz, C_6D_6): δ = 2.42 (NSi(CH$_3$)$_3$), 70.08 (d, $^{1}J_{P-C}$ = 5.55 Hz, PCH$_2$S), 128.76 (m, *o*-C), 128.95 (*p*-C), 133.66-133.88 (m, *m*-C), 137.46 (m, *i*-C)

^{29}Si-NMR (99.36 MHz, C_6D_6): δ = -4.53

^{31}P-NMR (121.49 MHz, C_6D_6): δ = -36.07

7.3.29 [Co{$Ph_2PCH_2S(NSiMe_3)_2$}$_2$] (30)

To a slurry of [Co{N(SiMe$_3$)$_2$}$_2$] (0.11 g, 0.29 mmol, 1.0 eq.) in pentane (5 mL) a solution of **11** (0.29 g, 0.57 mmol, 2.0 eq.) in pentane (10 mL) was slowly added at -78 °C. After warming to rt and stirring overnight, the blue-purple suspension was

filtered over celite, reduced in volume and stored at 4 °C, yielding blue crystals after two hours.

Empirical formula: $C_{38}H_{60}CoN_4P_2S_2Si_4$ **Molecular weight**: 870.25 g/mol

Yield (crystals): 0.05 g, 0.06 mmol, 21 %

Elemental analysis (found (calc.) [%]): C 51.58 (52.44), H 7.17 (6.95), N 6.59 (6.44), S 7.59 (7.37)

7.3.30 [Fe{$Ph_2PCH_2S(NSiMe_3)_2$}$_2$] (31) and [{$FeN(SiMe_3)_2$}-{$Li(NSiMe_3)_2SCHP(O)Ph_2$}(LiO)]$_2$ (32)

To a slurry of [Fe{$N(SiMe_3)_2$}$_2$] (0.21 g, 0.55 mmol, 1.0 eq.) in pentane (10 mL) a solution of **11** (0.58 g, 1.10 mmol, 2.0 eq.) in pentane (20 mL) was slowly added at -78 °C. After warming to rt and stirring overnight, the light brown suspension was filtered over celite, reduced in volume and stored at 4 °C, yielding colourless and red crystals after one month.

Empirical formula: $C_{38}H_{60}FeN_4P_2S_2Si_4$ (colourless)

Molecular weight: 867.17 g/mol

Empirical formula: $C_{50}H_{94}Fe_2Li_4N_6O_4P_2S_2Si_8$ (red)

Molecular weight: 1333.57 g/mol

7.3.31 [{$Cu(Me_2PCH_2S(NSiMe_3)_2)$}$_4${$Cu_2S$}$_4$] (33)

[Cu{$N(SiMe_3)_2$}] (0.20 g, 0.89 mmol, 2.0 eq.) was suspended in THF (15 mL). **4** (0.26 g, 0.45 mmol, 1.0 eq.) in pentane (15 mL) was slowly added at -78 °C. After stirring over night the solvent was removed *in vacuo* and the residue suspended in hexane (30 mL) and filtered over celite. The orange solution was reduced in volume and stored at 4 °C for two weeks, yielding colourless crystals.

Empirical formula: $C_{36}H_{104}Cu_{12}N_8P_4S_8Si_8$ **Molecular weight**: 2016.83 g/mol

^{1}H-NMR (300.13 MHz, C_6D_6): δ = 0.41 (s, 18 H, NSi(CH_3)$_3$), 0.42 (s, 18 H, NSi(CH_3)$_3$), 1.46 (d, 6 H, $^2J_{P-H}$ = 4.95 Hz, P(CH_3)$_2$), 1.53 (d, 6 H, $^2J_{P-H}$ = 3.99 Hz, P(CH_3)$_2$), 2.12 (dd, 4 H, $^2J_{H-H}$ = 13.50 Hz, $^2J_{P-H}$ = 4.15 Hz, PCH_2S), 2.28 (dd, 4 H, $^2J_{H-H}$ = 13.50 Hz, $^2J_{P-H}$ = 6.04 Hz, PCH_2S)

^{31}P-NMR (121.49 MHz, C_6D_6): δ = -75.78

7.3.32 [(tmeda)Rb{$Ph_2PCH_2S(NSiMe_3)_2$}$_2$Li] (34)

To a slurry of [Rb{$N(SiMe_3)_2$}] (0.14 g, 0.57 mmol, 1.0 eq.) in pentane (5 mL) a solution of **11** (0.30 g, 0.57 mmol, 1.0 eq.) in pentane (10 mL) was slowly added at -78 °C. After warming to rt and stirring overnight, the light brown suspension was filtered over celite, reduced in volume and stored at 4 °C, yielding yellow crystals after two hours.

Empirical formula: $C_{44}H_{76}LiN_6P_2RbS_2Si_4$ **Molecular weight**: 1019.94 g/mol

Yield (crystals): 0.26 g, 0.26 mmol, 45 %

Elemental analysis (found (calc.) [%]): C 51.60 (51.81), H 7.60 (7.51), N 8.32 (8.24), S 6.55 (6.29)

^{1}H-NMR (300.13 MHz, C_6D_6): δ = 0.30 (s, 36 H, NSi(CH_3)$_3$), 2.08 (s, 12 H, N(CH_3)$_2$), 3.43 (s, 4 H, PCH_2S), 7.02-7.13 (m, 12 H, *o*-H, *p*-H), 7.56 (s br, 8 H, *m*-H); the N(CH_2)$_2$N protons were not resolved from the baseline

^{7}Li-NMR (194.37 MHz, C_6D_6): δ = 1.81 (s br)

^{13}C-NMR (125.76 MHz, C_6D_6): δ = 3.37 (NSi(*C*H$_3$)$_3$), 45.85 (N(*C*H$_3$)$_2$), 57.53 (br, N(*C*H$_2$)$_2$N), 67.99 (br, P*C*H$_2$S), 128.29 (*o*-C), 128.65 (br, *p*-C), 132.47 (d, $^3J_{P-C}$ = 18.71 Hz, *m*-C), 133.53 (d, $^1J_{P-C}$ = 18.35 Hz, *i*-C)

^{29}Si-NMR (99.36 MHz, C_6D_6): δ = -5.63 (s br)

^{31}P-NMR (202.46 MHz, C_6D_6): δ = -33.03 (s br)

7.3.33 [(tmeda)K{$Ph_2PCH_2S(NSiMe_3)_2$}$_2$Li] (35)

To a slurry of [K{$N(SiMe_3)_2$}] (0.11 g, 0.57 mmol, 1.0 eq.) in pentane (5 mL) a solution of **11** (0.30 g, 0.57 mmol, 1.0 eq.) in pentane (10 mL) was slowly added at -78 °C. After warming to rt and stirring overnight, the yellow suspension was filtered over celite, reduced in volume and stored at -25 °C, yielding yellow crystals after four days.

Empirical formula: $C_{44}H_{76}LiN_6P_2KS_2Si_4$ **Molecular weight**: 973.57 g/mol

Yield (crystals): 0.16 g, 0.16 mmol, 29 %

^{1}H-NMR (300.13 MHz, C_6D_6): δ = 0.23 (s, 18 H, NSi(CH_3)$_3$), 0.30 (s, 18 H, NSi(CH_3)$_2$), 2.04 (s br, 16 H, (CH_3)$_2$N, N(CH_2)$_2$N), 3.40 (s br, 4 H, PCH_2S), 6.98-7.13 (m, 12 H, *o*-H, *p*-H), 7.46-7.68 (m, 8 H, *m*-H)

^{7}Li-NMR (116.64 MHz, C_6D_6): δ = 1.90 (s br)

^{31}P-NMR (121.49 MHz, C_6D_6): δ = -33.99 (s br), -33.30 (s br)

8 CRYSTALLOGRAPHIC SECTION

8.1 Crystal Application

The crystals were taken from the mother liquor using standard *Schlenk* techniques and placed in perfluorated polyether oil on a microscope slide. An appropriately sized crystal of high quality was selected under a polarization microscope with the help of the X-TEMP2 cooling device (Figure 8-1).[213] Thereby a crystal can be chosen under a protective nitrogen atmosphere and a desired temperature can be determined. The crystal was then mounted on the tip of a glass fibre, fixed to a goniometer head and shock cooled by the open-flow crystal cooling device. The polyether oil froze to a glas around the crystal protecting it, along with the nitrogen gas flow, from oxygen and moisture.

Figure 8-1: Mountig table with the X-TEMP2 cooling device.[214]

8.2 Data Collection and Processing

Data were collected on a Bruker SMART-APEXII rotating anode with D8 goniometer (Mo K_α radiation, λ = 71.073 pm; INCOATEC Helios mirror optics) or an Incoatec microfocus source with Quazar mirror optics (Figure 8-2).[215] All crystals were centered optically using a video camera after being mounted onto the diffractometer.

Data collection was carried out with the APEX2 program package.[216] Usually 48 frames in three different orientations were collected to check the crystal quality and determine the exposure time. The final measurement was then carried out in ω-scan mode with a step-width of 0.3°.

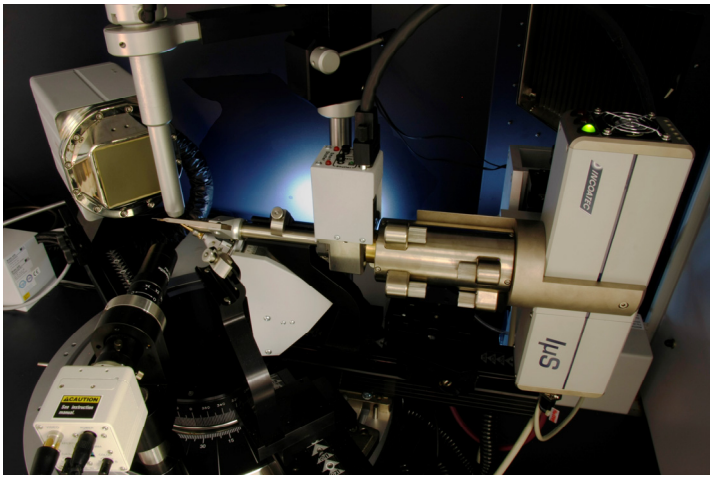

Figure 8-2: Setup of the INCOATEC micro focus source.[214]

The unit cell was searched and refined using APEX2.[216] The data were integrated with SAINT[217] and an empirical absorption correction with SADABS was applied.[218] XPREP was used to determine the space group and for data merging.[219]

8.3 Structure Solution and Refinement

The structures were solved by direct methods with SHELXS and refined on F^2 using the full-matrix least-squares methods of SHELXL.[220] From the integration the square of the structure factors F_o^2 was obtained which is directly proportional to the measured intensities. All non-hydrogen atoms were refined with anisotropic displacement parameters.

The results of the refinements were verified by comparison of the calculated (F_c) and the observed (F_o) structure factors. Commonly used criteria are the residuals $R1$ (Equation 8-1) and $wR2$ (Equation 8-2). The value of $wR2$ is thereby more significant because the model is refined against F^2.[221]

$$R1 = \frac{\sum_{hkl} \left\| F_o - F_c \right\|}{\sum_{hkl} \left| F_o \right|}$$

Equation 8-1: Definition of $R1$.[221]

$$wR2 = \sqrt{\frac{\sum_{hkl} w\left(F_o^{\,2} - F_c^{\,2}\right)^2}{\sum_{hkl} w(F_o^{\,2})^2}}$$

Equation 8-2: Definition of $wR2$.[221]

Ideally, the residual densities at the end of the refinement should be low (*i. e*. below 1.00 eÅ^{-3}). In addition, the deepest hole in the residual electron density map should be of comparable value. Due to model restrictions the residuals are normally found in the bonding regions. Higher residuals for heavy scatterers are acceptable as they arise mainly from absorption effects and *Fourier* truncation errors due to the limited recorded resolution range. The highest peak and deepest hole from difference *Fourier* analysis are listed in the crystallographic tables.

All hydrogen atoms bonded to sp^2 (sp^3) carbon atoms were assigned ideal positions and refined using a riding model with U_{iso} constrained to 1.2 (1.5) times the U_{eq} value of the parent carbon atom. Hydrogen atoms bound to heteroatoms were located on the electron density map and refined using distance restraints. This is necessary because of the low electronegativity of hydrogen. Thus, its electron density is usually delocalised in direction of the heteroatom and only pseudo hydrogen positions can be found.

8.4 Treatment of Disorder

Especially *t*Bu groups or solvent molecules in the crystal can show thermal motion. Thus one given position cannot be unambiguously determined – the molecules or parts of them are disordered over different sites (positional disorder). This is often the case with ending groups which can rotate or tilt. In addition, atom positions can be occupied by different elements at the same time (site occupancy disorder).

To resolve disorder with the so-called split-atom model, the structure has to be refined as good as possible, thereby the disorder can be described more accurately. The main position of the disordered group is first described isotropically. Afterwards, the second position is assigned either by naming the corresponding Q-peaks or using the coordinates from the *.lst file. Meanwhile, both sites are constrained to sum up to 1. Afterwards, the final refinement is undertaken as usual. Often it is helpful to assign disorder step by step in order to stabilise the refinement.[222]

In order to get physically sensible groups and to enhance the model it is often helpful or necessary to use constraints and restraints. A constraint is a mathematical operation fixing structural parameters on exact values (*e. g*. treatment of hydrogen atoms). Restraints introduce additional chemical or crystallographical information into the model. Restraints add to the data of the refinement and have to be observed within their standard deviations. Important restraints in SHELXL are SIMU and DELU

(as well ISOR) which affect the anisotropic displacement parameters.[223] DELU is the rigid bond restraint that fits the components of the anisotropic displacement parameters along the bonds resulting in uniform ADPs. SIMU is the similarity restraint which adjusts the ADPs of neighbouring atoms within a certain radius to be equal according to their esd's. ISOR forces the ADPs to adapt a more spherical, isotropic behavior, which is sometimes necessary to refine positions with minor occupation factors but should not be excessively used.

8.5 Crystallographic Details

8.5.1 [Li{$Ph_2PCH_2S(NtBu)_2$}]$_2$ (2)

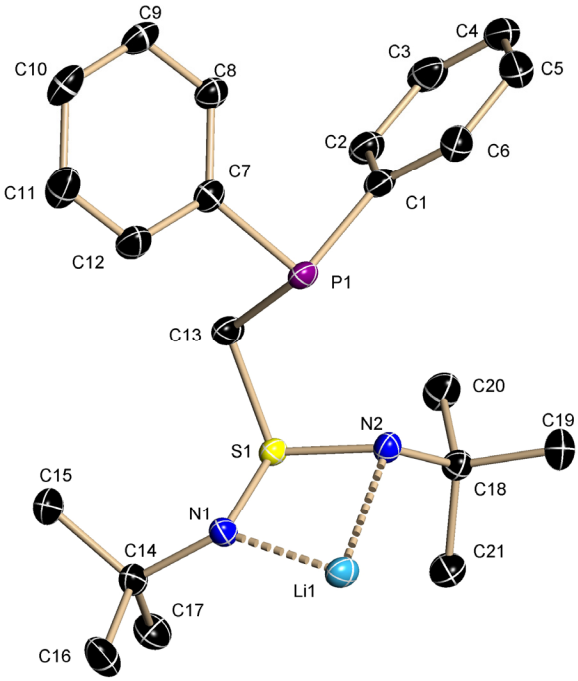

Asymmetric unit of **2**. The anisotropic displacement parameters are shown at the 50 % probability level, hydrogen atoms are omitted for clarity.

identification code	Ph-Schnecke	μ [mm^{-1}]	0.235
empirical formula	$C_{42}H_{60}N_4P_2S_2Li_2$	F(000)	408
molecular weight [g/mol]	760.93	max./min. transmission	0.8623/0.7544
crystal size [mm]	0.18 x 0.1 x 0.05	θ range [°]	1.88-28.28
temperature [K]	100(2)	completeness to θ_{max}	1.000
crystal system	triclinic	reflections collected	25994
space group	$P\bar{1}$	independent reflections	5259
a [Å]	9.6236(11)	R_{int}/R_σ	0.0399/0.0359
b [Å]	10.1512(12)	restraints/parameters	0/241
c [Å]	11.3253(13)	GoF	1.054
α [°]	73.936(2)	R1 (all data)	0.0564
β [°]	84.728(2)	R1 (I>2σ(I))	0.0391
γ [°]	88.960(2)	wR2 (all data)	0.1026
V [Å^3]	1058.7(2)	wR2 (I>2σ(I))	0.0976
Z	1	diff. peak/hole [eÅ^{-3}]	0.391/-0.381
ρ_{calc} [g cm^{-3}]	1.193	g1/g2	0.0518/0.3215

8.5.2 $[Li\{Me(Ph)PCH_2S(NSiMe_3)_2\}]_2$ (3)

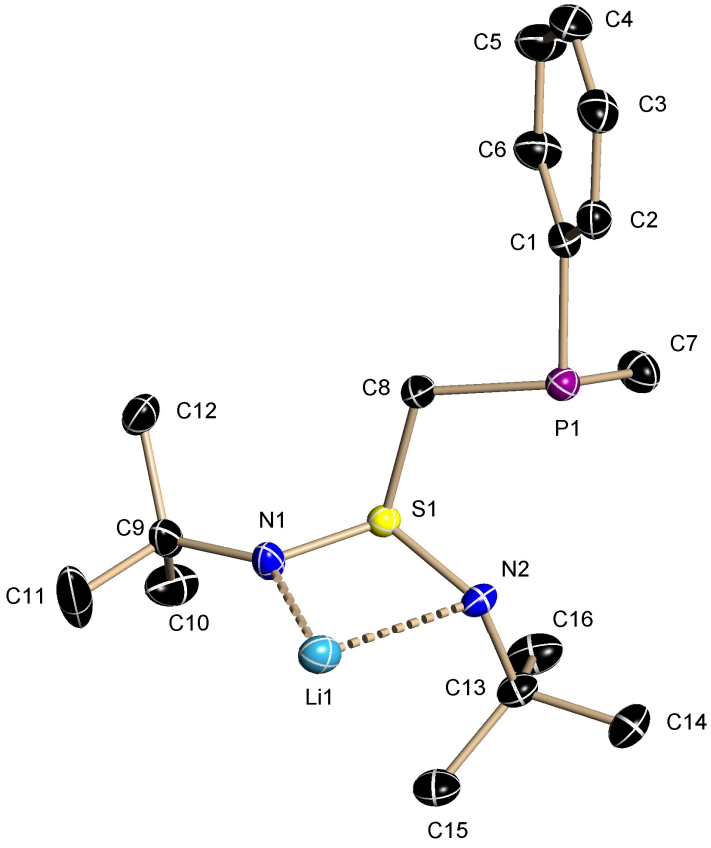

Asymmetric unit of **3**. The anisotropic displacement parameters are shown at the 50 % probability level, hydrogen atoms are omitted for clarity.

identification code	Me-Ph-Schnecke	*F*(000)	688
empirical formula	$C_{32}H_{56}N_4P_2S_2Li_2$	max./min. transmission	0.9703/0.9358
molecular weight [g/mol]	636.78	θ range [°]	1.96-26.37
crystal size [mm]	0.16 x 0.14 x 0.08	completeness to θ_{max}	0.999
temperature [K]	100(2)	reflections collected	39157
crystal system	monoclinic	independent reflections	3784
space group	$P2_1/c$	R_{int}/R_σ	0.0274/0.0128
a [Å]	10.5006(14)	restraints/parameters	0/197
b [Å]	20.753(3)	GoF	1.050
c [Å]	8.5699(11)	*R*1 (all data)	0.0325
β [°]	97.279(2)	*R*1 (*I*>2σ(*I*))	0.0305
V [Å^3]	1852.5(4)	*wR*2 (all data)	0.0788
Z	2	*wR*2 (*I*>2σ(*I*))	0.0778
ρ_{calc} [g cm^{-3}]	1.142	diff. peak/hole [eÅ^{-3}]	0.409/-0.247
μ [mm^{-1}]	0.256	g1/g2	0.0355/1.043

8.5.3 $[Li\{Me_2PCH_2S(NSiMe_3)_2\}]_2$ (4)

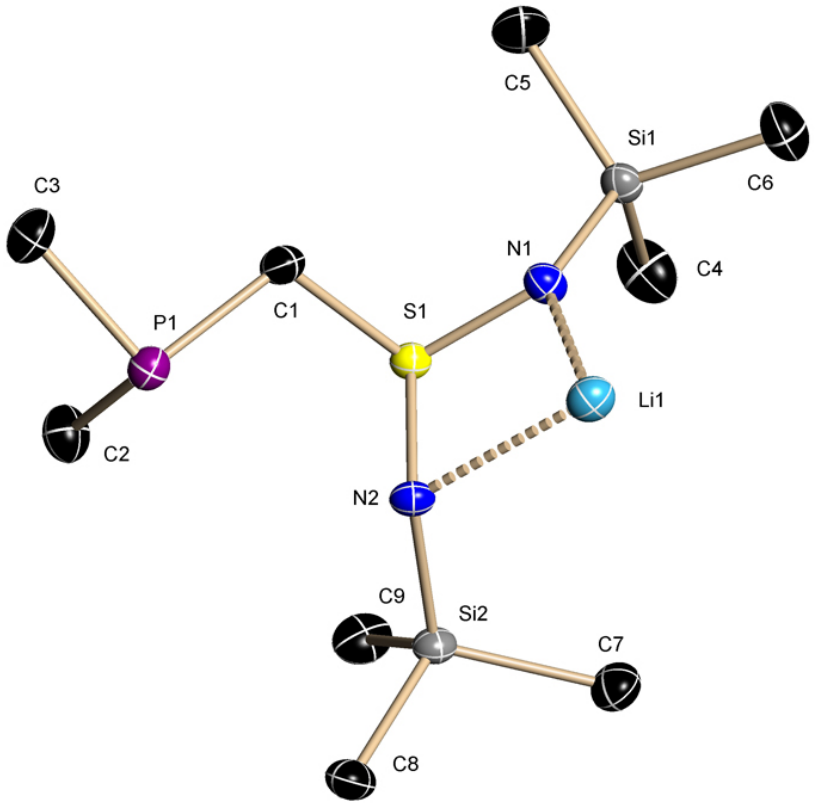

Asymmetric unit of **4** . The anisotropic displacement parameters are shown at the 50 % probability level, hydrogen atoms are omitted for clarity.

identification code	Krabbe	μ [mm^{-1}]	0.396
empirical formula	$C_{18}H_{52}N_4Si_4P_2S_2Li_2$	F(000)	312
molecular weight [g/mol]	576.93	max./min. transmission	0.9703/0.9262
crystal size [mm]	0.14 x 0.12 x 0.02	θ range [°]	2.18-26.37
temperature [K]	100(2)	completeness to θ_{max}	0.998
crystal system	triclinic	reflections collected	21105
space group	$P\bar{1}$	independent reflections	3546
a [Å]	10.2715(11)	R_{int}/R_σ	0.0145/0.0148
b [Å]	10.3560(11)	restraints/parameters	0/153
c [Å]	10.4832(11)	GoF	0.861
α [°]	68.6360(10)	R1 (all data)	0.0236
β [°]	65.7280(10)	R1 (I>2σ(I))	0.0216
γ [°]	60.9900(10)	wR2 (all data)	0.0619
V [Å^3]	869.77(16)	wR2 (I>2σ(I))	0.0607
Z	1	diff. peak/hole [eÅ^{-3}]	0.314/-0.223
ρ_{calc} [g cm^{-3}]	1.101	g1/g2	0.0391/0.5002

8.5.4 $[Li\{Ph_2PCH_2S(NSiMe_3)_2\}]_2$ (5)

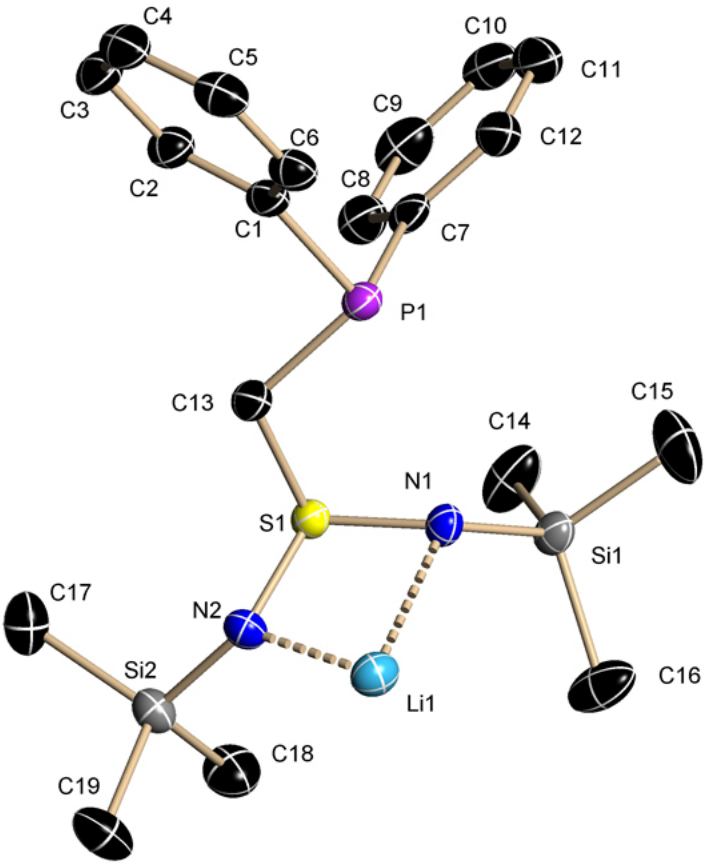

Asymmetric unit of **5**. The anisotropic displacement parameters are shown at the 50 % probability level, hydrogen atoms are omitted for clarity.

identification code	MMP163	*F*(000)	880
empirical formula	$C_{38}H_{60}Li_2N_4P_2S_2Si_4$	max./min. transmission	0.9422/0.5030
molecular weight [g/mol]	825.20	θ range [°]	1.83-26.74
crystal size [mm]	0.20 x 0.04 x 0.02	completeness to θ_{max}	0.999
temperature [K]	100(2)	reflections collected	28120
crystal system	monoclinic	independent reflections	5013
space group	$P2_1/n$	R_{int}/R_σ	0.0761/0.0550
a [Å]	9.2956(18)	restraints/parameters	0/241
b [Å]	14.412(3)	GoF	1.061
c [Å]	17.625(4)	*R*1 (all data)	0.0436
β [°]	91.707(3)	*R*1 (*I*>2σ(*I*))	0.0373
V [Å^3]	2360.1(8)	*wR*2 (all data)	0.1065
Z	2	*wR*2 (*I*>2σ(*I*))	0.1016
ρ_{calc} [g cm^{-3}]	1.161	diff. peak/hole [eÅ^{-3}]	0.463/-0.332
μ [mm^{-1}]	0.312	g1/g2	0.1325/3.7432

8.5.5 $[Li\{Me(Ph)PCH_2S(NSiMe_3)\}]_2$ (6)

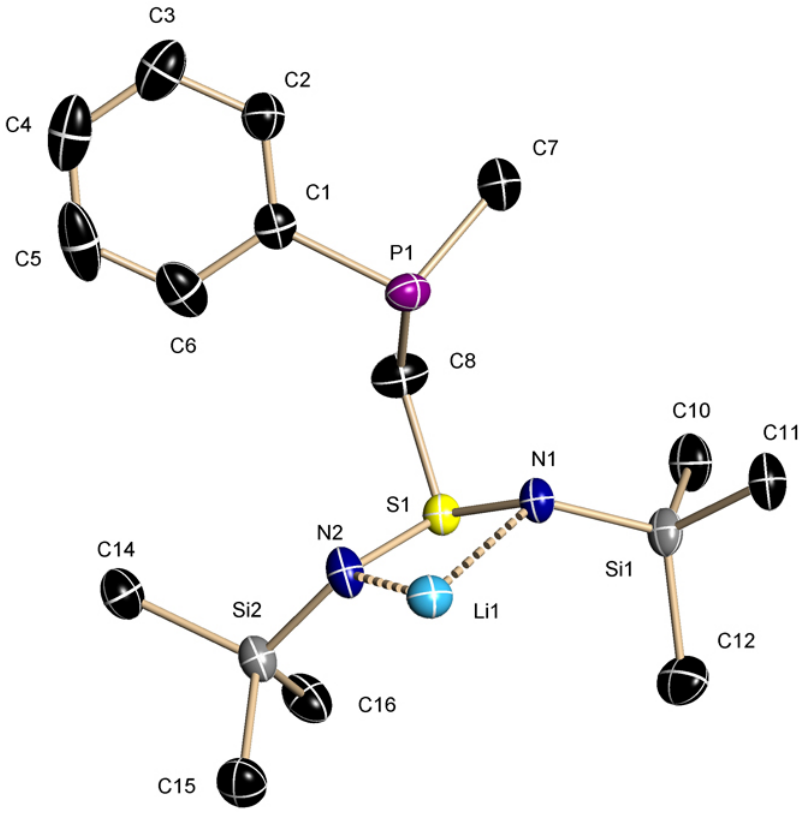

Asymmetric unit of **6**. The anisotropic displacement parameters are shown at the 50 % probability level, hydrogen atoms are omitted for clarity. The residual density is above 1.00 eÅ^{-3} because the data quality is not sufficient.

identification code	MMP103_1	μ [mm^{-1}]	0.352
empirical formula	$C_{28}H_{56}Li_2N_4P_2S_2Si_4$	F(000)	376
molecular weight [g/mol]	701.07	max./min. transmission	0.9422/0.8182
crystal size [mm]	0.2 x 0.2 x 0.1	θ range [°]	2.363-26.5295
temperature [K]	100(2)	completeness to θ_{max}	0.998
crystal system	triclinic	reflections collected	17074
space group	$P\bar{1}$	independent reflections	3991
a [Å]	10.5602(12)	R_{int}/R_σ	0.0448/0.0369
b [Å]	10.9235(13)	restraints/parameters	0/198
c [Å]	10.9438(13)	GoF	1.029
α [°]	79.480(2)	R1 (all data)	0.0749
β [°]	66.032(2)	R1 (I>2σ(I))	0.0539
γ [°]	61.491(2)	wR2 (all data)	0.1507
V [Å^3]	1013.6(2)	wR2 (I>2σ(I))	0.1375
Z	1	diff. peak/hole [eÅ^{-3}]	1.343/-0.296
ρ_{calc} [g cm^{-3}]	1.149	g1/g2	0.0756/1.6538

8.5.6 $[Li\{Et_2PCH(CH_3)S(NSiMe_3)\}]_2$ (7)

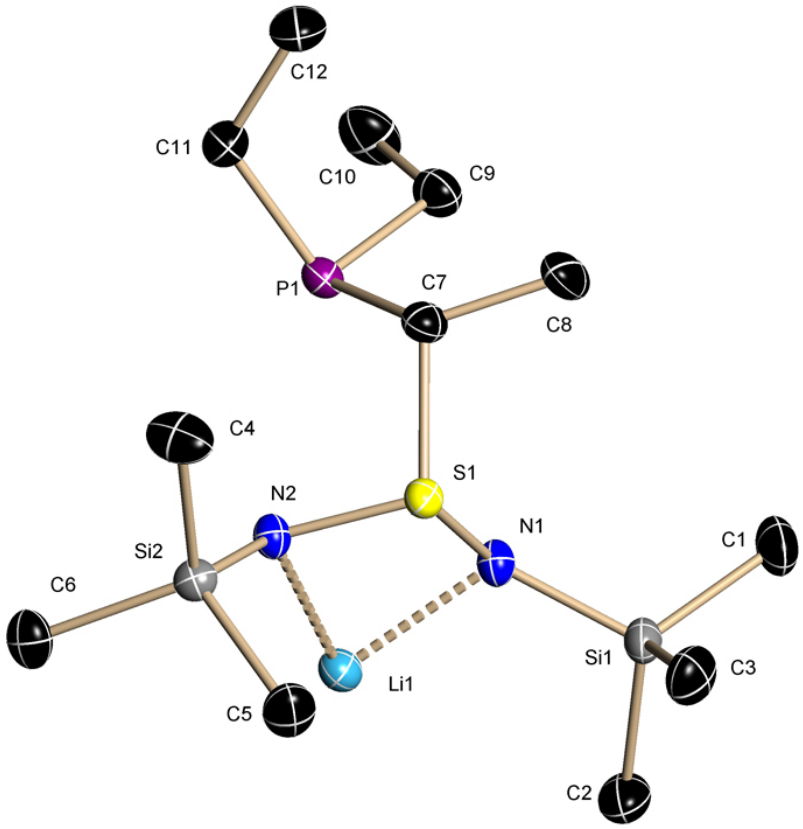

Asymmetric unit of **7**. The anisotropic displacement parameters are shown at the 50 % probability level, hydrogen atoms are omitted for clarity.

identification code	Spinne	μ [mm^{-1}]	0.357
empirical formula	$C_{24}H_{64}N_4Si_4P_2S_2Li_2$	F(000)	360
molecular weight [g/mol]	661.09	max./min. transmission	0.9422/0.8178
crystal size [mm]	0.8 x 0.3 x 0.04	θ range [°]	2.50-27.88
temperature [K]	100(2)	completeness to θ_{max}	0.996
crystal system	triclinic	reflections collected	39887
space group	$P\bar{1}$	independent reflections	4676
a [Å]	10.6002(6)	R_{int}/R_σ	0.0146/0.0074
b [Å]	10.6350(10)	restraints/parameters	0/181
c [Å]	10.7744(6)	GoF	1.068
α [°]	100.7850(10)	R1 (all data)	0.0299
β [°]	117.3660(10)	R1 (I>2σ(I))	0.0277
γ [°]	103.4460(10)	wR2 (all data)	0.0768
V [Å^3]	986.48(12)	wR2 (I>2σ(I))	0.0747
Z	1	diff. peak/hole [eÅ^{-3}]	0.686/-0.453
ρ_{calc} [g cm^{-3}]	1.113	g1/g2	0.0396/0.456

8.5.7 $[Li\{Me_2P(S)CH_2S(NSiMe_3)_2\}]_2$ (8)

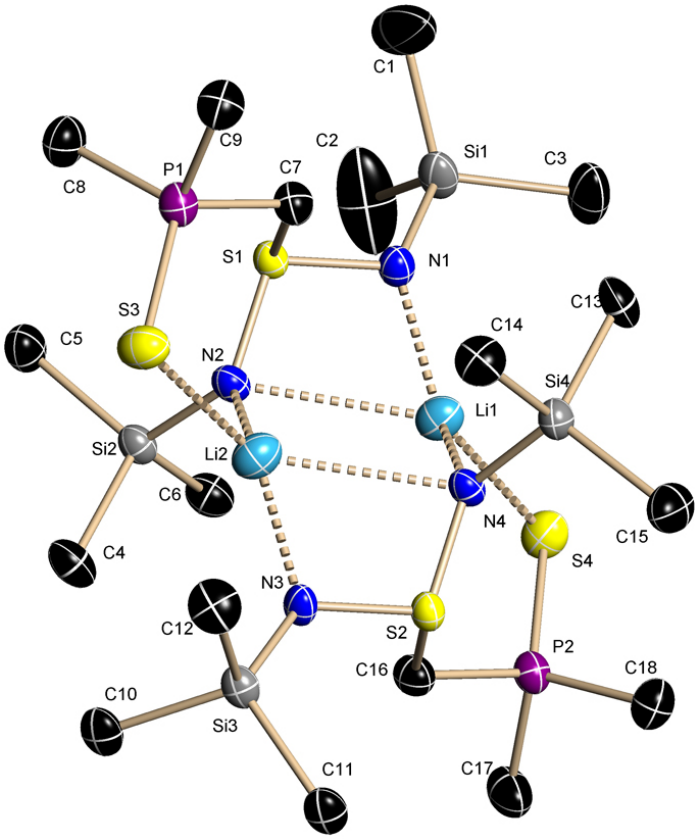

Asymmetric unit of **8**. The anisotropic displacement parameters are shown at the 50 % probability level, hydrogen atoms are omitted for clarity.

identification code	KrabbOx	*F*(000)	1376
empirical formula	$C_{18}H_{52}Li_2N_4P_2S_4Si_4$	max./min. transmission	0.9799/0.9238
molecular weight [g/mol]	641.06	θ range [°]	1.30-25.68
crystal size [mm]	0.12 x 0.06 x 0.04	completeness to θ_{max}	1.0
temperature [K]	100(2)	reflections collected	56599
crystal system	monoclinic	independent reflections	6870
space group	$P2_1/n$	R_{int}/R_σ	0.0824/0.0490
a [Å]	18.3672(19)	restraints/parameters	0/323
b [Å]	11.7143(13)	GoF	1.091
c [Å]	18.699(2)	*R*1 (all data)	0.0837
β [°]	115.876(2)	*R*1 (*I*>2σ(*I*))	0.0517
V [Å^3]	3619.8(7)	*wR*2 (all data)	0.1218
Z	4	*wR*2 (*I*>2σ(*I*))	0.1098
ρ_{calc} [g cm^{-3}]	1.176	diff. peak/hole [eÅ^{-3}]	0.591/-0.645
μ [mm^{-1}]	0.498	g1/g2	0.0399/6.1868

8.5.8 $[Li\{Me_2P(Se)CH_2S(NSiMe_3)_2\}]_2$ (9)

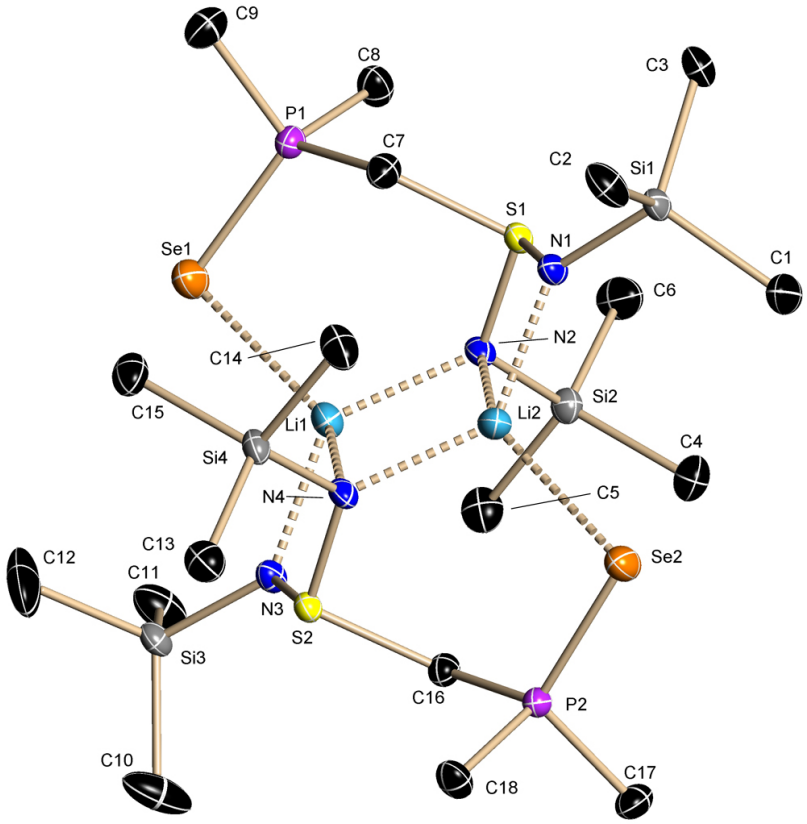

Asymmetric unit of **9**. The anisotropic displacement parameters are shown at the 50 % probability level, hydrogen atoms are omitted for clarity.

identification code	MMP223_2	*F*(000)	1520
empirical formula	$C_{18}H_{52}Li_2N_4P_2S_2Se_2Si_4$	max./min. transmission	0.7080/0.9422
molecular weight [g/mol]	734.86	θ range [°]	2.169-26.269
crystal size [mm]	0.22 x 0.1 x 0.1	completeness to θ_{max}	1.000
temperature [K]	100(2)	reflections collected	42058
crystal system	monoclinic	independent reflections	7260
space group	$P2_1/n$	R_{int}/R_σ	0.0553/0.0410
a [Å]	18.734(3)	restraints/parameters	0/323
b [Å]	11.6198(18)	GoF	1.023
c [Å]	18.839(3)	*R*1 (all data)	0.0495
β [°]	116.104(2)	*R*1 (*I*>2σ(*I*))	0.0325
V [Å^3]	3682.5(10)	*wR*2 (all data)	0.0847
Z	4	*wR*2 (*I*>2σ(*I*))	0.0782
ρ_{calc} [g cm^{-3}]	1.325	diff. peak/hole [eÅ^{-3}]	0.462/-0.713
μ [mm^{-1}]	2.353	g1/g2	0.0352/3.5681

8.5.9 $Ph_2PCH_2S(NSiMe_3)(HNSiMe_3)$ (10)

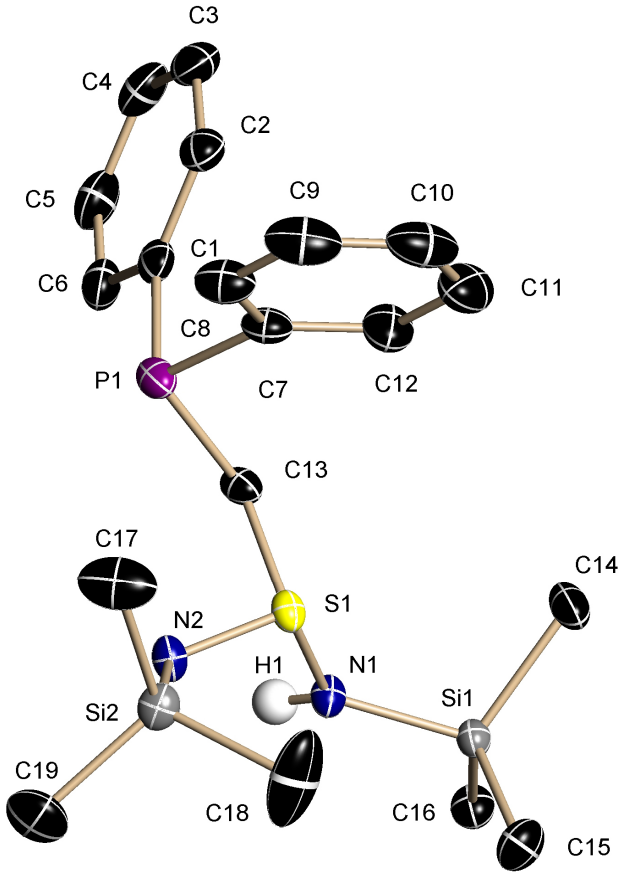

Asymmetric unit of **10**. The anisotropic displacement parameters are shown at the 50 % probability level, hydrogen atoms are omitted for clarity. H1 was freely refined using a distance restraint.

identification code	Moskito	*F*(000)	872
empirical formula	$C_{19}H_{31}Si_2N_2PS$	max./min. transmission	0.9422/0.8590
molecular weight [g/mol]	406.67	θ range [°]	2.59-27.88
crystal size [mm]	0.54 x 0.2 x 0.12	completeness to θ_{max}	0.999
temperature [K]	100(2)	reflections collected	43786
crystal system	monoclinic	independent reflections	5491
space group	$P2_1/n$	R_{int}/R_σ	0.016/0.0083
a [Å]	12.9937(7)	restraints/parameters	1/235
b [Å]	9.9367(6)	GoF	1.052
c [Å]	18.1145(10)	*R*1 (all data)	0.0289
β [°]	99.8430(10)	*R*1 (*I*>2σ(*I*))	0.0278
V [Å^3]	2304.4(2)	*wR*2 (all data)	0.0767
Z	4	*wR*2 (*I*>2σ(*I*))	0.0757
ρ_{calc} [g cm^{-3}]	1.172	diff. peak/hole [eÅ^{-3}]	0.596/-0.340
μ [mm^{-1}]	0.319	g1/g2	0.038/1.0873

8.5.10 [(tmeda)Li{$Ph_2PCH_2S(NSiMe_3)_2$}] (11)

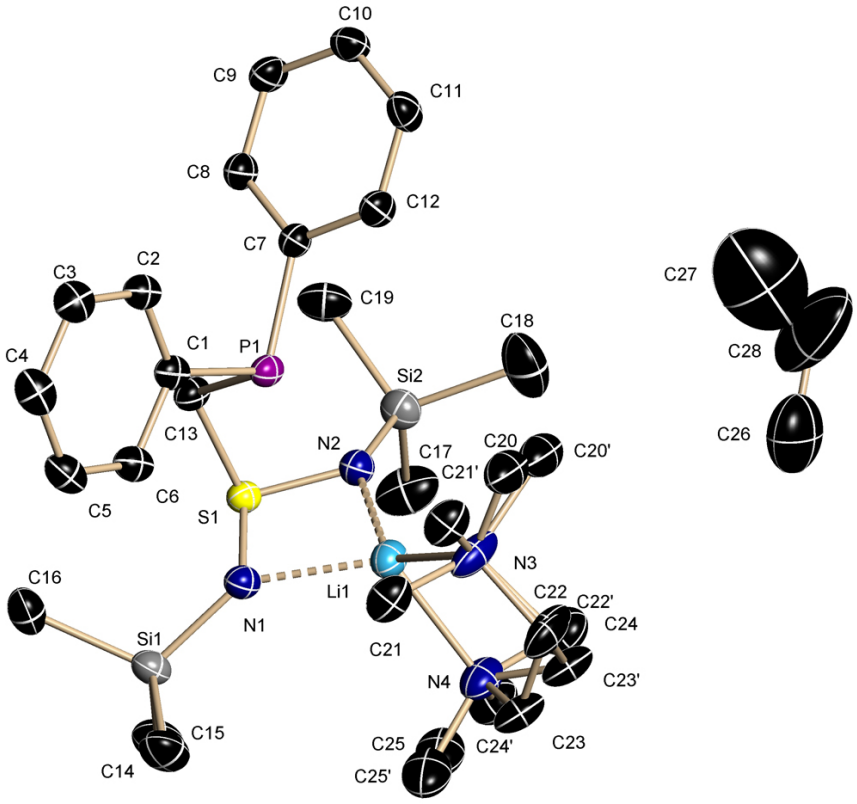

Asymmetric unit of **11**. The anisotropic displacement parameters are shown at the 50 % probability level, hydrogen atoms are omitted for clarity. The pentane molecule is only half occupied as it is situated on a crystallographic mirror plane and was refined using PART -1. The TMEDA ligand is disordered over two sites with occupancies of 67 and 33%, respectively.

identification code	MMPIAN06	*F*(000)	2456
empirical formula	$C_{28}H_{53}LiN_4PSSi_2$	max./min. transmission	0.9422/0.8424
molecular weight [g/mol]	571.89	θ range [°]	1.23-26.02
crystal size [mm]	0.18 x 0.04 x 0.02	completeness to θ_{max}	0.999
temperature [K]	100(2)	reflections collected	48696
crystal system	monoclinic	independent reflections	6847
space group	*C*2/*c*	R_{int}/R_σ	0.0632/0.0384
a [Å]	33.944(5)	restraints/parameters	0/387
b [Å]	9.5352(13)	GoF	1.071
c [Å]	21.921(3)	*R*1 (all data)	0.0520
β [°]	101.895(3)	*R*1 (*I*>2σ(*I*))	0.0382
V [$Å^3$]	6942.4(17)	*wR*2 (all data)	0.0974
Z	8	*wR*2 (*I*>2σ(*I*))	0.0903
ρ_{calc} [g cm^{-3}]	1.081	diff. peak/hole [e$Å^{-3}$]	0.344/-0.244
μ [mm^{-1}]	0.229	g1/g2	0.0288/8.9902

8.5.11 $[Li\{tBu_2P(O)CH_2S(NSiMe_3)_2\}]_2$ (12)

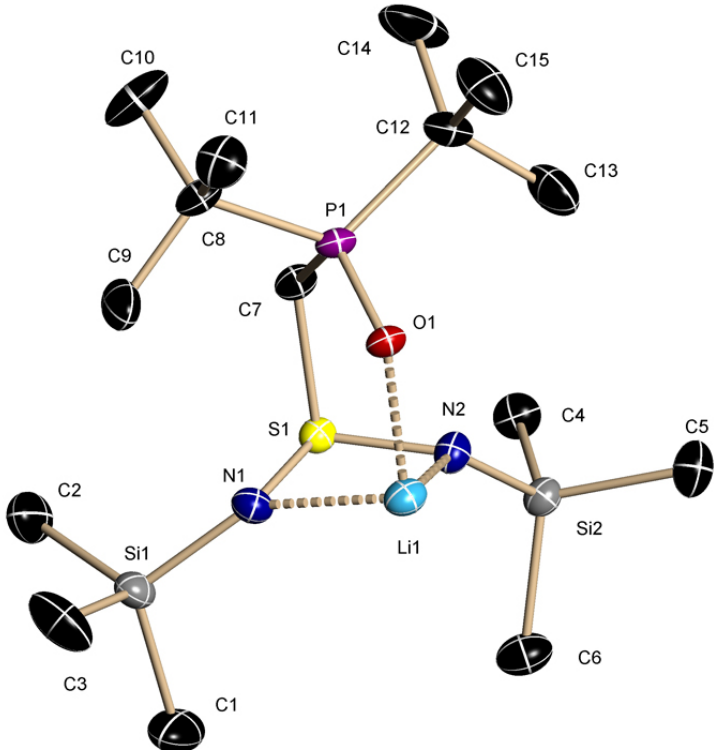

Asymmetric unit of **12**. The anisotropic displacement parameters are shown at the 50 % probability level, hydrogen atoms are omitted for clarity.

identification code	MMP174	μ [mm^{-1}]	0.311
empirical formula	$C_{30}H_{76}Li_2N_4O_2P_2S_2Si_4$	F(000)	424
molecular weight [g/mol]	777.25	max./min. transmission	0.9422/0.8690
crystal size [mm]	0.14 x 0.1 x 0.01	θ range [°]	1.88-26.73
temperature [K]	100(2)	completeness to θ_{max}	0.999
crystal system	triclinic	reflections collected	21034
space group	$P\bar{1}$	independent reflections	4985
a [Å]	10.2856(10)	R_{int}/R_σ	0.0386/0.0349
b [Å]	11.4857(12)	restraints/parameters	0/220
c [Å]	11.7940(12)	GoF	1.044
α [°]	70.915(2)	R1 (all data)	0.0536
β [°]	70.929(2)	R1 (I>2σ(I))	0.0391
γ [°]	66.854(2)	wR2 (all data)	0.1009
V [Å^3]	1178.8(2)	wR2 (I>2σ(I))	0.0936
Z	1	diff. peak/hole [eÅ^{-3}]	0.426/-0.247
ρ_{calc} [g cm^{-3}]	1.095	g1/g2	0.0508/0.5387

8.5.12 [Li{*t*Bu$_2$PCH$_2$S(NSiMe$_3$)$_2$}$_2${*t*Bu$_2$P(O)Me}] (13)

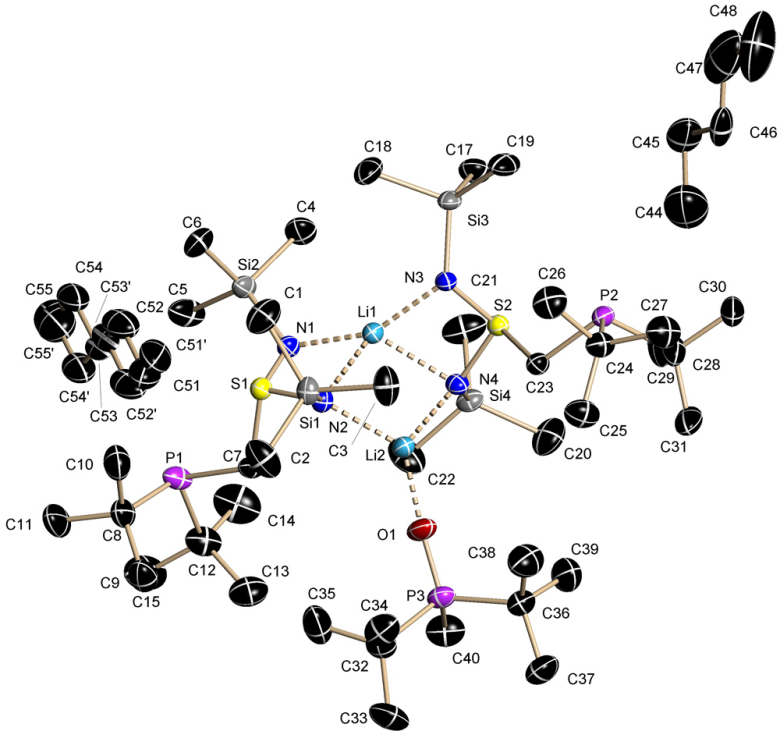

Asymmetric unit of **13**. The anisotropic displacement parameters are shown at the 50 % probability level, hydrogen atoms are omitted for clarity. The occupancy factors of the disordered pentane molecule on a special position refine to 63 and 37 %, respectively. The molecule was refined using SIMU, DELU and ISOR as well as EADP (C55/C55'), SADI and FLAT. As the pentane molecule lies on the mirror plane and because of the bad data quality it is complicated to assign the little electron density in a better way. When SQUEEZE of the PLATON[224] program package is used, the esds of the bond lengths and angles in the [Li{*t*Bu$_2$PCH$_2$S(NSiMe$_3$)$_2$}$_2$] moiety do not improve.

identification code	MMP197_2a	*F*(000)	2192
empirical formula	$C_{44}H_{109}Li_2N_4OP_3S_2Si_4$	max./min. transmission	0.9422/0.8927
molecular weight [g/mol]	993.64	θ range [°]	1.57-26.37
crystal size [mm]	0.2 x 0.2 x 0.1	completeness to θ_{max}	1.000
temperature [K]	100(2)	reflections collected	129001
crystal system	monoclinic	independent reflections	13114
space group	$P2_1/c$	R_{int}/R_σ	0.0342/0.0177
a [Å]	27.929(3)	restraints/parameters	121/659
b [Å]	11.1729(13)	GoF	1.043
c [Å]	22.139(3)	*R*1 (all data)	0.0653
β [°]	111.563(2)	*R*1 (*I*>2σ(*I*))	0.0564
V [Å^3]	6425.0(13)	*wR*2 (all data)	0.1553
Z	4	*wR*2 (*I*>2σ(*I*))	0.1475
ρ_{calc} [g cm^{-3}]	1.027	diff. peak/hole [eÅ^{-3}]	1.924/-0.480
μ [mm^{-1}]	0.263	g1/g2	0.0726/10.459

8.5.13 $[Li\{tBu_2PCH_2S(NSiMe_3)_2\}]_2$ (14)

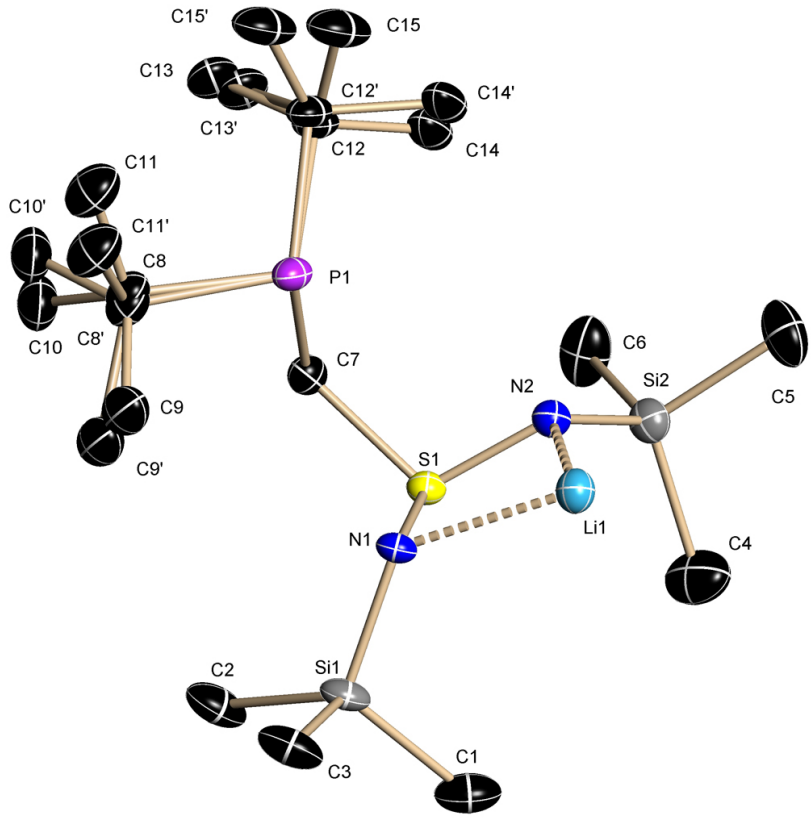

Asymmetric unit of **14**. The anisotropic displacement parameters are shown at the 50 % probability level, hydrogen atoms are omitted for clarity. The occupancy factors for the disordered *t*Bu groups refine to 87 and 13 % for C8-C11 and 84 and 16 % for C12-C15. The disorder was refined using SADI and EADP.

identification code	MMP256	*F*(000)	816
empirical formula	$C_{30}H_{76}Li_2N_4P_2S_2Si_4$	max./min. transmission	0.9422/0.7801
molecular weight [g/mol]	745.25	θ range [°]	2.05-26.13
crystal size [mm]	0.1 x 0.1 x 0.01	completeness to θ_{max}	0.997
temperature [K]	100(2)	reflections collected	34352
crystal system	monoclinic	independent reflections	4460
space group	$P2_1/c$	R_{int}/R_σ	0.1313/0.0812
a [Å]	11.1544(19)	restraints/parameters	14/243
b [Å]	19.906(3)	GoF	1.037
c [Å]	11.3602(19)	*R*1 (all data)	0.1000
β [°]	117.149(3)	*R*1 (*I*>2σ(*I*))	0.0527
V [Å^3]	2244.5(6)	*wR*2 (all data)	0.1069
Z	2	*wR*2 (*I*>2σ(*I*))	0.0931
ρ_{calc} [g cm^{-3}]	1.103	diff. peak/hole [eÅ^{-3}]	0.356/-0.294
μ [mm^{-1}]	0.321	g1/g2	0.0351/1.2936

8.5.14 [Li{(C_6H_4)NMe_2}] [*t*BuLi] (15)

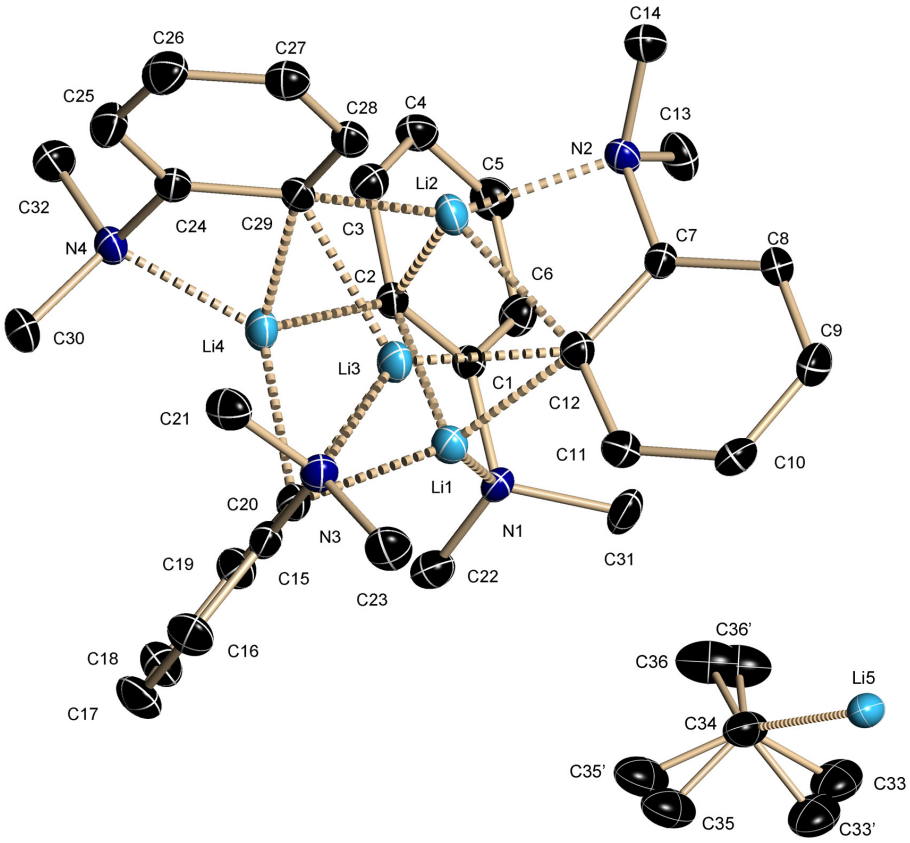

Asymmetric unit of **15**. The anisotropic displacement parameters are shown at the 50 % probability level, hydrogen atoms are omitted for clarity. The *t*Bu group of the *t*BuLi molecule is disordered, the occupancy factors refine to 52 and 48 %, respectively.

identification code	MMP182_L	max./min. transmission	0.9422/0.7689
empirical formula	$C_{36}H_{49}Li_5N_8$	θ range [°]	1.45-26.76
molecular weight [g/mol]	572.49	completeness to θ_{max}	0.999
crystal size [mm]	0.3 x 0.04 x 0.04	reflections collected	40145
temperature [K]	100(2)	independent reflections	3964
crystal system	tetragonal	R_{int}/R_σ	0.0393/0.0402
space group	$I\bar{4}$	restraints/parameters	6/429
a [Å]	27.993(4)	GoF	1.080
c [Å]	8.8744(12)	*R*1 (all data)	0.0457
V [Å^3]	6954.3(16)	*R*1 (*I*>2σ(*I*))	0.0379
Z	2	*wR*2 (all data)	0.0950
ρ_{calc} [g cm^{-3}]	1.094	*wR*2 (*I*>2σ(*I*))	0.0912
μ [mm^{-1}]	0.061	diff. peak/hole [eÅ^{-3}]	0.258/-0.183
F(000)	2464	g1/g2	0.0428/3.3274

8.5.15 $[Li\{Me_2N(C_6H_4)S(NSiMe_3)_2\}]_2$ (16)

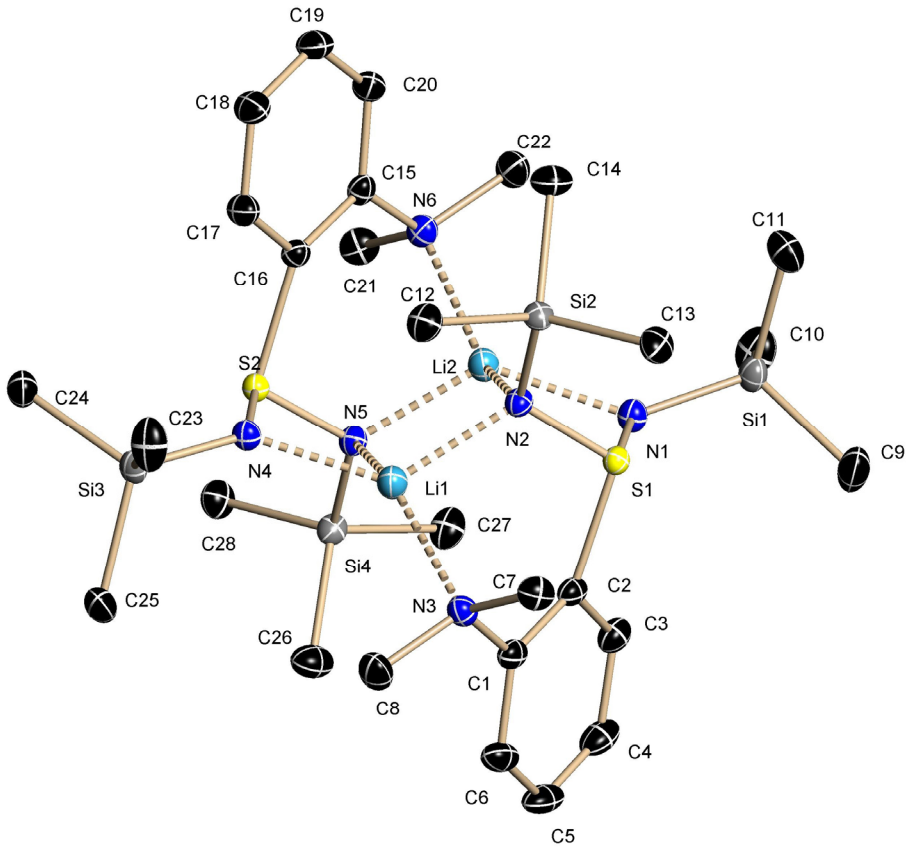

Asymmetric unit of **16**. The anisotropic displacement parameters are shown at the 50 % probability level, hydrogen atoms are omitted for clarity.

identification code	MMPMKLA20	*F*(000)	1440
empirical formula	$C_{28}H_{56}Li_2N_6S_2Si_4$	max./min. transmission	0.9893/0.9527
molecular weight [g/mol]	667.15	θ range [°]	2.44-27.88
crystal size [mm]	0.2 x 0.1 x 0.04	completeness to θ_{max}	0.999
temperature [K]	100(2)	reflections collected	67118
crystal system	monoclinic	independent reflections	9209
space group	$P2_1/c$	R_{int}/R_σ	0.0277/0.0167
a [Å]	15.9924(18)	restraints/parameters	0/395
b [Å]	11.9224(13)	GoF	1.031
c [Å]	20.441(2)	*R*1 (all data)	0.0339
β [°]	97.758(1)	*R*1 (*I*>2σ(*I*))	0.0277
V [Å^3]	3861.7(7)	*wR*2 (all data)	0.0760
Z	4	*wR*2 (*I*>2σ(*I*))	0.0720
ρ_{calc} [g cm^{-3}]	1.147	diff. peak/hole [eÅ^{-3}]	0.350/-0.244
μ [mm^{-1}]	0.288	g1/g2	0.0356/1.7641

8.5.16 [(thf)Li{$Me_2N(C_6H_4)S(NSiMe_3)_2$}]$_2$ (17)

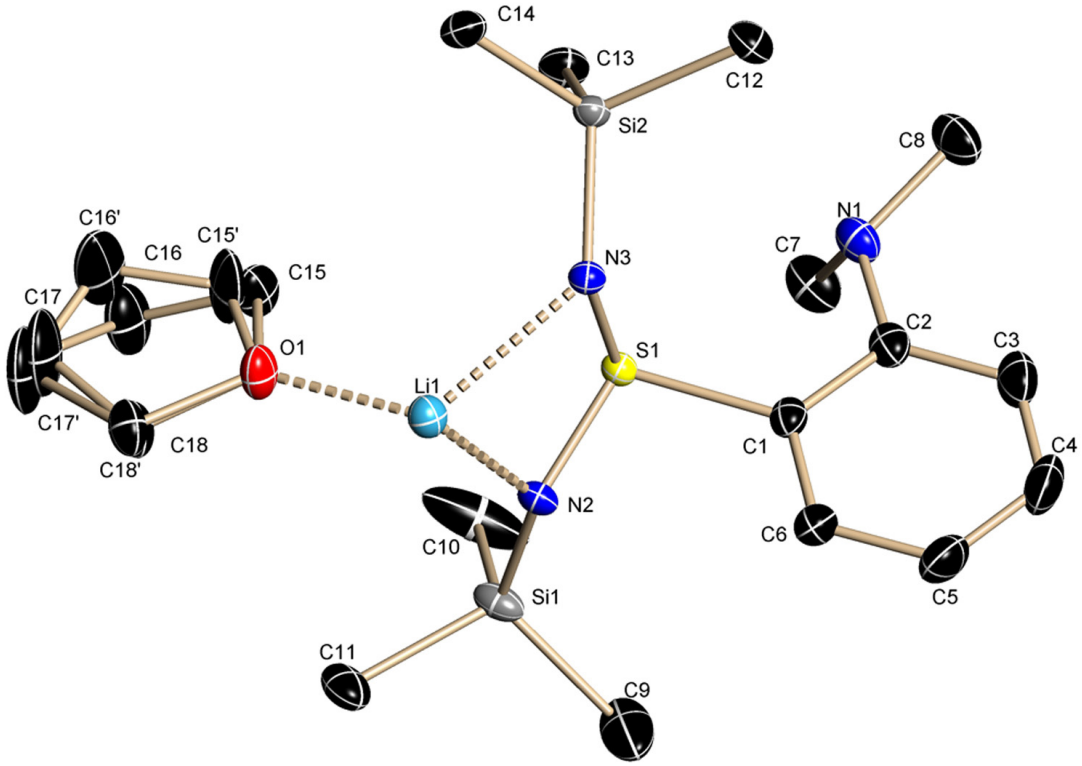

Asymmetric unit of **17**. The anisotropic displacement parameters are shown at the 50 % probability level, hydrogen atoms are omitted for clarity. The THF molecule is disordered over two sites with occupancies of 79 and 21%, respectively.

identification code	MMP230_1	μ [mm^{-1}]	0.251
empirical formula	$C_{36}H_{72}Li_2N_6O_2S_2Si_4$	F(000)	440
molecular weight [g/mol]	811.36	max./min. transmission	0.9422/0.8938
crystal size [mm]	0.38 x 0.24 x 0.1	θ range [°]	1.82-26.37
temperature [K]	100(2)	completeness to θ_{max}	1
crystal system	triclinic	reflections collected	20312
space group	$P\bar{1}$	independent reflections	4810
a [Å]	10.6363(7)	R_{int}/R_σ	0.0189/0.0151
b [Å]	10.7789(7)	restraints/parameters	0/268
c [Å]	11.9504(7)	GoF	1.077
α [°]	74.373(1)	R1 (all data)	0.0309
β [°]	72.043(1)	R1 (I>2σ(I))	0.0281
γ [°]	66.036(1)	wR2 (all data)	0.0750
V [Å^3]	1174.51(13)	wR2 (I>2σ(I))	0.0728
Z	1	diff. peak/hole [eÅ^{-3}]	0.340/-0.283
ρ_{calc} [g cm^{-3}]	1.147	g1/g2	0.0326/0.5806

8.5.17 $[K\{Me_2N(C_6H_4)S(NSiMe_3)_2\}]_2$ (18)

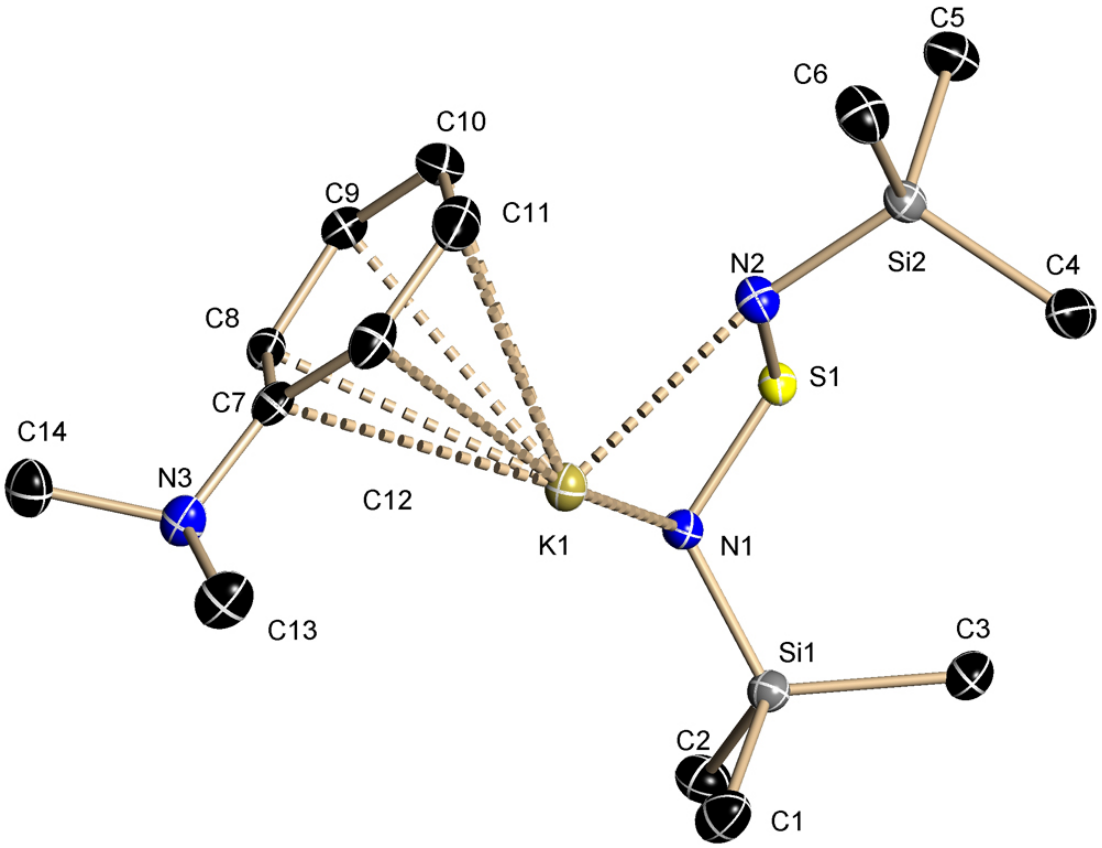

Asymmetric unit of **18**. The anisotropic displacement parameters are shown at the 50 % probability level, hydrogen atoms are omitted for clarity.

identification code	MMP213	*F*(000)	1568
empirical formula	$C_{28}H_{56}K_2N_6S_2Si_4$	max./min. transmission	0.9422/0.7983
molecular weight [g/mol]	731.47	θ range [°]	1.75-26.69°
crystal size [mm]	0.2 x 0.2 x 0.1	completeness to θ_{max}	0.999
temperature [K]	100(2)	reflections collected	22355
crystal system	monoclinic	independent reflections	4289
space group	*C*2/*c*	R_{int}/R_σ	0.0541/0.0438
a [Å]	17.743(2)	restraints/parameters	0/198
b [Å]	9.8015(10)	GoF	1.030
c [Å]	23.866(3)	*R*1 (all data)	0.0565
β [°]	102.288(7)	*R*1 (*I*>2σ(*I*))	0.0356
V [Å^3]	4055.3(8)	*wR*2 (all data)	0.0797
Z	4	*wR*2 (*I*>2σ(*I*))	0.0725
ρ_{calc} [g cm^{-3}]	1.198	diff. peak/hole [eÅ^{-3}]	0.363/-0.403
μ [mm^{-1}]	0.481	g1/g2	0.0275/5.947

8.5.18 [(*t*BuN)$_2$S·{LiMe$_2$N(C$_6$H$_4$)S(N*t*Bu)$_2$}$_2$] (19)

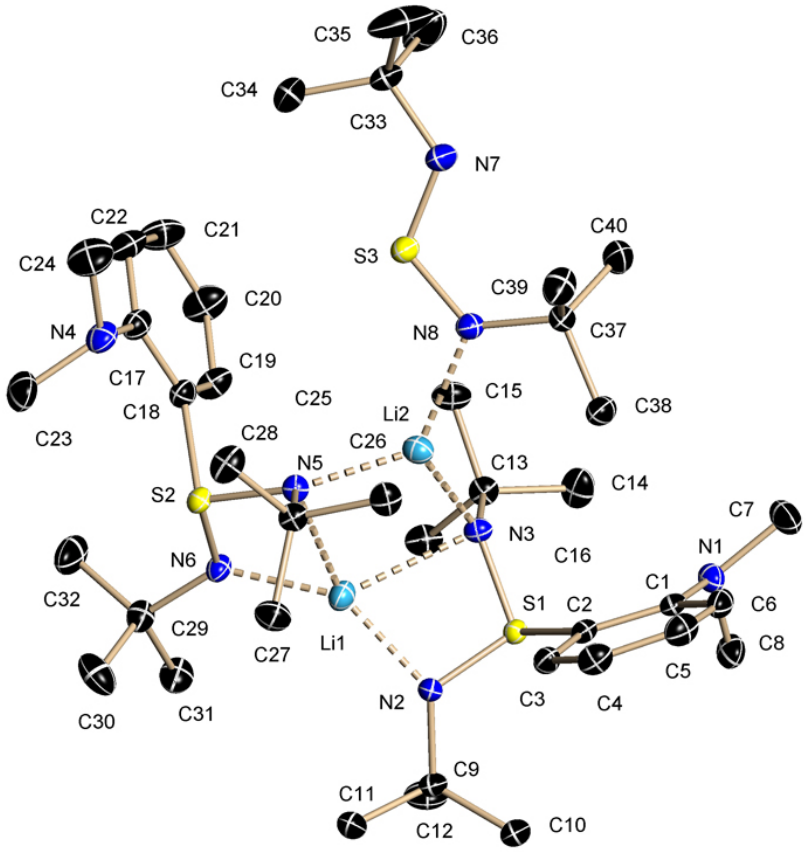

Asymmetric unit of **19**. The anisotropic displacement parameters are shown at the 50 % probability level, hydrogen atoms are omitted for clarity.

identification code	MMPMKLA18	*F*(000)	1696
empirical formula	$C_{40}H_{74}Li_2N_8S_3$	max./min. transmission	0.9893/0.9119
molecular weight [g/mol]	777.13	θ range [°]	1.36-26.79
crystal size [mm]	0.12 x 0.06 x 0.04	completeness to θ_{max}	0.998
temperature [K]	100(2)	reflections collected	74676
crystal system	monoclinic	independent reflections	10263
space group	$P2_1/n$	R_{int}/R_σ	0.0661/0.0382
a [Å]	10.7028(15)	restraints/parameters	0/500
b [Å]	21.801(3)	GoF	1.031
c [Å]	21.092(3)	*R*1 (all data)	0.0535
β [°]	101.945(3)	*R*1 (*I*>2σ(*I*))	0.0384
V [Å^3]	4814.8(12)	*wR*2 (all data)	0.0933
Z	4	*wR*2 (*I*>2σ(*I*))	0.0917
ρ_{calc} [g cm^{-3}]	1.072	diff. peak/hole [eÅ^{-3}]	0.289/-0.408
μ [mm^{-1}]	0.188	g1/g2	0.0383/2.6362

8.5.19 [Li{2-PyS(NSiMe$_3$)$_2$}]$_2$ (20)

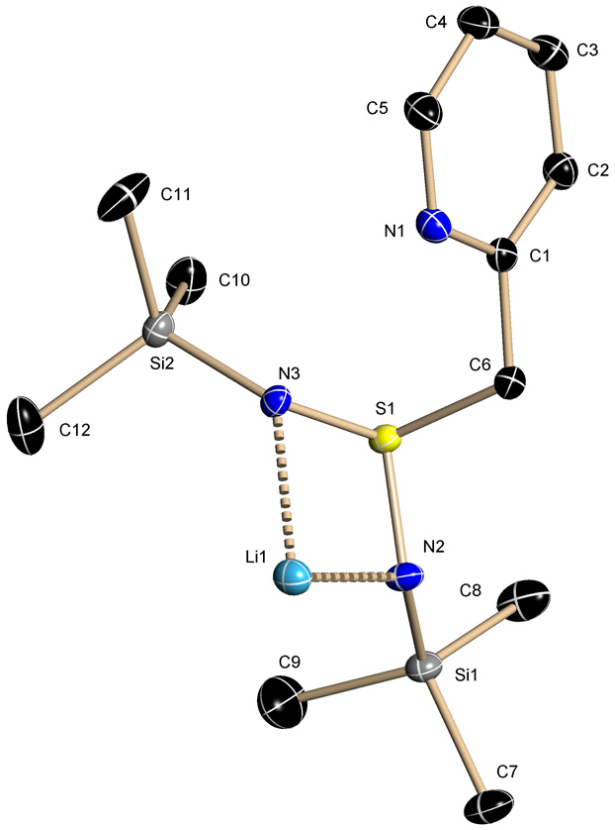

Asymmetric unit of **20**. The anisotropic displacement parameters are shown at the 50 % probability level, hydrogen atoms are omitted for clarity.

identification code	MMP271	μ [mm^{-1}]	0.310
empirical formula	$C_{24}H_{48}Li_2N_6S_2Si_4$	F(000)	328
molecular weight [g/mol]	611.04	max./min. transmission	0.9422/0.8838
crystal size [mm]	0.18 x 0.1 x 0.01	θ range [°]	2.17-27.89
temperature [K]	100(2)	completeness to θ_{max}	0.999
crystal system	triclinic	reflections collected	14695
space group	$P\bar{1}$	independent reflections	4187
a [Å]	9.5103(9)	R_{int}/R_σ	0.0135/0.0120
b [Å]	10.5415(10)	restraints/parameters	0/178
c [Å]	10.6013(10)	GoF	1.047
α [°]	63.6220(10)	R1 (all data)	0.0272
β [°]	68.6900(10)	R1 (I>2σ(I))	0.0249
γ [°]	86.5790(10)	wR2 (all data)	0.0682
V [Å^3]	880.43(14)	wR2 (I>2σ(I))	0.0668
Z	1	diff. peak/hole [eÅ^{-3}]	0.373/-0.248
ρ_{calc} [g cm^{-3}]	1.152	g1/g2	0.0317/0.4066

8.5.20 $[Li\{Me_2N(CH_2)_2N(CH_3)S(NSiMe_3)_2\}]_2$ (21)

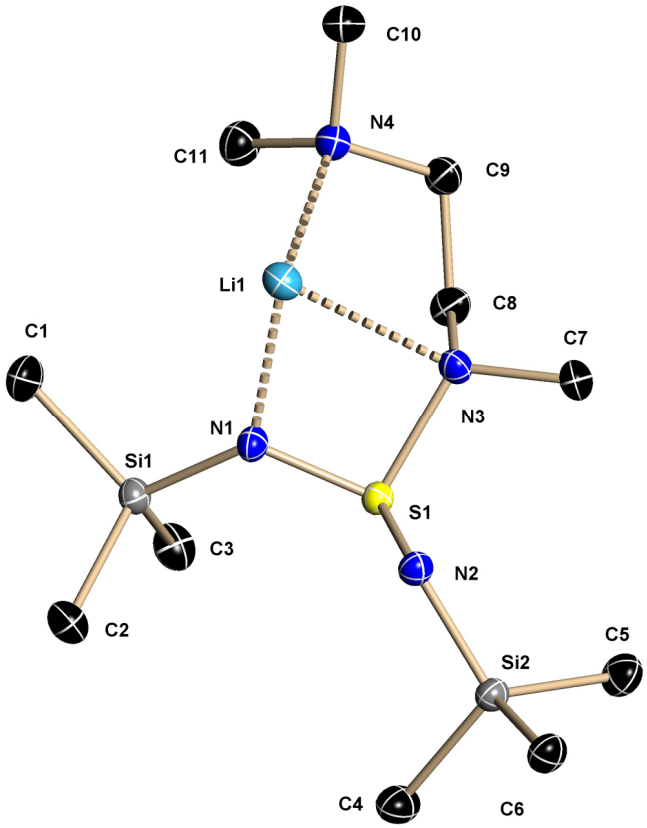

Asymmetric unit of **21**. The anisotropic displacement parameters are shown at the 50 % probability level, hydrogen atoms are omitted for clarity.

identification code	MMPMKLA19	μ [mm^{-1}]	0.287
empirical formula	$C_{22}H_{62}Li_2N_8S_2Si_4$	F(000)	316
molecular weight [g/mol]	629.18	max./min. transmission	0.9422/0.8652
crystal size [mm]	0.4 x 0.14 x 0.08	θ range [°]	2.64-28.31
temperature [K]	100(2)	completeness to θ_{max}	0.994
crystal system	triclinic	reflections collected	30141
space group	$P\bar{1}$	independent reflections	4620
a [Å]	10.0177(14)	R_{int}/R_σ	0.0166/0.0153
b [Å]	10.2175(13)	restraints/parameters	0/181
c [Å]	10.7308(13)	GoF	1.020
α [°]	95.461(1)	$R1$ (all data)	0.0257
β [°]	108.065(1)	$R1$ (I>2σ(I))	0.0240
γ [°]	112.888(1)	$wR2$ (all data)	0.0700
V [Å^3]	932.4(2)	$wR2$ (I>2σ(I))	0.0686
Z	1	diff. peak/hole [eÅ^{-3}]	0.372/-0.286
ρ_{calc} [g cm^{-3}]	1.120	g1/g2	0.0382/0.3008

8.5.21 $[Na\{Me_2N(CH_2)_2N(CH_3)S(NSiMe_3)_2\}]_2$ (22)

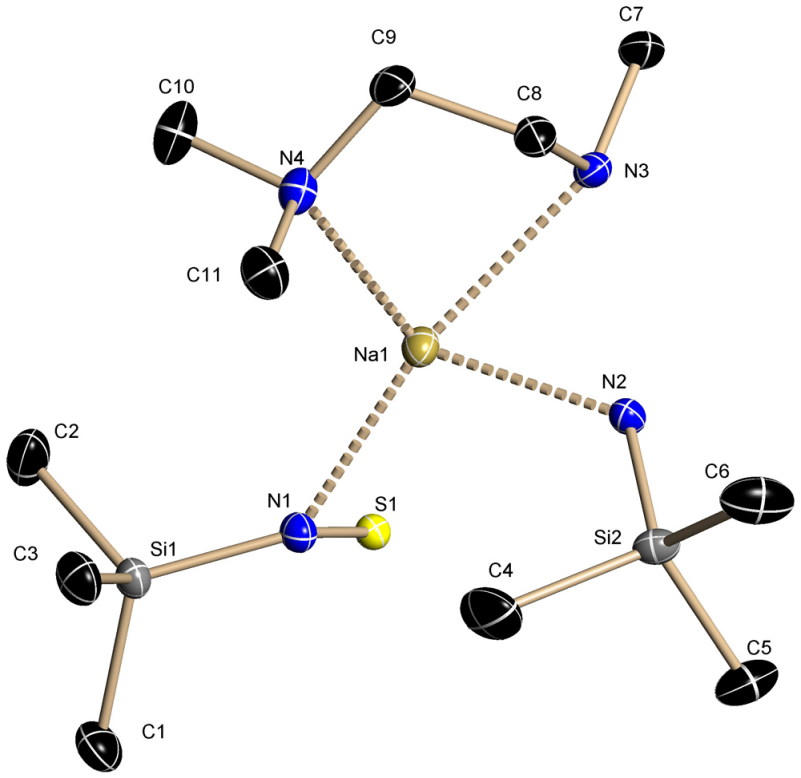

Asymmetric unit of **22**. The anisotropic displacement parameters are shown at the 50 % probability level, hydrogen atoms are omitted for clarity.

identification code	MMPEK04	μ [mm^{-1}]	0.306
empirical formula	$C_{22}H_{62}N_8Na_2S_2Si_4$	F(000)	360
molecular weight [g/mol]	661.26	max./min. transmission	0.9422/0.8641
crystal size [mm]	0.2 x 0.04 x 0.04	θ range [°]	2.09-26.03
temperature [K]	100(2)	completeness to θ_{max}	0.996
crystal system	triclinic	reflections collected	14548
space group	$P\bar{1}$	independent reflections	3831
a [Å]	10.1566(12)	R_{int}/R_σ	0.0177/0.0146
b [Å]	10.7350(12)	restraints/parameters	0/181
c [Å]	10.9361(12)	GoF	1.073
α [°]	90.997(2)	R1 (all data)	0.0272
β [°]	114.202(1)	R1 (I>2σ(I))	0.0250
γ [°]	113.399(1)	wR2 (all data)	0.0657
V [Å^3]	974.73(19)	wR2 (I>2σ(I))	0.0644
Z	1	diff. peak/hole [eÅ^{-3}]	0.323/-0.301
ρ_{calc} [g cm^{-3}]	1.127	g1/g2	0.0263/0.5024

8.5.22 $[Li_2K_3\{PhP(CH_2S(NSiMe_3)_2\}_2(OH)]$ (23)

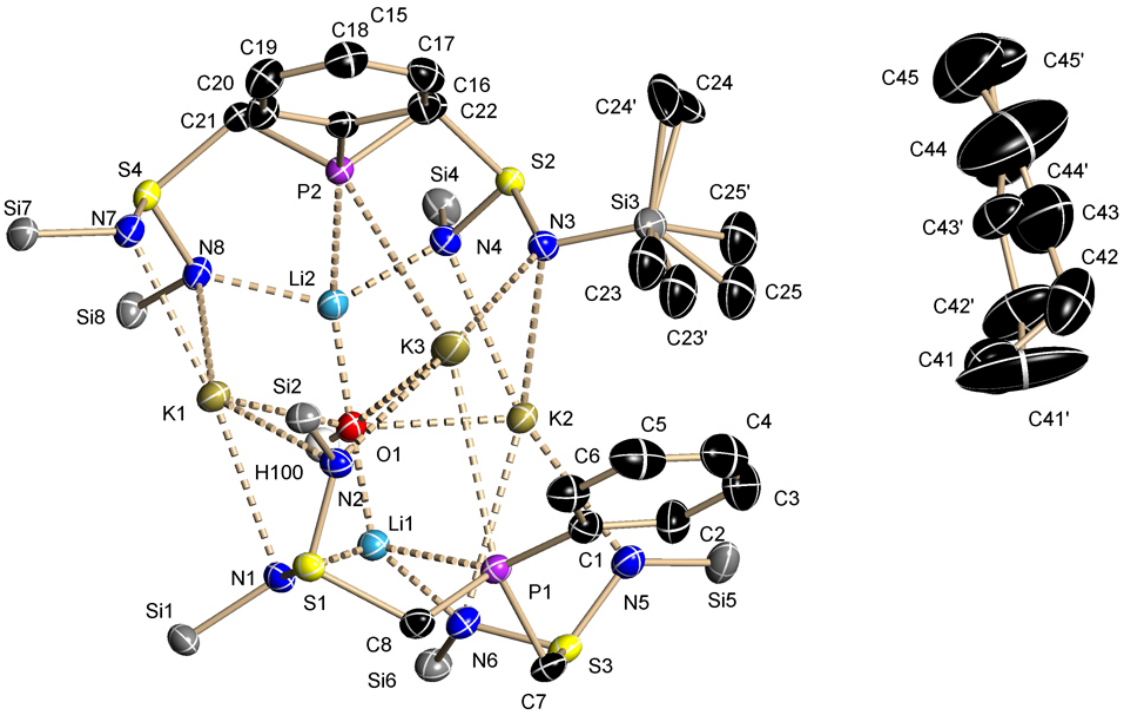

Asymmetric unit of **23**. The anisotropic displacement parameters are shown at the 50 % probability level, hydrogen atoms are omitted for clarity. The hydrogen atom on O1 was freely refined using distance restraints. The occupancy factors of the disordered pentane molecule refine to 57 and 43 %, respectively. The two solvent molecules were refined using SAME for the connectivities and SIMU, DELU and ISOR for the displacement parameters. Two of the $NSiMe_3$ groups are disordered as well. The occupancy factors for $Si(3)Me_3$ refine to 72 and 28 %, respectively. The group was refined using SADI restraints. For $Si(4)Me_3$ the values are 56 and 44 %, the group was refined using EADP.

identification code	MMP218	*F*(000)	2824
empirical formula	$C_{45}H_{103}K_3Li_2N_8OP_2S_4Si_8$	max./min. transmission	0.9422/0.8702
molecular weight [g/mol]	1318.48	θ range [°]	0.96-26.80°
crystal size [mm]	0.2 x 0.2 x 0.1	completeness to θ_{max}	0.999
temperature [K]	100(2)	reflections collected	184533
crystal system	monoclinic	independent reflections	15896
space group	$P2_1/c$	R_{int}/R_σ	0.0474/0.0222
a [Å]	21.5346(17)	restraints/parameters	58/738
b [Å]	14.3833(11)	GoF	1.072
c [Å]	24.3506(19)	*R*1 (all data)	0.0509
β [°]	99.826(1)	*R*1 (*I*>2σ(*I*))	0.0388
V [Å^3]	7431.7(10)	*wR*2 (all data)	0.0959
Z	4	*wR*2 (*I*>2σ(*I*))	0.0892
ρ_{calc} [g cm^{-3}]	1.178	diff. peak/hole [eÅ^{-3}]	0.853/-0.830
μ [mm^{-1}]	0.503	g1/g2	0.0354/8.0999

8.5.23 $[Li_4O_2\{CH_2(N(Me)CH_2S(NtBu)_2Li)\}_2]$ (24)

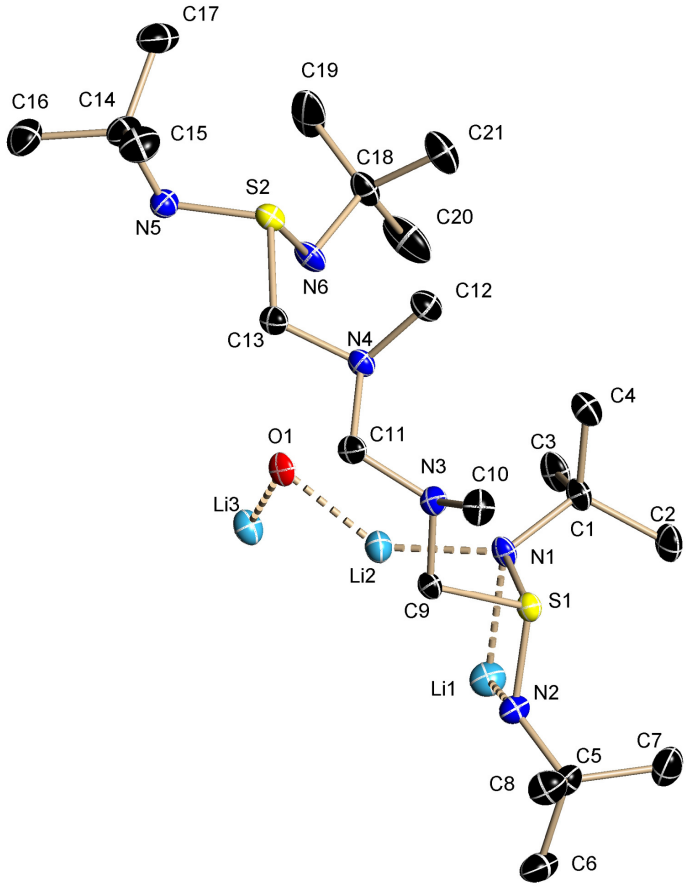

Asymmetric unit of **24**. The anisotropic displacement parameters are shown at the 50 % probability level, hydrogen atoms are omitted for clarity.

identification code	MMPEK10	*F*(000)	1056
empirical formula	$C_{42}H_{96}Li_6N_{12}O_2S_4$	max./min. transmission	1.000/0.674
molecular weight [g/mol]	971.19	θ range [°]	1.68-25.72
crystal size [mm]	0.15 x 0.1 x 0.1	completeness to θ_{max}	0.997
temperature [K]	100(2)	reflections collected	56834
crystal system	monoclinic	independent reflections	5526
space group	$P2_1/c$	R_{int}/R_σ	0.0830/0.0401
a [Å]	8.6080(9)	restraints/parameters	0/312
b [Å]	14.0907(14)	GoF	1.073
c [Å]	24.267(3)	*R*1 (all data)	0.0651
β [°]	99.829(2)	*R*1 (*I*>2σ(*I*))	0.0491
V [Å^3]	2900.3(5)	*wR*2 (all data)	0.1127
Z	2	*wR*2 (*I*>2σ(*I*))	0.1056
ρ_{calc} [g cm^{-3}]	1.110	diff. peak/hole [eÅ^{-3}]	0.623/-0.419
μ [mm^{-1}]	0.206	g1/g2	0.0294/3.8993

8.5.24 $[Li_4\{(NSiMe_3)_2SCH_2N(Me)CH_2N(Me)CH_2(O)\}\{NSN(SiMe_3)\}(OtBu)]_2$ (25)

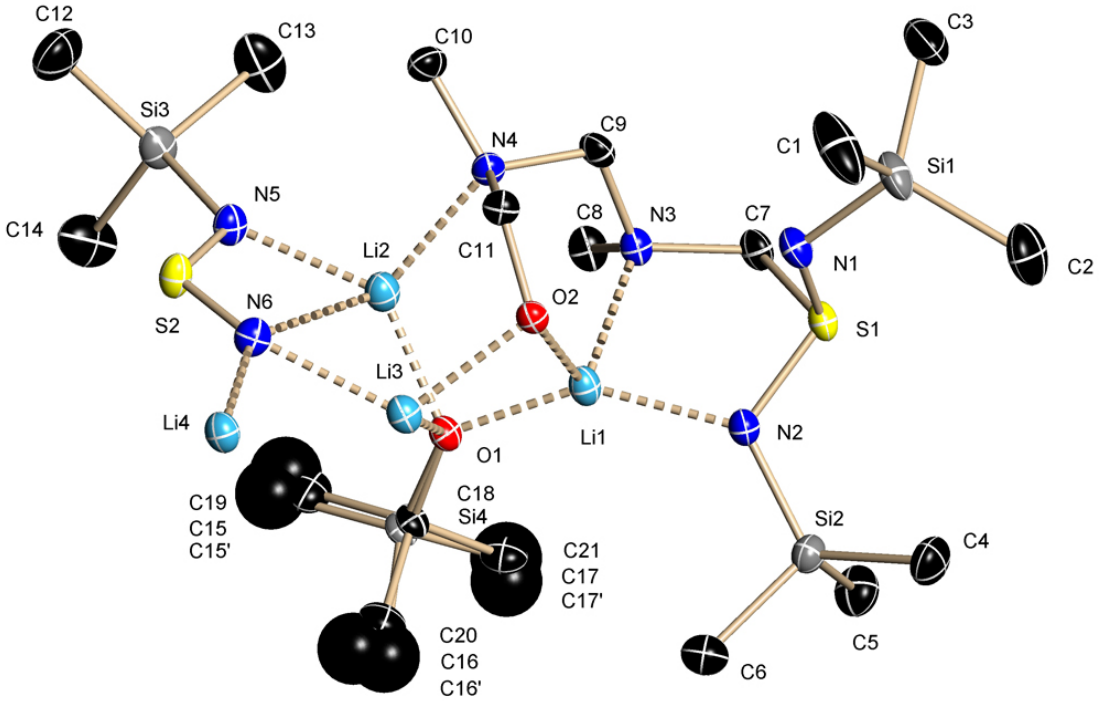

Asymmetric unit of **25**. The anisotropic displacement parameters are shown at the 50 % probability level, hydrogen atoms are omitted for clarity. The *t*Bu group on O1 is disordered with a disordered $SiMe_3$ group. The occupancy factors refine to 72 and 22 % and 6 % for the second site of the $SiMe_3$ group. Because of the small occupancy, the second orientation of the $SiMe_3$ group could not be refined anisotropically. The disorder was refined using DELU, ISOR and DFIX.

identification code	MMPEK07	*F*(000)	1209
empirical formula	$C_{35.44}H_{96.02}Li_8N_{12}O_4S_4Si_{6.57}$	max./min. transmission	0.9422/0.8318
molecular weight [g/mol]	1122.87	θ range [°]	1.64-26.37
crystal size [mm]	0.2 x 0.04 x 0.04	completeness to θ_{max}	1.000
temperature [K]	100(2)	reflections collected	40145
crystal system	monoclinic	independent reflections	6806
space group	$P2_1/n$	R_{int}/R_σ	0.0568/0.0313
a [Å]	9.938(2)	restraints/parameters	18/366
b [Å]	14.987(3)	GoF	1.077
c [Å]	22.310(5)	*R*1 (all data)	0.0504
β [°]	90	*R*1 (*I*>2σ(*I*))	0.0348
V [Å^3]	3322.9(13)	*wR*2 (all data)	0.0874
Z	2	*wR*2 (*I*>2σ(*I*))	0.0806
ρ_{calc} [g cm^{-3}]	1.122	diff. peak/hole [eÅ^{-3}]	0.386/-0.312
μ [mm^{-1}]	0.302	g1/g2	0.0348/1.8942

8.5.25 [Mg{$Me_2PCH_2S(NtBu)_2$}$_2$] (26)

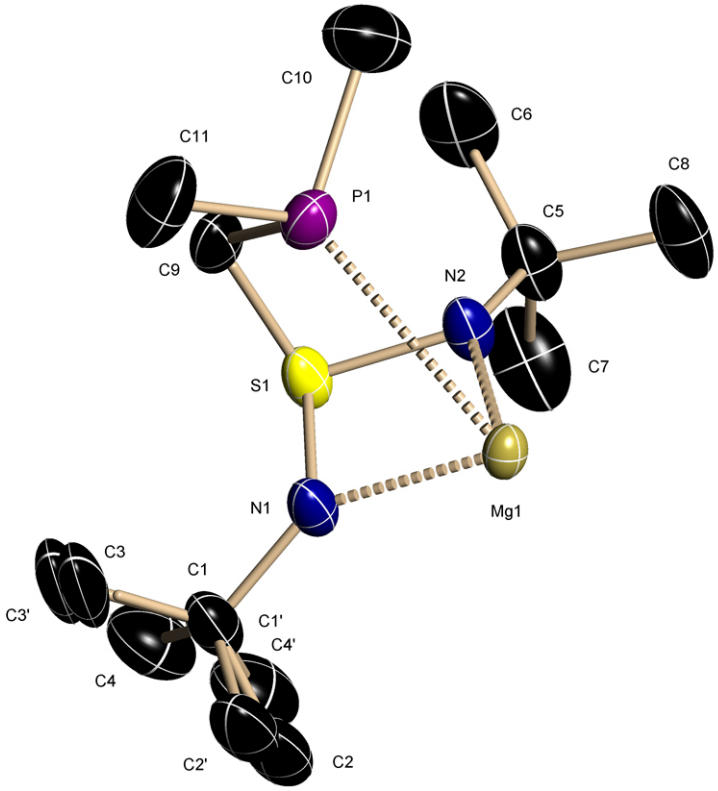

Asymmetric unit of **26**. The anisotropic displacement parameters are shown at the 30 % probability level, hydrogen atoms are omitted for clarity. One tBu group is disordered over two sites with occupancies of 60 and 40 %.

identification code	Mücke	*F*(000)	2288
empirical formula	$C_{22}H_{52}MgN_4P_2S_2$	max./min. transmission	0.98931/0.83307
molecular weight [g/mol]	523.05	θ range [°]	2.19-26.40
crystal size [mm]	0.2 x 0.1 x 0.02	completeness to θ_{max}	0.999
temperature [K]	250(2)	reflections collected	21122
crystal system	orthorhombic	independent reflections	3270
space group	*Fdd*2	R_{int}/R_σ	0.0407/0.0253
a [Å]	37.169(8)	restraints/parameters	31/162
b [Å]	10.175(2)	GoF	1.148
c [Å]	16.851(4)	*R*1 (all data)	0.0497
V [Å^3]	6373(2)	*R*1 (*I*>2σ(*I*))	0.0462
Z	8	*wR*2 (all data)	0.1172
ρ_{calc} [g cm^{-3}]	1.090	*wR*2 (*I*>2σ(*I*))	0.1156
μ [mm^{-1}]	0.303	diff. peak/hole [eÅ^{-3}]	0.227/-0.227
		g1/g2	0.0553/7.7268

8.5.26 $[Mg\{Me_2PCH_2S(NSiMe_3)_2\}_2]$ (27)

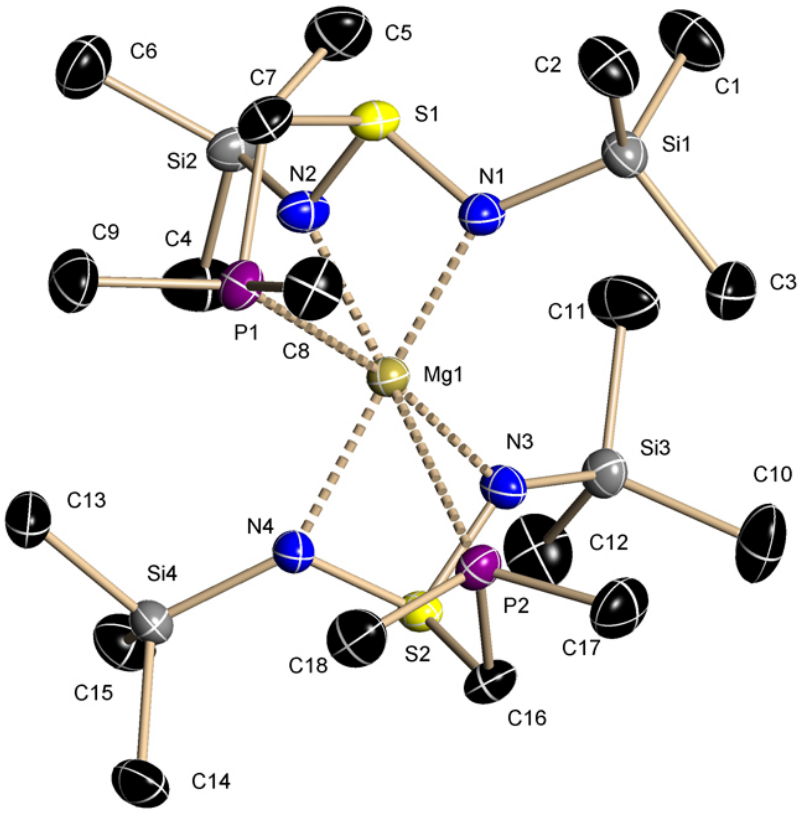

Asymmetric unit of **27**. The anisotropic displacement parameters are shown at the 50 % probability level, hydrogen atoms are omitted for clarity.

identification code	MKP17	*F*(000)	1272
empirical formula	$C_{18}H_{52}N_4Si_4P_2S_2Mg$	max./min. transmission	0.9422/0.8698
molecular weight [g/mol]	587.36	θ range [°]	2.68-29.13
crystal size [mm]	0.56 x 0.52 x 0.30	completeness to θ_{max}	0.998
temperature [K]	100(2)	reflections collected	156125
crystal system	monoclinic	independent reflections	9326
space group	$P2_1/n$	R_{int}/R_σ	0.0192/0.0072
a [Å]	10.2563(5)	restraints/parameters	0/296
b [Å]	17.8142(8)	GoF	1.019
c [Å]	19.2917(9)	*R*1 (all data)	0.0238
β [°]	99.2730(10)	*R*1 (*I*>2σ(*I*))	0.0213
V [Å^3]	3478.7 (3)	*wR*2 (all data)	0.0630
Z	4	*wR*2 (*I*>2σ(*I*))	0.0612
ρ_{calc} [g cm^{-3}]	1.122	diff. peak/hole [eÅ^{-3}]	0.286/-0.263
μ [mm^{-1}]	0.415	g1/g2	0.0374/0.6229

8.5.27 $[Ca\{Ph_2PCH_2S(NSiMe_3)_2\}_2]$ (28)

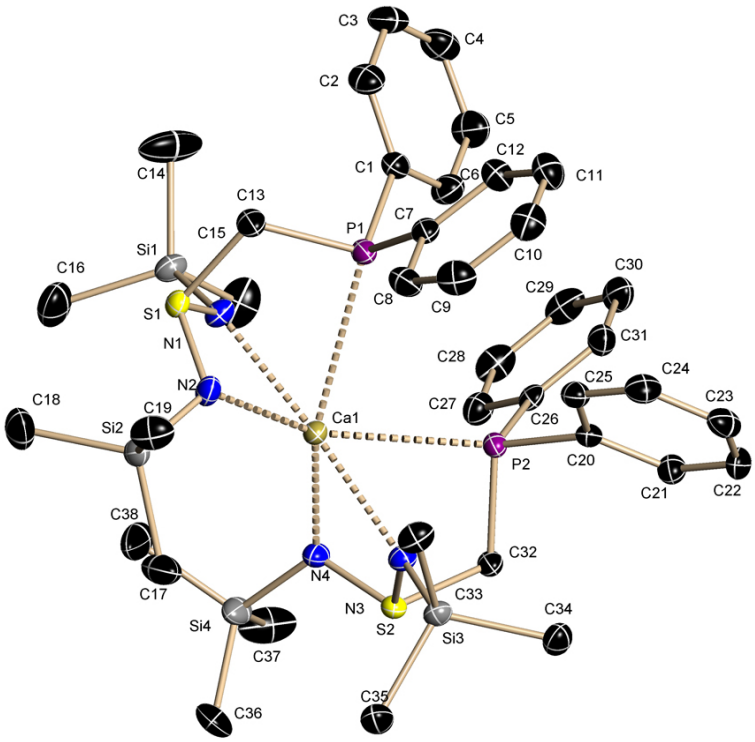

Asymmetric unit of **28**. The anisotropic displacement parameters are shown at the 50 % probability level, hydrogen atoms are omitted for clarity.

identification code	MMP273	*F*(000)	1816
empirical formula	$C_{38}H_{60}CaN_4P_2S_2Si_4$	max./min. transmission	0.9422/0.8075
molecular weight [g/mol]	851.40	θ range [°]	1.34-26.02
crystal size [mm]	0.16 x 0.02 x 0.02	completeness to θ_{max}	0.999
temperature [K]	100(2)	reflections collected	46417
crystal system	orthorhombic	independent reflections	9409
space group	$P2_12_12_1$	R_{int}/R_σ	0.0462/0.0305
a [Å]	10.2753(11)	restraints/parameters	0/472
b [Å]	20.867(2)	GoF	1.050
c [Å]	22.261(2)	*R*1 (all data)	0.0340
V [Å^3]	4773.1(9)	*R*1 (*I*>2σ(*I*))	0.0291
Z	4	*wR*2 (all data)	0.0691
ρ_{calc} [g cm^{-3}]	1.185	*wR*2 (*I*>2σ(*I*))	0.0668
μ [mm^{-1}]	0.416	diff. peak/hole [eÅ^{-3}]	0.295/-0.193
Flack-x-parameter [225]	0.04(3)	g1/g2	0.0343/1.346

8.5.28 $[Sr\{Ph_2PCH_2S(NSiMe_3)_2\}_2]$ (29)

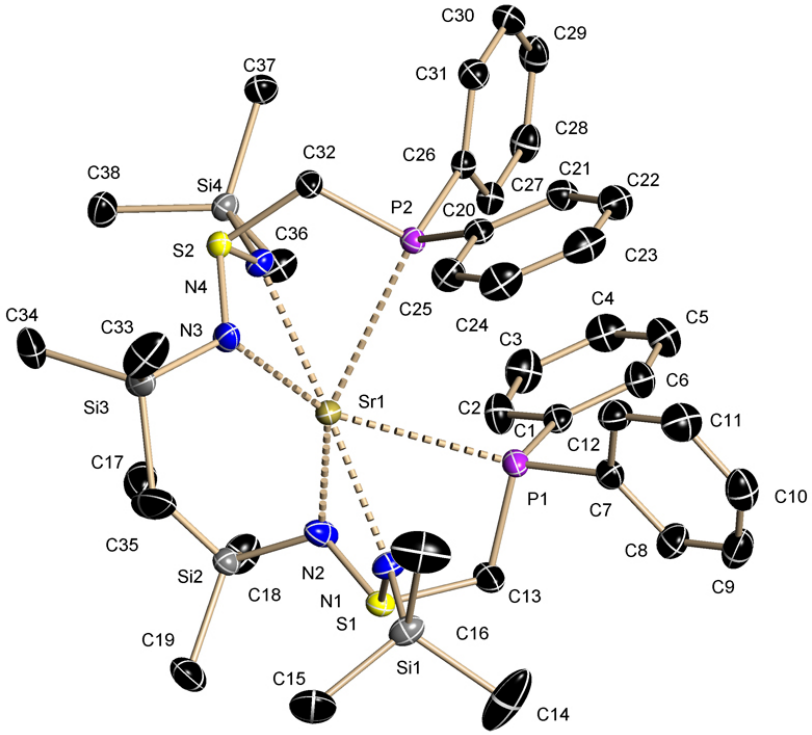

Asymmetric unit of **29**. The anisotropic displacement parameters are shown at the 50 % probability level, hydrogen atoms are omitted for clarity.

identification code	MMP266	*F*(000)	1888
empirical formula	$C_{38}H_{60}N_4P_2S_2Si_4Sr$	max./min. transmission	0.9422/0.8426
molecular weight [g/mol]	898.94	θ range [°]	1.34-26.77
crystal size [mm]	0.2 x 0.15 x 0.1	completeness to θ_{max}	0.999
temperature [K]	100(2)	reflections collected	120179
crystal system	orthorhombic	independent reflections	10269
space group	$P2_12_12_1$	R_{int}/R_σ	0.0262/0.0105
a [Å]	10.4329(17)	restraints/parameters	0/472
b [Å]	20.842(3)	GoF	1.053
c [Å]	22.140(4)	*R*1 (all data)	0.0181
V [Å^3]	4814.3(13)	*R*1 (*I*>2σ(*I*))	0.0173
Z	4	*wR*2 (all data)	0.0445
ρ_{calc} [g cm^{-3}]	1.240	*wR*2 (*I*>2σ(*I*))	0.0442
μ [mm^{-1}]	1.402	diff. peak/hole [eÅ^{-3}]	0.255/-0.142
Flack-x-parameter	0.066(2)	g1/g2	0.0232/1.356

8.5.29 [Co{$Ph_2PCH_2S(NSiMe_3)_2$}$_2$] (30)

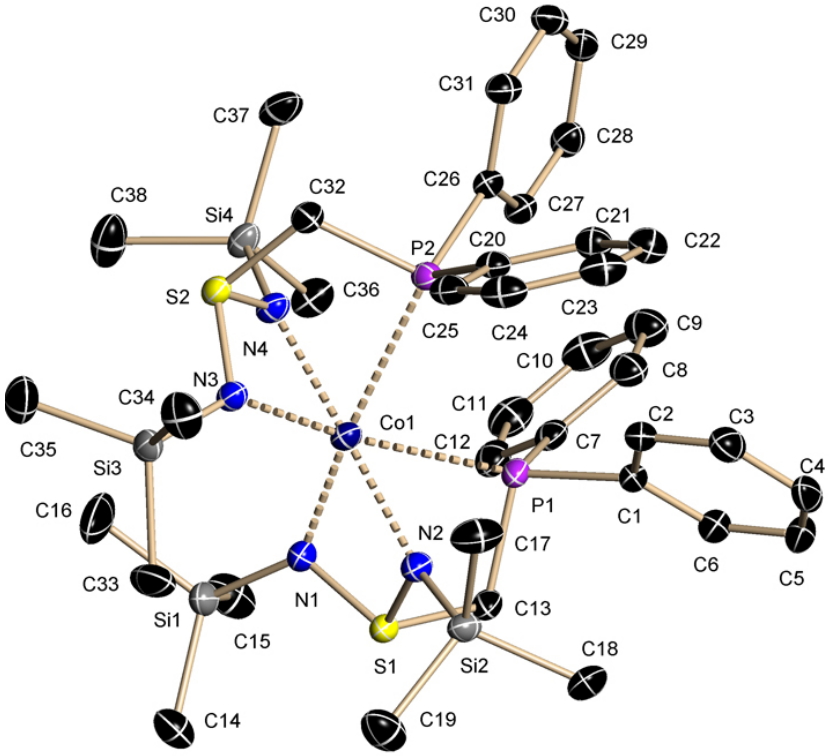

Asymmetric unit of **30**. The anisotropic displacement parameters are shown at the 50 % probability level, hydrogen atoms are omitted for clarity. The compound crystallises as a racemic twin with BASF values of 83 and 17 %, respectively.

identification code	MMP266	*F*(000)	1844
empirical formula	$C_{38}H_{60}CoN_4P_2S_2Si_4$	max./min. transmission	0.9422/0.8969
molecular weight [g/mol]	870.25	θ range [°]	1.82-28.29
crystal size [mm]	0.2 x 0.1 x 0.02	completeness to θ_{max}	0.999
temperature [K]	100(2)	reflections collected	95693
crystal system	orthorhombic	independent reflections	11283
space group	$Pna2_1$	R_{int}/R_σ	0.0385/0.0231
a [Å]	22.4210(17)	restraints/parameters	1/473
b [Å]	10.7606(8)	GoF	1.047
c [Å]	18.8363(14)	*R*1 (all data)	0.0275
V [Å^3]	4544.5(6)	*R*1 (*I*>2σ(*I*))	0.0244
Z	4	*wR*2 (all data)	0.0602
ρ_{calc} [g cm^{-3}]	1.272	*wR*2 (*I*>2σ(*I*))	0.0584
μ [mm^{-1}]	0.677	diff. peak/hole [eÅ^{-3}]	0.236/-0.195
Flack-x-parameter	0.170(7)	g1/g2	0.0284/1.288

8.5.30 [Fe{$Ph_2PCH_2S(NSiMe_3)_2$}$_2$] (31)

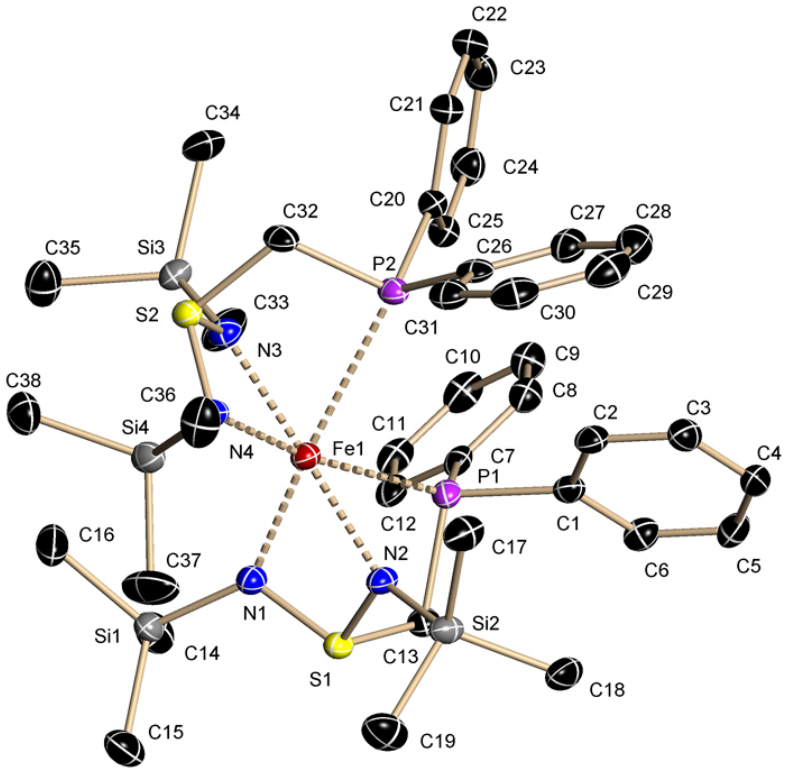

Asymmetric unit of **31**. The anisotropic displacement parameters are shown at the 50 % probability level, hydrogen atoms are omitted for clarity. The compound crystallises as a racemic twin with BASF values of 51 and 49 %, respectively. The Flack-x-parameter could not be determined.

identification code	MMPEK23	*F*(000)	1840
empirical formula	$C_{38}H_{60}FeN_4P_2S_2Si_4$	max./min. transmission	0.9422/0.8288
molecular weight [g/mol]	867.17	θ range [°]	1.81-25.51
crystal size [mm]	0.2 x 0.1 x 0.01	completeness to θ_{max}	0.974
temperature [K]	100(2)	reflections collected	82204
crystal system	orthorhombic	independent reflections	8158
space group	$Pna2_1$	R_{int}/R_σ	0.0423/0.0228
a [Å]	22.445(2)	restraints/parameters	1/473
b [Å]	10.7778(10)	GoF	1.013
c [Å]	18.8861(18)	*R*1 (all data)	0.0256
V [Å^3]	4568.8(7)	*R*1 (*I*>2σ(*I*))	0.0243
Z	4	*wR*2 (all data)	0.0621
ρ_{calc} [g cm^{-3}]	1.261	*wR*2 (*I*>2σ(*I*))	0.0612
μ [mm^{-1}]	0.627	diff. peak/hole [eÅ^{-3}]	0.453/-0.244
		g1/g2	0.037/1.918

8.5.31 [{FeN(SiMe$_3$)$_2$}{Li(NSiMe$_3$)$_2$SCHP(O)Ph$_2$}(LiO)]$_2$ (32)

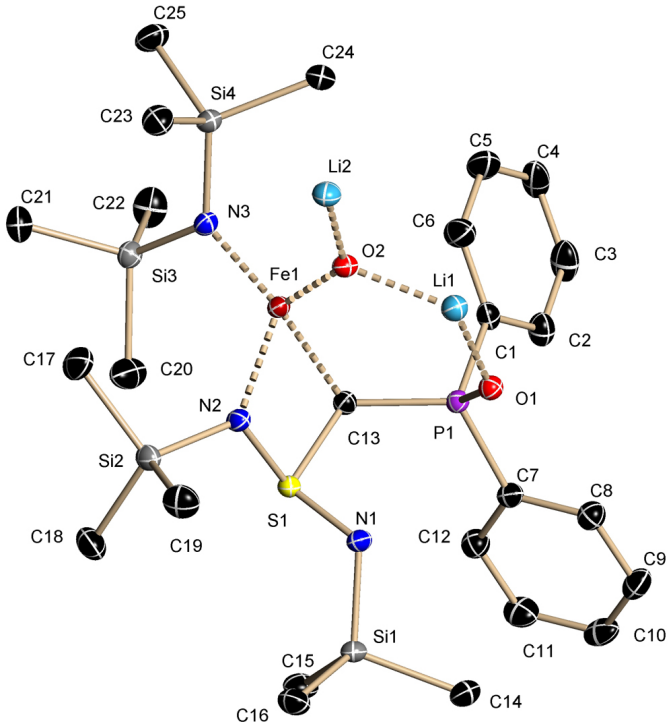

Asymmetric unit of **32**. The anisotropic displacement parameters are shown at the 50 % probability level, hydrogen atoms are omitted for clarity.

identification code	MMPEK23_rot	μ [mm^{-1}]	0.688
empirical formula	$C_{50}H_{94}Fe_2Li_4N_6O_4P_2S_2Si_8$	F(000)	706
molecular weight [g/mol]	1333.57	max./min. transmission	0.9893/0.9409
crystal size [mm]	0.24 x 0.2 x 0.01	θ range [°]	1.59-26.77
temperature [K]	100(2)	completeness to θ_{max}	0.998
crystal system	triclinic	reflections collected	33831
space group	$P\bar{1}$	independent reflections	7543
a [Å]	11.7823(13)	R_{int}/R_σ	0.0201/0.0153
b [Å]	12.6677(14)	restraints/parameters	0/364
c [Å]	14.2318(16)	GoF	1.047
α [°]	71.7790(10)	$R1$ (all data)	0.0246
β [°]	66.2720(10)	$R1$ (I>2σ(I))	0.0237
γ [°]	68.8660(10)	$wR2$ (all data)	0.0642
V [Å^3]	1778.5(3)	$wR2$ (I>2σ(I))	0.0627
Z	1	diff. peak/hole [eÅ^{-3}]	0.404/-0.249
ρ_{calc} [g cm^{-3}]	1.245	g1/g2	0.0288/1.0845

8.5.32 [{Cu(Me$_2$PCH$_2$S(NSiMe$_3$)$_2$)}$_4$(Cu$_2$S)$_4$] (33)

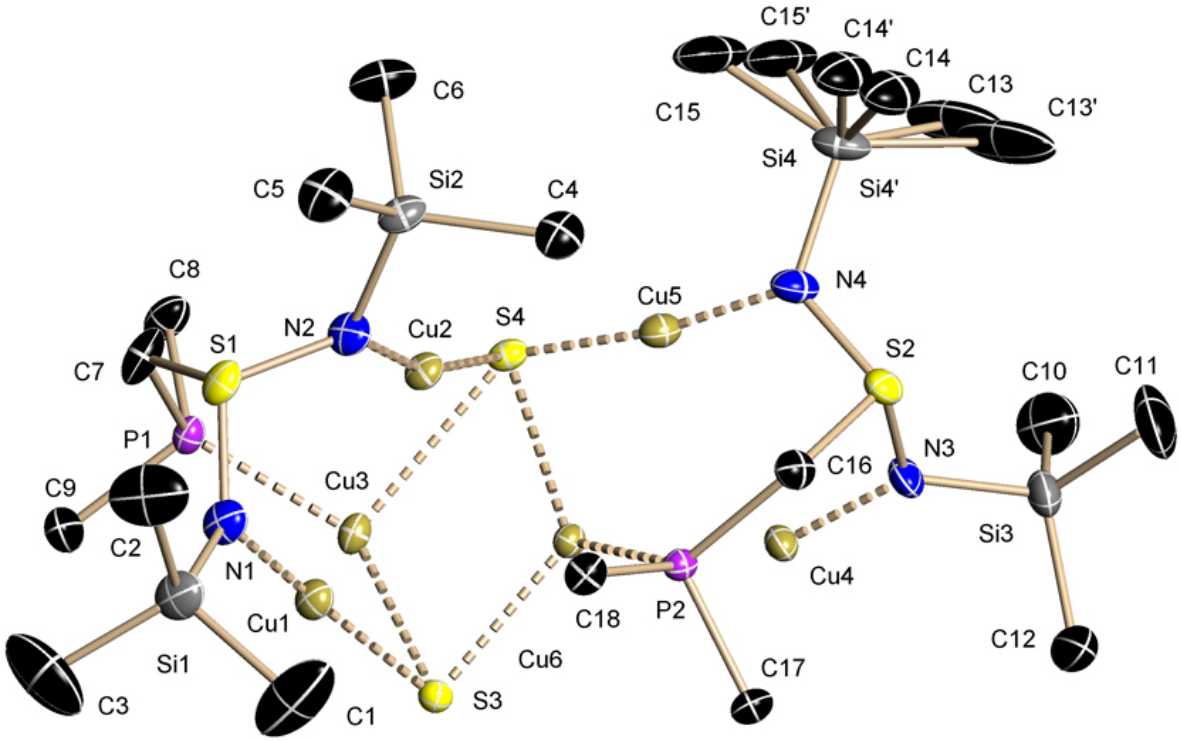

Asymmetric unit of **33**. The anisotropic displacement parameters are shown at the 50 % probability level, hydrogen atoms are omitted for clarity. The $NSiMe_3$ group on N4 is disordered and was refined using SAME. The occupancy factors refine to 86 and 14 %, respectively.

identification code	MMP236	*F*(000)	4096
empirical formula	$C_{36}H_{104}Cu_{12}N_8P_4S_8Si_8$	max./min. transmission	0.9422/0.8205
molecular weight [g/mol]	2016.83	θ range [°]	1.42-26.37
crystal size [mm]	0.18 x 0.1 x 0.02	completeness to θ_{max}	0.999
temperature [K]	100(2)	reflections collected	40145
crystal system	Monoclinic	independent reflections	8166
space group	*C*2/*c*	R_{int}/R_σ	0.0393/0.0137
a [Å]	31.087(3)	restraints/parameters	9/372
b [Å]	9.4333(8)	GoF	1.020
c [Å]	29.451(3)	*R*1 (all data)	0.0236
β [°]	112.4610(10)	*R*1 (*I*>2σ(*I*))	0.0199
V [Å^3]	7981.4(12)	*wR*2 (all data)	0.0499
Z	4	*wR*2 (*I*>2σ(*I*))	0.0482
ρ_{calc} [g cm^{-3}]	1.678	diff. peak/hole [eÅ^{-3}]	0.668/-0.603
μ [mm^{-1}]	3.567	g1/g2	0.0217/18.5376

8.5.33 [(tmeda)Rb{$Ph_2PCH_2S(NSiMe_3)_2$}$_2$Li] (34)

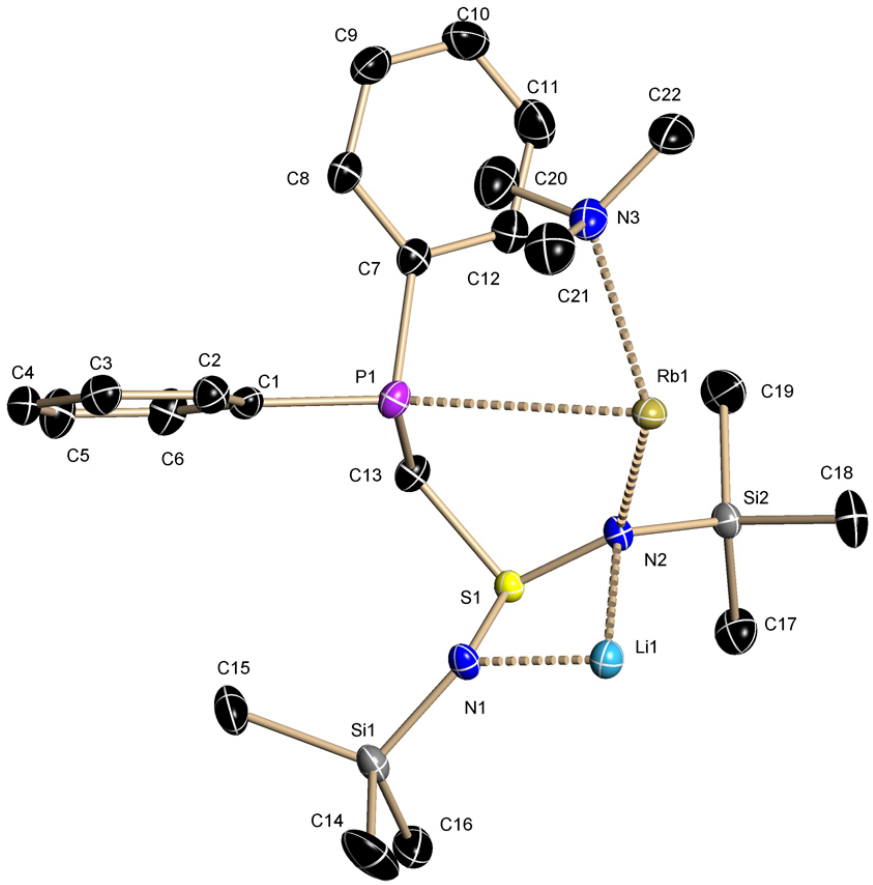

Asymmetric unit of **34**. The anisotropic displacement parameters are shown at the 50 % probability level, hydrogen atoms are omitted for clarity.

identification code	MMP276	*F*(000)	2160
empirical formula	$C_{44}H_{76}LiN_6P_2RbS_2Si_4$	max./min. transmission	0.942/0.8952
molecular weight [g/mol]	1019.94	θ range [°]	1.81-26.02
crystal size [mm]	0.2 x 0.15 x 0.1	completeness to θ_{max}	0.999
temperature [K]	100(2)	reflections collected	40145
crystal system	monoclinic	independent reflections	5449
space group	*C*2/*c*	R_{int}/R_σ	0.0393/0.0245
a [Å]	18.0553(17)	restraints/parameters	0/280
b [Å]	13.6709(13)	GoF	1.036
c [Å]	22.639(2)	*R*1 (all data)	0.0361
β [°]	97.149(2)	*R*1 (*I*>2σ(*I*))	0.0281
V [Å^3]	5544.6(9)	*wR*2 (all data)	0.0641
Z	4	*wR*2 (*I*>2σ(*I*))	0.0612
ρ_{calc} [g cm^{-3}]	1.222	diff. peak/hole [eÅ^{-3}]	0.536/-0.241
μ [mm^{-1}]	1.147	g1/g2	0.0236/8.3289

8.5.34 [(tmeda)K{$Ph_2PCH_2S(NSiMe_3)_2$}$_2$Li] (35)

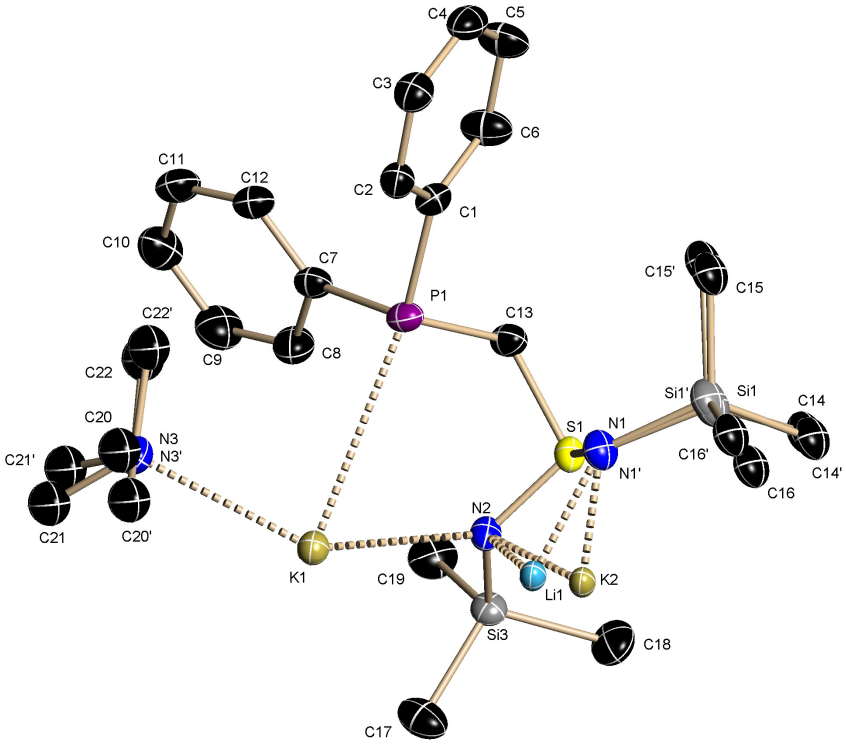

Asymmetric unit of **35**. The anisotropic displacement parameters are shown at the 50 % probability level, hydrogen atoms are omitted for clarity. The TMEDA molecule is disorder over two sites with occupancy factors of 83 and 17 %, respectively. One $SiMe_3$ group is disordered with occupancy factors of 50 and 50 %. The lithium cation is disordered with potassium with occupancy factors of 94 and 6 %, respectively. Because of insufficient crystal quality, the data is not satisfying. However, the unit cell presented here is the best solution.

identification code	MMPEK26	*F*(000)	2092
empirical formula	$C_{44}H_{76}K_{1.06}Li_{0.94}N_6P_2S_2Si_4$	max./min. transmission	0.9422/0.8605
molecular weight [g/mol]	975.50	θ range [°]	1.80-25.68
crystal size [mm]	0.1 x 0.1 x 0.02	completeness to θ_{max}	1.000
temperature [K]	100(2)	reflections collected	39141
crystal system	monoclinic	independent reflections	5267
space group	*C*2/*c*	R_{int}/R_σ	0.0389/0.0228
a [Å]	18.2492(11)	restraints/parameters	10/280
b [Å]	13.4012(8)	GoF	1.066
c [Å]	22.8301(14)	*R*1 (all data)	0.0585
β [°]	96.4140(10)	*R*1 (*I*>2σ(*I*))	0.0495
V [Å^3]	5548.4(6)	*wR*2 (all data)	0.1199
Z	4	*wR*2 (*I*>2σ(*I*))	0.1146
ρ_{calc} [g cm^{-3}]	1.168	diff. peak/hole [eÅ^{-3}]	1.470/-0.691
μ [mm^{-1}]	0.354	g1/g2	0.0438/19.8298

8.5.35 $[Ph_2PCSN(H)tBu]_2$

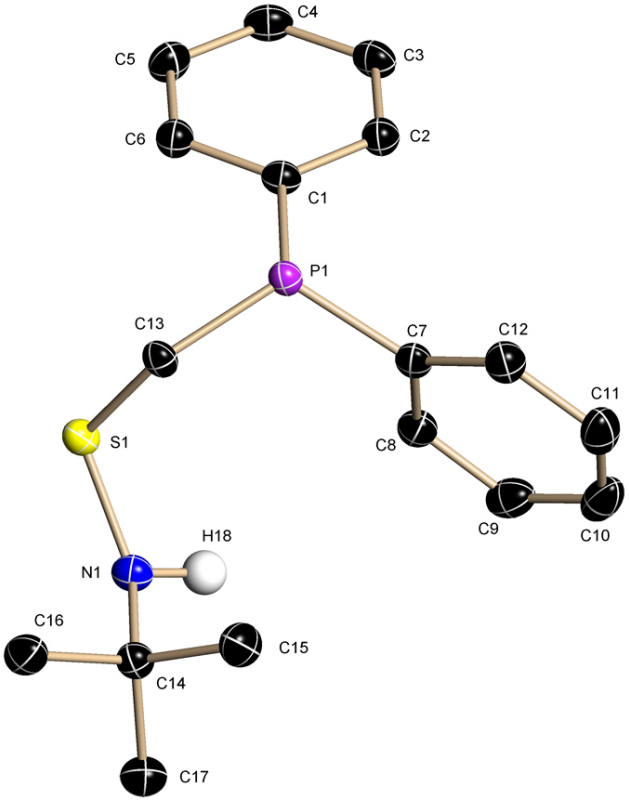

Asymmetric unit of $[Ph_2PCSN(H)tBu]_2$. The anisotropic displacement parameters are shown at the 50 % probability level, hydrogen atoms are omitted for clarity except for H18 which was freely refined using distance restraints.

identification code	Falter	μ [mm^{-1}]	0.300
empirical formula	$C_{34}H_{40}N_2P_2S_2$	F(000)	320
molecular weight [g/mol]	602.74	max./min. transmission	0.9800/0.8349
crystal size [mm]	0.15 x 0.08 x 0.06	θ range [°]	2.11-26.80
temperature [K]	100(2)	completeness to θ_{max}	0.997
crystal system	triclinic	reflections collected	23572
space group	$P\bar{1}$	independent reflections	3318
a [Å]	9.4276(14)	R_{int}/R_σ	0.0496/0.0295
b [Å]	9.7367(14)	restraints/parameters	1/203
c [Å]	10.5340(15)	GoF	1.027
α [°]	68.924(2)	R1 (all data)	0.0538
β [°]	89.615(2)	R1 (I>2σ(I))	0.0389
γ [°]	61.767(2)	wR2 (all data)	0.1031
V [Å^3]	779.1(2)	wR2 (I>2σ(I))	0.0984
Z	1	diff. peak/hole [eÅ^{-3}]	0.413/-0.392
ρ_{calc} [g cm^{-3}]	1.285	g1/g2	0.0455/0.5364

8.5.36 MMP40

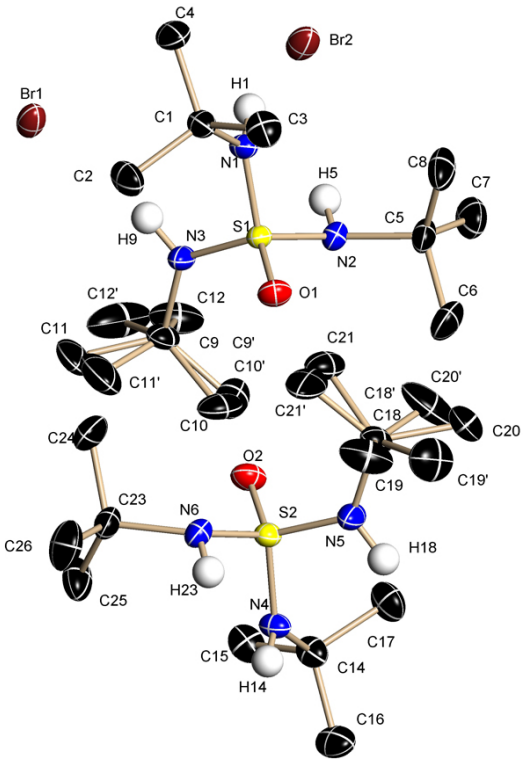

Asymmetric unit of MMP40. The anisotropic displacement parameters are shown at the 50 % probability level, hydrogen atoms are omitted for clarity except for H1, H5, H9, H14, H18 and H23 which were freely refined using distance restraints. The *t*Bu group on N3 is disordered with occupancy factors of 72 and 28 %, respectively. The *t*Bu group on N5 is disordered with occupancy factors of 81 and 19 %, respectively. Both were refined using SAME, EADP and EXYZ.

identification code	Smarties	*F*(000)	1456
empirical formula	$C_{12}H_{30}BrN_3OS$	max./min. transmission	0.9703/0.7969
molecular weight [g/mol]	344.36	θ range [°]	1.72-27.10
crystal size [mm]	0.2 x 0.2 x 0.1	completeness to θ_{max}	0.999
temperature [K]	100(2)	reflections collected	93217
crystal system	monoclinic	independent reflections	7874
space group	$P2_1/c$	R_{int}/R_σ	0.0346/0.0147
a [Å]	12.3613(7)	restraints/parameters	18/429
b [Å]	19.2447(12)	GoF	1.034
c [Å]	16.0995(10)	*R*1 (all data)	0.0265
β [°]	111.2920(10)	*R*1 (*I*>2σ(*I*))	0.0234
V [Å^3]	3568.5(4)	*wR*2 (all data)	0.0594
Z	8	*wR*2 (*I*>2σ(*I*))	0.0582
ρ_{calc} [g cm^{-3}]	1.282	diff. peak/hole [eÅ^{-3}]	0.573/-0.343
μ [mm^{-1}]	2.417	g1/g2	0.0299/1.504

8.6 Service Structures

8.6.1 $C_9H_8O_5$ (MMPHB01)

This structure was a service measurement for the group of Prof. Tietze.[226]

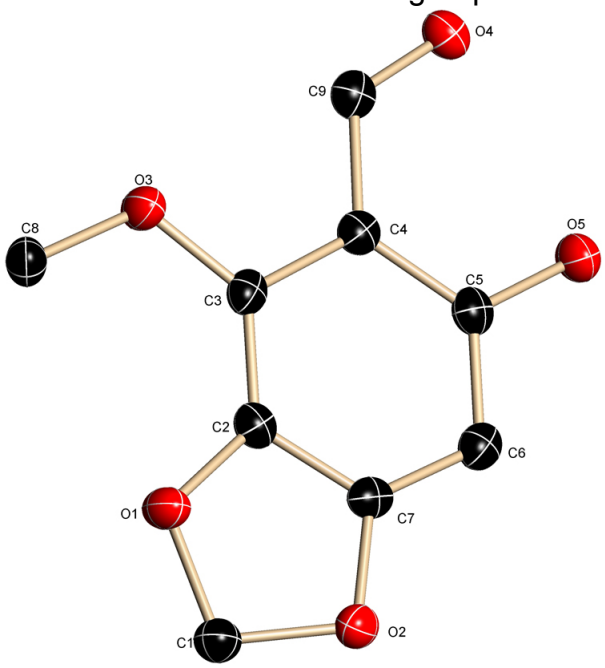

Asymmetric unit of $C_9H_8O_5$. The anisotropic displacement parameters are shown at the 50 % probability level, hydrogen atoms are omitted for clarity except for H5 which was freely refined using distance restraints.

identification code	Zicke	*F*(000)	408
empirical formula	$C_9H_8O_5$	max./min. transmission	0.9422/0.7780
molecular weight [g/mol]	196.15	θ range [°]	2.04-25.34
crystal size [mm]	0.2 x 0.14 x 0.01	completeness to θ_{max}	0.996
temperature [K]	100(2)	reflections collected	9944
crystal system	monoclinic	independent reflections	1439
space group	$P2_1/c$	R_{int}/R_σ	0.0469/0.0299
a [Å]	3.8332(14)	restraints/parameters	0/129
b [Å]	12.639(5)	GoF	1.035
c [Å]	16.337(6)	*R*1 (all data)	0.0564
β [°]	96.283(7)	*R*1 (*I*>2σ(*I*))	0.0363
V [Å^3]	786.7(5)	*wR*2 (all data)	0.0974
Z	4	*wR*2 (*I*>2σ(*I*))	0.0892
ρ_{calc} [g cm^{-3}]	1.656	diff. peak/hole [eÅ^{-3}]	0.189/-0.188
μ [mm^{-1}]	0.138	g1/g2	0.0473/0.3526

8.6.2 HWOA019

This was measured for H. Wolf from our own group.

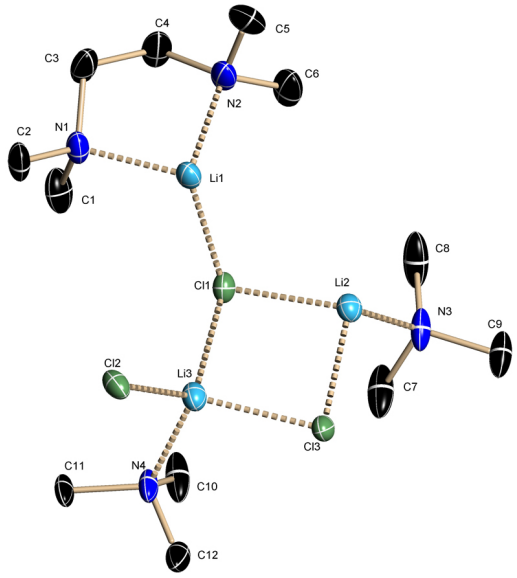

Asymmetric unit of HWOA019. The anisotropic displacement parameters are shown at the 50 % probability level, hydrogen atoms are omitted for clarity.

identification code	HWOA019	μ [mm^{-1}]	0.441
empirical formula	$C_{12}H_{32}Cl_3Li_3N_4$	F(000)	384
molecular weight [g/mol]	359.59	max./min. transmission	0.9422/0.8765
crystal size [mm]	0.2 x 0.2 x 0.1	θ range [°]	2.09-26.37
temperature [K]	100(2)	completeness to θ_{max}	0.997
crystal system	triclinic	reflections collected	18917
space group	$P\bar{1}$	independent reflections	4202
a [Å]	10.7463(8)	R_{int}/R_σ	0.0294
b [Å]	11.1086(8)	restraints/parameters	0.0230
c [Å]	11.1472(9)	GoF	1.249
α [°]	61.1730(10)	R1 (all data)	0.0455
β [°]	74.626(2)	R1 (I>2σ(I))	0.0328
γ [°]	62.4420(10)	wR2 (all data)	0.1124
V [Å^3]	1032.03(14)	wR2 (I>2σ(I))	0.0967
Z	2	diff. peak/hole [eÅ^{-3}]	0.357/-0.266
ρ_{calc} [g cm^{-3}]	1.157	g1/g2	0.0651/0.2132

Other service structures that were measured for our own group can be found in the corresponding diploma theses.[227,228]

9 REFERENCES

[1] S. Trofimenko, *J. Am. Chem. Soc.* **1966**, *88*, 1842.

[2] a) J. P. Jesson, S. Trofimenko, D. R. Eaton, *J. Am. Chem. Soc.* **1967**, *89*, 3248; b) S. Trofimenko, *J. Am. Chem. Soc.* **1967**, *89*, 3170.

[3] S. Trofimenko, *Chem. Rev.* **1993**, *93*, 943.

[4] F. T. Edelmann, *Angew. Chem.* **2001**, *113*, 1704; *Angew. Chem. Int. Ed.* **2001**, *40*, 1656.

[5] M. Paneque, S. Sirol, M. Trujillo, E. Gutiérrez-Puebla, M. A. Monge, E. Carmona, *Angew. Chem.* **2000**, *112*, 224; *Angew. Chem. Int. Ed.* **2000**, *39*, 218.

[6] C. Slugovc, K. Mereiter, S. Trofimenko, E. Carmona, *Chem. Commun.* **2000**, 121.

[7] Z. Hu, S. M. Gorun, *Inorg. Chem.* **2001**, *40*, 667.

[8] a) J. C. Calabrese, S. Trofimenko, J. S. Thompson, *J. Chem. Soc., Chem. Commun.* **1986**, 1122; b) S. Trofimenko, J. C. Calabrese, J. S. Thompson, *Inorg. Chem.* **1987**, *26*, 1507.

[9] a) S. G. N. Roundhill, D. M. Roundhill, D. R. Bloomquist, C. Landee, R. D. Willett, D. M. Dooley, H. B. Gray, *Inorg. Chem.* **1979**, *18*, 831; b) J. S. Thompson, T. J. Marks, J. A. Ibers, *J. Am. Chem. Soc.* **1979**, *101*, 4180; c) J. S. Thompson, T. Sorrell, T. J. Marks, J. A. Ibers, *J. Am. Chem. Soc.* **1979**, *101*, 4193.

[10] D. L. Reger, J. R. Gardinier, W. R. Gemmill, M. D. Smith, A. M. Shahin, G. J. Long, L. Rebbouh, F. Grandjean, *J. Am. Chem. Soc.* **2005**, *127*, 2303.

[11] E. V. Mutseneck, S. Bieller, M. Bolte, H.-W. Lerner, M. Wagner, *Inorg. Chem.* **2010**, *49*, 3540.

[12] J. Bielawski, M. K. Das, E. Hanecker, K. Niedenzu, H. Nöth, *Inorg. Chem.* **1986**, *25*, 4623.

[13] S. Bieller, M. Bolte, H.-W. Lerner, M. Wagner, *Chem. Eur. J.* **2006**, *12*, 4735.

[14] T. A. Betley, J. C. Peters, *Inorg. Chem.* **2003**, *42*, 5074.

[15] A. A. Barney, A. F. Heyduk, D. G. Nocera, *Chem. Commun.* **1999**, 2379.

[16] a) S. Trofimenko, *J. Am. Chem. Soc.* **1970**, *92*, 5118; b) H. Gornitzka, D. Stalke, *Angew. Chem.* **1994**, *106*, 695; *Angew. Chem. Int. Ed.* **1994**, *33*, 693; c) F. Breher, J. Grunenberg, S. C. Lawrence, P. Mountford, H. Rüegger, *Angew. Chem.* **2004**, *116*, 2575; *Angew. Chem. Int. Ed.* **2004**, *43*, 2521; d) A. Otero, J. Fernández-Baeza, A. Antiñolo, J. Tejeda, A. Lara-Sánchez, *Dalton Trans.* **2004**, 1499; e) A. Hoffmann, U. Flörke, M. Schürmann, S. Herres-Pawlis, *Eur. J. Org. Chem.* **2010**, 4136.

[17] D. Kratzert, D. Leusser, D. Stern, J. Meyer, F. Breher, D. Stalke, *Chem. Commun.* **2011**, *47*, 2931.

[18] W. H. Armstrong, A. Spool, G. C. Papaefthymiou, R. B. Frankel, S. J. Lippard, *J. Am. Chem. Soc.* **1984**, *106*, 3653.

[19] N. Kitajima, K. Fujisawa, C. Fujimoto, Y. Moro-oka, S. Hashimoto, T. Kitagawa, K. Toriumi, K. Tatsumi, A. Nakamura, *J. Am. Chem. Soc.* **1992**, *114*, 1277.

[20] T. C. Higgs, C. J. Carrano, *Inorg. Chem.* **1997**, *36*, 291.

[21] K. Ruth, S. Tüllmann, H. Vitze, M. Bolte, H.-W. Lerner, M. C. Holthausen, M. Wagner, *Chem. Eur. J.* **2008**, *14*, 6745.

[22] a) S. T. Prigge, A. S. Kolhekar, B. A. Eipper, R. E. Mains, L. M. Amzel, *Science* **1997**, *278*, 1300; b) S. T. Prigge, B. A. Eipper, R. E. Mains, L. M. Amzel, *Science* **2004**, *304*, 864.

[23] a) A. Otero, A. Lara-Sánchez, J. Fernández-Baeza, E. Martínez-Caballero, I. Márquez-Segovia, C. Alonso-Moreno, L. F. Sánchez-Barba, A. M. Rodríguez, I. López-Solera, *Dalton Trans.* **2010**, *39*, 930; b) S. Milione, F. Grisi, R. Centore, A. Tuzi, *Organometallics* **2006**, *25*, 266; c) S. C. Lawrence, B. D. Ward, S. R. Dubberley, C. M. Kozak, P. Mountford, *Chem. Commun.* **2003**, 2880; d) G. Türkoglu, C. Pubill Ulldemolins, R. Müller, E. Hübner, F. W. Heinemann, M. Wolf, N. Burzlaff, *Eur. J. Inorg. Chem.* **2010**, 2962.

[24] M. N. McCain, S. Schneider, M. R. Salata, T. J. Marks, *Inorg. Chem.* **2008**, *47*, 2534.

[25] a) E. E. Pullen, D. Rabinovich, C. D. Incarvito, T. E. Concolino, A. L. Rheingold, *Inorg. Chem.* **2000**, *39*, 1561; b) J. Grobe, R. Wehmschulte, B. Krebs, M. Läge, *Z. Anorg. Allg. Chem.* **1995**, *621*, 583.

[26] a) D. D. LeCloux, C. J. Tokar, M. Osawa, R. P. Houser, M. C. Keyes, W. B. Tolman, *Organometallics* **1994**, *13*, 2855; b) J. S. Fleming, E. Psillakis, J. C. Jeffery, K. L. V. Mann, J. A. McCleverty, M. D. Ward, *Polyhedron* **1998**, *17*, 1705; c) V. Chandrasekhar, B. Murugesapandian, *Acc. Chem. Res.* **2009**, *42*, 1047.

[27] A. Steiner, D. Stalke, *Inorg. Chem.* **1995**, *34*, 4846.

[28] M. A. Beswick, M. K. Davies, P. R. Raithby, A. Steiner, D. S. Wright, *Organometallics* **1997**, *16*, 1109.

[29] D. Leusser, J. Henn, N. Kocher, B. Engels, D. Stalke, *J. Am. Chem. Soc*. **2004**, *126*, 1781.

[30] J. Henn, D. Leusser, D. Ilge, D. Stalke, B. Engels, *J. Phys. Chem. A* **2004**, *108*, 9442.

[31] R. Fleischer, S. Freitag, D. Stalke, *J. Chem. Soc., Dalton Trans.* **1998**, 193.

[32] R. Fleischer, S. Freitag, D. Stalke, *Angew. Chem.* **1996**, *108*, 208; *Angew. Chem. Int. Ed.* **1996**, *35*, 204.

[33] T. Schulz, D. Stalke, *Chem. Eur. J.* **2010**, 2185.

[34] R. Fleischer, D. Stalke, *Coord. Chem. Rev.* **1998**, *176*, 431.

[35] C. Selinka, S. Deuerlein, T. Häuser, D. Stalke, *Inorg. Chim. Acta* **2004**, *357*, 1873.

[36] J. T. E. Meyer, T. Schulz, S. K. Pandey, D. Stalke, *Inorg. Chem.* **2010**, *49*, 2743.

[37] C. Selinka, D. Stalke, *Z. Naturforsch., B: Chem. Sci.* **2003**, *58*, 291.

[38] S. M. Deuerlein, PhD Thesis, Göttingen, **2007**.

[39] M. M. Meinholz, S. K. Pandey, S. M. Deuerlein, D. Stalke, *Dalton Trans.* **2011**, *40*, 1662.

[40] a) M. A. Casado, V. Hack, J. A. Camerano, M. A. Ciriano, C. Tejel, L. A. Oro, *Inorg. Chem.* **2005**, *44*, 9122; b) J. A. Camerano, M. A. Casado, M. A. Ciriano, C. Tejel, L. A. Oro, *Chem. Eur. J.* **2008**, *14*, 1897.

[41] a) R. G. Pearson, *J. Am. Chem. Soc.* **1963**, *85*, 3533; b) R. G. Parr, R. G. Pearson, *J. Am. Chem. Soc.* **1983**, *105*, 7512; c) R. G. Pearson, *J. Am. Chem. Soc.* **1985**, *107*, 6801.

[42] a) L. Lochmann, J. Pospíšil, D. Lim, *Tetrahedron Lett.* **1966**, 257; b) M. J. Schlosser, *J. Organomet. Chem.* **1967**, *8*, 9.

[43] a) Y. Kondo, M. Shilai, M. Uchiyama, T. Sakamoto, *J. Am. Chem. Soc.* **1999**, *121*, 3539; b) T. Imahori, M. Uchiyama, T. Sakamoto, Y. Kondo, *Chem. Commun.* **2001**, *23*, 2450.

[44] A. Krasovskiy, P. Knochel, *Angew. Chem.* **2004**, *116*, 3396; *Angew. Chem. Int. Ed.* **2004**, *43*, 3333.

[45] a) P. C. Andrikopoulos, D. R. Armstrong, D. V. Graham, E. Hevia, A. R. Kennedy, R. E. Mulvey, C. T. O'Hara, C. Talmard, *Angew. Chem.* **2005**, *117*, 3525; *Angew. Chem. Int. Ed.* **2005**, *44*, 3459; b) R. E. Mulvey, *Acc. Chem. Res.* **2009**, *42*, 743.

[46] S. Merkel, D. Stern, J. Henn, D. Stalke, *Angew. Chem.* **2009**, *121*, 6468; *Angew. Chem. Int. Ed.* **2009**, *48*, 6350.

[47] F. M. Piller, A. Metzger, M. A. Schade, B. A. Haag, A. Gavryushin, P. Knochel, *Chem. Eur. J.* **2009**, *15*, 7192.

[48] Available from Aldrich and Chemmetall GmbH

[49] A. Krasovskiy, V. Krasovskaya, P. Knochel, *Angew. Chem.* **2006**, *118*, 3024; *Angew. Chem. Int. Ed.* **2006**, *45*, 2958.

[50] a) C. R. Hauser, H. G. Walker Jr., *J. Am. Chem. Soc.* **1947**, *69*, 295; b) F. C. Frostick Jr., C. R. Hauser, *J. Am. Chem. Soc.* **1949**, *71*, 1350.

[51] J. García-Álvarez, D. V. Graham, E. Hevia, A. R. Kennedy, J. Klett, R. E. Mulvey, C. T. O'Hara, S. Weatherstone, *Angew. Chem.* **2008**, *120*, 8199; *Angew. Chem. Int. Ed.* **2008**, *47*, 8079.

[52] E. Hevia, D. J. Gallagher, A. R. Kennedy, R. E. Mulvey, C. T. O'Hara, C. Talmard, *Chem. Commun.* **2004**, 2422.

[53] W. Clegg, K. W. Henderson, A. R. Kennedy, R. E. Mulvey, C. T. O'Hara, R. B. Rowlings, D. M. Tooke, *Angew. Chem.* **2001**, *113*, 4020; *Angew. Chem. Int. Ed.* **2001**, *40*, 3902.

[54] A. R. Kennedy, J. Klett, R. E. Mulvey, D. S. Wright, *Science* **2009**, *326*, 706.

[55] P. Braunstein, F. Naud, *Angew. Chem.* **2001**, *113*, 702; *Angew. Chem. Int. Ed.* **2001**, *40*, 680.

[56] D. Hänssgen, H. Hupfer, M. Nieger, M. Pfendtner, R. Steffens, *Z. Anorg. Allg. Chem.* **2001**, *627*, 17.

[57] T. Schulz, Diploma thesis, Würzburg (GER), **2006**.

[58] R. Fleischer, D. Stalke, *Organometallics* **1998**, *17*, 832.

[59] D. Hänssgen, R. Steffens, *Z. Anorg. Allg. Chem.* **1983**, *507*, 178.

[60] H. H. Karsch, H. Schmidbaur, *Z. Naturforsch.* **1977**, *32B*, 762.

[61] L. M. Engelhardt, G. E. Jacobsen, C. L. Raston, A. H. White, *J. Chem. Soc., Chem. Commun.* **1984**, 220.

[62] L. T. Byrne, L. M. Engelhardt, G. E. Jacobsen, W.-P. Leung, R. I. Papasergio, C. L. Raston, B. W. Skelton, P. Twiss, A. H. White, *J. Chem. Soc., Dalton Trans.* **1989**, 105.

[63] L. Wang, E. Hauptman, L. K. Johnson, E. F. McCord, Y. Wang, S. D. Ittel, US6897275B2, **2005**.

[64] a) G. C. Eberhardt, W. A. Butte, *J. Org. Chem.* **1964**, *29*, 2928; b) D. J. Peterson, *J. Organomet. Chem.* **1967**, *8*, 199.

[65] G. Fraenkel, W. R. Winchester, *Organometallics* **1989**, *8*, 2308.

[66] S. Blaurock, O. Kühl, E. Hey-Hawkins, *Organometallics* **1997**, *16*, 807.

[67] P. Rademacher, *Strukturen Organischer Moleküle*, VCH, New York, **1987**.

[68] Cambridge Structural Database, v5.32, Cambridge Crystallographic Data Centre, Cambridge, **2010**.

[69] a) D. Stalke, *Proc. Indian Acad. Sci.* **2000**, *112*, 155; b) J. K. Brask, T. Chivers, *Angew. Chem.* **2001**, *113*, 4082; *Angew. Chem. Int. Ed.* **2001**, *40*, 3960.

[70] W. Clegg, K. Izod, W. McFarlane, P. O'Shaughnessy, *Organometallics* **1998**, *18*, 3950.

[71] MestreNova, three-spin system ABC (C–P–P); A: ν = 0 ppm, J_{AB} = 18.3 Hz, J_{AC} = 0 Hz, B: ν = 1000 ppm, J_{AB} = 18.3 Hz, J_{BC} = 8.6 Hz, C: ν = 1000.002 ppm, J_{CA} = 0 Hz, J_{CB} = 8.6 Hz.

[72] S. Deuerlein, D. Leusser, U. Flierler, H. Ott, D. Stalke, *Organometallics* **2008**, *27*, 2306.

[73] M. Hesse, H. Meier, B. Zeeh, *Spektroskopische Methoden in der organischen Chemie*, Thieme, Stuttgart, **2005**.

[74] O. J. Scherer, R. Wies, *Z. Naturforsch.* **1970**, *25b*, 1486.

[75] A. M. Aguiar, G. W. Prejean, J. R. S. Irelan, C. J. Morrow, *J. Org. Chem.* **1969**, *34*, 4024.

[76] a) Z. Fei, N. Kocher, C. J. Mohrschladt, H. Ihmels, D. Stalke, *Angew. Chem.* **2003**, *115*, 807; *Angew. Chem. Int. Ed.* **2003**, *42*, 783; b) G. Schwab, D. Stern, D. Leusser, D. Stalke, *Z. Naturforsch*. **2007**, *62b*, 711; c) G. Schwab, D. Stern, D. Stalke, *J. Org. Chem.* **2008**, *73*, 5242.

[77] T. Chivers, M. Krahn, M. Parvez, G. Schatte, *Chem. Commun.* **2001**, 1922.

[78] T. Chivers, M. Krahn, M. Parvez, G. Schatte, *Inorg. Chem.* **2001**, *40*, 2547.

[79] V. H. Gessner, C. Strohmann, *J. Am. Chem. Soc.* **2008**, *130*, 14412.

[80] a) D. Leusser, B. Walfort, D. Stalke, *Angew. Chem*. **2002**, *114*, 2183; *Angew. Chem. Int. Ed.* **2002**, *41*, 2079; b) B. Walfort, D. Stalke, *Angew. Chem*. **2001**, *113*, 3965; *Angew. Chem. Int. Ed.* **2001**, *40*, 3846.

[81] S. Freitag, W. Kolodziejski, F. Pauer, D. Stalke, *Dalton Trans.* **1993**, 3479.

[82] B. Walfort, A. P. Leedham, C. A. Russell, D. Stalke, *Inorg. Chem.* **2001**, *40*, 5668.

[83] J. C. Thomas, J. C. Peters, *Inorg. Chem.* **2003**, *42*, 5055.

[84] F. Eisenträger, A. Göthlich, I. Gruber, H. Heiss, C. A. Kiener, C. Krüger, J. U. Notheis, F. Rominger, G. Scherhag, M. Schultz, B. F. Straub, M. A. O. Volland, P. Hofmann, *New. J. Chem.* **2003**, *27*, 540.

[85] F. T. Edelmann, F. Knösel, F. Pauer, D. Stalke, W. Bauer, *J. Organomet. Chem.* **1992**, *438*, 1.

[86] T. Stey, D. Stalke in: Z. Rappoport, I. Marek (Eds.), *The Chemistry of Organolithium Compounds*, Wiley, New York, **2004**.

[87] M. Müller, H.-W. Lerner, M. Bolte, *Acta Cryst.* **2008**, *E64*, m803.

[88] a) A. R. Lepley, W. A. Khan, A. B. Giumanini, A. G. Giumanini, *J. Org. Chem.* **1966**, *31*, 2047; b) E. B. Pederson, *J. Chem. Soc., Perkin Trans. 2* **1977**, 473; c) S.-I. Murahashi, T. Naota, Y. Tanigawa, *Org. Synth. Col.* **1984**, *62*, 39.

[89] D. Bojer, I. Kamps, X. Tian, A. Hepp, T. Pape, R. Fröhlich, N W. Mitzel, *Angew. Chem.* **2007**, *119*, 4254; *Angew. Chem. Int. Ed.* **2007**, *46*, 4176-4179.

[90] E. Weiss, *Angew. Chem.* **1993**, *105*, 1565; *Angew. Chem. Int. Ed. Engl.* **1993**, *32*, 1501.

[91] A. Streitwieser, Jr., J. E. Williams, Jr., J. M. McKelvey, *J. Am. Chem. Soc.* **1976**, *98*, 4778.

[92] E. Kaufmann, K. Raghavachari, A. E. Reed, P. v. R. Schleyer, *Organometallics* **1988**, *7*, 1597.

[93] a) F. M. Bickelhaupt, M. Solà, C. F. Guerra, *J. Chem. Theor. Comput.* **2006**, *2*, 965; b) E. Matito, J. Poater, F. M. Bickelhaupt, M. Solà, *J. Phys. Chem.* **2006**, *B110*, 7189.

[94] E. Weiss, G. Henken, *J. Organomet. Chem.* **1970**, *21*, 265.

[95] H. J. Dietrich, *J. Organomet. Chem*. **1981**, *205*, 291.

[96] T. Kottke, D. Stalke, *Angew. Chem.* **1993**, *105*, 619; *Angew. Chem. Int. Ed.* **1993**, *32*, 580.

[97] C. Strohmann, V. H. Gessner, *J. Am. Chem. Soc.* **2007**, *129*, 8952.

[98] M. Schlosser, *Organoalkali Reagents* in *Organometallics in Synthesis, A Manual*. M. Schlosser (Ed.), John Wiley & Sons: New York, **2002**.

[99] H. Hope, P. P. Power, *J. Am. Chem. Soc.* **1983**, *105*, 5320.

[100] R. G. Pearson, *J. Am. Chem. Soc.* **1985**, *107*, 6801.

[101] S. Harder, J. Boersma, L. Brandsma, J. A. Kanters, W. Bauer, P. v. R. Schleyer, *Organometallics* **1989**, *8*, 1696.

[102] a) E. O. Stejskal, J. E. Tanner, *J. Chem. Phys.* **1965**, *42*, 288; b) E. O. Stejskal, *J. Chem. Phys.* **1965**, *43*, 3597.

[103] K. F. Morris, C. S. Johnson Jr., *J. Am. Chem. Soc.* **1992**, *114*, 3139.

[104] J. T. Edward, *J. Chem. Educ.* **1970**, *47*, 261.

[105] G. Kagan, W. Li, R. Hopson, P. G. Williard, *Org. Lett.* **2009**, *11*, 4818.

[106] I. Keresztes, P. G. Williard, *J. Am. Chem. Soc.* **2000**, *122*, 10228.

[107] D. Li, I. Keresztes, R. Hopson, P. G. Williard, *Acc. Chem. Res.* **2009**, *42*, 270.

[108] All NMR studies on this system were conducted by Ann-Christin Pöppler, to whom I am very grateful.

[109] R. D. Thomas, M. T. Clarke, T. C. Young, *J. Organomet. Chem.* **1987**, *328*, 239.

[110] R. D. Thomas, M. T. Clarke, R. M. Jensen, T. C. Young, *Organometallics* **1986**, *5*, 1851.

[111] V. Snieckus, *Chem. Rev.* **1990**, *90*, 879; M. C. Whisler, S. MacNeil, V. Snieckus, P. Beak, *Angew. Chem.* **2004**, *116*, 2256; *Angew. Chem. Int. Ed.* **2004**, *43*, 2206.

[112] *CRC Handbook of Chemistry and Physics* (Ed. D. R. Lide), Taylor & Francis, Boca Raton, **2006**.

[113] a) H. Gilman, F. J. Webb, *J. Am. Chem. Soc.* **1940**, *62*, 987; b) H. Gilman, S. M. Spatz, *J. Org. Chem.* **1952**, *17*, 860; c) D. J. Peterson, H. R. Hays, *J. Org. Chem.* **1965**, *30*, 1939; d) S. V. Kessar, P. Singh, *Chem. Rev.* **1997**, *97*, 721.

[114] A. I. Shatenslitein, H. A. Gvozdera, *Tetrahedron* **1969**, *25*, 2749.

[115] a) D. J. Peterson, *J. Organomet. Chem.* **1970**, *21*, 63; b) D. J. Peterson, J. F. Ward, *J. Organomet. Chem.* **1974**, *66*, 209.

[116] a) T. Cohen, J. R. Matz, *J. Am.Chem. Soc.* **1980**, *102*, 6900; b) C. A. Broka, T. J. Shen, *J. Am. Chem. Soc.* **1989**, *111*, 2981; c) C. Strohmann, B. C. Abele, *Angew. Chem.* **1996**, *108*, 2514; *Angew. Chem. Int. Ed.* **1996**, *35*, 2378.

[117] R. E. Gawley, Q. Zhang, *J. Org. Chem.* **1995**, *60*, 5763.

[118] a) A. Hildebrand, P. Lönnecke, L. Silaghi-Dumitrescu, I. Silaghi-Dumitrescu, E. Hey-Hawkins, *Dalton Trans.* **2006**, 967.

[119] C. Strohmann, V. H. Gessner, *Angew. Chem.* **2007**, *119*, 4650; *Angew. Chem. Int. Ed.* **2007**, *46*, 4566.

[120] C. Strohmann, V. H. Gessner, *Angew. Chem.* **2007**, *119*, 8429; *Angew. Chem. Int. Ed.* **2007**, *46*, 8281.

[121] H. H. Karsch, *Chem. Ber.* **1996**, *129*, 483.

[122] H. Ott, PhD thesis, Göttingen (GER), **2008**.

[123] K. Izod, J. C. Stewart, W. Clegg, R. W. Harrington, *Dalton Trans.* **2007**, 257.

[124] J. D. Smith, *Adv. Organomet. Chem.* **1998**, *43*, 267.

[125] M. A. Beswick, N. Choi, A. D. Hopkins, M. McPartlin, M. A. Paver, D. S. Wright, *Chem. Commun.* **1998**, 261.

[126] D. Hoffmann, W. Bauer, P. v. R. Schleyer, U. Pieper, D. Stalke, *Organometallics* **1993**, *12*, 1193.

[127] U. Pieper, D. Stalke, *Organometallics* **1993**, *12*, 1201.

[128] G. Bai, H. W. Roesky, M. Noltemeyer, H.-G. Schmidt, *Organometallics* **2002**, *21*, 2789.

[129] M. Herberhold, S. Gerstmann, W. Milius, B. Wrackmeyer, H. Borrmann, *Phosphorus, Sulfur, Silicon Relat. Elem*. **1996**, *112*, 261.

[130] a) D. Leusser, J. Henn, N. Kocher, B. Engels, D. Stalke, *J. Am. Chem. Soc*. **2004**, *126*, 1781; b) J. Henn, D. Leusser, D. Ilge, D. Stalke, B. Engels, *J. Phys. Chem. A* **2004**, *108*, 9442.

[131] T. Schulz, PhD thesis, Göttingen (GER), **2010**.

[132] a) D. Olbert, H. Görls, D. Conrad, M. Westerhausen, *Eur. J. Inorg. Chem.* **2010**, *12*, 1791; b) H. Nöth, S. Rojas-Lima, A. Troll, *Eur. J. Inorg. Chem.* **2005**, *10*, 1895.

[133] a) H. Ott, U. Pieper, D. Leusser, U. Flierler, J. Henn, D. Stalke, *Angew. Chem*. **2009**, *121*, 3022; *Angew. Chem. Int. Ed*. **2009**, *48*, 2978; b) P. Macchi, *Angew. Chem*. **2009**, *121*, 5905; *Angew. Chem. Int. Ed*. **2009**, *48*, 5793.

[134] V. H. Gessner, C. Däschlein, C. Strohmann, *Chem. Eur. J.* **2009**, *15*, 3320.

[135] a) H. Yuge, T. K. Miyamoto, *Inorg. Chim. Acta* **2002**, *329*, 66; b) M. Montfort, I. Resino, J. Ribas, X. Solans, M. Font-Bardia, *N. J. Chem.* **2001**, *25*, 1577 ; c) sligthly modified: F. Voigt, A. Fischer, C. Pietzsch, K. Jacob, *Z. Anorg. Allg. Chem.* **2001**, *627*, 2337.

[136] A. W. Addison, T. Nageswara Rao, J. Reedijk, J. van Rijn, G. C. Verschoor, *Dalton Trans.* **1984**, 1349.

[137] S. Sripothongnak, A. M. Pischera, M. P. Espe, W. S. Durfee, C. J. Ziegler, *Inorg. Chem.* **2009**, *48*, 1293.

[138] a) I. Cragg-Hine, M. G. Davidson, F. S. Mair, P. R. Raithby, R. Snaith, *J. Chem. Soc., Dalton Trans.* **1993**, 2423; b) M. L. Cole, A. J. Davies, C. Jones, P. C. Junk, *New J. Chem.* **2005**, *29*, 1404.

[139] F. Pauer, D. Stalke, *J. Organomet. Chem*. **1991**, *418*, 127.

[140] P. C. Andrews, D. R. Armstrong, C. L. Raston, B. A. Roberts, B. W. Skelton, A. H. White, *Dalton Trans.* **2001**, 996.

[141] P. B. Hitchcock, M. F. Lappert, P. G. Merle, *Dalton Trans.* **2007**, 585.

[142] D. J. Peterson, J. H. Collins, *J. Org. Chem.* **1966**, *31*, 2373.

[143] J. W. F. L. Seetz, G. Schat, O. S. Akkerman, F. Bickelhaupt, *J. Am. Chem. Soc.* **1982**, *104*, 6848.

[144] C. Strohmann, *Angew. Chem.* **1996**, *108*, 600; *Angew. Chem. Int. Ed.* **1996**, *35*, 528.

[145] V. H. Gessner, S. Dilsky, C. Strohmann, *Chem. Commun.* **2010**, *46*, 4719.

[146] a) F. M. Mackenzie, R. E. Mulvey, *J. Am. Chem. Soc.* **1996**, *118*, 4721; b) X. Wei, Q. Dong, H. Tong, J. Chao, D. Liu, M. F. Lappert, *Angew. Chem.* **2008**, *120*, 4040; *Angew. Chem. Int. Ed.* **2008**, *47*, 3976.

[147] R. E. Mulvey, *Chem. Soc. Rev.* **1998**, *27*, 339.

[148] C. Drost, C. Jager, S. Freitag, U. Klingebiel, M. Noltemeyer, G. M. Sheldrick, *Chem. Ber.* **1994**, *127*, 845.

[149] M. B. Hursthous, M. A. Hossain, M. Motevdli, M. Sanganee, A. C. Sullivan, *J. Organomet. Chem.* **1990**, *381*, 293.

[150] A. R. Kennedy, R. E. Mulvey, R. B. Rowlings, *J. Am. Chem. Soc.* **1998**, *120*, 7816.

[151] a) A. R. Kennedy, R. E. Mulvey, R. B. Rowlings, *Angew. Chem.* **1998**, *110*, 3321; *Angew. Chem. Int. Ed.* **1998**, *37*, 3180; b) A. R. Kennedy, R. E. Mulvey, C. L. Raston, B. A. Roberts, R. B. Rowlings, *Chem. Commun.* **1999**, 353; c) R. E. Mulvey, *Chem. Commun.* **2001**, 1049.

[152] D. J. Gallagher, K. W. Henderson, A. R. Kennedy, C. T. O'Hara, R. E. Mulvey, R. B. Rowlings, *Chem. Commun.* **2002**, 376.

[153] D. R. Armstrong, A. R. Kennedy, R. E. Mulvey, R. B. Rowlings, *Angew. Chem.* **1999**, *111*, 231; *Angew. Chem. Int. Ed.* **1999**, *38*, 131.

[154] A. J. Chalk, T. J. Hoogeboom, *J. Organomet. Chem.* **1968**, *11*, 615.

[155] R. Fleischer, D. Stalke, *J. Organomet. Chem.* **1998**, *550*, 173.

[156] a) S. Blair, K. Izod, W. Clegg, R. W. Harrington, *Eur. J. Inorg. Chem.* **2003**, 3319; b) S. Blair, K. Izod, W. Clegg, *Inorg. Chem.* **2002**, *41*, 3886.

[157] A. Pape, M. Lutz, G. Müller, *Angew. Chem.* **1994**, *106*, 2375; *Angew. Chem. Int. Ed.* **1994**, *33*, 2281

[158] a) F. Pauer, J. Rocha, D. Stalke, *Chem. Commun.* **1991**, *20*, 1477; b) R. Fleischer, B. Walfort, A. Gbureck, P. Scholz, W. Kiefer, D. Stalke, *Chem. Eur. J.* **1998**, *4*, 2266.

[159] a) M. R. Crimmin, I. J. Casely, M. S. Hill, *J. Am Chem. Soc.* **2005**, *127*, 2042; b) M. R. Crimmin, A. G. M. Barrett, M. S. Hill, P. B. Hitchcock, P. A. Procopiou, *Organometallics* **2007**, *26*, 2953; c) M. R. Crimmin, A. G. M. Barrett, M. S. Hill, P. B. Hitchcock, P. A. Procopiou, *Organometallics* **2008**, *27*, 497.

[160] F. Buch, J. Brettar, S. Harder, *Angew. Chem.* **2006**, *118*, 2807; *Angew. Chem. Int. Ed.* **2006**, *45*, 2741.

[161] W. E. Lindsell, F. C. Robertson, I. Souter, *Eur. Polym. J.* **1983**, *19*, 115.

[162] a) M. Kaupp, P. v. R. Schleyer, H. Stoll, H. Preuss, *J. Chem. Phys.* **1991**, *94*, 1360; b) M. Kaupp, P. v. R. Schleyer, *J. Am. Chem. Soc.* **1992**, *114*, 491.

[163] R. Fleischer, D. Stalke, *Inorg. Chem.* **1997**, *36*, 2413.

[164] G. Mösges, F. Hampel, M. Kaupp, P. v. R. Schleyer, *J. Am. Chem. Soc.* **1992**, *114*, 10880.

[165] a) S. Blair, K. Izod, W. Clegg, *Inorg. Chem.* **2002**, *41*, 3886; b) P. W. Roesky, *Inorg. Chem.* **2006**, *45*, 798; c) S. Datta, M. T. Gamer, P. W. Roesky, *Dalton Trans.* **2008**, 2839.

[166] T. P. Hanusa, *Chem. Rev.* **1993**, *93*, 1023.

[167] a) C. Eaborn, P. B. Hitchcock, K. Izod, Z.-R. Lu, J. D. Smith, *Organometallics* **1996**, *15*, 4783; b) H. Schumann, S. Schutte, H.-J. Kroth, D. Lentz, *Angew. Chem.* **2004**, *116*, 6335; *Angew. Chem. Int. Ed.* **2004**, *43*, 6208; c) S. Harder, *Angew. Chem.* **2004**, *116*, 2768; *Angew. Chem. Int. Ed.* **2004**, *43*, 2714.

[168] N. N. Greenwood, A. Earnshaw, *Chemie der Elemente,* 1. Aufl. (Nachdr.), VCH, Weinheim (GER), **1990**.

[169] R. D. Shannon, *Acta Cryst.* **1976**, *A32*, 751.

[170] K. Abdur-Rashid, T. Graham, C.-W. Tsang, X. Chen, R. Guo, W. Jia, D. Amoroso, C. Sui-Seng, WO2008141439A1, **2008**.

[171] a) T. B. Marder, *Angew. Chem.* **2007**, *119*, 8262; *Angew. Chem. Int. Ed.* **2007**, *46*, 8116; b) F. H. Stephens, V. Pons, R. T. Baker, *Dalton Trans.* **2007**, 2613.

[172] a) B. L. Small, M. Brookhart, A. M. A. Bennett, *J. Am. Chem. Soc.* **1998**, *120*, 4049; b) G. J. P. Britovsek, M. Bruce, V. C. Gibson, B. S. Kimberley, P. J. Maddox, S. Mastroianni, S. J. McTavish, C. Redshaw, G. A. Solan, S. Strömberg, A. J. P. White, D. J. Williams, *J. Am. Chem. Soc.* **1999**, *121*, 8728; d) C. Bianchini, G. Mantovani, A. Meli, F. Migliacci, F. Zanobini, F. Laschi, A. Sommazzi, *Eur. J. Inorg. Chem.* **2003**, 1620.

[173] M. M. P. Grutters, C. Müller, D. Vogt, *J. Am. Chem. Soc.* **2006**, *128*, 7414.

[174] M. Takata, K. Kashiwabara, H. Ito, T. Ito, J. Fujita, *Bull. Chem. Soc. Jpn.* **1985**, *58*, 2247.

[175] a) M. Atoh, K. Kashiwabara, J. Fujita, *Bull. Chem. Soc. Jpn.* **1985**, *58*, 3492; b) M. Atoh, H. O. Sørensen, P. Andersen, *Acta Chem. Scand.* **1997**, *51*, 1169.

[176] J. Bennett, R. J. Doyle, G. Salem, A. C. Willis, *Dalton. Trans.* **2006**, 4614.

[177] a) Y. A. Simonov, N. V. Gerbeleu, M. Gnadets, P. N. Bourosh, E. B. Koropchanu, O. A. Bologa, *Koord. Khim. (Rus. J. Coord. Chem.)* **2001**, *27*, 386; b) N. Bresciani-Pahor, M. Calligaris, L. Randaccio, P. J. Toscano, *J. Chem. Soc., Dalton Trans.* **1982**, 1009; c) B. D. Gupta, K. Qanungo, R. Yamuna, A. Pandey, U. Tewari, V. Vijaikanth, V. Singh, T. Barclay, W. Cordes, *J. Organomet. Chem.* **2000**, *608*, 106; d) T. Yamada, Y. Ohashi, *Bull. Chem. Soc. Jpn.* **1998**, *71*, 2527.

[178] a) S. C. Bart, E. Lobkovsky, P. J. Chirik, *J. Am. Chem. Soc.* **2004**, *126*, 13794; b) S. C. Bart, E. J. Hawrelak, E. Lobkovsky, P. J. Chirik, *Organometallics* **2005**, *24*, 5518; c) Q. Knijnenburg, A. D. Horton, H. van der Heijden, A. W. Gal, P. Budzelaar, M. Henricus, WO2003042131, **2003**; d) A. Mikhailine, F. Freutel, N. Meyer, R. H. Morris, P. O. Lagaditis, US20100145087A1, **2010**.

[179] V. V. K. M. Kandepi, J. M. S. Cardoso, E. Peris, B. Royo, *Organometallics* **2010**, *29*, 2777.

[180] a) C. Bianchini, G. Mantovani, A. Meli, F. Migliacci, F. Zanobini, F. Laschi, A. Sommazzi, *Eur. J. Inorg. Chem.* **2003**, 1620; b) B. L. Small, M. Brookhart, *Macromolecules* **1999**, *32*, 2120; c) T.

M. Smit, A. K. Tomov, V. C. Gibson, A. J. P. White, D. J. Williams, *Inorg. Chem.* **2004**, *43*, 6511; d) M. W. Bouwkamp, E. Lobkovsky, P. J. Chirik, *J. Am. Chem. Soc.* **2005**, *127*, 9660.

[181] a) M. Tamura, J. K. Kochi, *J. Am. Chem. Soc*. **1971**, *93*, 1487; b) A. Fürstner, A. Leitner, *Angew. Chem.* **2002**, *114*, 632; *Angew. Chem. Int. Ed.* **2002**, *41*, 609; c) A. Fürstner, A. Leitner, M. Méndez, H. Krause, *J. Am. Chem. Soc.* **2002**, *124*, 13856.

[182] R. J. Trovitch, E. Lobkovsky, M. W. Bouwkamp, P. J. Chirik, *Organometallics* **2008**, *27*, 6264.

[183] C. Bolm, J. Legros, J. Le Paih, L. Zani, *Chem. Rev.* **2004**, *104*, 6217.

[184] C. Sui-Seng, F. Freutel, A. J. Lough, R. H. Morris, *Angew. Chem.* **2008**, *120*, 954; *Angew. Chem. Int. Ed.* **2008**, *47*, 940.

[185] a) R. Noyori, S. Hashiguchi, *Acc. Chem. Res.* **1997**, *30*, 97; b) T. Ikariya, A. J. Blacker, *Acc. Chem. Res.* **2007**, *40*, 1300.

[186] P. O. Lagaditis, A. A. Mikhailine, A. J. Lough, R. H. Morris, *Inorg. Chem.* **2010**, *49*, 1094.

[187] A. Kermagoret, F. Tomicki, P. Braunstein, *Dalton Trans.* **2008**, *22*, 2945.

[188] D. Benito-Garagorri, E. Becker, J. Wiedermann, W. Lackner, M. Pollack, K. Mereiter, J. Kisala, K. Kirchner, *Organometallics* **2006**, *25*, 1900.

[189] A. Murso, D. Stalke, *Dalton Trans.* **2004**, 2563.

[190] V. Rautenstrauch, X. Hoang-Cong, R. Churlaud, K. Abdur-Rashid, R. H. Morris, *Chem. Eur. J.* **2003**, *9*, 4954.

[191] S. Gladiali, E. Alberico, *Chem. Soc. Rev.* **2006**, *35*, 226.

[192] G. Glatz, S. Demeshko, G. Motz, R. Kempe, *Eur. J. Inorg. Chem.* **2009**, 1385.

[193] J. Volbeda, A. Meetsma, M. W. Bouwkamp, *Organometallics* **2009**, *28*, 209.

[194] B. Walfort, T. Auth, B. Degel, H. Helten, D. Stalke, *Organometallics* **2002**, *21*, 2208.

[195] a) D. Fenske, H. Krautscheid, S. Balter, *Angew. Chem.* **1990**, *102*, 799; *Angew. Chem. Int. Ed.* **1990**, *29*, 796; b) D. Fenske, J.-C. Steck, *Angew. Chem.* **1993**, *105*, 254; *Angew. Chem. Int. Ed.* **1993**, *32*, 238; c) J.-P. Lang, H. Kawaguchi, K. Tatsumi, *Chem. Commun.* **1999**, 2315.

[196] D. Fenske, H. Krautscheid, M. Müller, *Angew. Chem.* **1992**, *104*, 309; *Angew. Chem. Int. Ed.* **1992**, *31*, 321.

[197] S. Dehnen, D. Fenske, *Chem. Eur. J.* **1996**, *2*, 1407.

[198] a) P. Pyykkö, *Chem. Rev.* **1997**, *97*, 597; b) H. L. Hermann, G. Boche, P. Schwerdtfeger, *Chem. Eur. J.* **2001**, *7*, 5333.

[199] U. Englich, K. Hassler, K. Ruhlandt-Senge, F. Uhlig, *Inorg. Chem.* **1998**, *37*, 3532.

[200] G. W. Rabe, S. Kheradmandan, L. M. Liable-Sands, I. A. Guzei, A. L. Rheingold, *Angew. Chem.* **1998**, *110*, 1495; *Angew. Chem. Int. Ed.* **1998**, *37*, 1404.

[201] K. Izod, W. Clegg, S. T. Liddle, *Organometallics* **2001**, *20*, 367.

[202] W. Clegg, A. M. Drummond, R. E. Mulvey, S. T. Liddle, *Chem. Commun.* **1998**, 2391.

[203] D. R. Armstrong, W. Clegg, A. M. Drummond, S. T. Liddle, R. E. Mulvey, *J. Am. Chem. Soc.* **2000**, *122*, 11117.

[204] T. Gelbrich, T. L. Threlfall, S. Huth, E. Seeger, *Polyhedron* **2006**, *25*, 937.

[205] M. Westerhausen, S. Weinrich, G. Kramer, H. Piotrowski, *Inorg. Chem.* **2002**, *41*, 7072.

[206] D. Ilge, D. S. Wright, D. Stalke, *Chem. Eur. J.* **1998**, *4*, 2275.

[207] I. Ruppert, V. Bastian, R. Appel, *Chem. Ber.* **1975**, *108*, 2329.

[208] G. van Koten, A. J. Leusink, J. G. Noltes, *J. Organomet. Chem.* **1975**, *85*, 105.

[209] a) T. Tsuda, T. Hashimoto, T. Saegusa, *J. Am. Chem. Soc.* **1972**, *94*, 658; b) T. Greiser, E. Weiss, *Chem. Ber.* **1976**, *109*, 3142.

[210] a) W. Schlenk, J. Holtz, *Ber. Dtsch. Chem. Ges*. **1917**, *50*, 262; b) W. Schlenk, *Die Methoden der Organischen Chemie* in *Die Methoden der Organischen Chemie* (Ed. J. Houben), G. Thieme, Leipzig, **1924**, p. 720.

[211] O. J. Scherer, G. Wolmershäuser, *Z. Anorg. Allg. Chem.* **1977**, *432*, 173.

[212] O. J. Scherer, R. Wies, *Z. Naturforsch.* **1970**, *25b*, 1486-1487.

[213] a) T. Kottke, D. Stalke, *J. Appl. Crystallogr*. **1993**, *26*, 615; b) D. Stalke, *Chem. Soc. Rev*. **1998**, *27*, 171.

[214] picture by Dr. Christian Kling

[215] T. Schulz, K. Meindl, D. Leusser, D. Stern, J. Graf, C. Michaelsen, M. Ruf, D. Stalke, *J. Appl. Crystallogr.* **2009**, *42*, 885.

[216] a) Bruker APEX v2.2-0, Bruker AXS Inst. Inc., Madison (WI, USA), **2007**; b) Bruker APEX v2009.11-0, Bruker AXS Inst. Inc., Madison (WI, USA), **2009**; c) Bruker APEX v2010.7-0, Bruker AXS Inst. Inc., Madison (WI, USA), **2010**.

[217] a) SAINT v7.46A in Bruker APEX v2.2-0, Bruker AXS Inst. Inc., Madison (WI, USA), **2007**; b) SAINT v7.68A in Bruker APEX v2009.11-0, Bruker AXS Inst. Inc., Madison (WI, USA), **2009**; c) SAINT v7.68A in Bruker APEX v2010.7-0, Bruker AXS Inst. Inc., Madison (WI, USA), **2010**.

[218] a) G. M. Sheldrick, SADABS 2008/1, Göttingen (GER), **2008**; b) G. M. Sheldrick, SADABS 2008/2, Göttingen (GER), **2008**.

[219] G. M. Sheldrick, XPREP in SHELXTL v6.12, Bruker AXS Inst. Inc., Madison (WI, USA), **2000**.

[220] G. M. Sheldrick, *Acta Crystallogr., Sect. A* **2008**, *64*, 112; V. V. Zhurov, E. A. Zhurova, A. A. Pinkerton, *J. Appl. Crystallogr.* **2008**, *41*, 340

[221] W. Massa, *Crystal Structure Determination*, Springer, Berlin, **2004**.

[222] P. Müller, *Crystallogr. Rev.* **2009**, *15*, 57.

[223] P. Müller, R. Herbst-Irmer, A. L. Spek, T. R. Schneider, M. R. Sawaya, *Crystal Structure Refinement - A Crystallographer's Guide to SHELXL* in *IUCr Texts on Crystallography, Vol. 8* (Ed. P. Müller), Oxford University Press, Oxford (UK), **2006**.

[224] PLATON v1.081, University of Glasgow, Glasgow (UK), **2005**.

[225] H. D. Flack, *Acta Cryst.* **1983**, *A39*, 876.

[226] H. Böckemeier, PhD thesis, Göttingen (GER), **2011**.

[227] E. Carl, Diploma thesis, Göttingen (GER), **2010** (EC50, EC99)

[228] R. G. Michel, Diploma thesis, Göttingen (GER), **2010** (RMA10, RMA16, RMA18, RMA23, RMA33)